Modelling thermoregulation for prosthetic design

Laura E Diment

Brasenose College

Supervisors: Jeroen HM Bergmann and Mark S Thompson



Institute of Biomedical Engineering

Department of Engineering Science

University of Oxford

A thesis submitted for the degree of

Doctor of Philosophy

Trinity Term 2019

Modelling thermoregulation for prosthetic design

Laura E Diment Brasenose College

Doctor of Philosophy Trinity Term 2019

Conventional manufacture of prosthetic sockets is artisanal, relying on limited objective data, which often leads to discomfort and tissue damage. Thermal discomfort is a key concern identified by amputees, particularly in hot climates. Despite this, it has had little research attention. This research increases knowledge of the body's heat transfer mechanisms and the effect of amputation and wearing a prosthesis on heat transfer and thermal discomfort through reviewing literature, running a clinical study with amputees and developing a computational bioheat model.

A questionnaire on discomfort, completed by 42 amputees in Bangalore, found heat and perspiration in the prosthetic socket were the most prevalent causes of discomfort. Skin temperatures and thermal discomfort measurements were collected from 30 lower-limb prosthesis users during exercise. After exercise, thermal discomfort was greater on the amputated leg, despite the skin on both legs cooling. The discomfort might signal that the heat generated by the muscles in the residual limb during exercise is stored in the muscles.

To explore the effect of the environment on muscle temperatures during exercise and post-exercise recovery, a cylindrical isolated-segment bioheat model of the thigh was developed in COMSOL Multiphysics and compared to empirical data of muscle temperatures. This model is the first to use finite element analysis to determine temperature distributions through the thigh during exercise and post-exercise recovery. It showed that thermal responses of individuals are varied and complex. From this understanding of the temperature responses of a healthy leg, the possible effects of amputation and prosthesis-use are discussed. The model increases knowledge of the heat transfer factors to consider in developing user-specific prosthetic sockets that reduce the body's thermal load.

The feasibility of integrating simulations, such as this model, with computer-aided design and 3D printing technology to improve customisation of prosthetic sockets was assessed by systematically reviewing the effectiveness of 3D printing prosthetics and other medical devices. The technology shows promise for supporting data-driven prosthetic socket design and manufacture but lacks research and clinical validation.

Acknowledgements

I am immensely grateful for all the support I received during my doctorate. Firstly, I thank my supervisors, Dr Jeroen Bergmann and Dr Mark Thompson for their guidance, not just in my doctoral research but also in developing a firm foundation for my academic career, and my examiners for helping me polish the final product.

I greatly appreciate the support of the General Sir John Monash Foundation, who funded the DPhil and whose focus on cross-discipline discussions to help find solutions to global challenges continues to be inspirational. I also gratefully acknowledge the funding received from the Wellcome Trust and Newton-Bhabha to finance the clinical trial in Bangalore. This clinical research would also not have been possible without Mobility India who organised recruitment and provided research facilities and translators, and the Indian Institute of Science who provided project support and accommodation.

A huge thank you to our friends and families back home, who made the best of our absence and never let the distance or time-difference prevent our regular Skype catch-ups, and especially to Syl, who helped me keep going and provided vital feedback in the drafting process. My deep appreciation also goes to the new friends that we've made here in England who made the academic road less lonely; the Brasenose College community, colleagues in the Botnar Research Centre and our Magdalen Road family, and most of all to Hannah, who was always there with hot-chocolate when I needed it.

Finally, heartfelt thanks to Thom for his unwavering encouragement and patience, and his willingness to follow me across the globe in support of my dream.

Publications

Work from this DPhil thesis has contributed towards the peer-reviewed journal publications and conference presentations detailed below.

Journal publications

Diment, L., Thompson, M. and Bergmann, J. (2019). Comparing thermal discomfort with skin temperature response of lower-limb prosthesis users during exercise. *Clinical Biomechanics*. 69(1); 148-155.

Diment, L., Thompson, M. and Bergmann, J. (2018). Three-dimensional printed upper-limb prostheses lack randomised controlled trials: A systematic review. *Prosthetics and Orthotics International*. 42(1); 7-13.

Diment, L., Thompson, M. and Bergmann, J. (2017). The efficacy and effectiveness of 3D printed medical devices: A systematic review. *BMJ Open*. 7(12). doi: 10.1136/bmjopen-2017-016891

Conference papers and posters

Diment, L., Thompson, M. & Bergmann, J. (2018). Developing thermal simulation of the effect of amputation on muscle heat during physical activity. In *ISPO UK Annual Scientific Meeting*. Southampton, UK.

Diment, L., Bergmann, J., Moulic, S., Thompson, M. (2017). The effect of a lower-limb prosthesis on skin temperature. In *ISPO UK Annual Scientific Meeting*. Cambridge, UK.

Diment, L., Bergmann, J., Thompson, M. (2016). 3D printed upper limb prosthetics are not backed by clinical evidence. In *Trent International Prosthetic Symposium*. Glasgow, UK.

Diment, L., Bergmann, J., Moulic, S., Thompson, M. (2016). Temperature and prosthetic discomfort. In *MEIbioeng 16*. Oxford, UK.

Diment, L., Bergmann, J., Moulic, S., Thompson, M. (2016). Data-driven prosthetic socket design: using sensors to assess discomfort. In *RECOUP International Conference on Ergonomics*. Bangalore, India.

Diment, L., Thompson, M., Bergmann J. (2018). Developing thermal simulation of the effect of amputation on muscle heat during physical activity. In *ISPO UK Annual Scientific Meeting*. Southampton, UK.

Contents

1. Introduction **1**

1.1. Overview of prosthetic sockets 1

1.1.1. Global outlook on the provision of prosthetics 1

1.1.2. Conventional prosthetic sockets 1

1.1.3. Prosthetic socket discomfort 3

1.1.4. A systemic approach to customised fitting 5

1.2. Research aims and thesis outline 6

2. Prosthetic socket discomfort **9**

2.1. Prevalence and types of discomfort 9

2.1.1. India's prosthetics outlook 9

2.1.2. Questionnaire on prosthetic discomfort 9

2.1.3. Types of discomfort experienced 11

2.1.4. Interpretation and study limitations 12

2.2. Physiology of thermoregulation and associated health issues 14

2.2.1. Physiology of thermoregulation 14

2.2.2. Health issues associated with overheating 17

2.3. Comparing amputee thermal discomfort and skin temperature during exercise 20

2.3.1. Background and aims 20

2.3.2. Measuring skin temperature and heat discomfort 22

2.3.3. Heat discomfort and physiological changes during exercise 28

2.3.4. Discussion of findings and reason to study muscle temperatures 34

3. Previous bioheat models and heat transfer theory **43**

3.1. Reason for a bioheat model 43

3.2. Previous bioheat models 45

3.2.1. Overview of bioheat modelling 45

3.2.2. Previous whole-body bioheat models 46

3.2.3. Previous isolated segment bioheat models 47

3.3. Empirical data on tissue temperatures 49

3.4. Theory of heat transfer 51

3.4.1. The passive and active heat transfer systems 51

3.4.2. Heat transfer within tissue 54

3.4.3. Heat exchange with the environment 61

3.4.4. Heat exchange between segments 64

3.4.5. Thermoregulatory responses 68

4. A bioheat model to predict muscle temperatures during physical activity **72**

4.1. Model aims and benefits 72

4.2. Model development strategy 73
4.2.1. Overview of the model design process 73
4.2.2. Choice of software: COMSOL Multiphysics 74
4.2.3. Finite element analysis 74
4.3. Building the model 76
4.3.1. Overview of COMSOL Multiphysics workflow 76
4.3.2. Geometry and materials for the cylindrical model 78
4.3.3. Global parameters and variables 79
4.3.4. Study set-up for passive heat transfer 83
4.3.5. Modelling exercise conditions 87
4.3.6. Modelling thermoregulatory responses 90
4.3.7. Modelling the large blood vessels separately 92
4.3.8. Numerical comparison of models 95
4.3.9. Optimising the metabolic rate during exercise 98
4.4. Geometry factors affecting heat transfer 99
4.5. Exploring the effect of insulation 104
4.6. A geometrically accurate model 105
4.7. Key findings and contributions 110
5. Feasibility of using 3D printing 113
5.1. Opportunity provided by 3D printing technologies 113
5.1.1. 3D printing capabilities 113
5.1.2. Adaptive material microstructures 115
5.1.3. CAD/CAM for developing countries 117
5.1.4. Necessity of critically appraising 3D printed prosthetics 118
5.1.5. Systematic review methodology 119
5.1.6. Critical appraisal of 3D printed prosthetic device studies 121
5.1.7. Outcomes and limitations of studies 126
5.2. Clinical efficacy and effectiveness of 3D printing 129
5.2.1. Overview of 3D printed medical devices 129
5.2.2. Systematic review methodology 131
5.2.3. Critical appraisal of randomised controlled trials 133
5.2.4. Outcomes and limitations 145
5.2.5. Application of findings to prosthetic socket design 149
6. Future directions 151
6.1. Validation of the amputee model 151
6.1.1. Prosthetic socket materials 151
6.1.2. Collecting muscle temperature data from amputees 152
6.2. Future model developments 152

6.2.1. Increasing accuracy 152
6.2.2. Assessing tissue damage 154
6.2.3. Incorporating pressure and friction analysis under dynamic loading 154
6.3. Further uses of the model 156
6.3.1. Athlete training protocols and post-exercise recovery interventions 156
6.3.2. Design guides for prosthetists 156
6.3.3. Web application for prosthetists 157
6.4. Monitoring temperature in the prosthesis 157
6.4.1. Reason for monitoring skin temperature 157
6.4.2. Comparing temperature sensing methods 158
7. Conclusions 169

Figures

Figure 1.1. Percentage of limb amputation at each level 4
Figure 2.1. User satisfaction with their prosthesis 11
Figure 2.2. Types of discomfort experienced by amputees in Bangalore 12
Figure 2.3. The skin's thermoregulatory mechanisms 16
Figure 2.4. General behaviour of the skin temperature over active muscle according to exercise type and intensity 17
Figure 2.5. Temperature testing locations on the amputated limb 23
Figure 2.6. Exercise protocol timeline 25
Figure 2.7 Sweat analysis using thresholding in MATLAB 27
Figure 2.8. Skin temperature at rest after 10 min with prosthesis on 30
Figure 2.9. Skin temperature response during exercise 31
Figure 2.10. Mean differences in temperature between locations 32
Figure 2.11. Rates of temperature change between an insulated leg and an exposed leg 37
Figure 3.1. Flow chart of the thermoregulatory system 53
Figure 4.1. A second-order tetrahedral mesh element 76
Figure 4.2. COMSOL workflow 77
Figure 4.3 Cylindrical model geometry 78
Figure 4.4 Mesh cross-section 79
Figure 4.5. Cross-section of model with cut-points 79
Figure 4.6. Model with and without heat loss from the skin at 20°C and 50% humidity 86
Figure 4.7. Comparing model steady-state temperatures to empirical data 87
Figure 4.8. Modelling muscle heat during exercise using the passive heat transfer system 89
Figure 4.9. Adding vasomotion to model the muscle temperatures during exercise and post-exercise recovery 91
Figure 4.10. Adding sweating to model the muscle temperatures during exercise and post-exercise recovery 92
Figure 4.11. Adding both sweating and vasomotion to model the muscle temperatures during exercise and post-exercise recovery 92
Figure 4.12. Medial and lateral sides with large blood vessels modelled separately. 94
Figure 4.13. The final model after adjusting the basal metabolic rate to align with the optimisation dataset 98
Figure 4.14. Validating the final model against the averages from the validation empirical dataset 99
Figure 4.15. The effect of thigh circumference and body size on muscle temperatures under: A. Hot-dry, B. Warm-humid, and C. Moderate conditions 101

Figure 4.16. The effect of body fat percentage on muscle temperatures 102
Figure 4.17. The effect of depth of thermocouple placement on the muscle temperature reading 103
Figure 4.18. Insulation increases the temperature during exercise and time for recovery 104
Figure 4.19. Joining and smoothing thigh muscles in Meshmixer 106
Figure 4.20. Anatomical model skin temperatures at rest, end of exercise and after recovery 107
Figure 4.21 Slices through the residual limb show internal temperature variations 108
Figure 5.1 Flow chart of selection and sorting of 3D printed prosthetics studies 121
Figure 5.2. Flow chart of selection and sorting of 3D printed medical device studies 134
Figure 5.3. Number of studies per level of evidence given by medical field. 135
Figure 6.1. Aerial view of suggested gait lab setup for dynamic 3D thermal imaging 160
Figure 6.2. Thermochromic liquid crystal structure 162
Figure 6.3. Example of temperature patterns that cannot be differentiated with a 2-direction weave 166
Figure 6.4. A hex-axial weave pattern typically used in basket weaving 167

Tables

Table 2.1. Responses to demographics questionnaire for all amputees 11
Table 2.2. Thermal dose at 43°C required to cause damage for skin, muscle and bone. 19
Table 2.3. Main findings for individual transfemoral amputees 28
Table 2.4. Main findings for individual transtibial amputees 29
Table 2.5. Summary of responses to demographics questionnaire 29
Table 2.6. Individual variables for ordinal logistic regression 33
Table 2.7. Relationship between thermal discomfort and various variables 33
Table 3.1. Summary of studies that measured leg muscle temperatures 50
Table 3.2. Material properties 59
Table 4.1. Global parameters 80
Table 4.2. Global variables 81
Table 4.3. Comparison of model variations 97
Table 5.1. CEBM Levels of Evidence 120
Table 5.2. Summary of human trials with a 3D printed prosthesis 122
Table 5.3. Critical appraisal of 3D printed prosthetic device studies 125
Table 5.4. Systematic literature search method for 3D printed medical devices 131
Table 5.5. Summary of RCTs 137
Table 5.6. Critical appraisal of studies with the highest level of evidence from each medical field 140
Table 5.7. Overview of studies with levels 2 and 3 of evidence from each medical field 141
Table 5.8. Critical appraisal of studies with levels 2 or 3 of evidence from each medical field 145
Table 6.1. Comparison of temperature sensing methods 168

Nomenclature and notational conventions

Measurements throughout this document are given in ***SI units*** (International System of Units) using the standard abbreviations.

Terminology	Description
Contralateral limb	This research is with unilateral amputees, so the contralateral limb is the healthy limb on the opposite side of the body to the amputation.
Countercurrent heat exchange	The veins and arteries run alongside each other so that some of the heat from the arteries is transferred, rewarming the blood in the veins to save the body energy.
Efficacy (device)	The performance of a device under ideal and controlled conditions.
Effectiveness (device)	The performance of a device under everyday conditions.
Mechanoreceptors	Nerve endings of neurons in the dorsal root ganglia that respond to changes in mechanical stimuli.
Metabolism	The consumption of energy by cells so they can perform work. This process also generates heat.
Power analysis	This determines the sample size required to detect a clinically important effect with a specified degree of confidence.
Skin wettedness	The ratio of the actual evaporative heat loss from the skin to the maximum evaporative heat loss for a given environmental condition.
Thermal load	The amount of energy required by the body to maintain a stable core temperature.
Thermoneutral temperature	The temperature at which the minimum amount of energy and oxygen are required of the human body to maintain a healthy and stable temperature.

Thermoneutral zone	The range of ambient temperatures at which no active metabolism changes, such as sweating or shivering, are required.
Thermoreceptors	Nerve endings of neurons in the dorsal root ganglia that respond to changes in temperature.
Thermoregulation	The body's active processes to increase or decrease heat loss from the body to maintain a stable core body temperature.
Thermosensitivity	The smallest change in temperature that an individual is able to detect.
Transfemoral amputation	An amputation through the femur, between the knee and the hip.
Transtibial amputation	An amputation through the tibia, between the ankle and the knee.
Unilateral amputee	An amputee with only one limb amputated.
Validity (external)	How well a study demonstrates that its conclusions are valid outside the context of the study.
Validity (internal)	How well a study demonstrates that the research question has been answered in an unbiased way.
Vasomotion	Dilation and constriction of the blood vessels to change the rate of blood flow.

Terminology	Abbreviation
Computer aided design	CAD
Computer aided manufacturing	CAM
Finite element analysis	FEA
Integrated circuit temperature sensor	IC
International Classification of Diseases	ICD
International Society for Prosthetics and Orthotics	ISPO
Metabolic equivalent score	MET
Mobility India Rehabilitation Service Provision	MI
Magnetic Resonance Imaging	MRI
Oxford Centre for Evidence-based Medicine	CEBM
Partial differential equation	PDE
Randomised Controlled Trial	RCT
Revolutions-per-minute	RPM
Root mean square error	RMSE
Short Form McGill Pain Questionnaire 2	SF-MPQ-2
Submaximal Clinical Exercise Tolerance Test	SXTT
Preferred Reporting Items for Systematic Reviews and Meta-Analyses	PRISMA
World Health Organization	WHO

Parameter	Symbol	Units
Absorptivity, surface	α	dimensionless
Area, surface	A	m^2
Coefficients for distribution or weighting	a	dimensionless
Density	ρ	kg/m^3
Distance	d	m
Emissivity, surface	ε	dimensionless
Energy converted to mechanical power	η	dimensionless
Evaporation coefficient	E	dimensionless
Force, volume	F	N/m^3
Heat capacity	C_p	J/(kg·K)
Heat flux	q	W/m^3
Heat of vaporisation	λ	J/kg
Heat transfer	Q	W
Heat transfer coefficient	h	$W/(m^2 \cdot K)$
Internal workload of the body	H	W/m^3
Irradiation, surface	G	W/m^2

Length	l	m
Lewis constant	L	dimensionless
Metabolic activity level	met	dimensionless
Metabolic rate	M	W/m^3
Perfusion rate	ω	$L/(s \cdot m^3)$
Permeability, skin moisture	δ_p	s
Power	P	W
Radiosity, surface	J	W/m^2
Reflectivity, surface	Φ	dimensionless
Refractive index	n	dimensionless
Relative humidity (RH)	φ	dimensionless
Resistance, thermal	R	m^2kPa/W
Resistivity	r	$kg \cdot m^3/(s^3 \cdot A^2)$
Reynolds number	Re	dimensionless
Stefan-Boltzmann law	e_b	W/m^2
Stefan-Boltzmann constant	σ	$W/(m^2 \cdot K^4)$
Temperature	T	K
Thermal conductivity	k	$W/(m \cdot K)$
Time	t	s
Velocity	v	m/s
Velocity, characteristic	U	m/s
Viscosity, dynamic	μ	$kg/(m \cdot s)$
Volume	V	m^3

1. Introduction

1.1. Overview of prosthetic sockets

1.1.1. Global outlook on the provision of prosthetics

Prosthesis use can improve quality of life by increasing function, independence, physical health, mental health, and social wellbeing.[1] Although figures on the global amputee population are difficult to obtain, estimates indicate that over 100 million people would benefit from a prosthesis or orthosis.[2] Of these, 80% live in developing countries.[3] Ageing populations and the increase in vascular-related diseases are causing the prevalence of disability to rise and, in most countries, the number of amputees is growing faster than the expansion of prosthetics services.[3] Despite the Convention on the Rights of Persons with Disabilities (CRPD) mandating access to good quality and affordable assistive products more than a decade ago,[4] only 1 in 10 in developing countries have access to appropriate assistive devices.[2] The Global Cooperation on Assistive Technology (GATE) has been launched by the World Health Organization (WHO) to create a systemic approach to fitting and distributing prosthetics globally, to support countries in their efforts to comply with the CRPD.[5] However, evidence on the best ways to design and disseminate prosthetics so that they are accessible, affordable and meet the users' needs is lacking.[6] There is currently limited objective data on prosthetic fitting and function available, and the subjective artisanal manufacturing methods conventionally used to fit a prosthesis do not support the creation of an efficient systemic approach. There is also a shortage of about 40,000 prosthetists.[7] In the UK, approximately 60,000 patients with an amputation or congenital limb deficiency attend specialist rehabilitation service centres each year, costing England's National Health Service (NHS) £60 million per year.[8]

1.1.2. Conventional prosthetic sockets

A prosthetic socket is the device-user interface that connects a conventional prosthetic limb to the residual limb of an amputee. Because each prosthesis user has unique health, functional, environmental and structural requirements, customisation of the socket is crucial

for creating a comfortable fit that maximises the user's range of motion and provides stability.[9]

The conventional way of fitting a prosthesis is to create a mould of the residual limb using plaster casting[10,11] or 3D scanning,[12,13] and develop a socket with a solid outer layer around this mould so that it holds its shape and distributes the pressure in a way that the user can tolerate. Both moulding processes require specialist knowledge to make sure pressure is applied at appropriate points to hold the limb on firmly without causing pain. For weight-bearing prostheses, the main suspension methods used are anatomic suspension systems, where the pressure is carefully focused on load-tolerant areas, or total surface bearing sockets (either vacuum-assisted suction or hydrostatic sockets), where the pressure is spread evenly across the residual limb.[14] The former is lower cost, so typically used in low-resourced regions, and the latter is considered state-of-the-art, used where price is not as significant an issue.[15] Sometimes older systems with belts or harnesses are used in low- and middle-income countries or for individuals likely to encounter substantial changes in residual limb volume.[15,16]

The fact that the residual limb shape varies with changes in weight, muscle tissue, loading, weather and hydration creates an additional challenge for socket design.[17] Using a total surface bearing suction socket, limb volume was found to reduce by 4 to 10% over an 8-hour workday.[18] Therefore, many amputees change the number or thickness of socks worn throughout the day to adapt to daily fluctuations in limb volume. The socket is the most frequently replaced part of the prosthesis,[19] with the NHS recommending prosthetic socket adjustment or replacement every one to two years to prevent health issues caused by a poorly fitting socket.[20,21]

The conventional processes for manufacturing sockets require specialised machinery, and fitting can take 2-3 weeks, consisting of multiple appointments, with additional sessions often required to modify the socket to improve comfort, and ongoing appointments for rehabilitation.[22,23] These artisanal manufacturing methods require subjective evaluation of what causes discomfort. They are non-standard, not repeatable and have little quantitative data input into the design. The casting, manufacturing and fitting processes are time, labour and material intensive.

Silicone liners are often used by those who can afford them, to improve suspension and comfort, because they distribute pressure more evenly, reduce friction and create the seal required for many suction and vacuum suspension systems. There are different methods to lock the silicone liner to the prosthesis; internal pin/lock systems, suction by hypobaric seals, sleeves, lanyards, and magnetic systems.[24] Though pressure and friction can be reduced by using a liner, the insulating properties of conventional sockets and liners often cause thermal discomfort due to the inability of the skin to dissipate heat and perspiration from the limb.[14,25]

Osseointegration has been considered as a way of directly loading the bone and removing the need for a socket. However, it is expensive, requires healthy bones to anchor the prosthesis, is not recommended for high-impact activities such as running, and has high infection rates at the percutaneous site.[26,27] There are also risks of more serious complications such as deep tissue infection, bone fracturing, and implant loosening.[26,27] Unless these issues are overcome, the design of external sockets that interface comfortably with the body is important for improving quality of life for amputees.

1.1.3. Prosthetic socket discomfort

Despite using a customised approach to fitting, discomfort is a major concern identified by both upper-limb and lower-limb prosthesis wearers internationally.[28–36] Improper fit or poor material choices can result in discomfort, skin problems, pressure sores, and deep tissue injury,[36–40] and these issues often lead to device abandonment.[36,41,42] The level of amputation is also a significant predictor of prosthesis non-use, and higher amputation levels (where a greater section of the limb has been removed) are associated with non-use and other poor prosthetic outcomes.[41] Figure 1.1 shows the percentage of limb amputations at each level.[43]

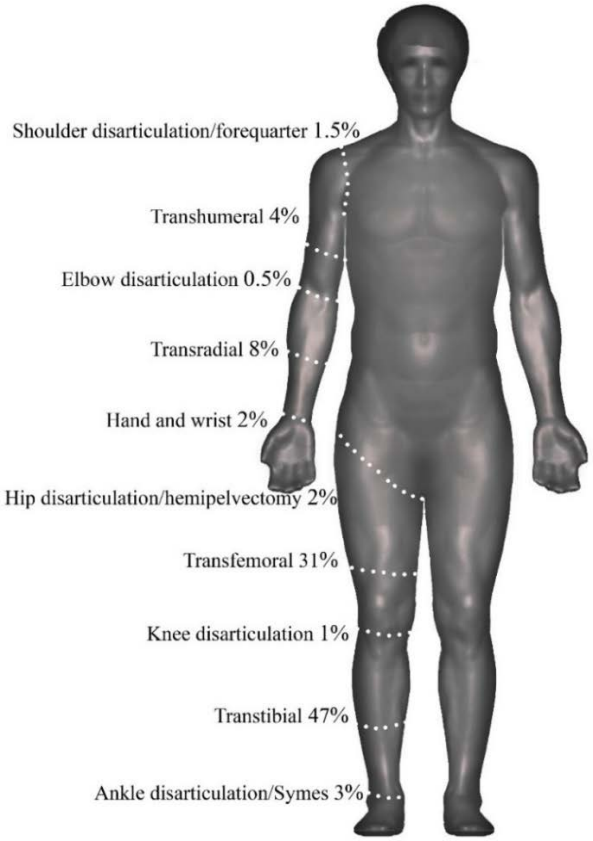


Figure 1.1. Percentage of limb amputation at each level

Previous studies show that over 35% of lower-limb amputees who visited an orthopaedic workshop presented with skin problems.[44] Pressure ulcers often occur, and heat and moisture forming between the device and the skin increase the risk of developing them.[45] Amputees most frequently requested improvements to the thermal properties of prosthetic sockets to deal with heat and sweating, and improvements to the adjustability of the sockets to respond to changes in residual limb size and shape.[46,47]

Even though 54% of prosthesis users stated that heat and/or sweat in the prosthetic socket was an issue (from 3,126 responses across 27 studies), comparatively little research has focused on how the socket's thermal properties affect discomfort.[31] This issue is likely to be even more prevalent in hot and humid climates. The majority of leg amputations are attributed to vascular diseases.[48–50] This population is typically older and is at risk of low levels of total physical activity, minimal participation in sport, and high levels of sedentary behaviour.[51,52] Despite the sedentary behaviour, thermal discomfort remains an issue for this population.[31] The other issue in this population is that vascular diseases can lead to peripheral neuropathy, where sensory loss can mean that the discomfort signals to the brain are disrupted, and tissue damage can occur before the individual experiences pain.[53] It is therefore important to understand the mechanisms of heat transfer to prevent tissue damage.

1.1.4. A systemic approach to customised fitting

Increasing the knowledge and objective data available on how a prosthesis interacts with an individual's body through the use of simulations and sensors, and feeding this into the design and manufacture of prosthetics, can reduce the trial-and-error inherent in current artisanal manufacturing. Because comfort is a complex issue, optimising the socket design for an individual through integration of comprehensive data on tissue mechanics, sensory responses and material properties, requires consideration of a range of factors that may influence the user's comfort.[54] User-specific simulations that predict tissue responses to variations in temperature, humidity and dynamic loading can improve prosthetic socket designs so they fit more naturally and comfortably onto the patient's residual limb. Feeding this information directly into the design and manufacturing process will enable prosthetic sockets to be developed that are more consistently comfortable, and more widely available. 3D printing technologies show promise for improving standardisation and repeatability of the manufacturing process,[55–57] and research into socket customisation for comfort has turned to 3D printing because it facilitates objective assessment of the user's needs and enables the socket to meet varied design priorities.[58,59] Research has been undertaken to monitor pressure[58,60] and friction[61–63] between the socket and the residual limb, but using 3D printing to objectively improve individual socket design to reduce the thermal load is a new concept that requires clinical validation.

The design of highly personalised assistive devices through integration of simulations, sensors, big-data and additive manufacturing has recently been the topic of large collaborations and investment in Europe.[64] This systemic approach to improving individual customisation reduces the load on prosthetists by decreasing the likelihood of requiring follow-up sessions to modify sockets. Storing the client's socket design digitally also enables direct modifications to the old design, rather than starting again. This may enable prosthetists to meet with more patients, and provides possibilities for remote fitting in locations where prosthetists are lacking.[65]

1.2. Research aims and thesis outline

This research contributes to the science and design of patient-specific prosthetic sockets for increased thermal comfort, with a focus on understanding the body's heat transfer mechanisms and how tissue heating during exercise in hot climates is affected by amputation and wearing a prosthetic socket. Skin temperature is known to affect discomfort and tissue health, but it is hypothesised that heat builds in the muscles when wearing a prosthetic socket, even when skin temperature does not change significantly. This internal heating may have negative effects for prosthesis users, and implications for prosthetic socket design requirements. Therefore, this research takes a multifaceted approach to increasing knowledge on heat transfer in an amputee's residual limb by collating literature, collecting data through a clinical study and computational modelling, as outlined below.

The research has been divided into 5 chapters:

Chapter 2 assesses the types of discomfort experienced by prosthesis users and the relationship between discomfort and skin temperature during exercise.

Many amputees in upper-income countries, where research has been focused, have heat-related issues when wearing a prosthetic leg. Lower-middle income countries often have hotter climates, and this is likely to lead to greater heat-related issues. This research presents the results of a clinical study with amputees in Bangalore, India, to assess the prevalence and types of discomfort experienced, and the skin temperatures during exercise. It is the first study to answer the question of whether monitoring skin temperature provides a good predictor of thermal discomfort, and to compare the temperatures between the amputated and healthy limbs. It includes older participants and those with amputations attributed to vascular diseases, addressing a wider demographic than previous studies.[66–70]

Chapter 3 explores the scientific literature on bioheat transfer and develops a numerical model of heat transfer in the thigh during exercise and post-exercise recovery.

Finding that skin temperature does not reflect the thermal discomfort levels, Chapter 3 focuses on the theory of bioheat transfer, to inform understanding of the internal heating that might affect thermal comfort and tissue health, and the disruption caused by amputation. It is based on previous bioheat models but has developed a way to predict temperatures in the

arterial blood flowing into the thigh and to model the large blood vessels to increase the accuracy of predictions of muscle temperatures in the thigh during exercise.

Chapter 4 aims to design and validate a bioheat model that predicts muscle temperatures in the thigh during exercise and post-exercise recovery under moderate, hot-dry and hot-humid conditions.

A bioheat model of human thermoregulation has been developed to simulate muscle temperatures during exercise and post-exercise recovery, using the theory developed in Chapter 3. This research develops the first finite element model to focus on understanding the muscle temperatures during exercise and to provide validation against empirical data. There is no data available in the literature on internal tissue temperatures of amputees during exercise and post-exercise recovery, so the bioheat model is validated using muscle temperature data from able-bodied participants. The chapter includes a discussion on how the model could be modified and validated to observe the effects of amputation and a prosthetic socket on an individual's thermoregulation during exercise and recovery.

Chapter 5 assesses the feasibility of combining simulations with 3D printing technology to support data-driven customisation of prosthetic sockets.

This chapter assesses the opportunity provided by 3D printing, to use a data-driven approach to design patient-specific assistive devices that can be manufactured directly from a 3D model. It reviews the scientific literature on 3D printing capabilities and presents a systematic review of the efficacy and effectiveness of current 3D printed prosthetics. Because this field lacks clinical evidence to support 3D printed prostheses for long-term use, a more general review of 3D printed patient-specific medical devices across all medical fields is also presented to determine the possibilities and efficacy of 3D printing technologies.

Chapter 6 outlines future directions for this research.

It discusses ways to validate the amputee model, assesses other uses and further additions to the model that could expand its usefulness in a clinical setting, and explores possibilities for monitoring temperatures in the socket to feed experimental data into the model to improve future prosthetic socket designs.

2. Prosthetic socket discomfort

2.1. Prevalence and types of discomfort

2.1.1. India's prosthetics outlook

Estimates on the number of amputees in India vary, but the 2011 census estimated that 5.4 million people had a mobility-related disability, including those with an amputation,[71] and the World Bank surmised that the efforts to quantify the amputee population size were likely to have significantly underestimated it.[72]

Understanding the discomfort caused by conventional prosthetic sockets is an important step towards improving socket designs. A study by Nagaraja et al.[35] showed that upper-limb prosthesis users in Bangalore, India rated discomfort as their primary area of dissatisfaction. However, lower-limb prosthesis users have not been assessed, and the cause of the discomfort has not been established.

Mobility India Rehabilitation Service Provision (MI) was chosen as the study site because it is located in a tropical climate, where heat discomfort is likely to be prevalent, and it is a renowned prosthetist training and research centre that services a large number of amputees (an average of 350 prosthesis and orthosis users per month).[73] It also has a range of manufacturing facilities and rehabilitation services on-site, so the fitting, manufacturing and rehabilitation process was thorough and consistent across study participants.

2.1.2. Questionnaire on prosthetic discomfort

A qualitative study of prosthesis user demographics and prosthetic discomfort was undertaken with the hypothesis that heat discomfort would be the most prevalent type of discomfort experienced in the prosthetic socket.

After receiving ethical approval through the Oxford Tropical Research Ethics Committee (OxTREC ref: 599-16), 42 participants were recruited through MI, between June and August 2016. Participants met the following inclusion criteria: over 18 years old, had an amputated or reduced limb, owned a prosthesis, and were able to give informed consent to

participating in the study. All amputees who matched the inclusion criteria and either visited the MI centre during the recruitment period, or were visited by the researcher and the community-based rehabilitation team, were invited to participate. The study took place at the rehabilitation service provision centre and in urban districts around Bangalore, where amputees involved in MI's community-based rehabilitation programme were located. A translator was provided by MI in cases where the participant did not speak fluent English.

Each participant completed a survey with questions on demographics, the participant's amputation, the use of their prosthesis and satisfaction with their prosthesis. Prosthetic satisfaction was assessed using a 6-point scale from *worst possible* to *best possible* and assessment criteria under 3 headings; *function, comfort,* and *appearance,* with *function* subdivided into *usefulness* and *reliability,* and *comfort* into *weight, socket fit* and *socket comfort* based on methods used in previous studies.[34,35] Average prosthesis satisfaction rating was taken by averaging the score across all assessment criteria for all participants. The survey was translated into Kannada by a native speaker to assist the translator with consistent and accurate communication of the questions.

The Short Form McGill Pain Questionnaire 2 (SF-MPQ-2)[74,75] was completed to assess the intensity of each of the discomfort symptoms the participant had felt in the past month. The SF-MPQ-2 is the 2009 revision of the McGill Pain Questionnaire (MPQ) that is the most widely used tool for measuring the quality and intensity of pain.[75,76] The SF-MPQ-2 was chosen to evaluate type and severity of discomfort because it has been previously validated in English,[75] and translated into Hindi, and Kannada, which made it easier for the translators to understand and explain the different types of discomfort to participants, and minimised the effect of translation bias. Participants were also asked whether they felt discomfort due to sweat or rubbing (areas of discomfort that have been reported by amputees[30,31,62] that were not covered in the SF-MPQ-2) and were asked to describe any other types of discomfort that they regularly experienced, to cover any areas that might have been missed by the SF-MPQ-2. The scale of 0 to 10 standardly used for the SF-MPQ2 was divided into: 0 = no discomfort, 1-3 = mild discomfort, 4-6 = moderate discomfort, and >7 = significant discomfort, as many participants were not familiar with the concept of rating sensation using a numerical scale. Participants were not told of the study's hypothesis that heat discomfort would be the most prevalent type, to minimise recall bias.

2.1.3. Types of discomfort experienced

The participant demographics (Table 2.1) show a wide range of variables, with large standard deviations in age, time since amputation and time between amputation and fitting of the initial prosthesis. The majority of participants were lower-limb amputees, primarily transtibial amputees.

Table 2.1. Responses to demographics questionnaire for all amputees

Topic	Factors	Responses
Demographics	Age in years (mean ± SD)	43.3 ± 14.5
	Gender (M/F)	35/7
	Side of amputation (L/R/both)	27/13/2
	Level of amputation (humerus/radius/femur/tibia)	1/3/16/24
	Years since amputation (mean (median) ± SD)	9.1 (5.5) ± 9.5
	Months from amputation to first prosthesis (mean (median) ± SD)	22.3 (12) ± 36.2
	Cause of amputation (traumatic/disease/congenital)	26/15/1
Prosthesis use	Hours of prosthetic wear per day (mean ± SD)	9.4 ± 4.7
	Training received (none/1 day/<1 week/<1 month/>1 month/NA)	7/4/9/0/18/4
	Activity level METs between 1 and 12 (mean ± SD)	4.8 ± 2.3

Most participants were happy with the function, comfort and aesthetics of their prosthesis, and none rated any aspect as *worst possible* (Figure 2.1). Participants gave their prosthesis an average satisfaction rating of 3.3/5, where 3 was considered *satisfactory* and 4 considered *good*. Despite 43% of participants stating that the fit of the socket was the best it could possibly be, socket comfort and weight of the prosthesis were the most common areas of dissatisfaction.

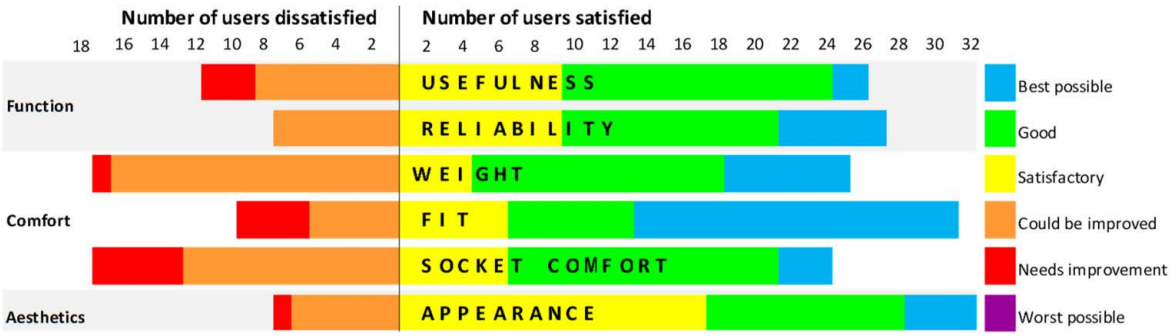


Figure 2.1. User satisfaction with their prosthesis

All participants felt at least a mild level of discomfort sometimes, but none felt more than a moderate discomfort while wearing their prosthesis. The main types of discomfort

experienced, based on SF-MPQ-2 scores, were the residual limb feeling hot, aching, getting tired and feeling heavy (Figure 2.2). Heat was the most prevalent issue, with 71% feeling at least a mild thermal discomfort inside the socket sometimes. The additional questions on whether sweat or friction caused discomfort were also met with large numbers of participants selecting these as issues, particularly sweat, which 62% considered to cause a moderate level of discomfort. In total, 79% had issues with heat, sweat or both. One participant stated that a burning sensation appeared when the nerve endings were touched. Despite the description of a burning sensation, it did not appear to be related to discomfort caused by heat.

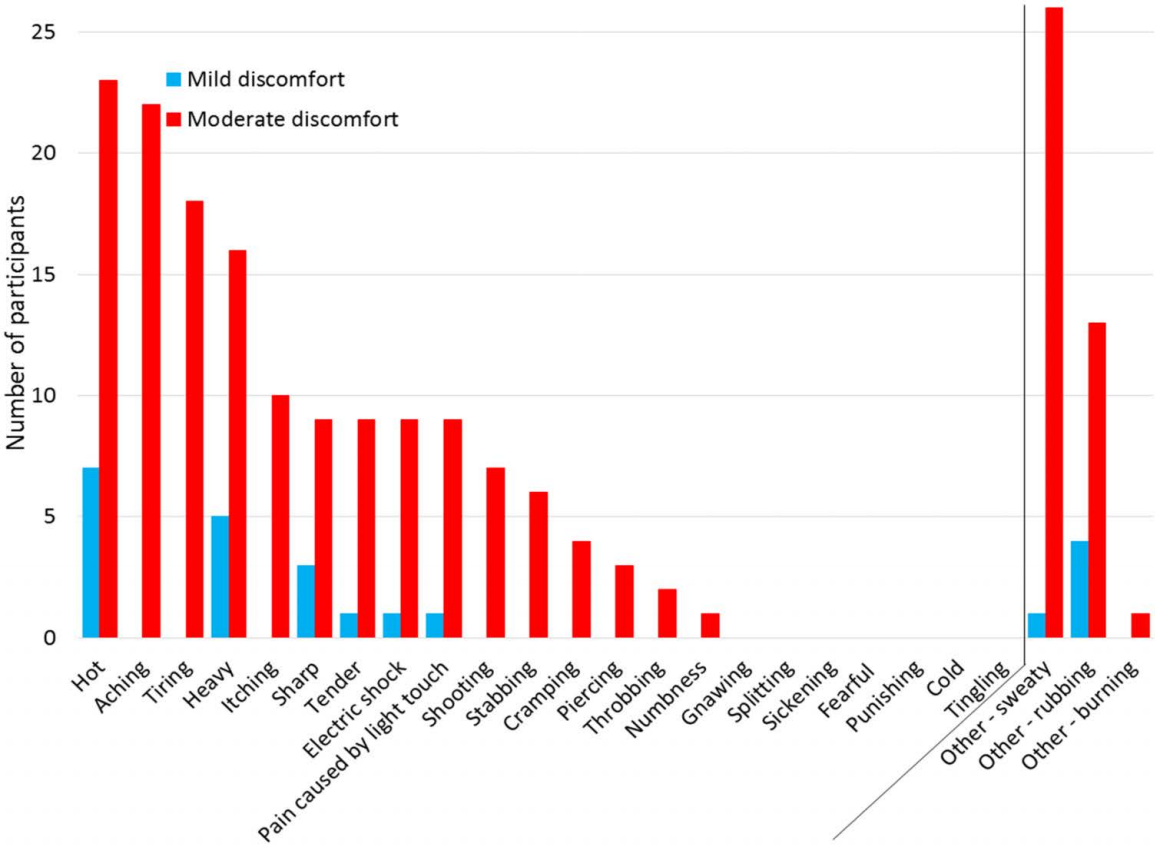


Figure 2.2. Types of discomfort experienced by amputees in Bangalore

2.1.4. Interpretation and study limitations

Heat in the prosthetic socket was the most commonly occurring cause of discomfort experienced by prosthesis users. Discomfort caused by sweating was also frequent and caused more respondents a moderate level of discomfort. This demonstrates that thermal discomfort is a significant issue for prosthesis users in Bangalore, and aligns with literature on prosthesis users globally,[31] though the issue was more prevalent at 79% than the 54% global average. This difference is likely due to the tropical climate in Bangalore.

The majority of participants had no problems with socket fit. However, socket comfort and weight of the prosthesis were the most common areas of dissatisfaction. This matches previous results from upper-limb prosthesis users in Bangalore,[35] and aligns with the fact that the most common types of discomfort experienced were heat, sweat, aching, tiredness and heaviness, all of which are related to the socket design and materials, rather than the fitting.

No participants rated any areas of discomfort as *significant discomfort* (>7/10), and most prosthesis users stated that they were satisfied with their prosthesis overall, despite all feeling at least a mild discomfort on occasion. This may be because the prosthesis has made a huge difference for amputees compared to life without a prosthesis, so they are willing to put up with a certain level of discomfort without feeling dissatisfied. It may also reflect positively on MI's ability to manage expectations. Additionally, because the trial was organised through MI, who provide free prostheses and ongoing rehabilitation and technical support to the participants, their clients may have felt a level of obligation to show satisfaction with the limb because of the generosity of the service provided. It is therefore imperative that conclusions made based on the qualitative data collected on satisfaction levels leave room for the complexity of the reasoning behind participant responses.

Prosthesis discomfort often leads to device abandonment.[41] Because amputees who are unhappy with their prosthesis and choose to abandon it are unlikely to remain in contact with their service provider, it is difficult to avoid recruitment bias when recruiting participants through a service provider, limiting the external validity of the study. However, MI provide free healthcare and have a community rehabilitation program where amputees can receive rehabilitation and follow-up in their homes, which dramatically reduces the number of amputees who abandon their prosthesis because of poor fitting or lack of support.

The study was also limited by using translators during the collection of qualitative data. This provided additional challenges with making sure the questions and subsequent answers were understood correctly. The documents were translated into Hindi and Kannada to minimise the effect of this translation bias, but given that some of the participants were illiterate, the use of a translator was required, adding a source of potential error.

The cause of amputation was more frequently disease-related than in the upper-limb prosthesis satisfaction study performed in Bangalore by Nagaraja et al.[35] Diabetic neuropathy mostly affects the legs and the participant demographic was older, so this difference is unsurprising.

The study shows that socket comfort and the weight of the prosthesis are the areas that cause the most dissatisfaction amongst prosthesis users in Bangalore, and that heat-related discomfort is the most frequently occurring type of discomfort experienced.

2.2. Physiology of thermoregulation and associated health issues

2.2.1. Physiology of thermoregulation

Thermal discomfort is typically used as a subjective "human sensor" to ensure action is taken when issues arise with thermoregulation.[77] Understanding the body's physiology and thermoregulatory system is necessary for understanding what effect excessive heat can have on the body tissues, and why thermal discomfort is experienced. Thermal comfort is related to skin and internal temperatures, as well as *skin wettedness*.*[78] Skin temperature is the largest determinant of thermal comfort at *thermoneutral*** core temperatures at rest, but as core temperature is displaced from thermoneutrality, or skin wettedness caused by perspiration increases, discomfort also increases.[77]

The cells of the human body are greatly influenced by temperature, so temperature must be highly regulated. Core temperature is typically maintained between 36.5-37.2°C at rest, though it naturally fluctuates throughout the day, and is affected by physical fitness, menstrual cycle, stress, age, nutrition, hydration, exercise and sleep.[79] The body has a complex and accurate thermoregulatory system to minimise temperature fluctuation. Core temperature can be maintained without shivering or sweating when external temperatures

* *Skin wettedness* is the proportion of the skin surface covered with sweat.

** *Thermoneutral* is the thermal range where the body does not require active thermoregulatory responses (sweating, shivering or vasomotion) to maintain a stable temperature.

are between 27°C and 32°C for an unclothed adult at rest, but outside this thermoneutral zone, thermoregulatory responses are required to maintain equilibrium between heat generation and dissipation.

The body creates and regulates heat via metabolic processes. *Metabolism* is a term used to describe the consumption of energy by cells so they can perform work. Metabolism includes the breaking down of organic matter by cellular respiration, and the building up of components of cells such as proteins and nucleic acids. Chemical energy is converted to heat and mechanical work by aerobic and anaerobic activities. The average person has a resting metabolic rate of 0.863 kcal/kg·h.[80] At rest, about 56% of heat is generated in the internal organs and approximately 18% in the muscles and skin. During physical exercise, the work done by the muscles increases metabolic heat production, with the heat produced by the muscles contributing to as much as 90% of total heat production.[81] Even at maximum efficiency, only about 23% of the energy generated is converted to mechanical work. The rest is converted to heat that needs to be transported to the skin and dissipated to the environment to maintain healthy tissue temperatures.[82,83] Heat produced by the body enters the bloodstream, where it is conveyed through the tissues to the skin. This circulation minimises temperature differences within the body.

During rest or light exercise, muscle metabolism is aerobic, and the source of fuel is lipids in the form of free fatty acids in plasma. During intense exercise, metabolism of the fatty acids cannot keep up with the demand, and glycogen is used for energy and metabolised anaerobically. As intense exercise continues, glycogen stores are eventually exhausted, and free fatty acids become the principal source of energy.[84] With exercise training, the body increases its ability to metabolise fatty acids.[84] This means that the metabolic processes are different for individuals, based on their fitness levels.

As the barrier between our internal and external environments, the skin is vital for thermoregulation.[85] Skin temperature is determined by the blood circulation to the skin, local metabolism, and heat exchange between the skin and the environment.[86] When external factors or increased metabolism cause the body's internal temperatures to increase, exposed skin uses three processes to increase heat-loss to the environment so a healthy core

temperature is maintained. Firstly, sweat, produced by the sweat glands, causes heat to evaporate into the surrounding air. Secondly, hair lies flat, removing the insulating layer of air around the skin so heat can escape more easily. Finally, inhibiting the vasomotor fibres serving blood vessels of the skin allows vasodilation of the blood vessels so more blood flows through the surface capillaries, increasing the surface area and amount of blood near the skin surface to increase heat loss through radiation (Figure 2.3).[87] Countercurrent heat exchange occurs between major arteries and veins. Most arteries lie deep, but veins are located superficially as well as deeper. This means that the vasodilation/vasoconstriction mechanisms control the arteriovenous heat exchange rate, passing more or less blood through the deeper veins to control temperature.[88,89]

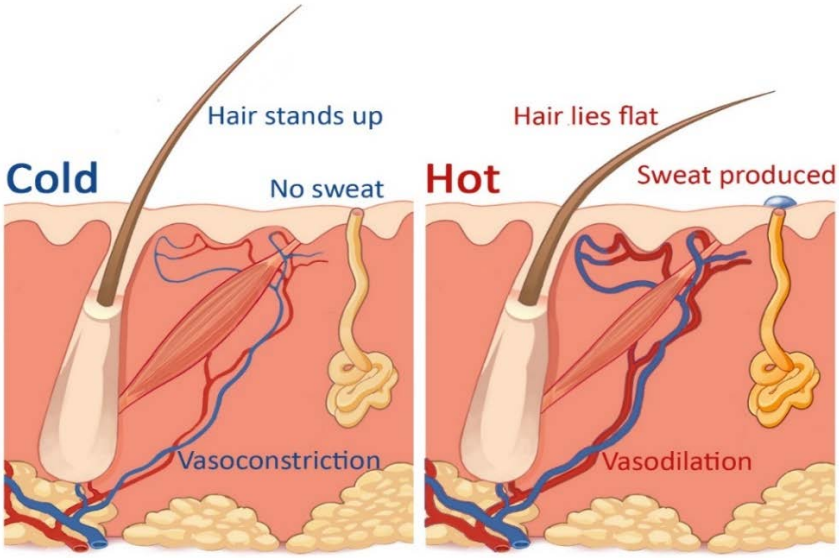


Figure 2.3. The skin's thermoregulatory mechanisms

Many factors influence the body's metabolic heat generation and the skin's capacity for heat loss. These include individual body factors (body size, proportions and muscle mass,[90,91] age,[92,93] sex,[92] hydration,[94] hormones,[95] fitness,[92] chronic health conditions such as diabetes,[92,96] and acclimation[97]), environmental conditions (clothing[93] and ambient conditions[92]), and exercise conditions (type, intensity and duration[98]). The heat dissipation from exposed skin over active muscles during low intensity aerobic exercise is typically dominated by evaporation, causing the skin temperature to decrease, while high intensity anaerobic exercise typically causes the skin temperature over active muscles to increase (Figure 2.4).[99]

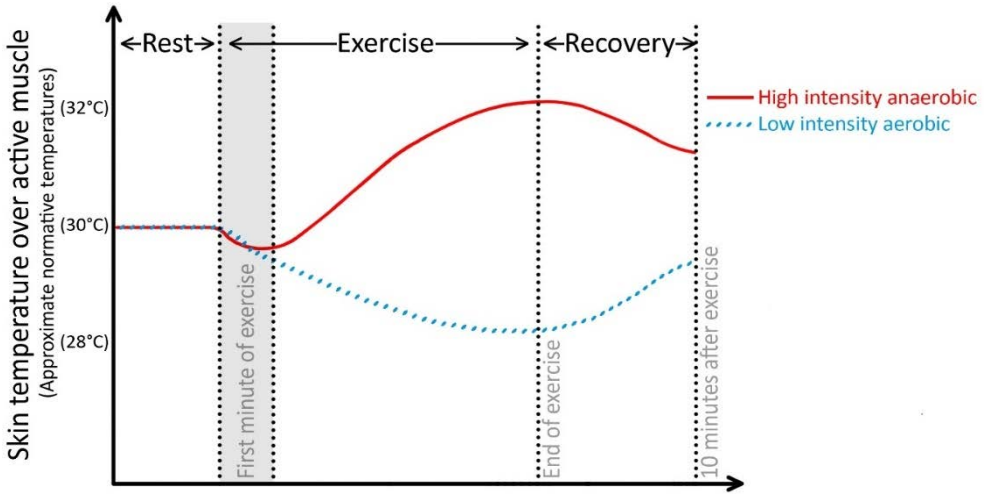


Figure 2.4. General behaviour of the skin temperature over active muscle according to exercise type and intensity[99–101]

Wearing a prosthesis can disrupt the body's cooling mechanisms, as pressure on the pores limits vasodilation and promotes the pressure–sweating reflex; where increased pressure limits perspiration and blood perfusion at the site.[102,103] Convective heat transfer is reduced because there is no air circulation at the skin, and the radiation and evaporation are significantly reduced by the insulating properties of the prosthetic socket and liner. This can result in heat and sweat building in the prosthetic socket,[25] and the heat generated in the muscles during exercise may remain in the muscles for longer durations.[104]

2.2.2. Health issues associated with overheating

Overheating tissue in the short or long-term can have adverse effects on health. If heat and sweat are unable to dissipate from the skin of the residual limb, the environment in the prosthetic socket becomes warm and moist, prone to skin breakdown, bacterial infection and health issues related to a prolonged increase in muscle or core temperatures.[37,38] This can affect not only the tissue health, but also comfort, activity levels and prosthesis suspension.[31]

Many of the health conditions explained below are more extreme than are likely to occur when exercising in a tropical climate with a prosthesis, but they provide useful insight into the effects of excessive heat stored in the body. It is also worth noting that not all heat in the body is damaging. Heat is often used for pain relief in situations such as acute soreness from over-exertion, neuropathic sensitivity, and stiffness and pain related to osteoarthritis, posture and cramping. This pain relief is typically attributed to its temporary effect on the pain

neurons, damping sensation, rather than healing the tissue.[105,106] However, it can also relax the muscles and increase the blood flow, which improves muscle flexibility and may help clear inflammatory mediators from the muscle tissue.[107] This externally applied heat has little effect on tissue 3 cm below the surface, so it does not cause core temperature to increase.[108]

A healthy person under normal environmental conditions at rest, has a constant body temperature,[93] and the core body temperature is regulated to within ±0.2°C of the normal value.[79] However, in exercise conditions, or environments that limit the skin's ability to dissipate heat, the rate of heat generated in the muscle can outweigh that being released to the environment, causing the body, and particularly the muscle tissue, to store the additional heat.[93] Active muscle temperatures can reach 2-3°C above core temperature.[93] This can cause rhabdomyolysis; the rapid breakdown of skeletal muscle cells, which often presents itself as muscular pain, swelling, and limited range of motion, and can lead to kidney damage.[109] Rhabdomyolysis can be caused by extreme physical exercise, normal exercise in extreme environments, high body temperature, heat stroke or lack of blood flow to a limb. Most often, rhabdomyolysis affects physically untrained people who overexert themselves in hot weather.[110] The prevalence of exertional rhabdomyolysis is unknown, and is mostly reported in military personnel, but a study with 225 high school students showed a 43.3% incidence after an endurance test which consisted of 1 minute of curl-ups, 1 minute of push-ups, and 8 minutes of squat-stand repetitions.[111] Muscle tissue properties also change with chronic heating, forming a highly vascularised fibrous tissue. How these changes affect tissue health is poorly understood.[112] The overheating in the muscles can travel through the circulatory system and increase core temperature by more than 2°C.[82,113] A high core temperature raises cardiac output, and increases demand for energy and oxygen by 10% per degree.[79] Core temperatures outside the normal range can result in heat stroke, cause changes in metabolic rates, disrupt organ function and cause tissue damage.[79]

An increase in core temperature can lead to increased fluid loss and dehydration, nausea, vomiting, lethargy, hypotension, hyperkalaemia, hypercarbia, metabolic acidosis, renal failure and acute kidney injury.[114–116] The central nervous system is also vulnerable to damage from increased core temperature, particularly if the effect is prolonged, and can cause short-term or sustained neurological and cognitive dysfunction, including adverse effects on attention, memory, and processing of information. Excessive internal temperatures

are linked to agitation, seizures, unsteadiness, and disturbance of consciousness.[114] Cognitive impairment has occurred in healthy participants when core temperature was raised to 38.8°C, and within 1 to 2 hours of temperature elevation. At 40°C, cell death begins to occur in certain cell lines,[114] 42°C causes circulatory collapse, and above 42.6°C, proteins and enzymes are denatured.[79] The duration of temperature elevation as well as the magnitude of the temperature are both important determinants of tissue thermal damage. Cumulative equivalent minutes at 43°C is the accepted metric for thermal dose assessment.[117] The heat required to damage different tissue types is shown in Table 2.2. Note that some of the measurements were taken in pig or rabbit instead of human because of their similarities to human tissue. Pain and temperature detection thresholds are also affected by temperature, with warm and cold detection thresholds increasing after heating the skin, and heat and mechanical pain thresholds decreasing.[117]

Table 2.2. Thermal dose at 43°C required to cause damage for skin, muscle and bone.[117]

	Minor, reversible damage	Significant and chronic damage	Complete necrosis
Skin	>20 minutes	>40 minutes	Between 5 and 250 hours
Muscle	>40 minutes	>80 minutes	Between 18 and 1200 hours
Bone	Heated for 16 minutes. Thirty days after treatment, the bone resorption was irreversible.		

The blood–brain barrier, under thermoneutral conditions, is a selective barrier of tight endothelial cells that prevents the movement of large or hydrophilic molecules, or toxic substances into the brain. However, this barrier is highly temperature-dependent, and significantly less selective at temperatures above 38°C. This increased permeability is hypothesised to be the predominant factor in the development of cerebral oedema in hyperthermic states.[114] Likewise, systemic excessive heat increases the permeability of the gastrointestinal tract, increasing the rate of gut bacterial translocation and the potential for endotoxins to enter other areas of the body.[114]

Though many of these symptoms are more extreme than typically experienced by prosthesis users in a tropical climate, it is obvious that excessive heat stored in the body can adversely affect health. It is therefore useful to monitor or predict the tissue temperatures in the residual limb.

Muscle temperature is a robust indicator of metabolism,[118,119] and is likely to correlate with thermal discomfort, because muscle cells are the primary cells to generate metabolic heat, and the main tissue type to store additional heat. However, muscle temperature is difficult to measure non-invasively.[120] Skin temperature response is more complex, reacting to changes in ambient conditions and the body's thermoregulatory stimuli. It therefore changes more rapidly than the internal tissues, which means it may not provide a good indicator of thermal issues if they penetrate deeper than skin. However, skin temperature is less invasive to measure than muscle temperature. The following section compares skin temperature to thermal discomfort to assess whether skin temperature is satisfactory for predicting thermoregulatory issues and recording the disruption to the thermoregulatory system caused by wearing a prosthesis during exercise.

2.3. Comparing amputee thermal discomfort and skin temperature during exercise

2.3.1. Background and aims

Thermal discomfort was the most prevalent type of discomfort experienced by prosthesis users in Bangalore's tropical climate. Despite the prevalence of the issue, little is known about the way prostheses impact the body's thermoregulatory system and their contribution to thermal discomfort. Understanding the thermal load of a prosthesis on the body's ability to thermoregulate is an important step towards developing a more thermally comfortable prosthetic socket. A build-up of heat on the skin during exercise was demonstrated in previous small studies by Klute et al.[66–69] Cutti et al.,[70] and Williams et al.,[121] who measured skin temperature within the transtibial prosthetic socket of amputees with traumatic aetiology during rest, exercise and post-exercise recovery. These studies demonstrated that with low to moderate exercise, temperature in the socket increased.

No studies have compared the temperatures to matched locations on the contralateral limb, and only one assessed the thermal discomfort experienced, assessing cold discomfort when exercising in the snow.[69] Additionally, the majority of leg amputations are attributed to vascular diseases.[48–50] This population is typically older and is at risk of low levels of total physical activity, minimal participation in sport, and high levels of sedentary behaviour. This means that they are unable to exercise for the lengths of time required in previous study

protocols.[51,52] Despite the sedentary behaviour, thermal discomfort remains an issue for this population.[31] The other issue in this population is that vascular diseases can lead to peripheral neuropathy, where sensory loss can mean that the discomfort signals to the brain are disrupted, and tissue damage can occur without pain warning.[53] It is therefore important to understand the mechanisms of heat transfer to prevent tissue damage.

This study undertaken in Bangalore, India, focused on determining whether a subjective assessment of thermal discomfort is an adequate indicator of the body's thermoregulatory response to the prosthetic socket's thermal load. Individual resting temperatures vary substantially, and temperatures differ between the amputated and contralateral limb.[122] Therefore, comparing the change in temperature between limbs, rather than assessing total temperature, enables a comparison of participants' responses to exercise and how well their bodies compensate for the increased thermal load of the prosthesis. By comparing the amount of change per minute, comparisons can be made across the population, even though some participants were not able to exercise for as long as others. Comparing rate-of-change in temperature also enabled a comparison between successive exercise intervals to assess whether there was a significant effect that might have been caused by adaption or fatigue in later exercise intervals.

The study aimed to assess: whether exercise caused greater thermal discomfort on the amputated limb in a prosthesis than on the contralateral limb; if the skin temperature response varied in rate-of-change between the residual limb in a prosthetic socket and the contralateral limb during exercise; and whether the rate-of-change of skin temperature on the residual limb related to the perceived thermal discomfort level.

Other questions explored were whether the location of temperature readings affected heating patterns, and whether other easily collected objective measures (skin thermosensitivity and sweat-rate) provided a robust correlation with the subjective measure of thermal discomfort. The thermosensitivity of the skin is dependent on the

thermoreceptors.* This sensitivity varies between individuals, particularly with comorbidities. Sweat-rate may be an indicator of thermal discomfort because the sweat glands are activated as a cooling process when the body heats. Though the skin does not have moisture sensors, the thermoreceptors and mechanoreceptors* together provide the brain with information on the moisture on the skin's surface.

2.3.2. Measuring skin temperature and heat discomfort

A subset of 30 of the respondents to the qualitative survey on prevalence and types of discomfort, presented in Chapter 2.1, were recruited through MI in Bangalore between June and August 2016. These 30 were all the participants who met the following inclusion criteria: over 18 years old, had been a unilateral lower-limb amputee for at least 6 months, had a prosthesis that was in good working order, and were able to give informed consent to participating in the study. The 6-month cut off was used because the residual limb shrinks by 17-40% in the first 6 months and stabilises around the 6-month mark.[123]

Participants used their own prosthesis and had varying levels of amputation. The study was approved through the Oxford Tropical Research Ethics Committee (OxTREC ref: 599-16) and took place at the rehabilitation service provision centre and in urban districts around Bangalore, where amputees involved in MI's community-based rehabilitation program were located. A translator was provided by MI in cases where the participant did not speak fluent English.

Each participant completed a survey with questions on demographics, the participant's amputation, the use of their prosthesis, and pain management. The demographics questionnaire was also provided in Kannada to help the translators.

The centre of the muscle at the back of the thigh (for transfemoral amputees) or calf (for transtibial amputees) was marked with a pen, as well as the same point at the front of the leg, equidistant from the base of the residual limb (Figure 2.5). These locations were also marked on the contralateral limb, and used to collect measures of temperature throughout the study.

* *Thermoreceptors* and *mechanoreceptors* in the skin are cutaneous nerve endings of neurons in the dorsal root ganglia that respond to changes in temperature and mechanical stimuli, respectively.

The locations were chosen because muscle cells are the primary cells to generate and store heat during exercise,[81] and therefore, measuring skin over the centre of the muscle mass is likely to give a good indicator of the temperature changes that occur during exercise. For transtibial amputees, temperatures were also measured at the lateral and medial femoral epicondyles to assess whether skin over bone has a different rate-of-change in temperature during exercise than skin over the active muscles.

Participants rested in a seated position for 10 minutes before the exercise test with their prosthesis on, so a baseline skin temperature recording could be taken at each location using a clinical infrared thermometer (Generation Guard, Victoria, Australia) with a 0.1°C resolution. Ambient humidity and temperature readings were collected. To minimise variability in air velocity, all trials were performed in a room with no fans or air conditioning.

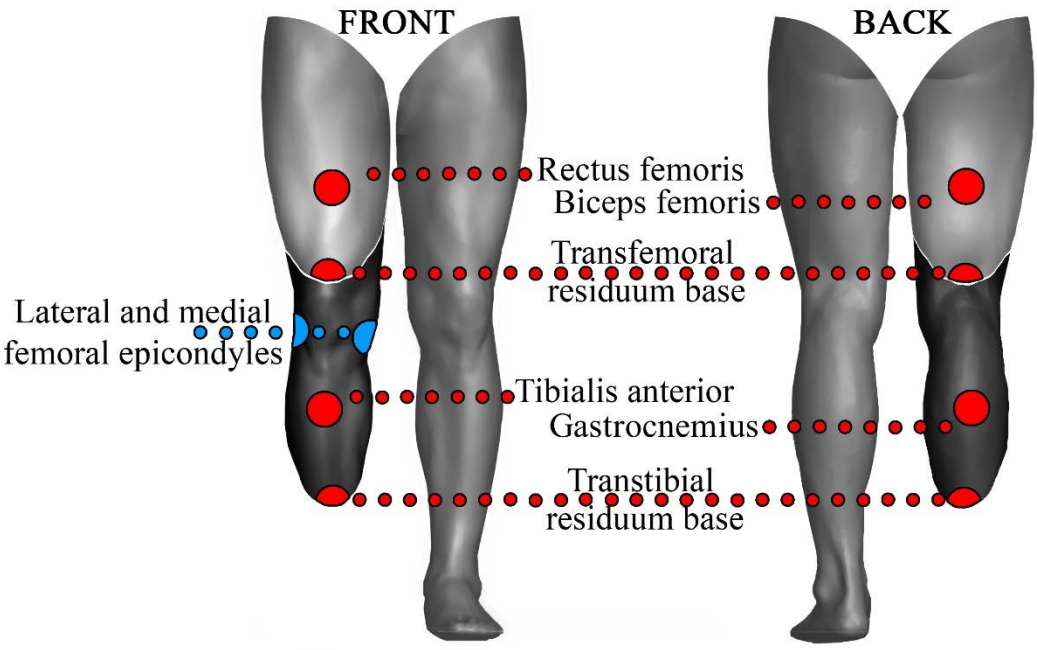


Figure 2.5. Temperature testing locations on the amputated limb

This study aimed to establish whether skin temperature is a good way of predicting thermal discomfort experienced by amputees. Thus, the magnitude of the temperature response was less important than ensuring the socket fit was not disrupted by sensors, and that the exercise was suitable for participants with limited fitness. Therefore, an infrared thermometer was used, rather than in-socket sensors, and a standard Submaximal Clinical Exercise Tolerance Test (SXTT)[124] exercise protocol was used with a MagneTrainer (3D

Innovations, USA). The SXTT was chosen because it only required participants to exercise on the cycle ergometer in two-minute intervals with a workload suitable for their fitness level. A one-minute rest was placed between each exercise interval, as described in Jones et al.,[125] which reduces issues with muscle fatigue in participants unaccustomed to cycling exercise, and made the exercise test accessible for prosthesis users with limited fitness. In this one-minute rest period, the prosthesis was removed for ~20 seconds to take the temperature readings. The temperature was recorded at each marker location, using the same protocol as the baseline temperature collection. The timing between doffing and taking the temperature readings was kept minimal and consistent across both legs and each time-point, with the order of readings randomised within and between participants.

Muscles respond more slowly than skin to temperature changes,[104] so if thermal discomfort increased without a significant change in skin temperature, it might signal that the heat generated by the muscles in the residual limb during exercise was being stored in internal tissues.

A self-administered Specific Activity Questionnaire[126] was completed prior to starting the exercise, to estimate the participant's metabolic equivalent score (MET). This was used to determine the incremental resistance to place on the pedals for each exercise interval. Music was played at 140 beats-per-minute during the exercise intervals, and participants were encouraged to pedal in time to the music to maintain a cycling frequency of 70 revolutions-per-minute (RPM). Assuming this pedalling rate, the protocols for increasing workload on the pedals were: MET scores of 1-4, 5-8, and >9 started at 20W, 20W and 30W, and increased by 5W, 10W and 15W each exercise interval, respectively, as set out by Gappmaier.[124] The endpoint of the test was exhaustion, judged by inability to maintain a cycling frequency of 50 revolutions-per-minute, or when the participant asked to stop. After this final exercise interval, temperatures were taken at each location, then participants rested for 5 minutes with their prosthesis off before the final temperature recordings were taken. The protocol timeline is given in Figure 2.6.

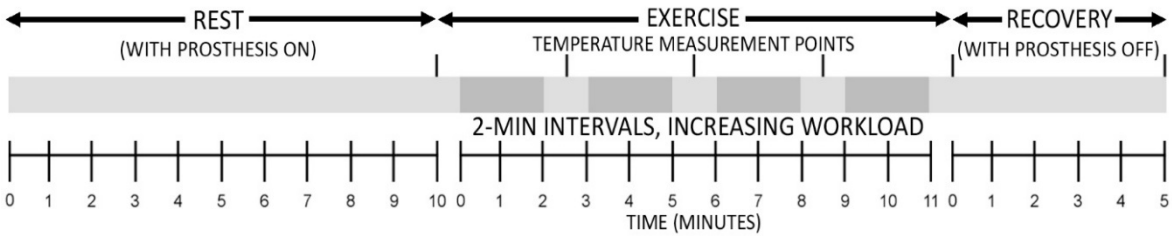


Figure 2.6. Exercise protocol timeline

Immediately before and after the exercise test, participants were asked to rate their heat-related discomfort and discomfort caused by perspiration individually on each leg, using a 6-point scale from *no discomfort* to *intense discomfort*. Participants were also asked to complete historic discomfort scores retrospectively, using the same scale to get an indication of the maximum discomfort caused by heat and perspiration experienced over the previous month for each leg. A Wilcoxon signed-rank test was used to assess whether thermal discomfort differed between the amputated and contralateral limbs after exercise.

Lilliefors tests showed that each temperature dataset followed a normal distribution, and a two-way repeated measures analysis of variance (ANOVA) did not find a difference between the rates of temperature change of transfemoral and transtibial amputees ($P>0.05$), so all participants were grouped together for analysis. A two-way repeated measures ANOVA was used to assess the temperature change over time to see whether there was a difference between the amputated and contralateral limbs and whether location of the temperature recording affected the response, with a p-value of <0.05 considered statistically significant. A two-way student's t-test was used to assess whether there was a difference in rate-of-change between the readings taken over areas of muscle on the residual limb (rectus femoris, biceps femoris and soleus) and readings taken over areas of bone (tibialis anterior, and lateral and medial femoral epicondyles).

Ordinal logistic regression was used to assess the relationship between the skin temperature changes that occurred on the residual limb during exercise and the perceived discomfort level, as well as to assess whether age, level of amputation or cause of amputation were associated with the discomfort experienced. The ordinal logistic regression function for the probability (Pr) is:

$$Pr(\theta_i - \boldsymbol{w} \cdot \boldsymbol{x}) = \frac{1}{1 + e^{-(\theta_i - \boldsymbol{w} \cdot \boldsymbol{x})}}$$

where $\boldsymbol{x}$ is the vector containing the set of observations from the study (temperature, age, level of amputation and cause of amputation), $\boldsymbol{w}$ is the vector containing the ordinal variable response of perceived thermal discomfort, and $\theta_1, \ldots, \theta_{K-1}$ are the set of discomfort thresholds (distinguishable divisions on the thermal discomfort scale) with the property that $\theta_1 < \theta_2 < \cdots < \theta_{K-1}$. The temperature of the residual limb at each time-point was calculated as the average of the 6 temperature readings taken (3 at the front and 3 at the back). The rate-of-change in temperature for each exercise interval was therefore calculated as the average temperature of the participant's limb after the exercise interval minus the average temperature before the interval, divided by the 2-minute exercise period. Because participants exercised for different lengths of time, and the rate-of-change was not significantly different between exercise intervals, the average rate-of-change in temperature for each participant was measured as the average of their completed exercise intervals.

Multicollinearity between predictors was assessed by calculating the variance inflation factors to ensure these predictors were independent of one another. The prosthetic thermal discomfort score used to compare discomfort to skin temperature was based on removing each discomfort score taken on the contralateral limb from the matched discomfort score taken on the residual limb. To get a measure of thermal discomfort that differentiated between participants more than a single discomfort score, the perspiration discomfort score and past-month discomfort scores were included, with the thermal discomfort weighted twice as important as perspiration discomfort, and in-trial scores weighted twice as important as historic scores.

Sweat rate has often been estimated by measuring skin conductance.[127,128] However, this only measures the path of least resistance, so is an inaccurate measure of overall sweating. Instead, a simple photographic scale was developed so that a 15cm^2 piece of thin, absorbent towel could be wrapped around the limb inside the prosthetic socket during exercise to absorb the sweat, and then placed on a tray and slid into a light box that was set up with a camera. To estimate the weight of sweat absorbed, a photograph of the towel at 10 seconds after its removal from the socket was compared to a pre-made calibration curve based on a database of 200 threshold-analysed photographs of weighed water droplets on 15cm^2 thin

towel, with the percentage of wetness on the towel calculated using a tone thresholding technique in MATLAB (Figure 2.7).

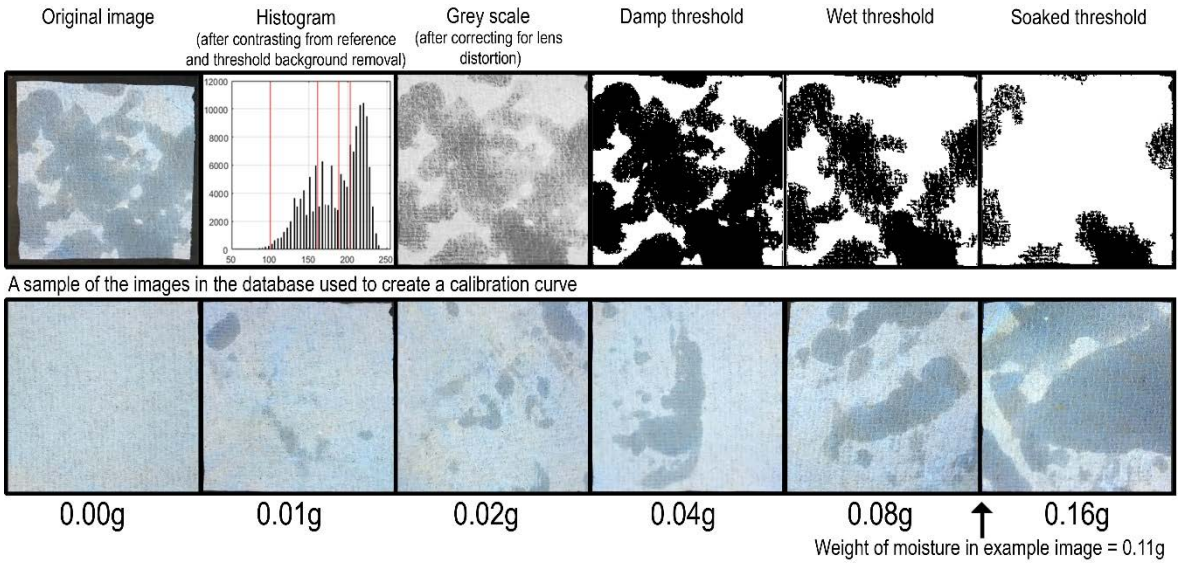


Figure 2.7 Sweat analysis using thresholding in MATLAB

Because the difference between the skin's sensitivity to temperature at sites affected by amputation and the same sites on the contralateral limb is insignificant,[129,130] and the wrist has a higher sensitivity than the thigh or calf,[131] skin thermosensitivity was tested at a single location on the contralateral anterior side of the wrist. This measure was taken before exercise because exercise-time varied between participants. This enabled a baseline comparison between participants.

Skin thermosensitivity was measured for only 23 participants due to unreliable access to hot water for testing. Each participant was blindfolded, and two cups of skin-temperature water (32±2°C) were placed in water baths, one at room temperature 27±3°C, and one at 40±4°C. Metal probes were placed in the cups to reach thermal equilibrium, then placed against the participant's inner wrist and returned to the cup, alternating which cup the probe was taken from, but without explaining this pattern to the participant. The stimuli were given at a frequency of 1Hz. The temperature difference in the cups was recorded when the participant was first able to detect a difference in temperature between the stimuli. This test was repeated 3 times and the average taken. The skin thermosensitivity test was developed based on the clinically validated Quantitative Sensory Testing (QST) thermal threshold

test,[132] but using low-cost equipment that could be easily transported and used without requiring access to electricity. A Spearman rank correlation was used to test whether the skin thermosensitivity correlated with the thermal discomfort score.

2.3.3. Heat discomfort and physiological changes during exercise

There were 11 transfemoral and 19 transtibial amputees who participated, most of whom were male. The main results for each transfemoral participant are presented in Table 2.3, and the main findings for each transtibial participant are presented in Table 2.4. A summary of the demographics of all participants is provided in Table 2.5. There was large variation between participants in age range, years since amputation, and how long after the amputation each participant received their first prosthesis. Most amputees received a prosthesis within the first year, but some waited up to 13 years (Table 2.5). Most of the prosthetic sockets were fitted and manufactured at Mobility India, where they use anatomic suspension systems to focus the pressure on load-tolerant areas of the leg. The manufacturing materials used were resins, thermoplastics and laminates. Most participants wore a sock inside the socket, with 3 using multiple socks to improve comfort and fit. Two participants wore silicone liners, and one wore a copolymer liner.

Table 2.3. Main findings for individual transfemoral amputees

Transfemoral amputees	1	2	3	4	5	6	7	8	9	10	11
Age (years)	31	61	23	30	55	20	42	45	25	41	53
Gender (M/F)	M	M	M	M	M	F	M	F	M	M	M
Time since amputation (years)	16	36	6	<1	18	<1	12	<1	4	1	11
Cause (Disease (D)/Trauma (T))	D	D	T	D	T	T	D	D	T	T	D
MET activity score	9	4	3	3	5	2	4	2	11	3	4
Experienced pain today (Y/N)	N	N	N	Y	N	Y	Y	N	N	Y	N
Thermal discomfort score	2	2.25	0.75	1.5	1.5	2	1.5	0	3.5	1	1
Mean temp. before exercise (°C)	32.9	30.1	31.8	31.1	34.6	30.9	31.3	30.7	31.6	31.8	31.3
Mean temp. after exercise (°C)	31.5	29.9	31.4	31.8	32.8	30.4	31.3	31.2	31.0	31.8	31.1
Duration of exercise (mins)	4	4	2	4	6	2	4	8	8	8	4
Rate of change in temp. at front (°C/min)	-0.37	-0.35	-0.27	0.11	-0.28	-0.23	0.00	0.11	-0.13	-0.03	-0.03
Rate of change in temp. at back (°C/min)	0.25	-0.15	0.10	-0.33	-0.20	-0.05	0.03	-0.02	0.02	-0.07	0.25
Difference: mean amputated – contralateral limb rate (°C/min)	-0.11	-0.01	0.31	-0.07	-0.21	-0.08	0.01	0.14	0.06	0.06	0.32

Table 2.4. Main findings for individual transtibial amputees

Transtibial amputees	1	2	3	4	5	6	7	8	9	10	11	12	13	14	15	16	17	18	19
Age (years)	35	31	21	48	40	45	65	33	30	53	41	36	65	45	62	59	65	67	65
Gender (M/F)	M	M	M	M	M	M	M	F	M	M	M	M	F	F	M	M	M	M	M
Time since amputation (years)	16	28	14	9	2	8	15	15	9	16	9	<1	3	3	2	<1	<1	4	5
Cause (Disease (D)/Trauma (T))	T	T	T	T	T	D	T	T	T	T	T	T	D	D	D	D	D	T	T
MET activity score	5	6	6	8	4	5	8	4	6	5	6	3	3	3	3	4	3	8	6
Experienced pain today (Y/N)	N	Y	N	Y	Y	N	N	Y	N	N	Y	Y	N	N	N	N	Y	N	N
Thermal discomfort score	1.5	4.25	4.25	5.75	2	4.5	0.75	2.25	2.25	1	2.25	4	3.25	0	2	0.5	3	3.75	1.75
Mean temp. before exercise (°C)	32.6	33.1	32.0	31.9	29.7	32.6	31.9	32.5	31.9	30.1	31.1	30.4	33.9	34.1	34.2	31.8	33.5	33.4	32.8
Mean temp. after exercise (°C)	31.9	32.8	32.3	31.2	28.4	32.9	31.6	30.2	31.1	30.1	31.9	31.0	33.5	33.5	33.7	32.7	32.3	33.9	34.0
Duration of exercise (mins)	6	6	6	6	6	6	6	6	6	6	6	6	2	2	2	2	2	8	8
Change in front temp. (°C/min)	-0.24	-0.07	0.08	-0.15	-0.06	0.04	-0.07	-0.14	-0.07	0.00	-0.03	0.14	-0.22	-0.02	-0.17	0.30	-0.38	0.13	0.02
Change in back temp. (°C/min)	0.01	-0.03	0.02	-0.08	0.11	0.06	-0.03	-0.64	-0.18	-0.01	0.28	0.05	-0.15	-0.61	-0.35	0.57	-0.83	0.21	0.26
Difference: mean amputated – contralateral limb rate (°C/min)	0.15	0.15	0.24	-0.10	0.09	-0.03	0.15	-0.42	0.06	-0.12	0.06	0.11	-0.19	-0.38	-0.43	0.43	-0.37	0.49	0.26

Despite many participants stating that they often experienced pain or discomfort due to the prosthesis, and 11 experiencing pain in the 24 hours leading up to the trial, most of the participants wore their prosthesis all day every day, and only 5 ever used pain relief medication (Table 2.5).

Table 2.5. Summary of responses to demographics questionnaire

Topic	Factors	Responses
Demographics	Age in years (mean (median) ± SD)	44.4 (43.5) ± 14.8
	Gender (M/F)	25/5
	Level of amputation (femur/tibia)	11/19
	Years since amputation (mean (median) ± SD)	8.8 (7) ± 8.7
	Months from amputation to first prosthesis (mean (median) ± SD)	16.3 (9) ± 28.2
	Cause of amputation (trauma/disease)	19/11
Prosthesis use	Hours of prosthetic wear per day (mean (median) ± SD)	10.2 (13) ± 5.2
	Training received (none/<1 day/<1 week/>1 week/forgotten)	7/4/4/14/1
	Activity level METs between 1 and 12 (mean (median) ± SD)	4.9 (4) ± 2.2
Education and occupation	Qualification level completed (none/primary/secondary/tertiary)	8/4/12/6
	Occupation before amputation (labourer/office worker/driver/ home maker/not applicable)	16/5/2/2/5
	Self-stated reduction in occupation prospects post-amputation (yes/no/not applicable)	8/22/5
Pain management	Experienced pain today (yes/no)	11/19
	Uses medication for pain relief sometimes (yes/no)	5/25
	Used pain medication today (yes/no)	1/29

The ambient temperature was 26.5°C ± 1.3°C (mean ± SD), and the relative humidity was 72.8% ± 5.4% (mean ± SD). With the prosthesis on, the baseline temperatures of the

residual limbs were not significantly different to the contralateral limbs ($p>0.05$). Figure 2.8 shows there was only 1.6˚C difference between the average temperature at the coldest location (the soleus on the amputated side) and the average temperature at the hottest one (the lateral epicondyle of femur on the amputated side).

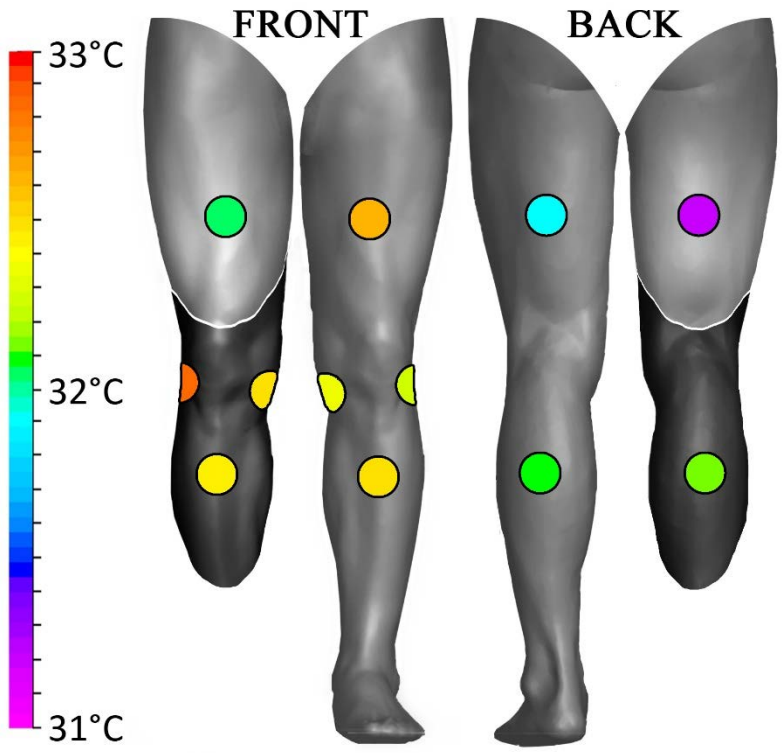


Figure 2.8. Skin temperature at rest after 10 min with prosthesis on

No participants exercised for more than 8 minutes, and only 19 of the 30 participants exercised for at least 6 minutes. Thirteen participants rated the residual limb as more uncomfortably hot after exercise than before, and 9 rated the residual limb as more uncomfortably hot than the contralateral limb after exercise. None of the participants rated the contralateral limb as more uncomfortably hot than the residual limb or felt that their amputated limb had cooled. The Wilcoxon signed-rank test showed that thermal discomfort was greater on the amputated side after exercise, with a mean score of 1.2/5, than on the contralateral side, which had a mean score of 0.6/5 ($Z = -2.719$, $p = 0.007$).

Despite participants stating that the amputated limb was more uncomfortably hot after exercise, the two-way repeated measures ANOVA showed that on average, the skin on both legs cooled during exercise (0.085°C/min, $p = 0.002$). The difference between legs was not significant ($p = 0.599$). However, front and back measurements varied significantly in temperature response ($p = 0.008$), with the skin at the back significantly warmer than the

front after exercise, in comparison to baseline. The difference in rate of change between the readings taken over areas of muscle on the residual limb and readings taken over areas of bone was insignificant ($p = 0.513$).

Figure 2.9 shows that the temperature responses during exercise for the amputated leg and the contralateral leg varied significantly between participants, with skin heating for some and cooling for others. The temperature changes were small, with large standard deviations of approximately 0.5°C on each limb. The average deviation between the 3 measurements taken at each location was 0.021°C.

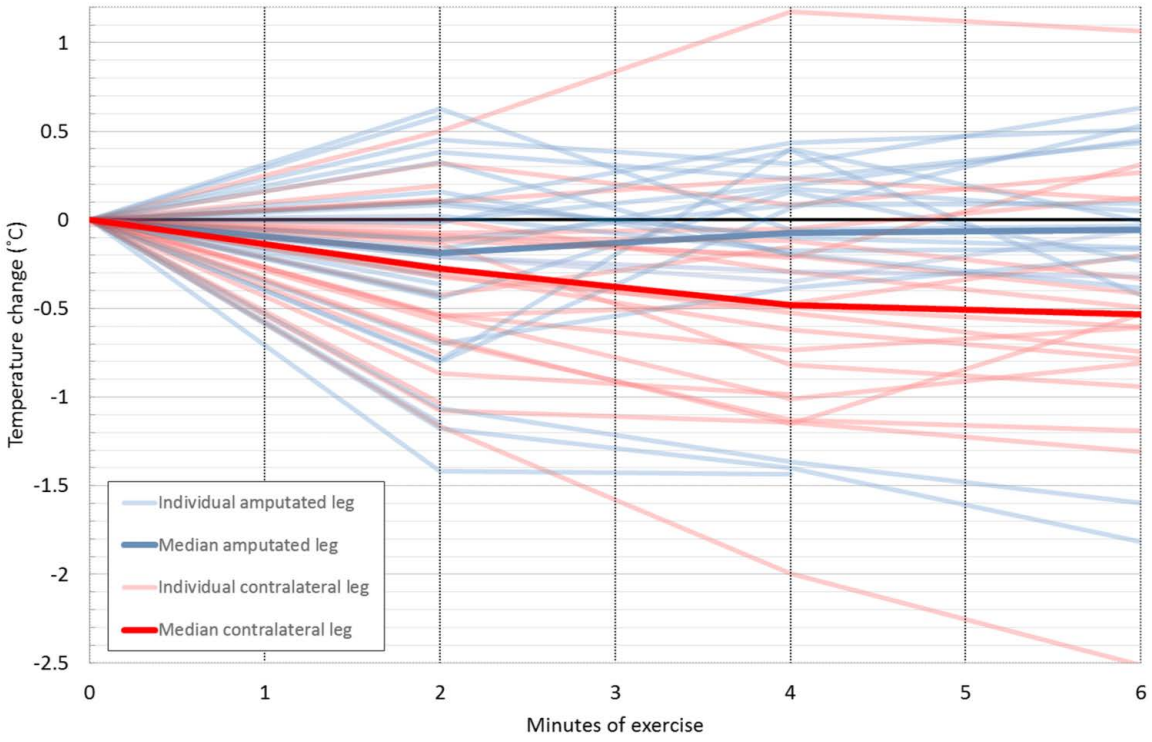


Figure 2.9. Skin temperature response during exercise

The differences in temperature between measuring locations is shown in Figure 2.10. The contralateral limb typically remained warmer than the amputated limb.

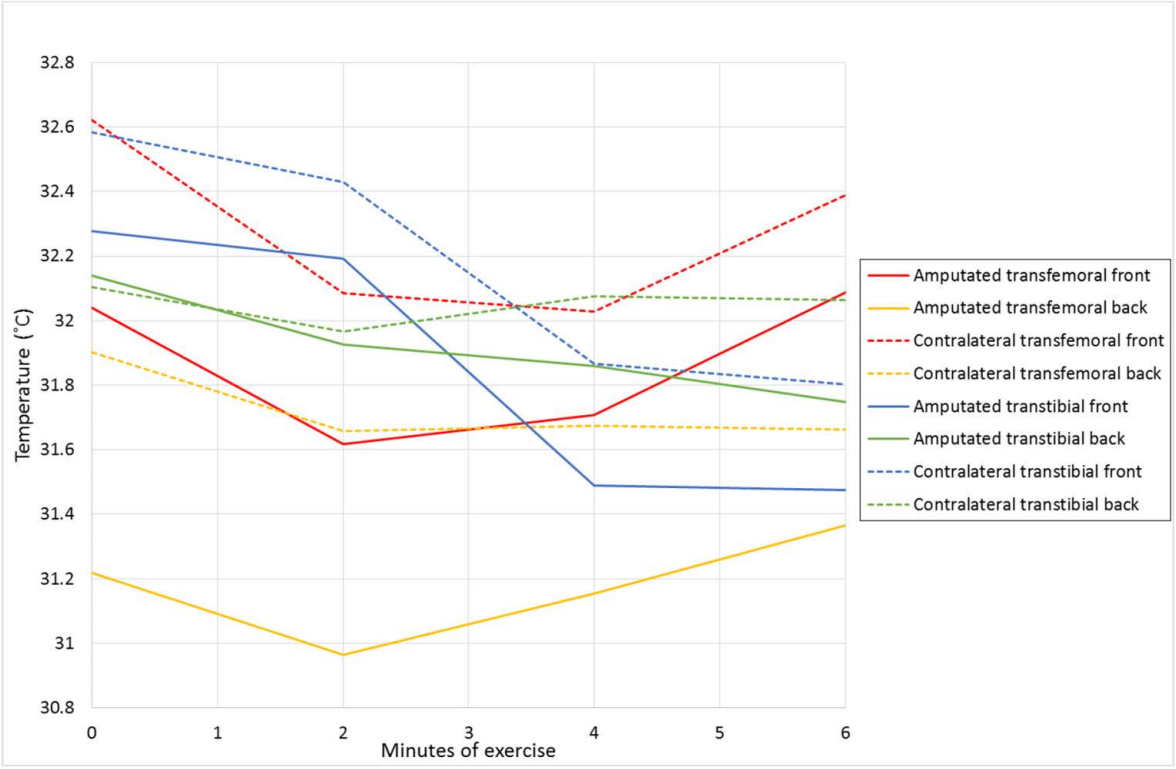


Figure 2.10. Mean differences in temperature between locations

The raw data used in the ordinal logistic regression is provided in Table 2.6. The variance inflation factors for each independent variable compared to all others were small (<1.45), so multicollinearity between predictors was not an issue.

Table 2.6. Individual variables for ordinal logistic regression

Participant	Thermal Discomfort	Average rate of temperature change (residual limb °C/min)	Age (years)	Level (0 = transfemoral, 1 = trans-tibial)	Cause (0 = injury, 1 = disease)
1	2	-.358	31	0	1
2	2.25	-.050	61	0	1
3	0.75	-.208	23	0	0
4	1.5	.158	30	0	1
5	1.5	-.303	55	0	0
6	2	-.217	20	0	0
7	1.5	-.023	42	0	1
8	0	.073	45	0	1
9	3.5	-.077	25	0	0
10	1	-.004	41	0	0
11	1	-.027	53	0	1
12	1.5	-.117	35	1	0
13	4.25	-.047	31	1	0
14	4.25	.050	21	1	0
15	5.75	-.114	48	1	0
16	2	-.222	40	1	0
17	4.5	.050	45	1	1
18	0.75	-.053	65	1	0
19	2.25	-.392	33	1	0
20	2.25	-.125	30	1	0
21	1	-.003	53	1	0
22	2.25	.128	41	1	0
23	4	.097	36	1	0
24	3.25	-.183	65	1	1
25	0	-.313	45	1	1
26	2	-.258	62	1	1
27	0.5	.433	59	1	1
28	3	-.604	65	1	1
29	3.75	.065	64	1	0
30	1.75	.150	65	1	0

The temperature change on the residual limb with exercise was not associated with an increase in the odds of experiencing thermal discomfort (Table 2.7). The only statistically significant relationship with thermal discomfort was the level of amputation, which showed that transfemoral amputees rated thermal discomfort higher than transtibial amputees did.

Table 2.7. Relationship between thermal discomfort and various variables

Variable	Odds ratio	Wald	95% Confidence Interval		Significance
			Lower bound	Upper bound	
Temperature	0.357	0.412	.015	8.279	0.521
Age	0.969	1.468	.920	1.020	0.226
Level of amputation	0.193	4.341	.041	.907	0.037
Cause of amputation	1.080	0.011	.253	4.614	0.918

To get an accurate indicator of sweat response, the plan had been for amputees to wear their prosthesis without socks during the exercise trial, to allow the towel, rather than the sock, to absorb any sweat. However, this plan was discontinued when the first participant was unable to comfortably wear the prosthesis without a sock. Poor socket fitting meant that participants were wearing up to 10 socks to keep their prosthesis on. The sweat test was performed with socks on, but there was not enough sweat absorbed by the towel during the short exercise period to register on the sweat scale.

The variation in skin thermosensitivity between participants was large. The mean skin thermosensitivity was 5.3°C, with a median of 4.3°C and a standard deviation of 3.1°C. Even the most thermally sensitive participant registered a difference of 0.9°C, which was a larger difference than the average temperature differences that occurred at any location on the skin during the trial. On average, participants with trauma-related causes were more sensitive to changes in temperature (by 1.21˚C) and rated thermal discomfort higher than those with amputations due to disease (by 0.4 out of 6), but the results were not statistically significant. The skin thermosensitivity correlated only very weakly with the prosthetic thermal discomfort score ($R = 0.19$, $p = 0.38$).

2.3.4. Discussion of findings and reason to study muscle temperatures

After exercise, heat discomfort was experienced by participants in their residual limb, more so than in their contralateral limb. However, the skin temperature on both limbs decreased during the exercise. No difference was detected between the rate of decrease in temperature between the amputated and contralateral limbs. Neither was any association found between the temperature change on the amputated limb during exercise and the subjective rating of thermal discomfort. The fact that heat discomfort was experienced despite the skin temperatures typically decreasing, and the differences in temperature being smaller than average skin thermosensitivity,[131] suggests that the body's thermoregulation is adversely affected by the prosthesis, and that skin temperature is not a suitable predictor of thermoregulatory issues.

Thermal discomfort is typically used as a subjective "human sensor" to ensure action is taken when issues arise with thermoregulation, but the disconnect between the skin temperature responses and the thermal discomfort suggests that in this population the

mechanism to detect thermal discomfort might be dysregulated on the amputated side, making it more difficult for the patient to correctly identify thermoregulatory issues and to adapt to the environmental constraints. This disruption to the system can lead to health issues related to a prolonged increase in core temperature, and may be partly due to peripheral neuropathy, which is particularly prevalent in diabetic amputees. Poor innervation of skin grafts can also limit an amputee's ability to feel discomfort as a warning of tissue damage.[133] It is therefore important to understand the thermoregulatory effects on the skin and in the muscles in order to create solutions that can counter thermoregulatory problems, rather than relying purely on a subjective measure of thermal discomfort. Though there was no difference between transfemoral and transtibial amputees in the average temperature change during exercise, transfemoral amputees rated thermal discomfort higher than transtibial amputees ($p = 0.037$). This may suggest that losing more of the leg disrupts the body's ability to thermoregulate to a greater extent. Higher amputation levels have previously been associated with worse prosthetic outcomes and higher rates of prosthesis non-use.[41]

During exercise, skin temperature responses vary according to the environment, and the exercise duration and intensity. For example, heat dissipation from exposed skin over active muscles during low intensity aerobic exercise is typically dominated by evaporation, causing the skin temperature to decrease, while high intensity anaerobic exercise typically causes the skin temperature over active muscles to increase.[99] However, many factors influence the skin's capacity for heat loss and the subsequent skin temperature response, including ambient conditions, size, hydration, age, sex, fitness, acclimation, chronic health conditions, and clothing, including a prosthesis.[93] The effect of these factors may explain why the skin temperature responses on both the amputated and contralateral limbs varied considerably from one participant to the next during exercise, despite using the same protocol in the same environmental conditions.

The prosthesis itself can disrupt the body's cooling mechanisms, as pressure on the pores limits surface blood vessel vasodilation, and the radiation and evaporation are significantly reduced by the insulating properties of the prosthetic socket.[25] Previous studies found that with longer periods of exercise without removing the prosthetic socket, temperatures in the socket increased.[66–70] This protocol instead recorded temperatures from

intermittent low to moderate intensity exercise. Given that in the general amputee population, a significant proportion of amputees are elderly and have limited fitness, this protocol may better represent the everyday physical exertion that leads to thermal discomfort.

It was expected that this intermittent exercise protocol with the prosthesis removed regularly would reduce the magnitude of the skin temperature response. However, the skin temperature response to a local environmental change, such as donning or doffing a prosthesis, is relatively slow,[68,134] and the rates of temperature change between an insulated leg and an exposed leg after exercise are not substantially different.[104] To confirm this, a case-study was performed with an able-bodied participant to assess the effect of exercising with an insulating layer and the effect of removing the insulating layer to take temperature measurements (Figure 2.11). The insulating layer was designed to have similar thermal properties to a prosthetic socket, and was worn on one leg. It consisted of a sock material as the inner lining, with a 2 mm thermoplastic sheet around it, moulded to the shape of the thigh from the epicondyles to the uppermost inner part of the thigh.

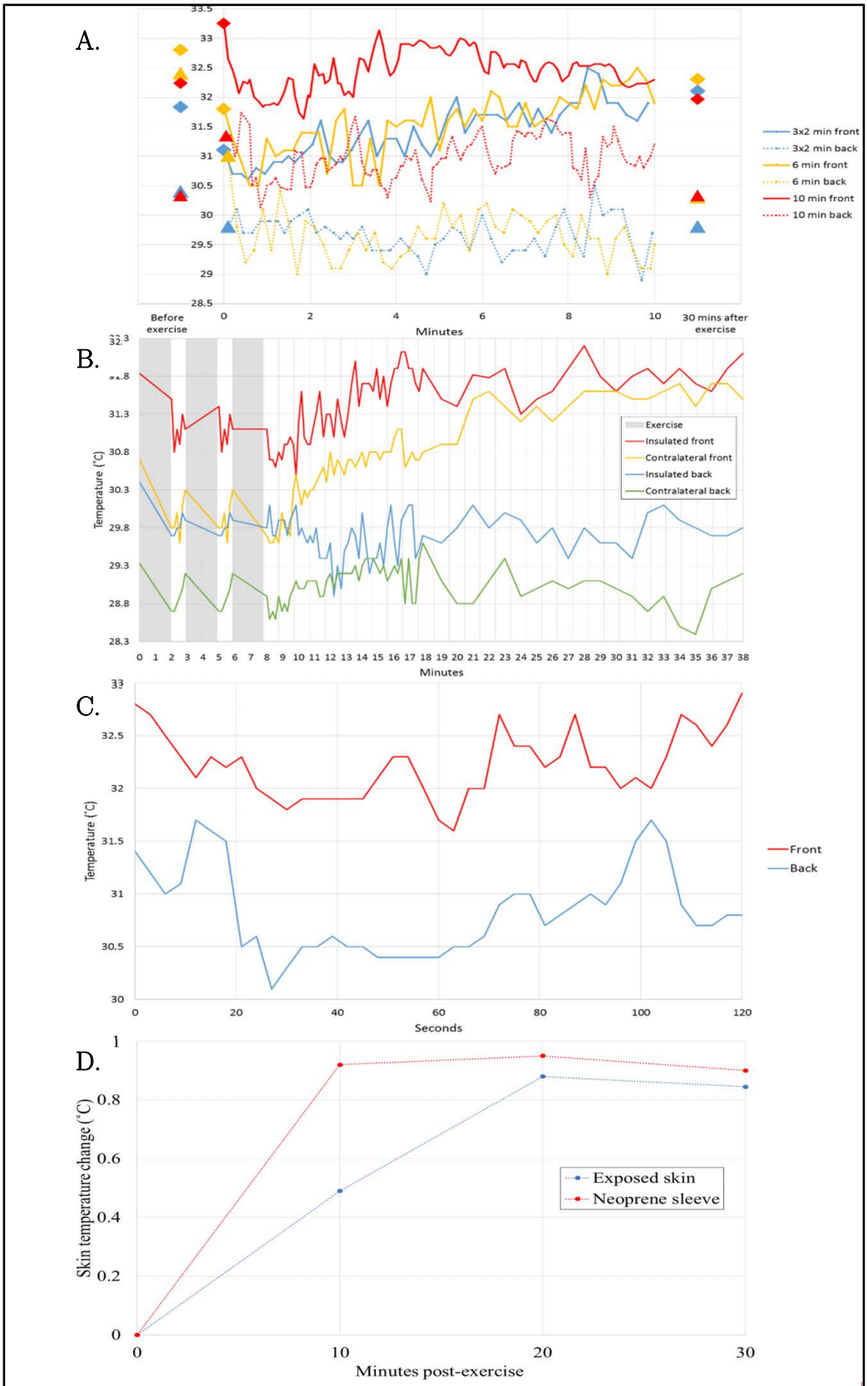


Figure 2.11. Rates of temperature change between an insulated leg and an exposed leg

*A. Insulated leg: after exercising for different lengths of time, the insulation was removed and the temperature change recorded. **B.** Comparing insulated and exposed legs: one thigh was insulated during three 2-minute exercise intervals, and removed for a minute between each. **C.** Insulated leg: First 2 minutes after exercising for 10 minutes. **D.** Thigh skin temperature change after exercise with and without a neoprene sleeve (based on data from Miller et al. 2005)[104]*

All readings were recorded digitally to reduce the data acquisition time and the time spent with the prosthesis off, aiming to keep the recording time consistent across both legs and each time-point, with the order of readings randomised to reduce measuring error and bias. Therefore a 1-minute rest to doff and don the prosthesis, leaving it off for ~20 seconds to take the temperature readings, was not expected to have a large, immediate influence on skin temperature. The study focused on the difference between the limb responses and the comparison with discomfort, rather than assessing the overall temperature change, to enable comparisons across the population despite individual resting temperatures varying substantially, and resting and doffing the prosthesis affecting the temperature response. The skin temperature in the socket decreased slightly on average over the exercise trial, suggesting that the removal of the socket between exercise intervals allowed some evaporative cooling to take place.

Using infrared thermometry to measure residual limb temperature differed from the previous studies, which used thermistors[66–69] or integrated circuit temperature sensors (ICs)[70] taped on the skin in the prosthetic socket and wired to a data acquisition system. The reason infrared thermometry was used is because adding sensors inside the socket could affect the fit and comfort of the socket. Thermistors and ICs also do not directly measure the skin temperature, require calibration, are too expensive to be disposable and therefore require sterilisation, create self-heating errors that can affect the temperature output, and the accuracy is relatively low compared to the small temperature changes expected on the skin during short, intermittent exercise.[135]

Despite the skin cooling, thermal discomfort increased during exercise in the residual limb and not the contralateral limb. This suggests that perhaps internal heating may be responsible for the thermal discomfort experienced. This theory is supported by the scientific literature that shows that if the body's ability to dissipate heat generated in the active muscles during exercise is limited, the additional heat is likely to be stored in the active muscles.[93] Muscle temperatures have been shown to respond almost instantaneously to changes in metabolism,[136] so they might associate more directly with thermal discomfort than skin temperatures. However, there is no easy way to measure muscle temperatures non-invasively.

During exercise, skin temperature responses vary according to the individual's capacity for heat loss (size, hydration, age, sex, fitness, acclimation and chronic health conditions),

clothing and prosthesis design, the environment, and the exercise duration and intensity.[93,99] The diverse individual variables make comparisons across the population challenging and may explain why the skin temperature responses on both the amputated and contralateral limbs varied substantially from one participant to the next during exercise, despite using the same protocol in the same environmental conditions. A computational model can assess the effect of independent variables and simulate internal temperatures. Therefore, the development of a model to simulate the effect of the prosthesis on thermoregulation is recommended. Peery et al.[137] developed a model to predict skin temperatures in a prosthetic socket at rest with no mechanical loading, but further work is required to investigate how physical activity with a prosthesis may affect muscle and core temperatures. This may better diagnose thermoregulatory issues in this population than using a subjective "human sensor" such as thermal discomfort, and explain why thermal discomfort is experienced.

The small temperature changes during exercise, large standard deviations, and substantial difference in absolute temperatures between participants make it difficult to ascertain the clinical significance of these results. Many participants also did not maintain a consistent cycling frequency of 70 RPM, fluctuating above and below the speed, which could affect the individual skin temperature response. The fact that participants were unable or unwilling to exercise for more than 8 minutes may indicate that many of the prostheses were not adequate for exercise conditions. This theory is supported by the participants' self-evaluated MET scores, which gave a median of 4; associated with a fitness level that feels fatigue or shortness of breath if doing exercise as vigorous as sweeping floors, raking leaves, painting, or walking at a standard pace. All but two of the participants were unused to riding a bicycle, so the use of different muscles may have contributed to fatigue and discomfort. However, a difference was not detected between the rates-of-change in temperature in successive exercise intervals, which suggests that the skin temperature was not substantially effected by fatigue or adaption to the exercise condition within this short exercise trial. Many participants were observed to have difficulties with donning and doffing their prosthesis, which also may have decreased their willingness to keep doing exercise intervals. A simulation enables longer, more intense exercise conditions to be evaluated than participants can manage with current prosthetics. It also allows a comparison of prosthetic materials and

designs without the expense of manufacturing each. This approach can lead to a more data-driven method of designing future prosthetic sockets for individual thermal comfort.

Despite 11 participants experiencing residual limb pain in the previous 24 hours, only 5 ever used pain relief medication for chronic residual limb pain and 24 wore their prosthesis for the majority of the day every day. This suggests that even though the prosthesis may have limited their ability to do physical exercise, most participants found significant benefit in having a prosthesis. The 5 participants who used pain relief medication used paracetamol, and one also sometimes used codeine. These both have temporary effects on body temperature and sensitivity to changes in temperature. However, no participants were using pain relief at the time of the trial. None of the other medications mentioned by participants have been linked to changes in thermoregulation or exercise performance.

The contralateral limb typically remained warmer than the amputated limb, despite the amputated limb being insulated by the prosthetic socket. This finding matches the scientific literature,[122] and suggests that there might be a reduction in blood flow in the amputated limb. This reduction in blood flowing to the skin surface may be limiting the heat loss from the body, and therefore the body's ability to thermoregulate, causing internal tissues to store additional heat. For transfemoral amputees, the main muscles used for cycling (the quadriceps and hamstrings) are not functional, so their gluteal muscles may be the main ones controlling the movements, and these are above the socket, so their heat may not be picked up in the current protocol.

Front and back of the leg were measured to improve the accuracy of the temperature reading for the limb. Though the front of the leg was typically slightly warmer during resting than the back (Figure 2.10), this was not the case after exercise. The rate of temperature change during exercise was different at the front of the socket to at the back, with the skin at the front of the leg cooling during exercise, but the skin near the larger muscle mass at the back of the leg not noticeably cooling during exercise. Assuming the evaporation rate was similar at the front to the back, then this outcome supports the idea that the working muscles may be storing the heat. There were differences in temperature between measuring locations as well. These differences demonstrate the importance of considering anatomy in future analysis and in the development of a bioheat model. Developing a patient-specific model

would enable the individual's factors that influence the body's capacity for heat loss to be considered, to assist in understanding the user's requirements for a prosthetic socket.

A standard numerical rating scale is widely used to measure pain, but has not been reliability tested for measuring discomfort caused by heat or perspiration, and the thermal discomfort score used in this paper, based on the heat and perspiration discomfort ratings, has not been validated. There is an inherent risk of bias when the participant is asked to think about heat and perspiration, as there is no way to blind the participant to the outcome assessment. This is another reason to develop an objective approach to assessing thermoregulatory issues, rather than using a subjective measure of heat discomfort.

Neither sweating nor skin thermosensitivity were robust indicators of thermal discomfort. There was not enough sweat absorbed by the towel during the short exercise period to register on the sweat scale, making the technique a poor way of assessing thermoregulatory issues. There were inherent inaccuracies in the skin thermosensitivity test used, caused by the time difference between the participant feeling the difference and stating it, and the water temperature being measured. This time lapse was greater if translation was required to confirm that a difference had been felt. Also, the probe from the hot water cooled faster in the air temperature, so decreased the difference on the wrist to the difference in the cups. To reduce the effect of these errors, the test was repeated 3 times, and a Spearman rank order correlation coefficient was used to compare the thermosensitivity to thermal discomfort, thereby taking into account the comparative sensitivity of the individual, not the magnitude of the sensitivity. However, this found only a very weak correlation between skin thermosensitivity and thermal discomfort.

These findings indicate that though heat discomfort was prevalent after exercising with a prosthesis, in this patient population, skin temperature does not explain the thermal discomfort experienced, and a subjective thermal discomfort score is inadequate for detecting thermoregulatory issues. Modern textiles that offer improved thermal regulation may be suitable for incorporating into future socket designs to reduce the thermal load on the body during physical activity,[138] but little is yet known about the design requirements for a thermally comfortable prosthetic socket. It is recommended that a bioheat model be

developed to increase understanding of the effects of a prosthesis on the body's thermoregulation and internal temperatures during exercise, and to enable a comparison of the thermal load on the body created by different socket designs.

3. Previous bioheat models and heat transfer theory

3.1. Reason for a bioheat model

This chapter explores the theory of heat transfer and the body's thermoregulatory system, to better understand the internal heating that might affect thermal comfort and tissue health.

There is a need for a new prosthetic socket design that can reduce the *thermal impact*[*] on the body during physical activity. Reducing the thermal impact is likely to reduce the discomfort experienced by amputees and increase quality-of-life, as discussed in Chapter 2. In addition to discomfort, there is also a risk of skin and deep tissue damage when wearing a prosthesis, due to the pressure and shear stresses, and heat and moisture that builds in a prosthetic socket. These issues are exacerbated by poor blood perfusion, which reduces the limb's ability to thermoregulate, and peripheral neuropathy, which limits the amputee's ability to detect thermal issues. Damage to skin and deep tissue are both common for amputees, particularly ones with vascular diseases.[30,31,37,139] A good understanding of the effect of an amputation and a prosthetic socket on the body's thermoregulation and temperature distributions is required before the thermal impact can be reduced through engineering design.

Chapter 2 demonstrated that thermal discomfort was an issue for prosthesis users in Bangalore, even with short exercise durations, and suggested that skin temperature was not a good predictor of the thermal impact of a prosthesis on the body. This result is in line with other studies.[99,104] Because skin temperature is not a good predictor of thermal discomfort, a bioheat model of human thermoregulation has been developed to simulate muscle temperatures during exercise and post-exercise recovery under moderate, hot-dry and hot-

[*] In this context, thermal impact is defined as the temperature of the body tissues above the temperatures under resting, thermoneutral conditions, per unit time (°C/s).

humid conditions. This chapter focuses on the theory, and Chapter 4 presents the model structure and results.

Muscle cells are the primary cells to generate and store heat during exercise, contributing as much as 90% of total metabolic heat production.[81] Therefore, the muscle temperatures may show a stronger association with thermal discomfort than other tissues. A number of studies have collected temperatures from various parts of the body during rest and physical activity.[140] It is relatively easy to collect skin temperature[135,141–144] and core temperature,[145–147] but muscle temperature is challenging to measure.[118] Muscle temperatures can be measured invasively at individual points using thermocouples,[104,136] and nuclear magnetic resonance (NMR) may be used to map the temperatures of a stationary person non-invasively.[148,149] Insulating the skin can also cause its temperature to rise to close to the muscle temperature, which can provide an estimate.[119,120] However, because of the skin's importance in thermoregulation, this method affects heat transfer too much to be useful for mapping muscle temperatures within a prosthetic socket. A computational bioheat transfer model enables prediction of internal temperatures that are not easy to collect empirically. It can provide a low-cost, non-invasive way to assess the risk of internal tissue heating during physical activity with a prosthesis.

Tissue temperature responses vary according to the individual's capacity for heat loss (size, hydration, age, sex, fitness, acclimation and chronic health conditions), as well as their body composition (volume, surface area, thigh circumference, body fat percentage, and blood circulation through the large and peripheral blood vessels). They are also affected by insulation (clothing and the prosthetic socket), the environment, and exercise duration and intensity.[93,99] The diverse individual variables make comparisons across the population challenging. A bioheat transfer model can control for independent variables, enabling study of how the muscle temperatures are affected by different heat-transfer factors. It can also predict the impact of changes in heat load on an individual, which can assist in designing a prosthetic socket for the individual, and in minimising the risk of tissue damage and fatigue for individuals in environmental conditions where tissue overheating is a concern.

A real-time bioheat model could be used by prosthetists in the clinic to predict the heating patterns of an individual's leg during the prosthetic socket casting process. The software could provide a visual guide to the prosthetist on areas of the limb that would

benefit from reduced thermal loading. Prosthetists and technicians could create holes in certain areas of the socket, thin the material, change the type of material or add active cooling processes in particular areas to enable breathability, change the thermal conductivity or support the body's natural thermoregulation. Bioheat modelling could also, in the future, be directly incorporated into computer-aided design and manufacturing of prosthetic sockets (see discussion in Chapter 4.7).

3.2. Previous bioheat models

3.2.1. Overview of bioheat modelling

The heat transfer that occurs in the human body can be modelled based on empirical data or analytically, based on understanding the physics involved. More commonly, a combination of both is used. Empirical models predict thermal responses by deriving equations directly from experimental data. Because collecting internal tissue temperatures at different locations under different environmental conditions is challenging, empirical models tend to only work for simple and very specific conditions and are not useful for extrapolating to other conditions than those of the initial empirical study. However, computational models also typically rely on empirical data to supplement the analytics, due to the complexity of numerically predicting metabolic activity in complex and highly individual tissue architectures.[150] The model developed in this research is based on heat transfer theory, but incorporates empirically derived physiological parameters where the theory alone is not well understood or validated, based on data obtained from the scientific literature.

Models of heat transfer in perfused biological tissue can be divided into vascular models and continuum models.[151] The intricacy and uniqueness of a person's blood vessel architecture make the individual contributions of vessels to the fluid flow and heat dissipation through tissue challenging to model. Because the tissues also actively generate heat, with a rate that varies with changes in energy expenditure and the environment, and each person's vasculature varies, vascular models are impractically complicated for mapping macro-level temperature differences. A continuum model is better suited to modelling heat transfer within tissue, and is used in most human thermal models. It describes the complex

small tissue structures in terms of the collective behaviour of the tissue, relying on the fact that the small blood vessels in tissues have a large surface area, so conduction of heat from the vessels to the tissue dominates the heat transfer. It considers the thermal conductivity, specific heat, and blood perfusion rate of the tissue as a whole.[152]

3.2.2. Previous whole-body bioheat models

Because of the complexity of the human body, simplifications and assumptions must be made to bioheat models to balance accuracy against computational complexity. For this reason, previous whole-body bioheat models have almost exclusively been made up of simple axisymmetric segments; typically cylinders.

Wissler's original six-segment model, published in 1961, used one cylinder to represent the head, one for the torso, and one for each limb.[153] It contained only one tissue type with uniform heat production and blood distribution. This model was followed shortly after by one by Stolwijk that considered the different tissue types.[154] This model has become the basis of most modern-day bioheat models. As technology and knowledge of the human body advance, these models have become increasingly accurate and complex, improving calculations for thermoregulation,[155] blood heat transfer,[156] and arterial blood temperature drop along the extremities.[157] The effects of clothing,[158–160] varied and transient environments,[156–158,161,162] exercise conditions,[83,134] and individual size[158,162–164] on human thermoregulation have also been modelled, and the cylindrical geometries have been modified by tapering the segment radius or creating elliptical cross-sections to better represent the body's anatomy.[165,166]

These models provide an estimate of the average temperatures of each tissue type in each segment, rather than mapping thermoregulation across the body or calculating temperature at specific locations. Temperatures in the human body are highly dependent on the geometry and inhomogeneity of the body,[167] and the study in Bangalore found significant differences in front and back of leg skin temperature responses during exercise (Section 2.3). Therefore, these multi-segment whole-body models do not provide accurate enough geometries and temperature predictions to be useful for assessing spatially localised temperature changes on the skin, and internal leg temperatures during physical activity. Many of these models have been validated against empirical data for average skin temperatures and core temperatures for various environmental conditions, but none have

been validated against empirical muscle temperature data due to the difficulty in obtaining average muscle temperature data.

Advances in modern computing have removed the computational power limitations that led to simple axisymmetric multi-segment models. Li and Wang[168] stepped away from the multi-segment whole-body model design and experimented with a human-shaped skin shell with the internal tissue layers divided as a percentage within this shell, and a finite element method used to calculate temperature across each mesh element individually, treating the body as a whole instead of linked segments. This model provided a more advanced means of simulating the effect of the external environment and clothing on skin temperature of a stationary human. To understand heating during physical activity, however, it is necessary to accurately model the internal tissues of the leg as well, because internal tissue geometries affect the temperature response to exercise. Building upon these previous models to develop a model that can predict muscle temperatures and show spatially localised temperature differences is necessary to compare current prosthetic socket designs and to design future sockets to vary material properties across the socket to improve comfort and function for the individual.

3.2.3. Previous isolated segment bioheat models

Due to their computational complexity, whole-body finite element models have not yet been developed with accurate geometries or to model temperatures at specific points. However, isolated segment models have been developed to model thermoregulation in a particular area of the body with more detail.[137,169,170] The following discussion will focus on models of the leg.

Mitchell et al.[171] developed a simple model of the whole leg, treating the cross-section of the leg tissues as circular. Their aim was to assess the time required to cool a resting leg to a steady-state temperature as a means of anaesthesia before amputation surgery. Average temperature at the centre of the leg was predicted, and thermocouples were inserted into the muscles of participants, below the amputation site, to provide internal temperature data to validate the model against. The core leg temperature dropped by 20 to 30°C, and these large changes were able to be approximated by the simple model.

More recently, Kalra et al.[169] developed a bioheat model of the thigh that used accurate tissue geometries based on the Visible Human dataset to simulate a resting leg under cooling conditions. The aim was to determine the effects of geometry and physiology on temperature distribution to assess whether external cooling methods cooled the body's core. The model demonstrated that anatomical accuracy in geometry is important, and that central vasoconstriction is a crucial factor in predicting localised temperatures when applying external cooling to the segment. A known limitation of isolated segment models is that there are many unknowns that make it complex to simulate thermoregulatory physiological responses. Kalra et al.[169] attempted to resolve this issue by inserting mean skin and core temperatures directly from empirical experiments, to approximate the central vasoconstriction and shivering. The purpose of the model was to assess a cooling body, so vasodilation, sweating and evaporation were ignored. This provided a close enough accuracy for short-duration studies under similar conditions for an immobile human, but would not be satisfactory for different environmental conditions, physical activity or longer duration studies.

Peery et al.[137] developed a finite element model of the passive thermoregulatory system in the leg to predict the steady-state skin temperature distribution of a transtibial prosthesis-user at rest with no mechanical loading, ignoring the effects of muscle metabolism and sweating. The exterior shape and locations of internal tissue layers were based on CT data from a transtibial residual limb of a supine amputee. The prosthesis was modelled as a single, 10 mm thick layer on the outside of the skin, and the model was generated using a tetrahedral mesh. The model focused on skin temperature mapping, comparing results to resting skin temperature data from inside the socket of 5 young-adult male amputees. Though internal temperatures were not analysed, the effect of the proximity of the muscle layer on skin temperature was observed. Results of both the model and empirical dataset showed that, at rest, skin temperatures were cooler near bone than over muscle, supporting the findings of the study in Bangalore that suggests that an axisymmetric model of the leg would not capture local temperature variations. The skin temperature results of the model fell within the wide variation of results from the individual amputees. However, the model did not adjust for, or attempt to explain, the variability in empirical data.

These isolated-segment models ignore the convective heat transfer from the large blood vessels and the countercurrent heat exchange that occurs between them. They also ignore

the body's thermoregulatory responses. During physical activity, thermoregulatory responses are necessary for maintaining healthy internal temperatures. In particular, the sweating mechanism and the corresponding evaporation rate dominate the rate of heat loss from the skin during low-intensity exercise.[99] These local thermoregulatory responses are based on the whole-body temperature distributions and responses, not just the heat created by work done in the local muscle. Likewise, convective heat transfer via the blood flowing through the major blood vessels is an important heat-exchange pathway for thermoregulation during physical activity.[172] Heat is transferred to the limbs through this circulatory system and additional heat from work done in the muscles is dissipated back through the circulatory system, particularly if environmental and clothing conditions hinder the heat transfer from the skin to the environment. If these blood-flow and thermoregulatory responses were fixed rates, they could easily be accounted for in an isolated segment model. However, during exercise, and in varied environmental conditions, the influence of the blood-flow through the major vessels and the thermoregulatory responses on the heat transfer occurring on the leg varies in complex ways. The previous isolated segment models of the leg by Mitchell,[171] Peery[137] and Kalra do not address these complexities.[169] They are therefore not suitable for modelling muscle temperatures during physical activity. These models are also not set up to be modifiable for user-specific parameters.

No previous bioheat models are able to assess the temperature distributions in the leg during exercise and recovery. Therefore, a new bioheat model has been developed based on the work developed in previous bioheat models. It is the first model validated against empirical muscle temperature data collected during exercise and recovery. This empirical data was obtained from the scientific literature.

3.3. Empirical data on tissue temperatures

A human bioheat model is only useful if it accurately simulates the body's heat transfer mechanisms. Therefore, it is important to be able to validate the bioheat model using empirical data. There is no published data on the muscle temperatures of amputees during rest, exercise and post-exercise recovery. Therefore, the model developed in this research

has been designed and validated based on the available muscle temperature data, collected from non-amputee participants in moderate, hot-dry and hot-humid climates.

Currently, the main research team developing a dataset of muscle temperatures under various exercise conditions is the Human and Environmental Physiology Research Unit in Ottawa, Canada, led by Professor Glen Kenny.[77,92,96,98,120,136,173–175] Long et al.[176] and Miller et al.[104] have also measured muscle temperature during recovery after exercise, with Miller et al. comparing muscle and skin temperatures of exposed skin to skin insulated using a neoprene sleeve. Bristow et al.[177] measured muscle temperatures at various depths for a stationary person with external cooling applied. Table 3.1 provides a summary of the studies that measured leg muscle temperatures. All used healthy, able-bodied participants and all inserted thermocouples into the muscles to collect temperature. Other than Flouris 2015b,[119] who measured muscle temperatures in the calf, all measured muscle temperatures in the thigh, and other than Bristow et al.,[177] all performed an exercise trial on a cycle ergometer.

Table 3.1. Summary of studies that measured leg muscle temperatures

Author date	Aim	Muscle site	Other sites	Participants
[177] Bristow 1994	Compare shallow and deep muscle temperatures during **external cooling**.	Vastus lateralis (15/30/45 mm from skin)	Esophagus	5
[120] Flouris 2015a	Compare muscle temperatures in **moderate**, **hot-dry**, and **hot-humid** climates during exercise and recovery.	Vastus lateralis	N/A	36
[119] Flouris 2015b	Compare **skin and muscle** temperatures during exercise and recovery.	Tibialis anterior	Skin over muscle	26
[136] Kenny 2003	Compare shallow and deep muscle temperatures during exercise and recovery.	Vastus medialis (10/25/40 mm from femur)	Esophagus	7
[98] Kenny 2006	Compare muscle temperatures (shallow and deep) during **moderate and high intensity exercise** and recovery.	Vastus medialis (10/25/40/55 mm from femur)	Esophagus	7
[174] Kenny 2007	Compare shallow and deep muscle temperatures post-exercise.	Vastus medialis (10/25/40/55 mm from femur)	Mean skin, Esophagus	16
[175] Kenny 2008	Measure muscle temperature during exercise and recovery.	Vastus lateralis	Mean skin, Esophagus, Rectum	8
[173] Kenny 2009	Measure muscle temperature during **intermittent bouts of exercise**.	Vastus lateralis	Mean skin, Esophagus, Rectum	10
[176] Long 2005	Compare muscle cooling **with and without ice** after exercise.	Rectus femoris	N/A	6
[104] Miller 2005	Compare **skin and muscle** temperatures of an **exposed leg** to a leg in a **neoprene sleeve** post-exercise.	Vastus lateralis	Skin over muscle	24

The purpose of this model is to simulate heat transfer during exercise and post-exercise recovery in conditions where tissue overheating is a concern. It is being used to study how much heat is stored in the muscles, and the time taken for this heat to dissipate. Because the issue of excessive heat and sweat in a prosthetic socket is exacerbated by hot and humid climates, the effect of changing the humidity and ambient temperature is important. Therefore, the empirical dataset selected for model validation is that by Flouris et al.,[120] who recorded muscle temperatures in the vastus lateralis muscle of the thigh of 36 participants throughout rest, exercise, and post-exercise recovery in a controlled environment of moderate temperature and humidity, a hot-dry environment, and a warm-humid environment. The model has also been used to explore the effect of disrupting the heat transfer to the environment by using an insulating layer on the skin's surface, as occurs when wearing a prosthetic socket.

The effect of above-knee amputation has been explored, rather than below knee, because thigh muscle temperatures have more commonly been measured empirically, providing more data for validation. Above-knee amputation also has greater tissue loss, causing greater disruption to the normal thermoregulatory system, and is associated with greater discomfort and worse prosthetic outcomes.[41] Muscle temperature data was not able to be collected from amputees, so this research focuses on designing and validating a model for healthy participants. The model is then extrapolated to explore the possible effects of amputation and of a prosthetic socket.

3.4. Theory of heat transfer

3.4.1. The passive and active heat transfer systems

This research focuses on temperatures in the thigh. Therefore, it is useful to model the thigh as the segment of interest, and to develop the theory of heat transfer from a perspective of heat entering and leaving this segment. The heat flux of tissue in the thigh segment (q_{ti}) can be determined by modelling the heat exchange that occurs within the segment, and the heat entering and exiting the segment through heat exchange with neighbouring body segments and between the skin and the environment as follows:

$$q_{ti} = heat\ exchange\ within\ the\ segment + heat\ exchange\ with\ other\ segments + heat\ exchange\ with\ the\ environment$$

The components of heat transfer can be divided into passive heat transfer factors, and active responses of the body's thermoregulatory system. The **passive system** simulates the heat transfer within the biological tissue; through conduction, blood circulation, and metabolism (Section 3.4.2). It also models the heat lost to the surroundings; by conduction, convection, radiation, and evaporation (Section 3.4.3). When the body is outside the thermoneutral range or a temperature disturbance occurs (such as a change in physical activity or external environment), temperature sensors in the skin and in the internal tissues signal the hypothalamus, which controls the **active system**. These active functions affect the amount of heat produced by the body and the amount released to the environment, using *vasomotion*[*], shivering and sweating (Section 3.4.5). Figure 3.1 shows these two interacting systems.

[*] Changes in the diameter of the blood vessels, dilating or constricting the walls to change the blood flow.

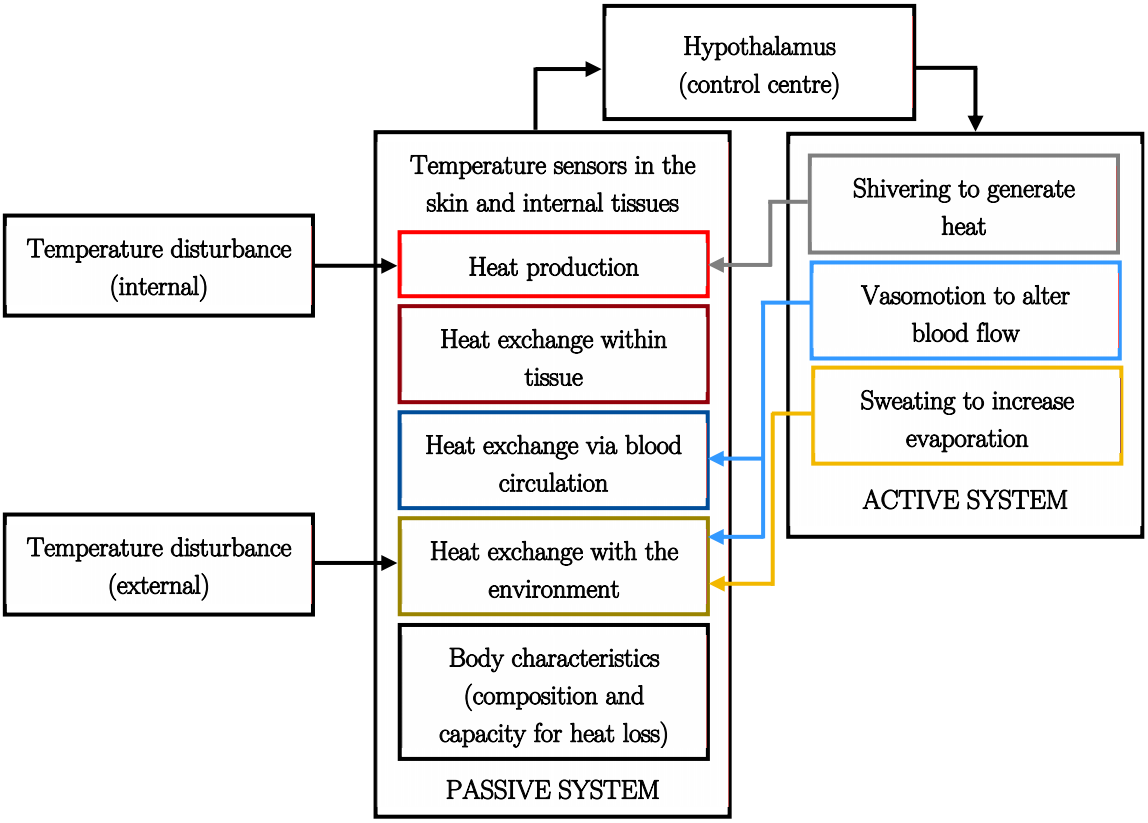


Figure 3.1. Flow chart of the thermoregulatory system

The physics of the passive heat transfer mechanisms has mostly been established and validated in literature.[155] Conversely, the body's metabolism and thermoregulation are complex and not well understood.[134] Previous bioheat models and empirical experiments came to various conclusions on which factors most impact heat transfer, particularly regarding geometry, metabolism and thermoregulation. None provide a good understanding of heat transfer in the muscles during exercise in hot conditions. The range of factors that affect heat transfer include: ambient conditions (temperature, humidity, and air-flow); body composition (volume, surface area, thigh circumference, body fat percentage, and blood circulation through the large and peripheral blood vessels); capacity for heat loss (fitness, acclimation, hydration, age, sex, chronic disease and fatigue); and thermoregulatory mechanisms (sweating, shivering, and vasomotion of the blood vessels).

The thigh tissue heat (q_{ti}) can be modelled as:

$$q_{ti} = \underbrace{\{q_{ti,cond} + q_{ti,conv} + q_{ti,m,bas} + q_{ti,m,work}\}}_{heat\ exchange\ within\ the\ segment} + \underbrace{\{q_{bl,in} - q_{bl,out}\}}_{heat\ exchange\ with\ other\ segments} + \underbrace{\{q_{sk,cond} + q_{sk,conv} + q_{sk,rad} + q_{sk,evap}\}}_{heat\ exchange\ with\ the\ environment}$$

where ti is tissue within the segment, bl is blood entering and exiting the segment, and sk is skin interacting with the environment. Heat is generated in the body through cellular metabolic reactions. The basal metabolic heat generation ($q_{m,bas}$) changes with ambient conditions. Heat is also generated through work done in the muscles ($q_{m,work}$), which increases with exercise and with shivering. The heat is transferred via conduction (q_{cond}), convection (q_{conv}), radiation (q_{rad}) and evaporation (q_{evap}).

3.4.2. Heat transfer within tissue

The heat transfer in biological tissue has been modelled based on Pennes bioheat equation (Eq. 1), the most well-known continuum bioheat model.[178] It explains one-dimensional steady-state heat transfer within a homogeneous, infinite tissue volume. It relies on the fact that heat flows from warmer regions to colder regions, and that the amount of thermal energy stored in the tissue equals the amount of thermal energy supplied to the system, minus both the amount of thermal energy lost to the surroundings and the amount of work performed by the system (based on the first law of thermodynamics).[178] Initially designed for predicting temperature in the human forearm, Pennes bioheat equation describes the energy balance of tissue metabolism and blood perfusion based on the following assumptions:[179]

- Blood reaches the capillary bed at artery temperature, equilibrium occurs at this capillary level, and the blood leaves the tissue at tissue temperature.
- The material properties of the tissue and the blood perfusion through the tissue are isotropic.

Many modifications to Pennes bioheat equation have been proposed and more complex models have been developed as knowledge of the thermoregulatory system improves. Most notably, the assumption that no heat is stored in the blood stream has been debated. However, the simple term used in Pennes bioheat equation produces a temperature prediction accuracy similar to the more detailed models,[155] so Pennes bioheat equation remains the standard for bioheat models,[179] and has been used in this research to predict heat transfer within tissue.

The rate of thermal energy accumulation of the tissue, based on the passive system, is given by:

$$\rho_{ti} \cdot C_{ti} \cdot \frac{\partial T_{ti}}{\partial t} = \nabla \cdot (-k \nabla T_{ti}) + \omega_{ti} \rho_{bl} C_{bl} (T_{bl,a} - T_{ti}) + q_{ti,m,bas} \; [W/m^3] \quad (1)$$

where ρ is density, C is specific heat capacity, T is temperature, k is thermal conductivity, ω is blood perfusion rate, and $q_{ti,m,bas}$ is the basal heat generation caused by cell metabolism.

Conduction is the thermal energy diffusion through the tissue from a warmer region to a colder region, as defined by Fourier's law:

$$q_{ti,cond} = \nabla \cdot (-k \nabla T_{ti}) \; [W/m^3] \quad (2)$$

The material property, k, represents the thermal conductivity of the tissue. This value for each tissue was obtained from the scientific literature (see Table 3.2).[155] The negative local temperature gradient, $-\nabla T_{ti}$, shows that the heat transfer is in the direction of decreasing temperature.

Convection is the rate at which the porous tissue is perfused by the thermal energy from the capillary blood, based on Fick's first principle:

$$q_{ti,conv} = \omega_{ti} \rho_{bl} C_{bl} (T_{bl,a} - T_{ti}) \; [W/m^3] \quad (3)$$

The density, ρ_{bl}, and specific heat capacity, C_{bl}, are modelled as constants of 1060 kg/m^3, and 3650 J/(kg·°C), respectively, because these values vary little in the tissue temperature ranges that occur in the body.[155] The blood temperature in the femoral artery as it enters the leg segment, $T_{bl,a}$, is 36.8°C under thermoneutral conditions,[180] but comes from the body's core, so requires adjustment based on environmental and exercise conditions (see Section 3.4.4 on how core body temperature effects the femoral artery temperature entering the thigh segment).

Blood perfusion rates through tissue, ω_{ti} $[L/s]$, can be modelled by assuming that changes in blood flow are determined by changes in metabolic activity: $\omega_{ti} = \omega_{bas,tn} + \Delta\omega_{ti}$, where $\omega_{bas,tn}$ is the basal rate of blood perfusion through the tissue under thermoneutral conditions and $\Delta\omega_{ti}$ is the change in local tissue perfusion rate from the $\omega_{bas,tn}$ value, defined as a linear relationship between the metabolic activity and blood flow:

$$\Delta\omega_{ti} = \frac{0.93}{\rho_{bl} C_{bl}} \cdot \Delta q_{ti,m,bas} \quad (4)$$

where 0.93 is an empirically derived proportionality constant,[181] and $\Delta q_{ti,m,bas}$ is the change in the body's basal metabolic rate outside thermoneutral conditions (explained in Eq. 9). This blood perfusion rate is also affected by the vasomotor responses of the active system (Section 3.4.5).

Circulation through the large blood vessels is modelled separately because the blood perfusion term in Pennes bioheat equation assumes that the local blood vessels transfer heat to the surrounding tissue so that they equilibrate, without the blood vessels storing any additional heat. Though this provides a close approximation in the small blood vessels, where their comparatively large surface area to blood flow causes conduction to dominate the heat transfer, convection dominates the heat transfer in blood vessels with >2.0 mm radius, due to the fast-flowing blood and comparatively small surface area for heat transfer.[182,183] Heat exchange between the blood vessels and the contacting tissues distributes some of the arterial heat into the surrounding tissues,[155] but much of the heat continues to circulate, and countercurrent heat exchange occurs between artery and vein pairs. Therefore, the femoral artery and femoral vein are modelled separately in the thigh.

Blood circulation through the large vessels can be modelled by balancing the mass, momentum and total energy using the equation for thermal energy conservation in a fluid, and the Navier-Stokes equations that govern the motion of fluids.

The thermal energy conservation equation in a fluid is:

$$q_p + q_{vd} + q_{bl} = \rho_{bl} C_{bl} \left(\frac{\partial T}{\partial t} + \boldsymbol{u} \cdot \nabla T_{bl} \right) + \nabla \cdot (-k \nabla T_{bl}) \tag{5}$$

where q_{bl} is any heat source other than that created by viscous dissipation (q_{vd}) and work done by pressure changes as a result of heating under adiabatic compression (q_p), ρ_{bl} is blood density, C_{bl} is the heat capacity of the blood, and $\boldsymbol{u}$ is the velocity field.

Though the flow conditions in the body are nonisothermal, and blood is a non-Newtonian fluid, the temperature range within the circulatory system is small and the blood density varies little. Therefore, the temperature variations have little impact on the flow calculations, so q_{vd} can be neglected. The blood flow velocity is also much smaller than the speed of sound, so q_p can be ignored because the pressure waves are fast enough that they effectively reduce to a mass conservation constraint.[184] Therefore, the circulatory model can be simplified to an incompressible Newtonian fluid.

The Reynolds number measures the relative importance of the inertial and viscous effects of a fluid. High Reynolds numbers mean the inertial effects dominate over viscous effects, and small perturbations affect flow momentum and trigger new flow structures, creating turbulent flows. In comparison, a low Reynolds number means the viscous effects damp out perturbations in the flow field, creating laminar flows.[184] The Reynolds number is $Re = \frac{\rho_{bl} U_{bl} d}{\mu_{bl}}$ where U_{bl} is the characteristic velocity (the average blood velocity in the blood vessel), d is the characteristic distance (the average diameter of the blood vessel), and μ is the dynamic viscosity of the blood. Because the characteristic velocities and distances are not clearly defined, the Reynolds number considered for this model is based on work by Caro et al.[185] that gives an average peak Reynolds number for the femoral artery as 1000. For flow in a pipe, the critical Reynolds number is around 2300. There is a transitional stage below this, but flows with Reynolds numbers below 2000 can be considered laminar.[186] Therefore, a laminar flow model has been used for this modelling.

The Navier-Stokes equations for incompressible flow are the conservation of momentum equation:

$$\rho_{bl}\left(\frac{\partial u}{\partial t} + \boldsymbol{u} \cdot \nabla \boldsymbol{u}\right) = -\nabla p + \nabla \cdot (\mu(\nabla \boldsymbol{u} + \nabla \boldsymbol{u}^T)) + \boldsymbol{F} \tag{6}$$

and the continuity equation which represents the conservation of mass:

$$\nabla \cdot \boldsymbol{u} = 0 \tag{7}$$

where p is the pressure, $\boldsymbol{F}$ is the volume force, and μ is the dynamic viscosity.

Countercurrent heat exchange occurs between artery and vein pairs due to their close proximity, allowing the veins to carry heat from the arteries back to the core to conserve energy and maintain the core temperature.[150,156] Bioheat models have attempted to account for countercurrent heat exchange between the large arteries and veins by adding a heat exchange coefficient to each body segment, to adjust the arterial and venous temperatures based on heat exchange in the segment proximal to it.[155,156] This heat transfer in the large blood vessels can be modelled as:

$$q_{bl,a} + q_{bl,v} = H_a\left(T_{bl,a} - T_{ti}\right) + H_v\left(T_{bl,v} - T_{ti}\right)$$

The heat exchange coefficients between the major arteries and the tissues (H_a) and the major veins and the tissues (H_v) per unit volume, are proportionality factors generated based on the assumption that the heat transfer rate between the large blood vessels and the surrounding tissue is proportional to the difference between the tissue and blood temperatures.[187] These heat exchange coefficients have been estimated in previous models, based on trial-and-error until they agreed with empirical results.[155] The location of vessels and direction of blood flow were ignored. This provided relatively good approximations of average tissue temperatures in the limbs under the limited conditions of the empirical datasets, but cannot provide temperature distributions within the thigh. Therefore, it is not a useful method for analysing the key areas of the residual limb to focus prosthetic socket design improvements on to reduce the thermal load on an amputee. This model is the first to physically mesh and model the blood flow through the major vessels in the thigh. Because the femoral artery and vein are modelled in realistically close proximity to one another, the model calculates this countercurrent heat exchange without requiring an empirically derived coefficient.

Basal metabolic heat generation, caused by cell metabolism, is the basal metabolic rate at thermoneutral ambient conditions, adjusted by the change in the body's thermal state due to the difference between ambient temperature and thermoneutral temperature:

$$q_{ti,m,bas} = q_{ti,m,bas,tn} + \Delta q_{ti,m,bas} \; [W/m^3] \tag{8}$$

This differs for each tissue type depending on the material properties. The average basal metabolic rates of individual tissue materials under thermoneutral conditions, $q_{ti,m,bas,tn}$, were obtained from literature (Table 3.2).[155] Thermoneutral conditions for an unclothed body at rest are between 27°C and 32°C.[79]

The difference between the actual basal metabolic rate and the basal rate corresponding to thermoneutral conditions, $\Delta q_{ti,m,bas}$, can be characterised by the Q10 model, which reflects how local tissue temperatures affect biochemical reactions:

$$\Delta q_{ti,m,bas} = q_{ti,m,bas,tn} \cdot [2^{\frac{T_{ti} - T_{ti,bas,tn}}{10}} - 1] \tag{9}$$

where $T_{ti} - T_{ti,bas,tn}$ is the change in local tissue temperature from the basal value under thermoneutral conditions. The Q10 model was used in previous bioheat models,[155,169] based on experimental work.[188]

Table 3.2. Material properties[155]

	Heat capacity (*Cp*) (J/(kg·K))	**Density (*ρ*) (kg/m³)**	**Thermal conductivity (*k*) (W/(m·K))**	**Basal metabolism ($q_{ti,m,bas,tn}$) (W/m³)**	**Basal blood perfusion ($\omega_{bas,tn}$) (L/s)**
Bone	1700	1357	0.75	0	0
Muscle	3768	1085	0.42	684	$0.538 \cdot 10^{-3}$
Fat	2300	850	0.16	58	$0.0036 \cdot 10^{-3}$
Skin	3680	1085	0.47	368	$1.05 \cdot 10^{-3}$
Blood	3650	1060	0.52		

Metabolic heat is also generated due to voluntary **work done** by the muscle tissue ($q_{ti,m,work}$, given in W/m³) and through **shivering** ($q_{ti,m,\mathrm{shiv}}$, in W/m³), which is part of the active thermoregulatory system.

Work performed by the body increases temperatures in the active muscles, in proportion to the workload.[155,157]

$$q_{ti,m,work} = \frac{\partial(a_{m,w} \cdot h_{work})}{\partial V_{mu}} \left[W/m^3\right] \tag{10}$$

where $a_{m,w}$ is a coefficient that distributes the overall extra metabolism due to exercise over specific areas of the body, V_{mu} is the muscle volume corresponding to the area of interest, and h_{work} is the internal workload of the body. Because the physics of metabolic heat generation is poorly understood, the heat generation rate corresponding to different exercise conditions is modelled based on experimental data collated in the Compendium of Physical Activities.[189] Approximately 60% of the heat generated by work done in the muscles is generated in the legs during standing activities. However, during cycling, the legs produce almost all the heat.[154,155] How this proportion varies with type and intensity of physical activity requires further research. For this model, the minimum $a_{m,w}$ has been set at 0.6 for the legs, when the person is resting, and the rate has been increased linearly in proportion to the exercise level, to a maximum of 90%.[190]

$$a_{m,w} = 0.6 + \frac{0.32 \cdot met_x - 0.32}{16}$$

This value is for both legs, so to get $a_{m,w,seg}$, it has been assumed that the distribution of work done by the muscles is even across the muscle mass of the legs. On average, one thigh contains 31.70% of the muscle of the legs.[191] Therefore,

$$a_{m,w,seg} = 0.317\left(0.6 + \frac{0.32 \cdot met_x - 0.32}{16}\right) \quad (11)$$

The muscle volume of the thigh can be predicted for an individual, based on input of the thigh circumference, height and body-fat percentage of the person. The internal workload of the body, h_{work}, is the energy produced by the muscle activity that does not appear as external work. Therefore, h_{work} is the difference between the present heat generation in the body and the basal metabolism.

$$h_{work} = met_x \cdot \mathrm{M}_{rest} \cdot (1 - \eta) - M_{bas}\ [W] \quad (12)$$

The resting metabolic rate is standardly given as 58.2 W/m^2, which is multiplied by the body surface area to give the rate for an individual.[189] However, this rate varies between individuals, and a study by Byrne, 2005,[192] suggests that the standard 58.2W/m^2 rate typically quoted in research overestimates resting metabolic rate by an average of 20%, so this study has therefore used Byrne's average instead. This rate is then multiplied by the current metabolic activity score corresponding to the type of activity being performed, met_x, and the basal metabolic rate, M_{bas}, is 80% of the resting metabolic rate.[189]

The fraction of the heat remaining in the body that is not converted to external mechanical power, $(1 - \eta)$, has been estimated using the protocol of Fiala et al,[155] based on a regression analysis of data from a small empirical study by Wyndham et al.[190] It showed that η rose with increase in metabolic activity, up to a maximum of approximately 20% of the metabolism being converted to external work.

$$\eta = 0.2 \cdot \tanh(0.39 \cdot met_x - 0.6).^{155} \quad (13)$$

This calculation of η is not validated outside the small empirical range tested, and should be reviewed. However, it aligns relatively well with other values found in the scientific literature,[193,194] so has been used within this model. To validate that these calculations provide a sensible output, a person of the average size given in the empirical dataset was used (1.87 m^2) with a resting metabolic rate of 48.5 W/m^2. This gave a resting metabolic rate in the muscle of the thigh of 604 W/m^3, which is similar to that provided in Fiala et al.,[155] given in Table 3.2.

The effect of shivering, $q_{ti,m,\mathrm{shiv}}$, has not been explored in this model because its onset requires simultaneous cold signals from both the skin and core,[195] which should not occur when exercising in moderate, warm-humid or hot-dry conditions. Empirical data from the

scientific literature showed no shivering response in the ambient temperature range of interest.[134]

3.4.3. Heat exchange with the environment

The **heat flux** from the skin surface to the environment (q_{sk}) consists of four parts:

$$q_{sk} = q_{sk,cond} + q_{sk,conv} + q_{sk,rad} + q_{sk,evap} \; [W/m^2]$$

When the body is in contact with an external solid object, such as clothing or a prosthesis, a small amount of heat is transferred via **conduction** ($q_{sk,cond}$), but this is not considered in the current model because it is negligible for adults,[88] and the empirical data used for comparison had most of the skin exposed.[120]

Convective ($q_{sk,conv}$) heat exchange between skin and the ambient air was modelled using natural convection:

$$q_{sk,conv} = h_{sk,conv}(T_{sk} - T_{air}) \; [W/m^2] \tag{14}$$

where $q_{sk,conv}$ is the convective heat flux, $h_{sk,conv}$ is the convective heat-transfer coefficient, T_{sk} is the skin temperature at the point being measured, and T_{air} is the ambient temperature. The convective heat-transfer coefficient for air can be modelled as:

$$h_{sk,conv} = \sqrt{a_{nat}\sqrt{T_{sk} - T_{air}}} \tag{15}$$

where a_{nat} is a weighted coefficient of the natural convection at a specific location of the body. Based on a regression analysis of empirical results by Wang et al,[196] $a_{nat} = 5.3$ for the legs. This gives a value for $h_{sk,conv}$ of approximately 4 W/(m2·K) at moderate temperatures, which aligns with other values found empricially.[197] As the ambient temperature increases, the difference between body and ambient temperature decreases. Without the effect of sweat or forced convection, the difference between ambient and skin temperature also decreases, until they are equal and $h_{sk,conv} = 0$. At ambient temperatures higher than body temperatures, the skin absorbs heat from the atmosphere via natural convection.

Forced convection due to air velocity can be added to the $h_{sk,conv}$ term for situations with mixed convection. The type and level of physical activity creates a varying relative airspeed due to body motion. However, previous models have found this variation in airspeed insignificant,[155] and the end goal of this model is to assess temperatures in a prosthetic socket, where there is no air-flow. Therefore, forced convection due to air velocity has been ignored in this model.

Radiation is the stream of electromagnetic waves emitted from a body. The radiative heat flux, $q_{sk,rad}$, is the difference between the irradiation, G, and the outgoing radiosity, J.

$$q_{sk,rad} = G - J \ [W/m^2]$$

The human body can be modelled as opaque, with no radiation transmitted through it. This means that at any point on the skin's surface, the radiosity is the sum of reflected and emitted radiation:

$$J = \Phi G + \varepsilon e_b T$$

where Φ is the skin's reflectivity, ε is the emissivity, and the Stefan-Boltzmann law, $e_b T$, models the increase in energy radiated across all wavelengths as the temperature increases. This increase in radiated energy is in proportion to the fourth power of the skin temperature in Kelvin, T, adjusted by the refractive index, n, and the Stefan-Boltzmann constant σ.

$$e_b T = n^2 \sigma((T_{sk})^4 - (T_{air})^4)$$

Radiation is emitted by the skin at temperatures within a limited range, and can be approximated to that of a diffuse grey surface, where the emissivity, ε, and absorptivity, α, of the skin are considered independent of the direction and wavelength of the radiation.[198]

$$\alpha = \varepsilon = 1 - \Phi$$

This approximation is not appropriate for skin under external radiation, such as direct solar radiation, which requires separation of the diffuse-grey surface model into two spectral bands (one for short wavelengths and one for long wavelengths), and computation of view factors to account for the variation in irradiation due to the body's geometry. Fiala et al.[155] presents a method of estimating the irradiation for the human body, to reduce the computational complexity of these calculations. However, my model is ultimately designed to investigate skin inside a prosthesis, and current prosthetic socket materials are insulators. This means little external heat travels through the socket to the skin. Also, the validation

dataset is from participants exercising within a controlled indoor environment. Therefore, these additional calculations have not been included. Here, only surface-to-ambient radiation has been modelled, ignoring the irradiation (G). The refractive index of the surface is assumed to be $n = 1$, with no shadowing effects in the view factor computation. Therefore:

$$q_{sk,rad} = \varepsilon\sigma((T_{sk})^4 - (T_{air})^4)\ [W/m^2] \quad (16)$$

where $\varepsilon = 0.98$ is the surface emissivity of the skin, $\sigma = 5.67\times10^{-8}$ W/(m^2·K^4) is the Stefan-Boltzmann constant, and T_{sk} and T_{air} are the skin and ambient temperatures in Kelvin, respectively.

Evaporative ($q_{sk,evap}$) heat loss from the skin surface is determined by the water vapour diffusion through the skin and the evaporation of sweat. As the moisture on the skin vaporises, it takes the heat with it, which cools down the skin. This heat flux depends on the amount of evaporated water and the latent heat of evaporation:[195]

$$q_{sk,evap} = h_{sk,evap} w (p_{sk,sat} - p_{air})\ [W/m^2] \quad (17)$$

where $h_{sk,evap}$ is the evaporative heat transfer coefficient, w is skin wettedness, $p_{sk,sat}$ is the vapour pressure of water at the skin surface, which is the pressure of saturated air at the skin temperature, and p_{air} is the vapour pressure of the ambient air.[195]

For an unclothed person exposed to air, $h_{sk,evap}$ is calculated using the Lewis ratio, L_{air}.

$$h_{sk,evap} = L_{air} \cdot h_{sk,conv} \quad (18)$$

where $h_{sk,conv}$ is given in Eq. 15, and $L_{air} = 16.5$ K/kPa for air. Note that evaporation only cools, so if ambient temperature is above the skin temperature, and therefore $h_{sk,conv}$ is negative, $h_{sk,evap}$ is 0.

Skin wettedness, w, is the ratio of the actual evaporative heat loss to the maximum possible evaporative heat loss with completely wet skin under the same environmental conditions.

$$w = \frac{p_{sk} - p_{air}}{p_{sk,sat} - p_{air}} \quad (19)$$

The vapour pressure of the ambient air, p_{air}, is measured using the ambient relative humidity, φ.

$$p_{air} = \varphi \cdot p_{air,sat} \quad (20)$$

The vapour pressure on the skin surface, p_{sk}, depends the latent heat of evaporation, λ_{H_2O} (which is 2256 kJ/kg), the skin moisture permeability, δ_p (which is 3 W/m^2·kPa),[155] and the rate of sweat forming, $\frac{dm_{Sw}}{A_{sk}dt}$, as elicited by the active system (explored in Section 3.4.5):

$$p_{sk} = \frac{\lambda_{H_2O}\frac{dm_{Sw}}{A_{sk}dt} + \delta_p \cdot p_{sk,sat} + p_{air}}{1 + \delta_p} \quad (21)$$

There are many published approximations for calculating the saturated water vapour pressure, p_{sat}. This model uses the Magnus form approximation to provide the coefficients, based on the Clausius-Clapeyron relation, because it is a simple approximation and one of the most accurate.[199]

$$p_{sat} = 6.1094 \cdot e^{\left(\frac{17.625 * T}{T + 243.04}\right)} \quad (22)$$

If p_{sk} is greater than $p_{sk,sat}$, then the maximum evaporation rate is reached.

Some heat is also lost from the body to the environment through evaporation from the oral, nasal, and respiratory passages via **respiration**, but this heat loss has no significant effect on leg temperatures,[155] and so has been ignored in this model.

3.4.4. Heat exchange between segments

If the heat entering and exiting the body segment of interest (the thigh) during rest, exercise and post-exercise can be mathematically derived, then a segment model can be used, rather than a whole-body model, significantly reducing the computational time for the model.

There is a small amount of heat entering and exiting the thigh segment via **conduction** between the torso, thigh and lower-leg. This rate is similar to conductive heat transfer rates within the segment itself, because the adjoining segments have similar tissue properties. Therefore, this can be modelled as symmetry at the interface between segments, to represent the segment being part of a larger structure.[200]

In contrast, the **convective** heat transfer from the major blood vessels entering and exiting the thigh segment contributes substantially to the amount of heat within the tissue. The aorta and femoral artery have large diameters, which means that their surface area to

volume ratio is small, compared to smaller blood vessels. The blood flows fast, with little heat transferred via conduction to the surrounding tissues. The temperature of the femoral artery at the entry to the thigh segment therefore maintains a similar heat to the aorta, and can be modelled based on a general estimation of the body's core temperature. Empirical results show that under resting, thermoneutral conditions, the body's core temperature[194] and femoral artery temperature[180] both average 36.8°C. This temperature requires adjustment based on anthropometrics, environmental conditions, physical activity, and clothing factors.[201]

The prediction of femoral artery temperature (T_{bl}) during rest, exercise and post-exercise recovery used in this model is based on a mathematical model developed by Givoni and Goldman.[193]

$$\text{If } t > t_{lag},\ T_{bl} = T_{bl,0} + \Delta T_{bl}\left(1 - e^{-k(t-t_{lag})}\right) \tag{23}$$

where $T_{bl,0}$ is the femoral artery temperature at the time-point where the exercise or ambient condition changes, and ΔT_{bl}, is the difference between the initial condition, $T_{bl,0}$, and the new final equilibrium temperature under the new conditions, $T_{bl,end}$.

$$\Delta T_{bl} = T_{bl,end} - T_{bl,0} \tag{24}$$

The change in temperature is amended to include the lag-time for the body to adjust between the previous condition and the current one, using k to represent a time constant in *K*/hour and t_{lag} to represent the lag-time in hours, both of which are influenced by the convective, radiative and evaporative cooling from the skin. This calculation represents the initially slow difference in rate-of-change in temperature from that prior to the change in exercise condition, followed by an acceleration in the rate-of-change, which decelerates as the temperature approaches the new equilibrium.

Femoral artery temperature at rest

This study focuses on temperature responses to different ambient conditions, but does not assess changing ambient conditions, so the adjustment for temperature change and body lag-time are not required for resting conditions. The resting femoral artery temperature, $T_{bl,rest}$, under the current ambient conditions can be determined by calculating the difference

in basal heat from thermoneutral basal heat (using Eq. 9, Section 3.4.2), minus the heat lost to the surroundings, which can be estimated based on the average heat capacity for the body, $C_{p,body} = 3768\ [J/(kg \cdot K)]$,[155] and the volume of the body, V_{body}:

$$T_{bl,rest} = T_{bl,thermoneutral} + \frac{\Delta q_{ti,m,bas} - q_{sk,conv} \cdot A_{sk} - q_{sk,rad} \cdot A_{sk} - q_{sk,evap} \cdot A_{sk}}{C_{p,body} \cdot V_{body}} \quad (25)$$

The resting femoral artery temperature varies by less than ±0.2°C in steady-state once the body has adjusted to the ambient temperature,[79] so the thermoneutral femoral artery temperature, 36.8°C, was initially assumed as the resting temperature for this model, but modelling this variation improved the fit of all model variations, so it has been included in the model.

The validation dataset by Flouris et al.[120] had an average mass of 73 kg and a body surface area of 1.87 m^2. This gives an approximate body volume of 0.0692 m^3.[202] The heat loss rates for the whole body ($q_{sk,conv}$, $q_{sk,rad}$ and $q_{sk,evap}$) have been assumed to be the same as for the thigh segment, using Eq. 14, 16 and 17 in Section 3.4.3, except that a clothing factor has been added:

$$q_{sk,conv} = \frac{h_{sk,conv}}{I_{clo}} (\bar{T}_{sk} - T_{air})\ [W/m^2]$$

$$q_{sk,rad} = \frac{\varepsilon\sigma}{I_{clo}} ((\bar{T}_{sk})^4 - (T_{air})^4)\ [W/m^2]$$

$$q_{sk,evap} = h_{sk,evap} w (p_{sk,sat} - p_{air}) \cdot \left(\frac{i_m}{I_{clo}}\right)\ [W/m^2]$$

where I_{clo} is the clothing thermal insulation, which is given in the empirical validation dataset by Flouris et al.[120] as 0.25 clo*, and i_m is the permeability index of the clothing. At a walking speed of 0.9 m/s and no wind speed, i_m was empirically found to be 0.44,[203] so this value has been used. The mean skin temperature, $\bar{T}_{sk}$, is not able to be calculated for the whole body using a segment model, but can be estimated by using the mean skin temperature of the modelled body segment, $\bar{T}_{sk,seg}$.

Femoral artery temperature during exercise

* 1 clo = 0.155 $K \cdot m^2 \cdot W^{-1}$

During low to moderate exercise, evaporative cooling is the main driver of heat loss from the skin, as long as evaporation from the skin is not hindered (such as when the skin is insulated or the relative humidity is high).[99] The initial temperature for the exercise phase of the study is the resting temperature, $T_{bl,work,0} = T_{bl,rest} =$ 36.8°C.

When exercising, higher metabolic rates have a shorter lag time for the body to adjust to a change in exercise conditions. This lag time, $t_{lag,work}$, can be modelled as:

$$t_{lag,work} = 27.84 - 0.072 \cdot met_x \cdot \mathrm{M}_{rest} + 5.93 \cdot 10^{-5} \cdot (met_x \cdot \mathrm{M}_{rest})^2 \qquad (26)$$

based on empirical data by Gonzalez et al.,[194] which gives a time of ~6-20 minutes for the body to adjust to the change in exercise condition. These time-scales fit with the times found experimentally by Givoni and Goldman.[193] During the computed lag-time as exercise is begun after resting, T_{bl} changes from the resting pattern to the exercising pattern. This model has assumed linearity in the rate of change during the lag phases to improve the accuracy over previous models that jumped directly from resting condition to exercise condition:

$$T_{bl} = \frac{dT_{bl,initial}}{dt} + \left(\frac{dT_{bl,final}}{dt} - \frac{dT_{bl,initial}}{dt}\right) \cdot \frac{t - t_{initial}}{t_{final} - t_{initial}} \qquad (27)$$

During the lag time after beginning exercise, this initial condition is the constant rest condition, $T_{bl,rest}$:

$$T_{bl,initial} = T_{bl,rest}$$

and the final condition is the rate of change in temperature after the body has adjusted to the exercise condition, $T_{bl,work}$:

$$T_{bl,work} = T_{bl,rest} + \left(T_{bl,work,end} - T_{bl,rest}\right)\left(1 - e^{-k_{work}(t - t_{lag,work})}\right) \qquad (28)$$

The time constant, k_{work}, is an empirically derived coefficient.[193] As k_{work} increases, the time to reach equilibrium decreases. Conditions that result in a core temperature change of around 0.5°C, take about 2 hours to reach equilibrium.[193] This can be modelled as:

$$k_{work} = 2 - 0.5\sqrt{T_{bl,work,end} - T_{bl,rest}} \qquad (29)$$

Note that the final temperature, $T_{bl,work,end}$, is not the temperature reached at the end of the exercise time, but the new steady-state temperature reached if maintaining the new exercise condition until the body temperature reaches its new equilibrium. This can be

modelled using the same method as Eq. 25, but including the metabolic heat load of the whole body, h_{work} (calculated using Eq. 12, Section 3.4.2):

$$T_{bl,work,end} = T_{bl,rest} + \frac{h_{work} - q_{sk,conv} \cdot A_{sk} - q_{sk,rad} \cdot A_{sk} - q_{sk,evap} \cdot A_{sk}}{C_{p,body} \cdot V_{body}} \; [K] \quad (30)$$

Femoral artery temperature during post-exercise recovery

During post-exercise recovery, ($T_{bl,rec}$), the metabolic rate returns to the resting metabolic rate. However, the recovery rate depends on the maximum temperature reached, and femoral artery temperature may continue to increase after exercise stops. Evaporative cooling is relatively unimportant in the post-exercise recovery phase, compared to convective and radiative cooling, because the sweat rate decreases during the recovery period. Even if the skin is completely wet at the end of the exercise phase, the evaporative cooling averages about 70 % of the evaporative capacity.[193]

The initial temperature for this phase of the study is the final temperature at the end of exercise, $T_{bl,a,rec,0} = T_{bl,a,work,end}$, and the final temperature at the new equilibrium is the same as the original resting temperature $T_{bl,a,rec,end} = T_{bl,a,rest}$. Therefore:

$$T_{bl,rec} = T_{bl,work,end} + \left(T_{bl,rest} - T_{bl,work,end}\right)\left[1 - e^{-k_{rec}(t - t_{lag,rec})}\right] \quad (31)$$

The time-constant of recovery, k_{rec}, and time-lag, $t_{lag,rec}$, can be modelled as functions of cooling power, P [W], based on empirical data:[193]

$$k_{rec} = 1.5(1 - e^{-1.5 \cdot P}) \quad (32)$$

$$t_{lag,rec} = 0.25e^{-0.05 \cdot P} \quad (33)$$

where:

$$P = 0.27\left(\frac{i_m}{I_{clo}}\right)(44 - p_{air}) + \left(\frac{0.174}{I_{clo}}\right)(36 - T_{air}) - 1.57 \quad (34)$$

to account for the clothing worn. For a moderate ambient condition of 24°C, this lag-time is ~13 minutes, which aligns with literature findings.[193,194] The lag-time is again modelled by simplifying it to a linear change from the rate-of-change in temperature during exercise to the rate-of-change in temperature during recovery, using Eq. 27.

3.4.5. Thermoregulatory responses

When internal or external thermal changes occur, the thermoregulatory physiological reactions of vasomotion, shivering and sweating are adjusted based on concurrently

occurring thermal stimuli from different sites of the body.[134] The evaporative heat loss is significantly affected by sweat rate, $\frac{dm_{Sw}}{A_{sk}dt}$, during exercise, and vasomotion of the peripheral blood vessels changes the blood perfusion rate through tissue, ω_{ti}. As with previous bioheat models, this model relies on empirical data to design the active system, because the complexity of the thermoregulatory system means there are not yet validated analytics to explain the physiological changes that occur.[134,150] The active system used in this model has been developed based on work by Fiala et al.,[134] which reviewed studies of human thermal responses to various boundary conditions, and recreated the conditions in a computational model of the passive heat transfer system, with the empirical responses used as input data and distributed over the muscle tissues for the shivering response (Sh), and over the skin surface for vasoconstriction (Cs), vasodilation (Dl) and sweating (Sw) responses, to obtain the distribution coefficients a_{Sh}, a_{Cs}, a_{Dl} and a_{Sw}, respectively. Vasomotion was separated into vasodilation and vasoconstriction, because these afferent signals were found to coexist under some moderate temperature conditions. Fiala found that the afferent signals could be predicted for a large range of boundary conditions, based on mean core and skin temperature changes only, rather than requiring temperatures from specific internal tissues. The regression coefficients were examined for their dependence on ΔT_{sk} and ΔT_{co} over a range of ambient and internal conditions:

$$F = b_{F,0} + b_{F,sk}\Delta T_{sk} + b_{F,co}\Delta T_{co}$$

where F is the regulatory response to be modelled (shivering, sweating, vasoconstriction or vasodilation). The intercept, $b_{F,0}$ was only required for the shivering response, where there is a shift in the threshold for shivering from the body's thermo-neutral state toward cold conditions. The behaviour of these regression coefficients could be described by a hyperbolic tangent ($tanh$) of x, with upper and lower limits linked by a transition phase.

Vasomotion of peripheral blood vessels

Peripheral vasoconstriction, Cs, and vasodilatation, Dl, of the skin blood flow are activated to regulate internal temperature, bringing more or less of the blood to the skin surface, and therefore modifying the amount of heat loss from the skin.

The approximate relationship between ΔT_{sk} and Cs is:

$$Cs = 35[tanh(0.34\Delta T_{sk} + 1.07) - 1]\Delta T_{sk} + 3.9\Delta T_{sk}\frac{d\bar{T}_{sk}}{dt} \quad (35)$$

Peripheral vasodilation, Dl, shows a non-linear relationship with both ΔT_{sk} and ΔT_{co}, but no difference with the rate of change in ambient temperature:

$$Dl = 21[tanh(0.79\Delta T_{sk} - 0.70) + 1]\Delta T_{sk} + 32[tanh(3.29\Delta T_{co} - 1.46) + 1]\Delta T_{co} \quad (36)$$

Vasodilation does not occur when the ΔT_{sk} is negative, so the lower asymptote of the function for $b_{Dl,sk}$ is zero.[134]

Cs and Dl affect the blood perfusion rate of the skin. Therefore:

$$\omega_{sk} = \omega_{sk,bas} + \frac{0.93 \cdot a_{Dl} \cdot Dl}{\rho_{bl} \cdot C_{p,bl}} \cdot q_{m,bas,tn} \cdot \left(\frac{2^{\frac{T_{sk} - T_{sk,tn}}{10}}}{1 + a_{Cs} \cdot Cs \cdot e - \eta^{Dl}} - 1 \right) \quad (37)$$

where a_{Dl} and a_{Cs} are the vasodilation and vasoconstriction distribution coefficients, respectively. For each leg, $a_{Cs} = 0.10$,[169] and $a_{Dl} = 0.115$.[134] To avoid instabilities in the prediction of body core temperature when Cs and Dl appear simultaneously, $e - \eta^{Dl}$ is included in the calculation, with $-\eta = \frac{1}{80}$.[134]

Exercise also causes an increase in blood perfusion in the active muscles.[204] Previous models have mentioned the importance of this heat transfer factor but have not included it.[169] This model uses a small percentage of total muscle blood flow, multiplied by the metabolic rate, to account for this. This factor was ignored when building, comparing and selecting the best design of bioheat model, and then determined by setting it to the value that gave the smallest root mean square error (RMSE) during exercise, compared to the empirical average of the optimisation dataset by Flouris et al.[120]

Sweating

In hot conditions, vasodilatation is accompanied by the production and evaporation of sweat. The amount of sweat produced and the evaporation rate from the skin surface depend on the internal and external temperature and pressure conditions, as explained in Eq. 17, Section 3.4.3:

$$q_{sk,evap} = h_{sk,evap} w \left(p_{sk,sat} - p_{air} \right) [W/m^2]$$

where skin wettedness, w, is influenced by the vapour pressure on the skin surface, p_{sk}, which depends on the rate of sweat forming, $\frac{dm_{Sw}}{A_{sk}dt}$. The amount of sweat formed, based on Fiala et al.'s multiple regression analysis of empirical studies, is:[134]

$$Sw = [0.8\,tanh(0.54\Delta T_{sk} - 0.19) + 1.2]\Delta T_{sk} + [5.7\,tanh(1.98\Delta T_{co} - 1.03) + 6.3]\Delta T_{co} \quad (38)$$

The maximum amount of sweat produced by the body is 23 g/min. The rate of sweat formation can be modelled as:

$$\frac{dm_{Sw}}{dt} = a_{Sw} \cdot A_{sk} \cdot Sw * 2^{\frac{T_{sk}-T_{sk,0}}{10}} \quad (39)$$

The sweat distribution coefficient for a leg, a_{Sw}, is 0.1305, according to averages used in Fiala et al.[134]

If p_{sk} is greater than $p_{sk,sat}$, then the maximum evaporation rate is reached, and the excess sweat drips from the skin. This pooling of sweat is important to consider when modelling prosthetic sockets because in most prosthetic socket designs, the moisture is unable to escape from the socket. The amount of sweat accumulated can be modelled as the amount of sweat produced minus the amount evaporated:[155]

$$\frac{dm_{Sw,acc}}{dt} = \frac{dm_{Sw}}{dt} - \frac{(P_{sk,sat}-P_{air})}{\lambda_{H_2O}} \cdot A_{sk} \quad (40)$$

4. A bioheat model to predict muscle temperatures during physical activity

4.1. Model aims and benefits

This chapter develops a bioheat model in COMSOL Multiphysics using the heat transfer modelling explained in Chapter 3. The model is designed to predict muscle temperatures in the thigh during exercise and post-exercise recovery in hot and humid environments. It is the first to focus on the muscle temperatures and to be validated against empirical muscle temperature data during exercise and post-exercise recovery in moderate, warm-humid, and hot-dry environments.

Due to the complexity of the thermoregulatory system, previous bioheat models that were designed to simulate temperatures under changing metabolic rates, modelled the whole body, using simple geometries to provide average temperatures in each limb, rather than exploring the heat distributions across the limb (see details in Section 3.2.2). This model instead, mathematically estimates the changing heat entering and leaving the body segment of interest; the thigh (see theory in Section 3.4.4). This means an isolated segment model can be used to reduce the model's computational time, increasing its usefulness in a clinical setting. Using finite element analysis (FEA) enables an approximate solution to be found for each mesh element, providing a much more detailed analysis of heat distributions than other methods of numerically solving partial differential equations (PDEs) (see theory in Section 4.2.3).

Various model designs are compared to optimise the design for modelling muscle temperatures of able-bodied individuals in hot and humid climates. This model of able-bodied individuals can provide useful information for athletes to monitor tissue health and develop training protocols and post-exercise recovery interventions. Given the focus of this research on amputee populations, this knowledge of heat transfer in non-amputee participants has been used to explore the possible effects of amputation and of a prosthetic socket on muscle heat during and post-exercise.

4.2. Model development strategy

4.2.1. Overview of the model design process

The bioheat model, developed in COMSOL Multiphysics, is based on: analytics of the passive heat-transfer in the body; previously validated bioheat models for rest, exercise and post-exercise recovery conditions; and regression analysis of empirical datasets. A simple geometry simplifies the process of understanding which physics accounts for the largest variability in temperature outputs. Therefore, the model has been initially developed as concentric cylinders that represent bone, muscle, fat and skin in the thigh.

The model was developed to include metabolism changes due to exercise (Section 3.4.2), the heat transfer that occurs within the thigh (Section 3.4.2), the heat transfer between the thigh and the environment (Section 3.4.3), and the heat transfer between the thigh and the rest of the body (Section 3.4.4). This model was tested after the addition of each heat-transfer factor, to make sure the output changed as expected, and was compared to empirical data of people during rest, exercise and post-exercise recovery under moderate, warm-humid and hot-dry environments (Section 4.3.4).[120]

The physics of the body's active thermoregulatory processes remains poorly understood, so much of the work in this model is based on regression analysis from empirical datasets, which are not necessarily valid outside the empirical conditions tested (see theory in 3.4.5). Therefore, to increase the model's temperature prediction accuracy in hot and humid environments, the model was optimised by testing different variations of the model, with various heat transfer factors that rely on empirical data included or excluded (Sections 4.3.6 - 4.3.8). These model variations included modelling the large blood vessels separately to account for the convective and countercurrent heat exchange, modelling the vasoconstriction and vasodilation of the blood vessels, and modelling the sweat production, which affects the evaporation rate from the skin's surface.

Each combination of factors was tested for all 3 exercise conditions (moderate, warm-humid and hot-dry), using the average data from all participants in Flouris et al.,[120] to determine the best overall combination of heat transfer factors for the model. These different

model variations were compared on the amount of error in predicting the empirical temperatures. The error was based on the difference in maximum temperature reached during exercise, and the root mean square error (RMSE) during exercise and in the first 30 minutes post-exercise (Section 4.3.8). Once the best model had been selected, the effect of individual body factors, such as size and body fat percentage, on the muscle temperatures were explored.

4.2.2. Choice of software: COMSOL Multiphysics

COMSOL Multiphysics version 5.4 software was used to develop the model because it has well-established and validated thermodynamics and bioheat transfer capabilities, as well as capabilities in fluid flow, structural mechanics, and many other areas that makes it easy to add various physics modules and couple them into a single simulation. COMSOL was also the software used by the most advanced previous thermal leg model.[169] This integrated work environment allows blood flow and sweating to be included in the heat transfer considerations, and supports the future addition of dynamic loading conditions to assess pressure and friction and their influence on heating. The university has software licences for COMSOL, including the Heat Transfer Module, and COMSOL provides the option of developing easy-to-use applications based on the simulations. Once the simulations have been developed into an app, they can be run on computers without COMSOL Multiphysics installed. The developer can control which parameters the end-user can manipulate and ensure the app provides simple visual outputs and graphs, so a non-specialised consumer can benefit from software developed on it. This could be beneficial for training clinicians to use the simulations in the prosthesis fitting process.

4.2.3. Finite element analysis

A variety of approaches, including finite-element, finite-difference, and finite-volume methods, can be used to numerically solve partial differential equations (PDEs) to determine the tissue temperatures in bioheat models influenced by the active and passive body systems. Finite element analysis (FEA) has been chosen for this research, despite being computationally heavier, because it is more suitable for multi-physics problems. It allows coupling of different kinds of functions that approximate the solution within each element, such as coupling heat transfer and fluid flow. It also allows adaptive mesh refinement around areas of interest, making it better for complex and changing geometries such as the human

body. (A finite-difference method is more appropriate for block-shaped models, and a finite-volume method for fluid-flow-only problems.)

FEA divides a 3D computer-aided design (CAD) model into small elements of geometrically simple shapes represented by a set of simple functions, such as linear or quadratic polynomials with a finite number of degrees of freedom (DOFs). These simple functions locally approximate the original complex PDEs that describe the physics of interest. A large sparse matrix equation system is generated from the combined element equations. The system of algebraic equations provides an approximation of the solution to the PDE, with a denser mesh providing a closer approximation to the actual solution but also increasing computational complexity.

For this model, tetrahedral mesh elements were used for the *Bioheat Transfer* physics because they can be used to mesh any 3D volume, regardless of geometry, and they are the only kind of element that can be used with COMSOL's **Adaptive Mesh Refinement** function. To refine the mesh, mesh convergence is used to compare the solutions obtained from different meshes, taking a fine mesh as an approximation to the actual solution and evaluating the error on coarser meshes:

$$er = u_{h1} - u_h$$

where er is the amount of error, and u is the numerical equation with an element size of h or $h1$. This determines how coarse to make the general mesh to get an accurate enough answer without increasing the computational time by too much, as recommended by COMSOL software.[205] Once the general mesh size has been selected and a solution computed for u_h, mesh adaption is then also used to improve the meshing. It plots the error estimates for u_h across the object, then generates a refined mesh, with the mesh elements correlating to the size of the error, so smaller mesh elements are built where the initial error is larger. Because this model solves a convective time-dependent problem, using multiple steps to assess the human body under thermoneutral and steady-state conditions before running the main time-dependent study, this mesh refinement is performed as part of the first step, rather than requiring an additional solution.

The tetrahedral elements were meshed using quadratic Lagrange discretisation (Figure 4.1), which uses second-order Poisson-type PDEs to describe heat transfer in the biomaterials, in the form:

$$f = \nabla \cdot (-D\nabla u)$$

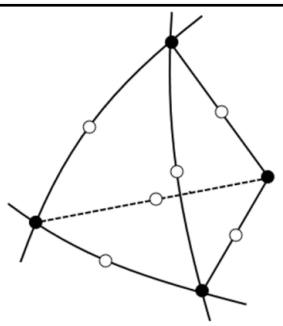


Figure 4.1. A second-order tetrahedral mesh element

Unlike the second-order Poisson-type PDEs used to describe heat transfer in the tissue layers, transport-type PDEs are used to describe the heat transfer in the blood stream. The governing equations are similar to Poisson's equation, but with a velocity vector, $\boldsymbol{v}$, that results in a governing equation that is closer to a first-order PDE:

$$f = \nabla \cdot (-D\nabla u + \boldsymbol{v}u)$$

where *D* is the diffusion coefficient and *u* is the unknown function. This means that fluid flow in the circulatory system is modelled with the velocity and pressure both resolved using first-order polynomial elements (P1 elements). This P1+P1 discretisation uses linear functions to reduce the number of degrees of freedom to solve, which requires substantially less computation and is accurate enough for this model because COMSOL uses in-built streamline and crosswind diffusion stabilisation methods,[206] and the problem has a high enough Reynolds number (see explanation in Section 3.4.2).

4.3. Building the model

4.3.1. Overview of COMSOL Multiphysics workflow

The model has been developed using the standard COMSOL Multiphysics workflow (Figure 4.2). All parameters and variables were set in *Global Definitions*. *Functions, component couplings* and *geometry selections* were defined under the component's *Definitions* so they could be called from elsewhere in the model.

The initial simple model was built using the inbuilt COMSOL Multiphysics geometry functions. However, Section 4.6 explores realistic geometries, importing .stl files that were developed based on MRI data. The material properties for bone, muscle, fat, skin and blood were based on averages from the scientific literature.

The heat transfer physics was modelled using the *Bioheat Transfer* node, with the flow in the major blood vessels modelled using the *Laminar Flow* node. The two physics nodes were linked as *Nonisothermal Flow* in the *Multiphysics* node, so that the temperature from the *Bioheat Transfer* could be used as an input for the *Laminar Flow* and the pressure and velocity from the *Laminar Flow* influenced the convective heat transfer in the *Bioheat Transfer*.

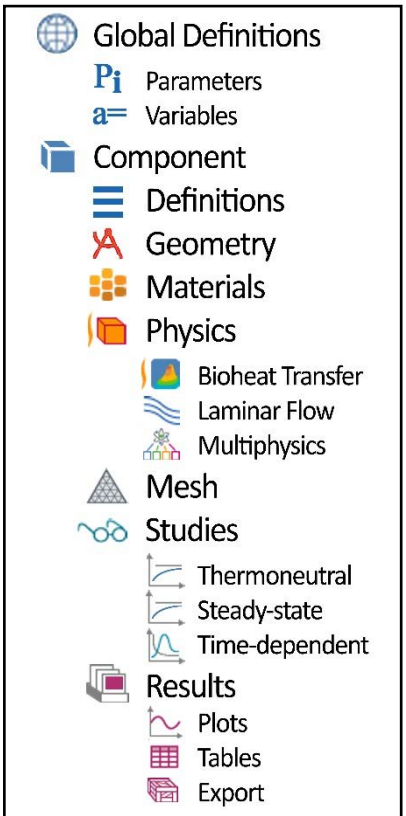


Figure 4.2. COMSOL workflow

Sensitivity analysis and adaptive mesh refinement tools were used to determine the appropriate mesh element sizes. A stepwise design process was used to add each heat-transfer factor to the model individually and observe the change in output, to make sure the factors behaved as expected. The final simulation was set up to run a stationary study to collect basal tissue temperatures, then to run the main studies, which included a stationary step to determine the initial steady-state tissue temperatures, and a time-dependent step for each ambient condition.

Cut-points were used to collect the muscle temperatures at comparable locations to those collected empirically, and at points that enabled heat variations across the limb to be observed. *Point-graphs* of the cut-points throughout the time-dependent trials were compared to the temperature data from empirical trials. Averages over tissue domains and time-periods were calculated in COMSOL, along with integrations to determine the root-mean square error, mean difference, and difference in gradients between modelled graphs and the empirical datasets. All results were exported for post-processing.

4.3.2. Geometry and materials for the cylindrical model

The model is designed to simulate heat transfer in the muscles during physical activity and post-exercise recovery in hot and humid climates, so it has been set up to match the conditions of the empirical study by Flouris et al,[120] who recorded muscle temperatures in the vastus lateralis muscle of 36 participants during exercise and post-exercise recovery in various controlled environments.

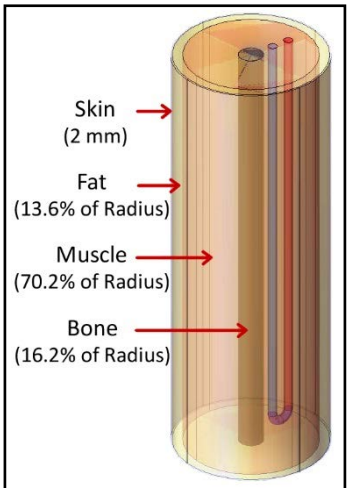


Figure 4.3 Cylindrical model geometry

The results from Bangalore (Chapter 2.3) and in literature[169] suggest that geometry is an important factor affecting heat transfer and causing differences between individuals, but the effect of geometry on heat transfer is poorly understood. Running a geometrically accurate model is time-consuming, computationally costly, and makes understanding which aspects of the geometry most affect heat-transfer, such as the skin surface area, muscle mass or thickness of the fat layer, challenging.

A simple model of concentric cylinders was built to simplify the process of understanding which physics accounts for the largest variability in temperature outputs. These cylinders represent bone, muscle, fat and skin (Figure 4.3). The tissue layer thicknesses were selected to have the same volumetric compositions as an established simple model.[169]

The thigh circumferences were not provided by Flouris et al.[120] Instead, for this bioheat model, they were calculated based on work by Vaughan et al.[207] to predict body circumferences.

$$thigh\ circ. = 36.26 - 0.08985 \cdot age + 1.998 \cdot sex + 0.4007 \cdot weight - 0.08038 \cdot height \quad (41)$$

Note that sex is set as a binary number (m=0/f=1). This gave an average thigh circumference for Flouris' data of 522 mm, and therefore a radius of 83.1 mm. The leg segment length of 461 mm was set based on Kalra's model, but because this segment model represents the upper leg, a section of the larger body system, *symmetry* was added to both ends, following Kalra's protocol.[200] This rendered the thigh length inconsequential.

The femoral artery and vein were modelled separately, as cylinders with a radius of 0.5 mm, based on empirical averages.[208] The distance from the bone to the vein and artery was based on Kalra's cross-sectional CT data of the thigh.[169] The artery enters the leg-segment from the top, and runs vertically down the medial side. The vein runs parallel with the artery, closer to the femur, with the outlet of the vein at the top of the segment beside the artery inlet (Figure 4.3).

The material properties were set to match those in Kalra et al.[169] (Table 3.2, p. 59). The blood vessels were modelled with boundary layers to assist the blood flow, and the *fine* element size restrictions built into COMSOL, using first-order transport-type PDEs, as explained in 4.2.3. The skin layer was modelled with an *extra-fine* mesh because of its thinness. A sensitivity analysis, performed relative to a 2 mm mesh, found that the remaining mesh was relatively insensitive to changes in element size below 10 mm, so the tetrahedral mesh element sizes were physics controlled using a *fine* element size with refinement around the high-detail areas of the model. Figure 4.4 shows a cross-section of the mesh to demonstrate the variation in mesh element sizes.

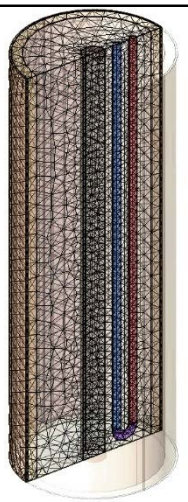


Figure 4.4 Mesh cross-section

4.3.3. Global parameters and variables

To make sure each heat transfer factor was programmed correctly and gave a sensible output, *cut-points* were placed in the centre of each tissue thickness (Figure 4.5) and the model run after each factor was added. Section 4.3.4 shows the changing output with different passive heat transfer factors added to the model. Because previous bioheat models did not model the blood flow in the major vessels, and these calculations complicate the heat transfer response, the initial model used 2D-axial

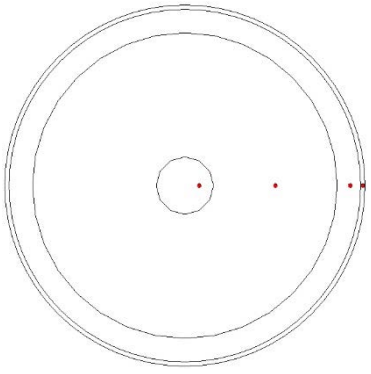


Figure 4.5. Cross-section of model with cut-points

symmetry. The effect of modelling of the major blood vessels separately is explored in section 4.3.7.

This section lists the parameters and variables used in the final model, with the studies set up to match the settings of Flouris et al.'s empirical trial.[120] This includes 3 separate time-dependent studies, with one for each of the ambient conditions tested in the research by Flouris et al.[120]

The ambient conditions, model size and tissue properties that were fixed parameters through all studies were set as *global parameters* (Table 4.1).

Table 4.1. Global parameters

Name	Expression	Unit	Description	Theory
t	0	min	Time set to 0 for stationary studies	
Amb_pres	1	atm	Ambient pressure	3.4.3
Radius	83.1	mm	Radius of thigh	3.4.2
Height	461	mm	Length of femur	3.4.2
V_body	0.0692	m^3	Whole body volume	3.4.4
A_body_sk	1.87	m^2	Whole body skin surface area	3.4.4
M_rest	48.5	W/m^2	Resting metabolic heat generation rate	3.4.2
M_body_rest	A_body_sk*M_rest	W	Resting metabolism	3.4.2
c_bl	3650	J/(kg·K)	Specific heat of blood	3.4.2
rho_bl	1060	kg/m^3	Density of blood	3.4.2
sk_perm	3	$W/(m^2 \cdot kPa)$	Skin moisture permeability	3.4.3
lat_H2O	2256	kJ/kg	Latent heat of evaporation	3.4.3
T_bl_rest	36.8	˚C	Resting arterial blood temperature	3.4.4
I_clo	0.25	clo	Clothing thermal insulation (1 clo = 0.155 $K \cdot m^2 \cdot W^{-1}$)	3.4.4
i_m	0.44	-	Permeability index of the clothing	3.4.4
L_air	16.5	K/kPa	Lewis ratio	3.4.3

Global variables were divided into separate nodes for; variables used in *all studies*, variables used in the *thermoneutral study* to collect the basal tissue temperatures, variables used in the *stationary steps* of the main studies to collect steady-state temperatures, variables used in the *time-dependent steps*, and variables specific to *each study* (Table 4.2). The correct *Global Variables* nodes for each study were selected using the *Physics and Variables Selection* option within the study settings.

Table 4.2. Global variables

Name	Expression	Unit	Description	Theory
All studies				
V_mu	comp1.vol_mu(1*1*1)	m^3	Segment muscle volume	3.4.2
A_sk	comp1.A_sk(1*1)	m^2	Segment skin surface area	3.4.3
qm_bas_dif	2^(T_delta/10)	W/m^3	Difference between basal and thermoneutral metabolism	3.4.2
qm_work_body	(qm_work_x*M_body_rest*(1-eta_met)-0.8*M_body_rest)	W	Heat generated through work done by the muscles	3.4.2
eta_met	0.2*tanh(0.39*qm_work_x-0.6)	-	Fraction of energy converted to power	3.4.2
M_seg	0.317*(0.6+(0.32*qm_work_x-0.32)/16) *qm_work_body	W	Heat generated through work done by the muscles in the segment	3.4.2
qm_work_seg	M_seg/V_mu	W/m^3	Heat rate generated by the muscles in the segment	3.4.2
h_sk_conv	sqrt(5.3*sqrt(abs(comp1.T-Amb_temp)))	$W/(m^2 \cdot K)$	Convective heat transfer coefficient at the skin	3.4.3
q_conv	h_sk_conv*(comp1.T-Amb_temp)	W/m^2	Heat loss through convection	3.4.3
q_rad	(0.98*5.67*10^-8*(T_sk^4-Amb_temp^4))[W/m^2/K^4]	W/m^2	Heat loss through radiation	3.4.3
h_evap	(comp1.T>Amb_temp)*(L_air*h_sk_conv) + (comp1.T<=Amb_temp)*0	m/s	Evaporative heat transfer coefficient at the skin	3.4.3
q_evap	h_evap*wet_sk*(p_sk_sat-p_air)	W/m^2	Heat loss through evaporation	3.4.3
wet_sk	(p_sk<=p_sk_sat)*(p_sk-p_air)/(p_sk_sat-p_air)+(p_sk>p_sk_sat)*1	-	Skin wettedness ratio	3.4.3
p_sk_sat	100*exp(18.956-(4030/(comp1.T+235-273)))/1000	Pa	Vapour pressure of saturated skin	3.4.3
p_air_sat	100*exp(18.956-(4030/ (Amb_temp +235-273)))/1000	Pa	Vapour pressure or saturated air	3.4.3
p_air	Rel_humid*p_air_sat	Pa	Air pressure	3.4.3
w_mu	(0.538*10^-3)+(0.93/(rho_bl*c_bl)*684 *qm_bas_dif)	1/s	Blood perfusion rate in muscle	3.4.2
w_fa	(0.0036*10^-3)+(0.93/(rho_bl*c_bl) *58*qm_bas_dif)	1/s	Blood perfusion rate in fat	3.4.2
w_sk	(t==0)*(1.05*10^-3)+(0.93/(rho_bl*c_bl)*368 *qm_bas_dif)+(t>0)*(1.05*10^-3)+(0.93*0.115 *Dl_sk/(rho_bl*c_bl)*368*(qm_bas_dif/(1+0.1 *Cs_sk*exp(-1/80)^Dl_sk)-1))	1/s	Blood perfusion rate in skin	3.4.5
T_sk	comp1.aveop_sk(T)	˚C	Mean skin temperature for segment	3.4.4
Thermoneutral				
Amb_ temp	30	˚C	Ambient temperature	3.4.3
Rel_humid	0.6	-	Relative humidity	3.4.3
T_bl	36.8	˚C	Femoral artery temperature	3.4.4
qm_work_x	comp1.qm_work_1(t)		Metabolic activity score	3.4.2
T_delta	0	˚C	Difference between current temperature and thermoneutral temperature	3.4.2
p_sk	(sk_perm*p_sk_sat+p_air)/(1+sk_perm)	Pa	Vapour pressure on the skin surface	3.4.3
Stationary				
T_t_neutral	withsol('sol1',comp1.T)	K	Temperature from thermoneutral study	3.4.2
T_delta	comp1.T-T_t_neutral	K	Difference between current temperature and thermoneutral temperature	3.4.2
p_sk	(sk_perm*p_sk_sat+p_air)/(1+sk_perm)	Pa	Vapour pressure on the skin surface	3.4.3
T_bl	T_bl_rest	˚C	Femoral artery temperature	3.4.4
Time-dependent				
T_t_neutral	withsol('sol1',comp1.T)	K	Temperature from thermoneutral study	3.4.2
T_delta	comp1.T-T_t_neutral	K	Difference between current temperature and thermoneutral temperature	3.4.2
p_sk	((t>0)*(lat_H2O*dmSw_dt/(A_sk*(t+1))) +sk_perm*p_sk_sat +p_air)/(1+sk_perm)	Pa	Vapour pressure on the skin surface	3.4.3
dmSw_dt	0.1170*Sw*2^((comp1.T-T_t0)/10)*A_body_sk	g/(min·K)	Rate of sweat formation	3.4.5

Sw	(0.8*tanh(0.59*(comp1.T-T_t0)-0.19)+1.2)*(comp1.T-T_t0) +(5.7*tanh(1.98*(T_bl_lag_rec_start-T_bl_rest)-1.03)+6.3)*(T_bl_lag_rec_start-T_bl_rest)	g/min	Amount of sweat formed across the whole body	3.4.5
T_bl	during_work_lag + during_work + during_rec_lag + during_rec	K	Femoral artery temperature	3.4.4
during_work_lag	(t<=t_lag_work)*(T_bl_rest + (T_bl_work-T_bl_rest)*(1-exp(-t)))	K	Femoral artery temperature during lag after beginning exercise	3.4.4
during_work	((t>t_lag_work)&&(t<=t_end)) *(during_work_lag +(T_bl_work_end -T_bl_rest)*(1-exp(-k_work*(t-t_lag_work)))	K	Femoral artery temperature during lag exercise	3.4.4
T_bl_work_end	T_bl_rest + (qm_work_body - q_conv*A_body_sk - q_rad*A_body_sk -q_evap*A_body_sk)/(3768*V_body)	K	Temperature at new steady-state	3.4.4
T_bl_rec_start	T_bl_rest + ((qm_work_x(t_exercise) *M_body_rest*(1-eta_met)-0.8*M_body_rest) -q_conv*A_body_sk - q_rad*A_body_sk -q_evap*A_body_sk)/(3768*V_body)	K	Fixed temperature at new steady-state	3.4.4
during_rec_lag	((t>t_end)&&(t<=t_lag_rec)) *(T_bl_rec + (T_bl_lag_rec_start - T_bl_rec) *((t_lag_rec-t)/(t_lag_rec-t_end)))	K	Femoral artery temperature during lag after finishing exercise	3.4.4
during_rec	(t>t_lag_rec)*(T_bl_rest+(T_bl_lag_rec_start - T_bl_rest)*exp(-k_rec*((t-t_end)/(t_lag_rec-t_end))))	K	Femoral artery temperature during recovery	3.4.4
t_lag_work	27.84 - 0.072* qm_work_x*M_rest + 5.93 *10^-5*qm_work_x*M_rest)^2	min	Time between change in met_rate and body response when exercising	3.4.4
t_lag_rec	t_end+15*exp(-0.5*P)	min	Time between change in met_rate and body response after exercising	3.4.4
T_bl_work	T_bl_rest+(T_bl_work_end-T_bl_rest)*(1-exp(-k_work*(t-t_lag_work)))	K	Femoral artery temperature during exercise	3.4.4
k_work	2 - 0.5*sqrt(abs(T_bl_work_end-T_bl_rest))	-	Time constant for delay when exercising	3.4.4
k_rec	1.5*(1-exp(-1.5*P))		time constant for delay after exercising	3.4.4
P	(0.27*(0.73)*(44 - p_air) + (0.174/0.96)*(36 -Amb_temp) - 1.57)/60	min	Cooling power	3.4.4
Dl_sk	(21*tanh(0.79*((comp1.T-T_t0)-0.7)+1) *(comp1.T-T_t0)+32*tanh(3.29* ((comp1.aveop_bl(T)-T_c0)-1.46)+1) *(comp1.aveop_bl(T)-T_c0))	W/K	Dilation of blood vessels to increase skin blood flow	3.4.3
Cs_sk	35*tanh(0.34*((comp1.T-T_t0)+1.07)-1) *(comp1.T-T_t0) 3.9*(comp1.T-T_t0)	W/K	Constriction of blood vessels to decrease skin blood flow	3.4.3
Moderate environment				
Amb_temp	24	˚C	Ambient temperature	3.4.3
Rel_humid	0.56	-	Relative humidity	3.4.3
qm_work_x	comp1.qm_work_1(t)	-	Metabolic activity score	3.4.2
T_t0	withsol('sol2',comp1.T)	K	Steady-state temperature	
T_c0	withsol('sol2',comp1.aveop_bl(T))	K	Core temperature at time 0	
t_end	90	min	Time when exercise ends	
Warm-humid environment				
Amb_temp	30	˚C	Ambient temperature	3.4.3
Rel_humid	0.6	-	Relative humidity	3.4.3
qm_work_x	comp1.qm_work_1(t)	-	Metabolic activity score	3.4.2
T_t0	withsol('sol5',comp1.T)	K	Steady-state temperature	
T_c0	withsol('sol5',comp1.aveop_bl(T))	K	Core temperature at time 0	
t_end	90	min	Time when exercise ends	
Hot-dry environment				
Amb_temp	40	˚C	Ambient temperature	3.4.3
Rel_humid	0.24	-	Relative humidity	3.4.3
qm_work_x	comp1.qm_work_2(t)	-	Metabolic activity score	3.4.2
T_t0	withsol('sol7',comp1.T)	K	Steady-state temperature	
T_c0	withsol('sol7',comp1.aveop_bl(T))	K	Core temperature at time 0	
t_end	60	min	Time when exercise ends	

The model was robust to differences in specified thermoneutral ambient temperature within the thermoneutral range of 27°C - 32°C,[79] so 30°C has been used throughout this research as the thermoneutral ambient temperature, as in Fiala et al.[155] One of the empirical datasets by Flouris et al.[120] was also run at 30°C, which makes the temperature a convenient choice for validation purposes.

4.3.4. Study set-up for passive heat transfer

An *Empty Study* was added to chain all the studies in order, running the *thermoneutral study* first, followed by each of the main studies *(moderate, warm-humid and hot-dry ambient conditions)*, which each included a stationary step and a time-dependent step. This reduced the runtime and increased the ease of comparisons between the outputs.

The stationary step of each study used input temperatures from the solution of the thermoneutral study. Likewise, the time-dependent studies were run with the steady-state temperatures from the stationary step as the initial tissue temperatures. While building and testing the model, intermediate time-stepping was used, with a maximum of 1-minute time-steps when large changes were expected in the output gradient due to a change in exercise level, and 10-minute maximum time-steps as the graph output stabilised, to speed up the model run-time. However, for ease of comparison when comparing the model variations to one-another, temperatures were stored every minute throughout the trials.

Bioheat Transfer physics was used to model the heat transfer in biological tissue, based on Pennes bioheat equation (Eq. 1, Section 3.4.2).[178] All domains were set as *Biological Tissue*, with separate *Bioheat* settings set up for each tissue type.

Conduction was calculated according to (Eq. 2, Section 3.4.2) with the thermal conductivity, k, set for each tissue according to the material properties in Table 3.2, p. 59. To test that the passive, conductive heat transfer between the tissues correctly diffused heat from a warmer region to a colder region until reaching equilibrium, the initial temperatures of the tissues were set to their thermoneutral resting temperatures, and arterial blood temperature was set to a fixed rate of 36.8°C. With no internal heating or heat loss from the

segment, the steady-state temperature of all tissues equilibrated to 36.8°C, as expected (Figure 4.6.A).

Basal metabolic heat generation was calculated according to Eq. 8, Section 3.4.2. The thermoneutral basal metabolic heat rates of each tissue type $q_{ti,m,bas,tn}$ were added to the appropriate tissue domains, according to the rates given in the scientific literature, presented in Table 3.2, p 59. The change in the body's basal metabolic rate due to ambient conditions, $\Delta q_{ti,m,bas}$, was set as a *global variable***.** The expression, $\Delta q_{ti,m,bas}$, in the main study, called the *global variable* $T_{ti,0} = withsol('sol1', T)$, to obtain the thermoneutral tissue temperatures stored in *Solution 1* $(sol1)$ at the completion of the thermoneutral stationary study. Figure 4.6.B. shows the increase in heat over time when no heat loss occurs. The energy generated by the basal metabolism in each tissue type, input into the model, is:

$$Input\ energy\ [J] = \left(q_{ti,m,bas,tn} + \Delta q_{ti,m,bas}\right) * Area * Time$$

If each tissue were in isolation, this would create temperature changes in the bone, muscle, fat and skin of 0°C, 8.55°C, 0.40°C and 0.32°C, respectively, over a 100-minute trial, with the muscle being the primary tissue to heat. However, because conductive heat transfer spreads the heat between tissues, the actual tissue changes were 1.77°C, 1.86°C, 1.53°C and 1.49°C, respectively. The muscle heated only slightly more than the surrounding tissues.

Boundary conditions were set to model the heat loss to the surroundings via **convection**, **radiation** and **evaporation**. **Conductive** heat exchange with the environment was ignored because it is negligible (see theory in Section 3.4.3). Convection, $q_{sk,conv}$, was added to the skin boundary as a *Heat Flux* → **Convective Heat Flux**, calculated using Eq. 14, Section 3.4.3, with the **Heat Transfer Coefficient,** $h_{sk,conv}$, set as a *global variable*, based on Eq. 15, Section 3.4.3. The radiative heat exchange, $q_{sk,rad}$, was also added to the skin boundary as a *Heat Flux*, but using the specific *Surface-to-Ambient Radiation* function, based on Eq. 16, Section 3.4.3.

Evaporative heat exchange, $q_{sk,evap}$, was added to the skin boundary as a *Heat Flux* → **General Inward Heat Flux**, calculated using Eq. 17, Section 3.4.3. The **Heat Transfer Coefficient,** $h_{sk,evap}$, was set as a *global variable*, based on the skin wettedness, **wet_sk**,

(Eq. 19, Section 3.4.3), which is affected by the ambient relative humidity, **Rel_humid**, the ratio of actual evaporative heat loss to the maximum evaporative heat loss, calculated using *global variables* **p_sk**, **p_sk_sat** and **p_air_sat**, as explained in Section 3.4.3, and the rate of sweat forming, $\frac{dm_{Sw}}{A_{Sk}dt}$, as given in Eq. 39, Section 3.4.5.

Figure 4.6 Parts C, D, E and F show the change in tissue temperature if the ambient temperature is dropped at time 0 from the thermoneutral temperature of 30°C to 20°C, with the ambient humidity set to 50% throughout. Figure 4.6.C has only convective heat exchange from the skin surface, Figure 4.6.D has only radiative heat exchange with the environment, Figure 4.6.E has only evaporative heat exchange from the skin surface, and Figure 4.6.F includes convective, evaporative and radiative heat loss.

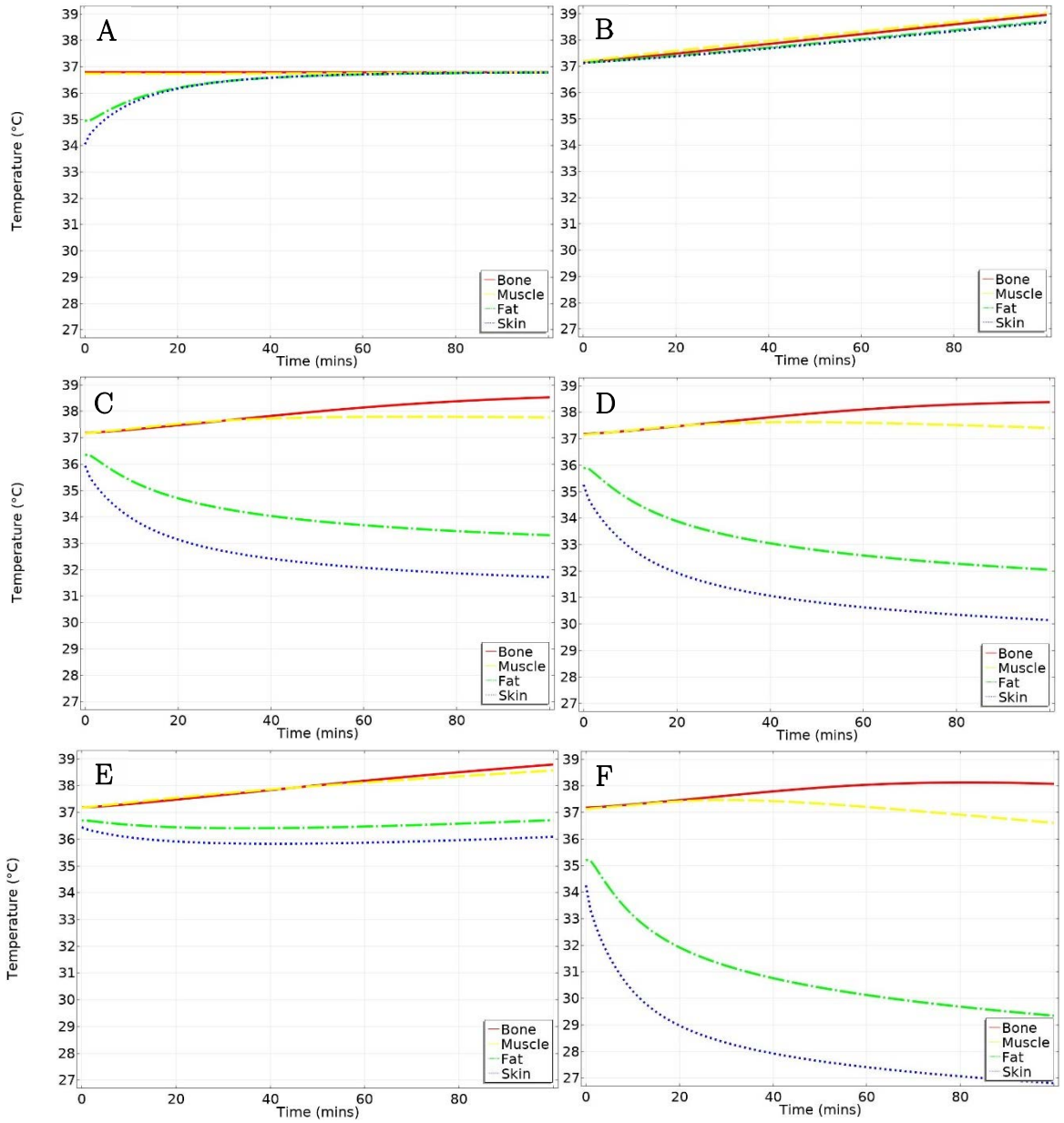


Figure 4.6. Model with and without heat loss from the skin at 20°C and 50% humidity

***A.** Insulated with 38.6°C blood and no metabolic heating; **B.** Insulated with basal metabolic heating; **C.** Basal metabolic heating with convective heat transfer from skin; **D.** Basal metabolic heating with radiative heat transfer from skin; E. Basal metabolic heating with evaporative heat transfer from skin; F. Basal metabolic heating with convective, radiative and evaporative heat transfer from skin*

Note that the evaporative cooling rate is small in comparison to the radiative and convective cooling rates under this rest condition, which matches previously demonstrated physiological responses.[193] Adding all the types of heat loss from the skin together results in a net heat loss (Figure 4.6.F). This is to be expected because the model does not include the active thermoregulatory processes to maintain steady internal temperatures with the drop in ambient conditions. There is also a larger difference between the temperatures of the bone

and skin than is seen empirically. This is because the convective heat transfer through the blood vessels is not yet considered.

The **convective** heat transfer of circulating blood, that contributes to the heat travelling through the segment, was calculated using Eq. 3, Section 3.4.2, with the blood density, ρ_{bl}, specific heat of blood, C_{bl}, and blood perfusion rates through tissue, ω_{ti} set as *global parameters*. These properties of blood and of each tissue type were set to match those given in Table 3.2, p. 59, with the environmental adjustments to the blood perfusion rates for each tissue calculated according to Eq. 4, Section 3.4.2.

After adding all the passive heat-transfer factors to the bioheat model, a *cut-point* was created at the location matching that of the thermocouple probe that was used to collect the empirical data by Flouris et al.[120] This was located in the muscle tissue at 22 mm depth below the skin surface. The model was run with the same three ambient conditions as tested empirically (24°C with 56% relative humidity, 30°C with 60% humidity, and 40°C with 24% humidity), running the model until the tissues reached steady-state. Figure 4.7 compares the steady-state temperatures from the *cut-point* of the model (offset on the x-axis for ease of comparison) to the resting temperatures from the empirical data. It shows good correlation between the model and the empirical data for all 3 empirical conditions, giving an error within 2 times the recording thermocouple's accuracy.

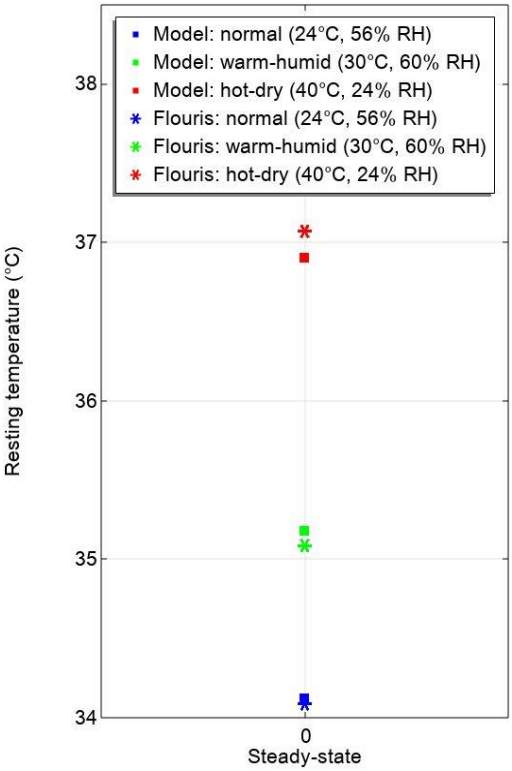


Figure 4.7. Comparing model steady-state temperatures to empirical data

4.3.5. Modelling exercise conditions

The empirical dataset by Flouris et al.[120] included 36 participants, who cycled at 40% of their peak oxygen uptake under various environmental conditions; 16 cycled in a moderate

environment for 90 minutes, 18 cycled in a warm-humid environment for 90 minutes, and 19 cycled in a hot-dry environment for 60 minutes. There were 17 participants who participated in two of the exercise conditions. All trials included 120 minutes of rest post-exercise. Flouris et al.[120] found no statistically significant differences between the averages in age, weight, height, or body fat % between the participant groups for the 3 exercise conditions. From each exercise condition, 6 participants have been randomly selected to form a validation dataset. Results from the remaining participants formed a dataset to use for selection and optimisation of the best bioheat model design for predicting muscle heat during exercise and recovery.

The muscles generate heat during exercise. Therefore, $q_{ti,m,work}$ has been added to the **Metabolic Heat Source** of the muscle tissue, using Eq. 10, Section 3.4.2. The metabolic activity score that corresponds with the level of exercise at each point in time has been set up as a *definition***,** using the *piecewise function***, qm_work_x(t)**. There are two variations of this function because variables cannot be called within a piecewise function, so the different length of exercise used in the hot-dry study was set using a separate piecewise function.

The arterial blood temperature entering the thigh segment, T_{bl}, varies with exercise and ambient conditions. It was calculated separately for each change in exercise condition; the initial resting condition, the exercise time-period, and the post-exercise recovery time. These were each stored as *time-dependent global variables*. The rest condition was used for the stationary studies. The exercise end-time was used to select the correct temperature for the exercise condition and post-exercise recovery condition in the time dependent studies:

$$T_{bl} = (t \leq t_{exercise\ end}) * \frac{dT_{bl,\text{exercise}}}{dt} + (t > t_{exercise\ end}) * \frac{dT_{bl,\text{recovery}}}{dt}$$

The tissue temperatures, T_{ti}, were continually updated during the time-dependent studies.

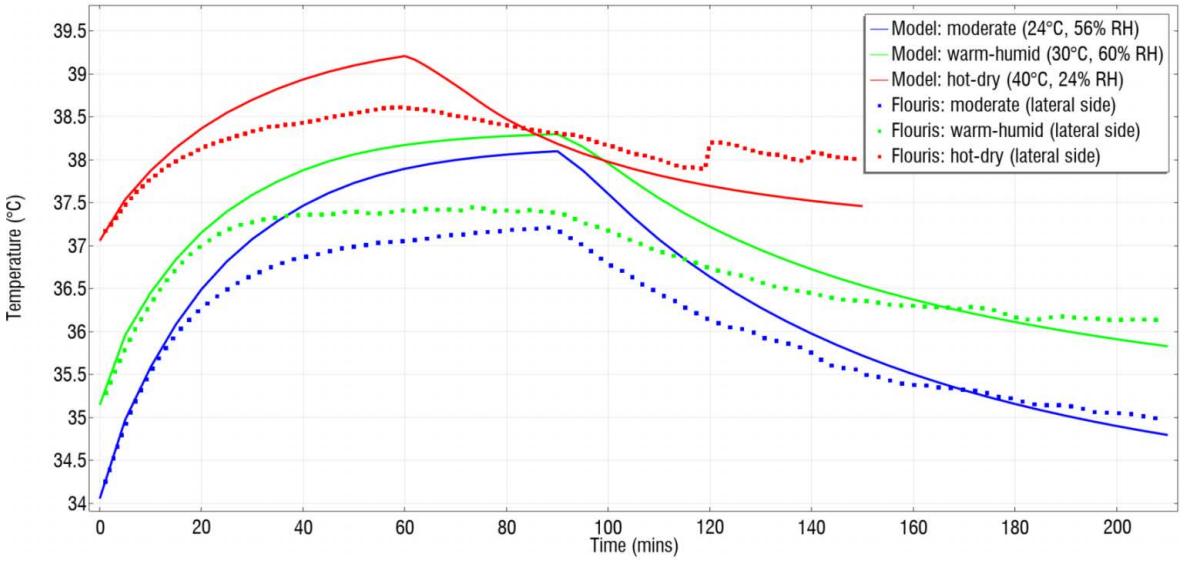


Figure 4.8. Modelling muscle heat during exercise using the passive heat transfer system

As shown in Figure 4.8, without the active system or large blood vessels modelled, the model overestimates the heat in the muscles during exercise because the heat dissipation from the skin and to the other body segments is significantly reduced. It also underestimates the time taken for the temperature to cool back down to the resting temperature because the fixed-temperature estimation of arterial blood does not take into account the heat entering the arterial blood from the muscles and the circulation between the leg and the larger mass of the whole-body.

Issues with adding heat transfer factors to a model based on experimental results include that the assumptions made are not necessarily valid outside the range of the empirical dataset, and that the factors may not provide insights into causation or the underlying mechanisms. Adding multiple factors at once, based on experimental results, without assessing the individual errors, uncertainties, and confounding can cause the model to become inaccurate and unreliable. Therefore, this research examines the impact of adding the active heat transfer factors to the model, comparing the amount of error between the output muscle temperatures from each model and the empirical dataset under the 3 ambient conditions. This enables a decision to be made on whether the heat factor is sensible and improves the temperature prediction in the present ambient conditions. The three factors examined here are:

- Separately modelling laminar flow through the major blood vessels to account for convective heat transfer and counter-current heat exchange between veins and arteries.
- Modifying the blood perfusion rate through the tissue based on vasoconstriction and vasodilation of the blood vessels.
- Modelling the production of sweat, which changes the evaporation rate from the skin's surface.

4.3.6. Modelling thermoregulatory responses

Vasomotion of the peripheral blood vessels regulates the internal temperatures by bringing more or less of the blood to the skin surface, and therefore modifying the amount of heat loss from the skin (see theory in Section 3.4.5). Vasoconstriction (Cs) and vasodilation (Dl) responses are modelled separately because these afferent signals can coexist under some moderate temperature conditions. This model inputs Cs_{sk} and Dl_{sk} as *global variables* and calls them from a separate *global variable* named ω_{sk} that models the blood flow through the skin layer, with Cs_{sk} and Dl_{sk} multiplied by their empirically derived distribution coefficients of 0.1 and 0.115, respectively.[134] The blood flow variable, ω_{sk} is called from within the *Bioheat Transfer* node under the biological tissue properties for skin, and used in the calculation of convective heat transfer. Exercise also causes an increase in blood flow to the muscles,[204] so an adjustment was made to the basal blood flow in the muscles to account for this (see theory in Section 3.4.5). Figure 4.9 shows that adding vasomotion to the model slightly improves the fit of the model (Table 4.3 provides a comparison of the RMSE). This particularly affects the rate at which the temperature during exercise reaches its new steady-state temperature.

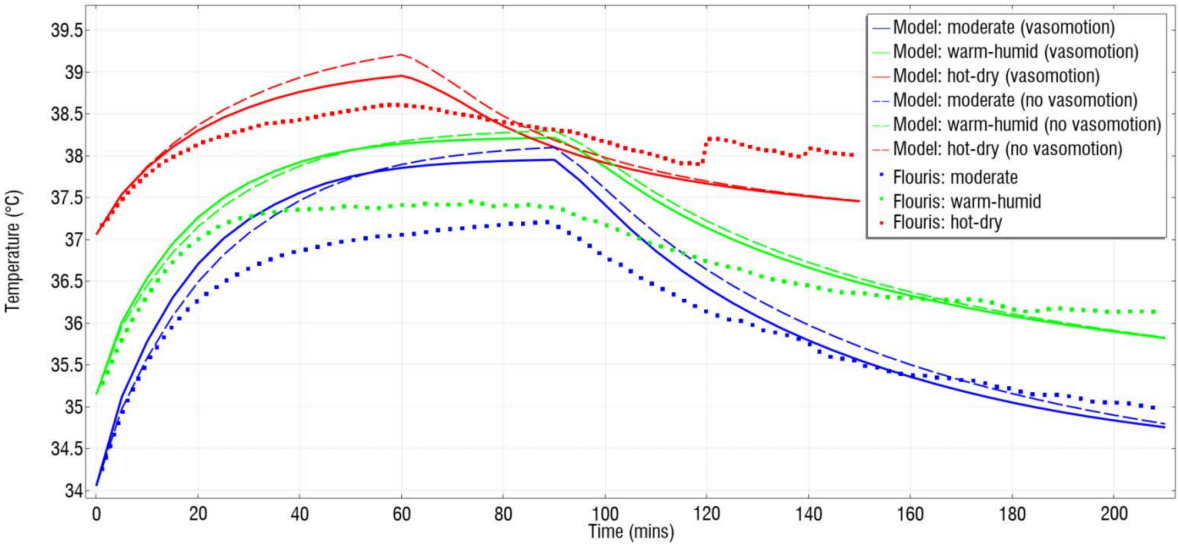


Figure 4.9. Adding vasomotion to model the muscle temperatures during exercise and post-exercise recovery

In hot conditions, vasodilation is accompanied by sweat production (Sw) to increase the rate of evaporation from the skin surface. However, this evaporation rate depends on the ambient air pressure, which is affected by the relative humidity. This calculation of skin wettedness, wet_{sk}, is influenced by the vapour pressure on the skin surface, p_{sk}, which depends on the rate of sweat forming, $\frac{dm_{Sw}}{A_{sk}dt}$ (see theory in Section 3.4.5). The sweat response, Sw, is modelled as a *global variable*, based on the regression analysis of empirical data performed by Fiala et al.,[134] and is used in the calculation of the vapour pressure on the skin surface, p_{sk}. This affects the *Evaporation Heat Flux* used on the skin surface in the *Bioheat Transfer* node. Figure 4.10 shows the effect of sweating (without including vasomotion). This improves the fit of the model under the moderate conditions the most, shows some improvement for the warm-humid condition and has no effect on the hot-dry condition. This is to be expected because evaporation relies on the heat-transfer coefficient for air, which, under natural convection only, as modelled here, requires the surrounding air to be cooler than the body for evaporation to occur. During exercise conditions, there is air movement generated around the limb, which would cause evaporation even at hot ambient temperatures, but this has not been considered for the current model because conventional prosthetic sockets do not enable air flow around the residual limb.

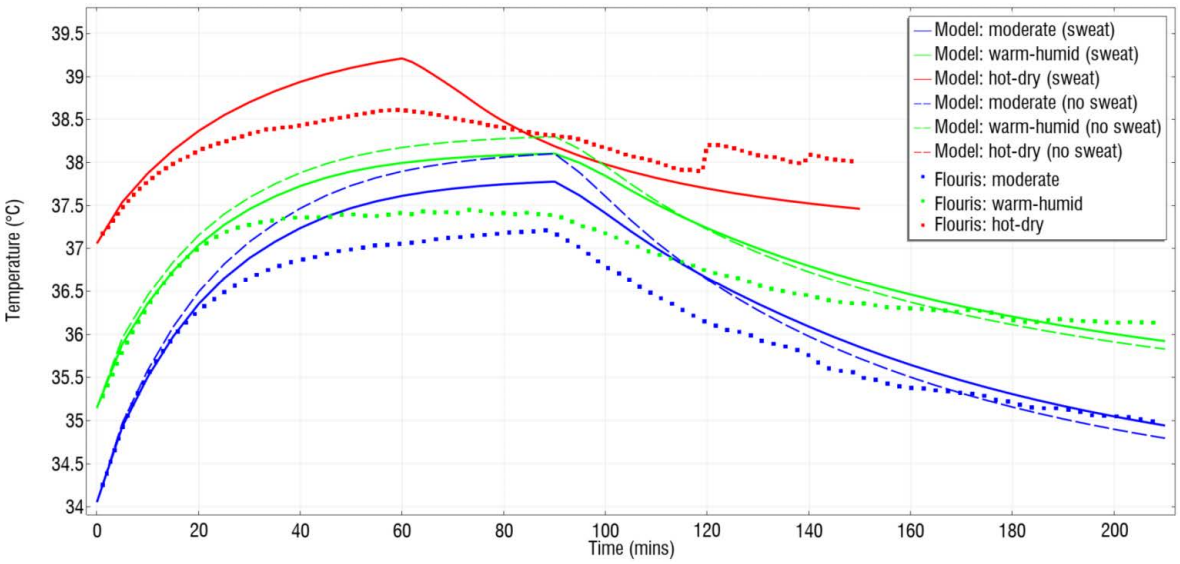


Figure 4.10. Adding sweating to model the muscle temperatures during exercise and post-exercise recovery

Combining both sweat and vasomotion gives a relatively good approximation of temperature responses under the three conditions. However, the model consistently over-estimates heating during exercise and does not reflect the slower initial rate of change in muscle cooling in the hot-dry condition.

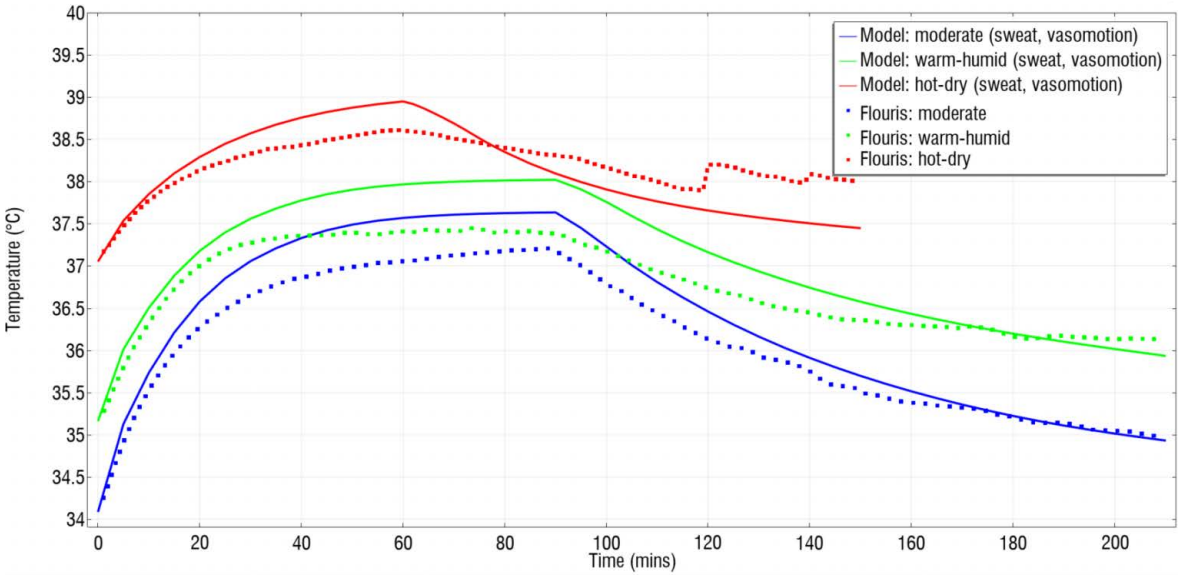


Figure 4.11. Adding both sweating and vasomotion to model the muscle temperatures during exercise and post-exercise recovery

4.3.7. Modelling the large blood vessels separately

Previous thigh segment models used a fixed arterial blood temperature, and did not model the large blood vessels separately,[137,171] or used an input of core temperature as the

arterial blood temperature, collected experimentally from the individual throughout the clinical study.[169] The former method is only suitable for rest-conditions, as it does not include the rate-of-change in temperature. The latter method is unfeasible without access to the individual's core temperature, which would require the individual to physically complete the simulation protocol with a sensor monitoring the core temperature variations with changing exercise conditions. This is not an option when using a bioheat model to predict an amputee's internal temperatures before they have their socket made. These methods were used previously because of the challenges in predicting core temperature during changing environmental and exercise conditions without modelling the whole-body.[169]

Whole-body models have adjusted for the convective heat transfer through the large blood vessels and counter-current heat exchange between veins and arteries by adding heat exchange coefficients to each body segment, generated based on trial-and-error until they agreed with empirical results (Section 3.4.2).[155,156] Instead, in this model, the large blood vessels have been individually meshed and modelled using laminar blood flow (see theory in 3.4.2), with the estimated changing arterial blood temperature used at the entry-point to the leg segment (see theory in 3.4.4). The realistically close proximity of the modelled blood vessels, and the direction and speed of the blood flow account for the countercurrent heat exchange without requiring a trial-and-error estimation. This method is more computationally heavy. However, modern computers and FEA software make this method feasible.

To assess the effect of modelling blood flow, the *Laminar Flow* physics node was added to the model and *COMSOL Multiphysics Non-isothermal Flow* coupling was used to link the physics between the heat transfer and fluid-flow calculations in the modelled blood vessels. In the *Bioheat Transfer* physics node, the blood domain was set as a **Fluid** with the fluid type set as Gas/Liquid, and the density, heat capacity and ratio of specific heats determined by the blood material properties. The artery inlet was set to the arterial blood temperature entering the segment, T_{bl}, and the velocity and pressure of the fluid were set to take input from the multiphysics coupling with the *Laminar Flow* node.

In the *Laminar Flow* node, the blood flow in the blood domain was modelled using the Navier-Stokes equations to determine the pressure and velocity in the circulatory system, as explained in Section 3.4.2. The inflow velocity was set to 0.8 m/s, based on the scientific literature findings of average flow velocity in the superficial femoral artery.[209] The outlet pressure was set to 40 mmHg, the average resting pressure in the common femoral vein.[210] The viscosity was determined by the blood material properties, and the temperature was set to take input from the multiphysics coupling with the *Bioheat Transfer* node. This slightly improved the fit of the model under the moderate and warm-humid environmental conditions (Figure 4.12). A *cut-point* was added to the medial side of the segment at the same 22 mm depth as the lateral measurements. Temperatures from this point were also added to the graph as a comparison. These responses differed from those on the lateral side at cooler ambient temperatures. The lack of empirical data to validate the findings of the temperatures on the medial side under the different environmental conditions mean these results should be used with caution, but do suggest that individual modelling of the major blood vessels should be taken into consideration when assessing the heating of the muscle tissues and the temperature distributions through the limb.

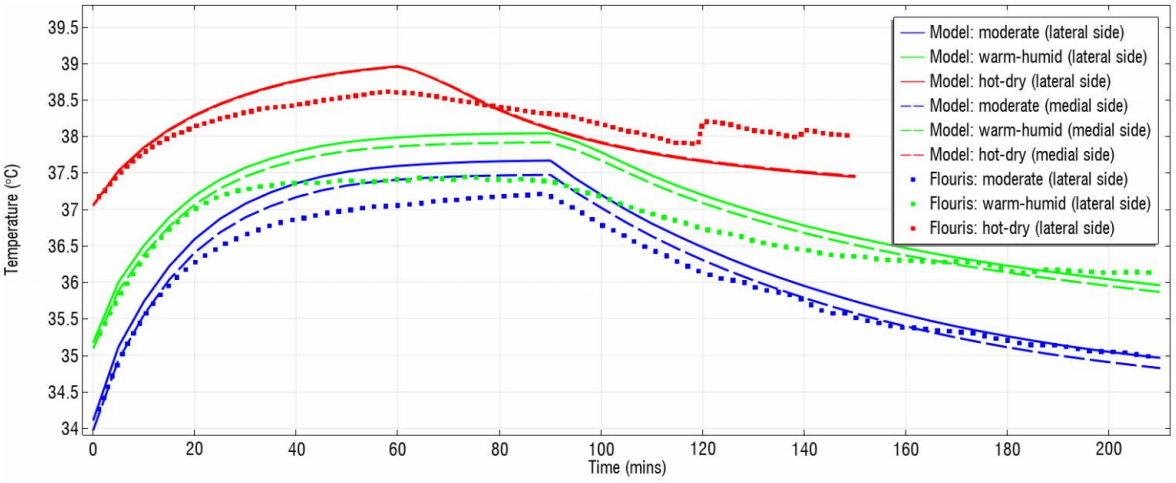


Figure 4.12. Medial and lateral sides with large blood vessels modelled separately. Empirical data from the lateral side has been included for reference.

All these model variations overestimate muscle heating during exercise. The model uses a highly simplified geometry. Figure 4.12 suggests that the locations of blood vessels affect the heat at particular points in the muscle, so using the average thigh circumference along the length of the cylinder, rather than using an accurate thigh shape is likely to also affect the output. The model is also based on a linear relationship between the basal metabolic rate

standardly given in the scientific literature and the metabolic activity score assigned to cycling at 40 % of peak oxygen uptake, as determined by Ainsworth.[189] However, this basal metabolic rate varies substantially between individuals, particularly with age, gender and fitness,[192] so it is unsurprising that it does not match the empirical dataset of athletic cyclists. The basal metabolic rate has been left at its current level to numerically determine the best model for assessing muscle heat during exercise and post-exercise recovery. Once the best model has been selected, this rate is then adjusted to reduce the root-mean-square error between the model output and optimisation dataset of empirical data.

4.3.8. Numerical comparison of models

The importance of physiological interactions between different heat transfer factors is not known, and testing the effect of each parameter individually does not take into consideration any confounding effects. Therefore, to assess each combination of factors, a full-factorial analysis was performed to compare the effects of each heat transfer factor graphed in the previous section (vasomotion, sweating, and separate modelling of major blood vessels), and every combination of factors. Each of the 8 model variations was run using the average participant data from the optimisation dataset under moderate ambient conditions, warm-humid conditions and hot-dry conditions, to determine the best model on average across the range of environmental conditions.

There are a variety of ways to compare the different models to the empirical data, and to judge the best model. Here, the main factors considered, when comparing models on their usefulness for predicting muscle temperatures in hot and humid climates, were:

1. How close the **end-of-exercise muscle temperature** was to the empirical dataset at the location that matched the thermocouple placement. The maximum thigh tissue temperature is an important predictor of tissue health. This maximum occurs at, or very close after the end of exercise, when the heating due to the muscle metabolism is at its highest. Based on thresholds of thermal damage for different tissues, the WHO suggests that the maximum local tissue temperature of any tissue should remain below 39°C to avoid thermal damage.[211,212]

2. **The root mean square error (RMSE)** between the model output and the empirical data as a way to judge the goodness-of-fit of the model. This provides an indicator of how well the overall temperature profile of the model matches the empirical data, giving an indication of the amount of heat stored over time. The cumulative thermal dose is the standard determinant of tissue thermal damage because damage occurs at lower temperatures if exposed for longer periods of time.[117] The cumulative thermal dose is more commonly used when external heating is applied to the tissue, such as in radiation therapy. However, muscles can be damaged due to over-exertion, and changes occur in the structure of the muscle tissue when exposed to sustained temperatures above the thermoneutral temperatures.[112] It is therefore, not only useful to compare the maximum temperature reached, but also the amount of difference between the models over time. Because the main drivers of heat transfer during exercise differ from those during recovery, the measures of RMSE were separated into the exercise interval and the post-exercise recovery period. This gives a measure of not only how the muscle heats during exercise, but also how long the heat remains in the muscle after the cessation of exercise. The first 30 minutes of recovery was used for this analysis, to avoid the section of empirical data that was erratic and suggested erroneous clinical measurements.

The data was stored in tables in the *Results* section of COMSOL, and exported as .csv files. Each table column was set as a *Derived Value* using *Node Groups* to group the columns into tables. The comparison between graphs was performed as a post-processing step in Excel. Conditional formatting was used to visually compare each model on each measure, with the worst model on a specific measure under the specific environmental condition coloured red and the best coloured blue.

The best model was chosen based on which one had the smallest errors in comparison to the clinical data, across the 3 environmental conditions. This selection method does not consider the computational time, whether the size of the improvement is physiologically meaningful, or whether it is more useful to have a model that under-predicts or over-predicts muscle temperatures. These differences are worth considering in the future, but complicate the model selection process, so are not considered in this current iteration of the model design, where the focus is on accurate muscle temperature prediction. The choice of “best model” has been selected as the best model across all 3 ambient conditions, rather than skewing the

selection towards the best one for the hottest conditions. This choice was made to make the model more versatile.

Table 4.3. Comparison of model variations

	Included heat factors	Environment	Difference in max. temp.	RMSE (exercise)	RMSE (recovery)
1	No blood vessels No sweating No vasomotion	Moderate	0.837	0.596	0.734
		Warm-humid	0.884	0.445	0.659
		Hot-dry	0.252	0.564	0.337
2	No blood vessels No sweating Vasomotion	Moderate	0.587	0.554	0.284
		Warm-humid	0.727	0.451	0.419
		Hot-dry	0.066	0.264	0.153
3	No blood vessels Sweating No vasomotion	Moderate	0.548	0.392	0.788
		Warm-humid	0.712	0.345	0.642
		Hot-dry	0.153	0.564	0.273
4	No blood vessels Sweating Vasomotion	Moderate	0.298	0.333	0.325
		Warm-humid	0.545	0.329	0.421
		Hot-dry	0.010	0.264	0.120
5	Blood vessels No sweating No vasomotion	Moderate	0.878	0.628	0.750
		Warm-humid	0.884	0.445	0.659
		Hot-dry	0.252	0.564	0.337
6	Blood vessels No sweating Vasomotion	Moderate	0.582	0.537	0.258
		Warm-humid	0.720	0.435	0.389
		Hot-dry	0.070	0.269	0.158
7	Blood vessels Sweating No vasomotion	Moderate	0.504	0.349	0.736
		Warm-humid	0.685	0.316	0.608
		Hot-dry	0.159	0.571	0.279
8	Blood vessels Sweating Vasomotion	Moderate	0.265	0.293	0.289
		Warm-humid	0.522	0.303	0.396
		Hot-dry	0.016	0.272	0.125

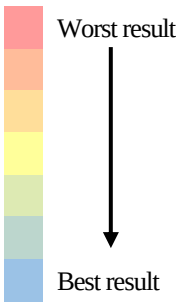


Table 4.3 shows that model variation 8, with sweat, vasomotion and separately modelled large blood vessels performed best on the greatest number of factors, as would be expected. It was slightly worse at modelling the hot-dry condition than model variation 4, without the large blood vessels modelled separately. However, these two results were close on all three measures of difference, so model variation 8 has been chosen as the optimum model for analysing muscle temperatures across the range of environmental conditions tested.

4.3.9. Optimising the metabolic rate during exercise

As mentioned previously, all model variations overestimated muscle heating during exercise. This may be because the geometry is simplified or because the metabolic rates assumed in the model differ from the empirical dataset. Using the best model design, selected in the previous section, the metabolic rate has been adjusted to minimise the RMSE during exercise. Reducing the metabolic rate increase for each point on the metabolic activity score by Ainsworth[189] by 15% gave a good accuracy across all environmental conditions (Figure 4.13). This result seems physiologically feasible, given the findings of Byrne et al.[192] on how much age, gender and fitness contribute to individual metabolic rates, and that the empirical dataset was of athletes accustomed to cycling.

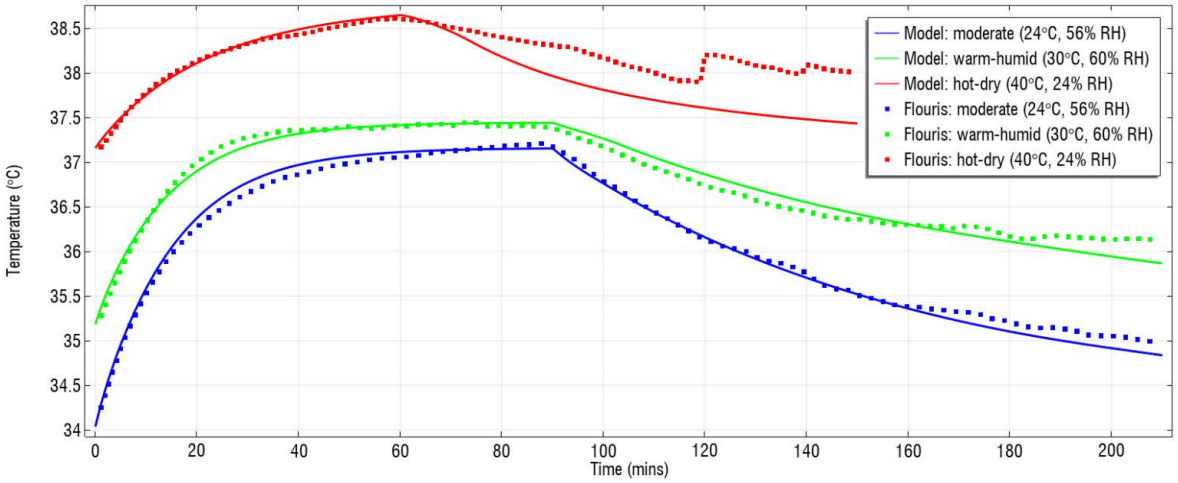


Figure 4.13. The final model after adjusting the basal metabolic rate to align with the optimisation dataset

After optimising the metabolic rate to match the empirical optimisation dataset, all three ambient conditions were within 0.07°C of the empirical data at the end of exercise and the RMSEs during exercise were 0.076, 0.067 and 0.037 for moderate, warm-humid and hot dry environments respectively. The RMSEs for recovery were 0.078, 0.121 and 0.396 for each ambient condition, respectively.

To test if this model is robust to different datasets, after being optimised on this optimisation empirical dataset, it has been compared to the separate validation dataset of 6 participants under each environmental condition. The thigh radius input was adjusted to 83.6mm (Eq. 41, Section 4.3.2) to match this new dataset. The model results showed good correlation with the empirical validation results (Figure 4.14). At the end of exercise, the

three ambient conditions were out by 0.004°C, 0.261°C and 0.106°C, respectively, for the moderate, warm-humid and hot-dry conditions. The exercising RMSEs were 0.078, 0.162 and 0.177, respectively, and the recovery RMSEs were 0.142, 0.331 and 0.474, respectively for the moderate, warm-humid and hot-dry conditions.

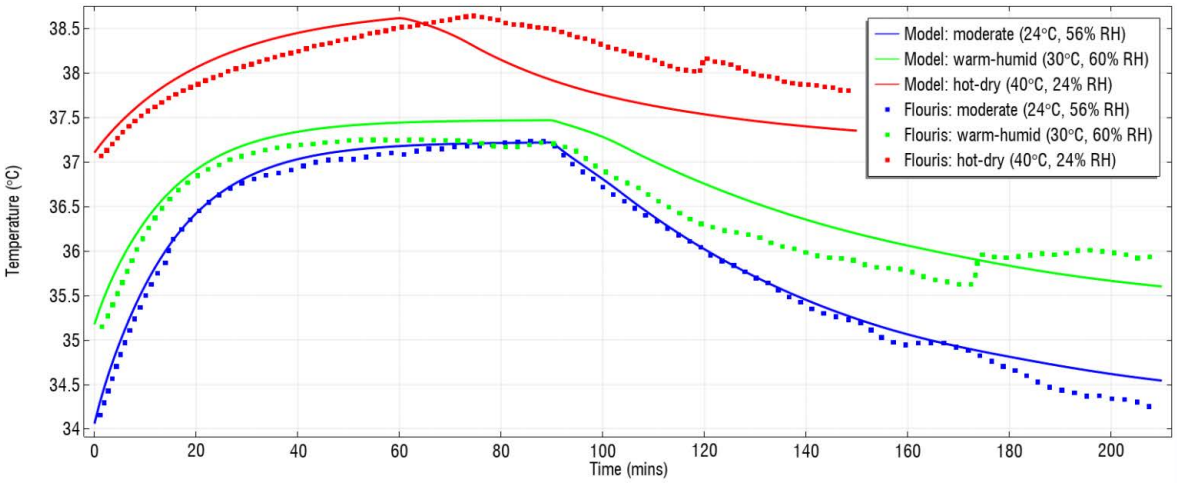


Figure 4.14. Validating the final model against the averages from the validation empirical dataset

This shows that the model is relatively robust, though it under-estimated cooling time under hot-conditions for both the optimisation and validation datasets. The sudden reheating at 120 minutes, seen in both the optimisation and validation empirical datasets, is likely to be a systematic error introduced by the protocol, such as moving the participant or offering them a drink, rather than a physiological response.

4.4. Geometry factors affecting heat transfer

Ideally, it would be good to test the model on individuals, inputting their estimated thigh circumference and body fat percentage and comparing the model output to the empirical response. However, the researchers who provided the empirical data have only provided the average outputs of the optimisation and validation datasets for each of the empirical conditions, so this validation is not possible. This section instead explores the importance of body composition factors on the temperature response by observing variations in the model output with different inputs, and discusses what these differences might mean clinically, but it requires future research to validate these findings. The model has been run with varying

thigh circumferences and muscle-to-fat ratios. It also observes the differences in shallow and deep muscle temperatures.

The maximum and minimum estimated thigh circumferences from the empirical dataset were used as an indicator of the range of normal data across a population. These were 615 mm and 449 mm, respectively. Likewise, the maximum and minimum skin surface areas were 2.20 m^2 and 1.54 m^2, respectively. The whole body volume was adjusted in proportion to the skin surface area. The four combinations of maxima and minima are compared in Figure 4.15 to give an indication on how changing the thigh circumference or the whole body size affect the muscle temperature. The muscle temperature was measured on the lateral side at a depth of 22.5% of the radius, as this gives the 22 mm average depth used in Flouris et al.[120] for Flouris' average thigh circumference.

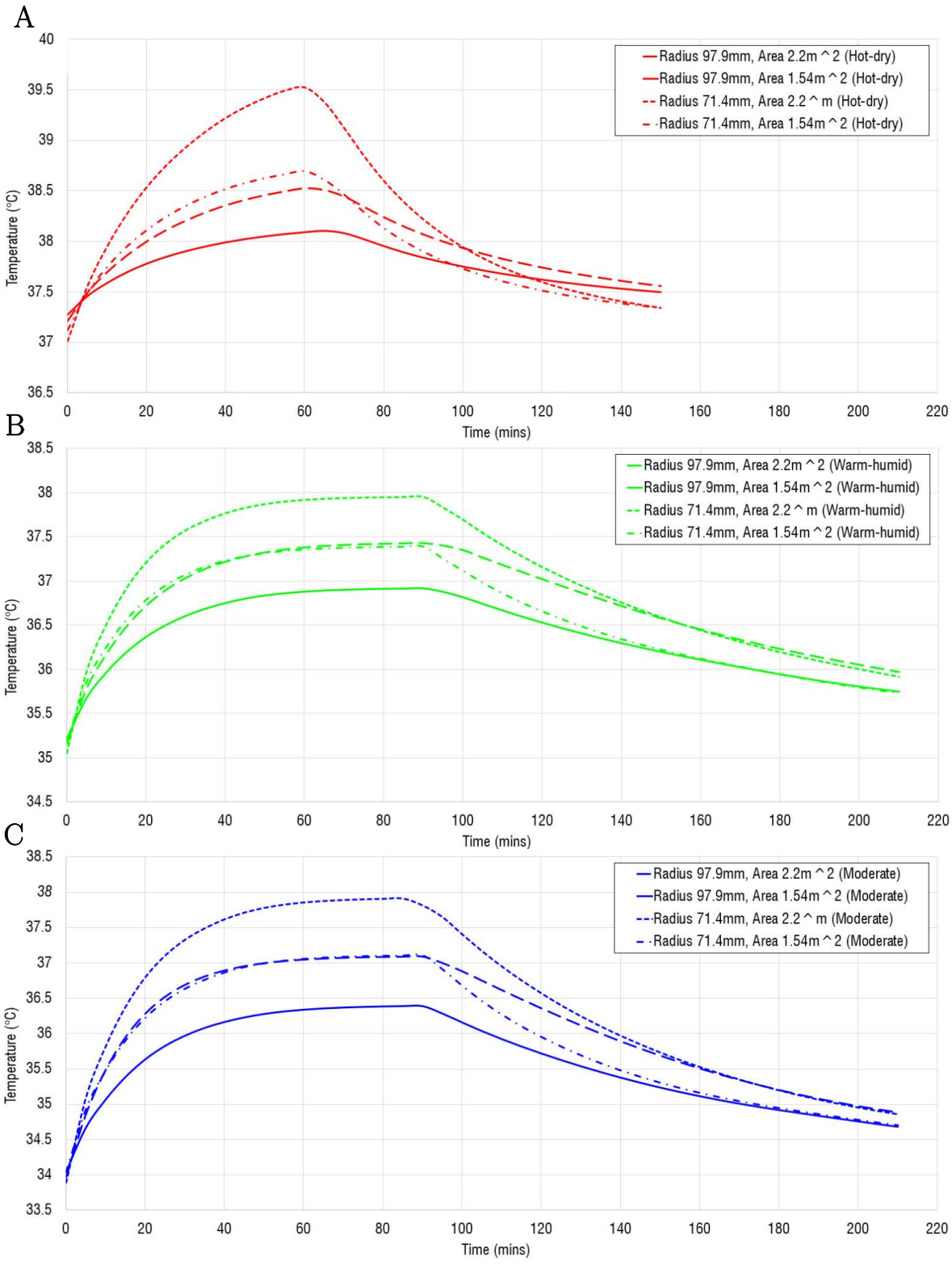


Figure 4.15. The effect of thigh circumference and body size on muscle temperatures under: A. Hot-dry, B. Warm-humid, and C. Moderate conditions

Figure 4.15 shows that within the normal range of thigh sizes, the overall size of the thigh contributes substantially to the muscle temperature outputs, and so does the total body

size, regardless of the environmental conditions. Larger bodies take longer to heat and to recover after exercise. This shows the importance of customising a bioheat model to the individual's size to predict the thigh muscle temperatures. Note that the model does not take into account individual metabolic rates, which are known to vary substantially between individuals,[192] because these differences are poorly understood. This is an area that could benefit from future research.

It is also useful to assess how internal tissue composition affects the model. The average participant body fat percentage in the empirical dataset used for comparison was 18.57%. The dataset ranged from 5.31% to 28.92%. This model predicts temperatures entering the leg segment based on body size, but only using an average estimation of body composition. Therefore, this average has been kept as a fixed percentage, and only the differences in fat % in the thigh were assessed (Figure 4.16). The average thigh body fat percentage was similar to the whole body, at 23.6%. The radius of the muscle tissue layer in the model was adjusted to compare 10% body fat to 30% body fat.

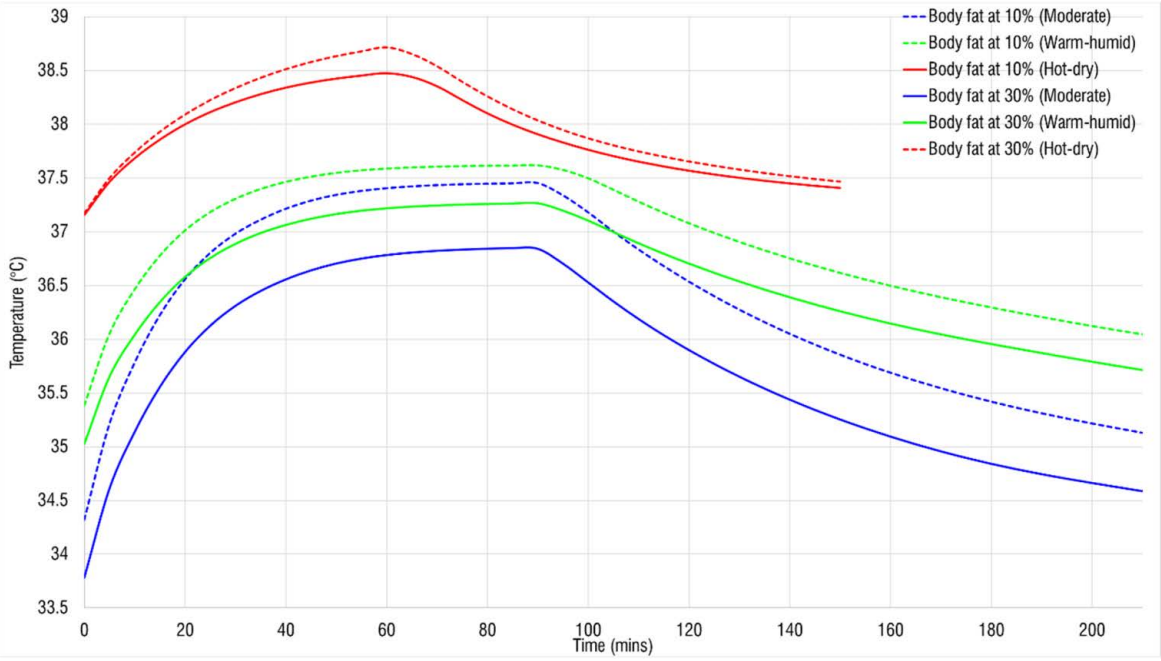


Figure 4.16. The effect of body fat percentage on muscle temperatures

These results show different muscle temperature responses with different internal compositions. This suggests that individual size and body composition are important factors to consider when simulating muscle temperatures.

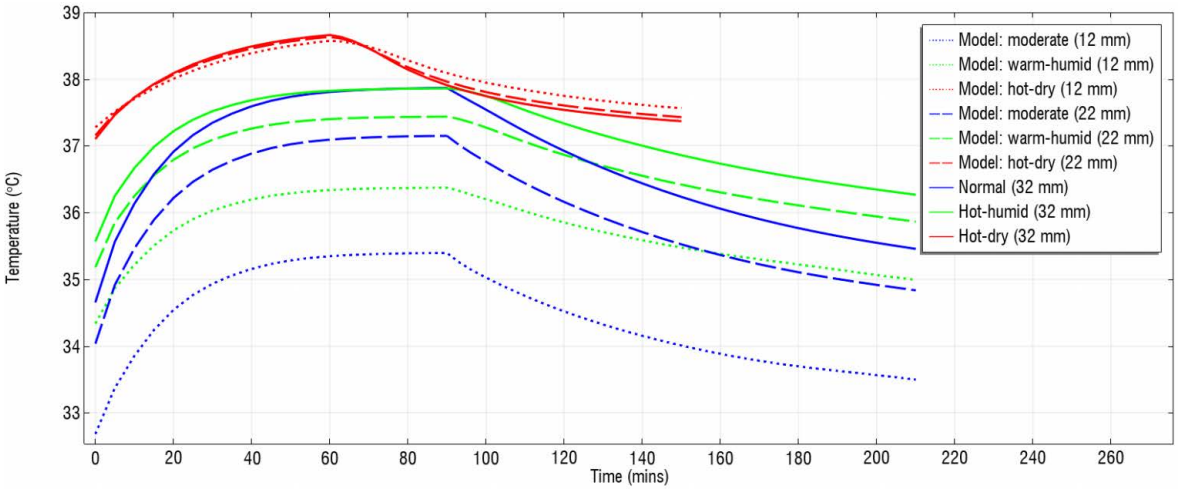


Figure 4.17. The effect of depth of thermocouple placement on the muscle temperature reading

Depth of temperature measurement into the muscle tissue appears to also have a significant effect on the temperature output (Figure 4.17). This aligns with empirical findings.[98,136,174] It is also likely that there are differences from the proximal to distal end of the limb, because the blood flows away from the heart, and the thigh is slightly conical in shape. The current cylindrical model does not consider the flow direction in the smaller blood vessels or the smaller circumference at the distal end, so does not adequately show these longitudinal temperature variations.

The validation of this model shows that using a simple cylindrical segment model can achieve relatively good accuracy in predicting muscle temperature. This model accurately predicts muscle temperatures in moderate conditions, but performs less well under hotter conditions. Particularly of note is the consistent under-estimation of the time it takes to recover after exercise in the hot-dry condition. This may be because empirically derived coefficients have been used where the physics is not well understood, and these empirical trials were typically performed under moderate ambient temperatures, so do not necessarily provide accurate predictions outside the tested ambient range. Under-estimating the recovery time in hot conditions may have clinical implications, as tissues can be damaged at lower temperatures if exposed for longer periods of time,[117] and the model will not detect this excessive sustained thermal loading.

The thigh is close to cylindrical and other models have shown that a cylinder can provide a relatively accurate prediction of temperatures under resting conditions.[171] However, this

research also demonstrates the importance of internal and external geometry on temperature distributions. To understand the areas of the residual limb to focus cooling on, it is recommended that more realistic geometries are evaluated.

Without having empirical results to compare these results to, it is not possible to determine if these results are accurate. If the results reliably predict actual differences in muscle temperature response, then the large variation in individual responses means it is important to use individualised predictions and designs to reduce the thermal load on the individual. If the results overestimate the differences between individuals, further research needs to go into how to model individual variance with a bioheat model.

4.5. Exploring the effect of insulation

A layer of insulation was added around the segment to represent the insulation of a prosthetic socket. This layer has been given the properties of a thermoplastic commonly used in conventional prosthetic sockets, with a thermal conductivity of 0.15 (W/m·K) and a typical socket thickness of 4.6 mm.[25] The model output shows an increase in temperature and a prolonged post-exercise recovery time (Figure 4.18). This makes sense, given that the skin heat loss is hindered, so heat that builds in the muscle takes longer to dissipate.

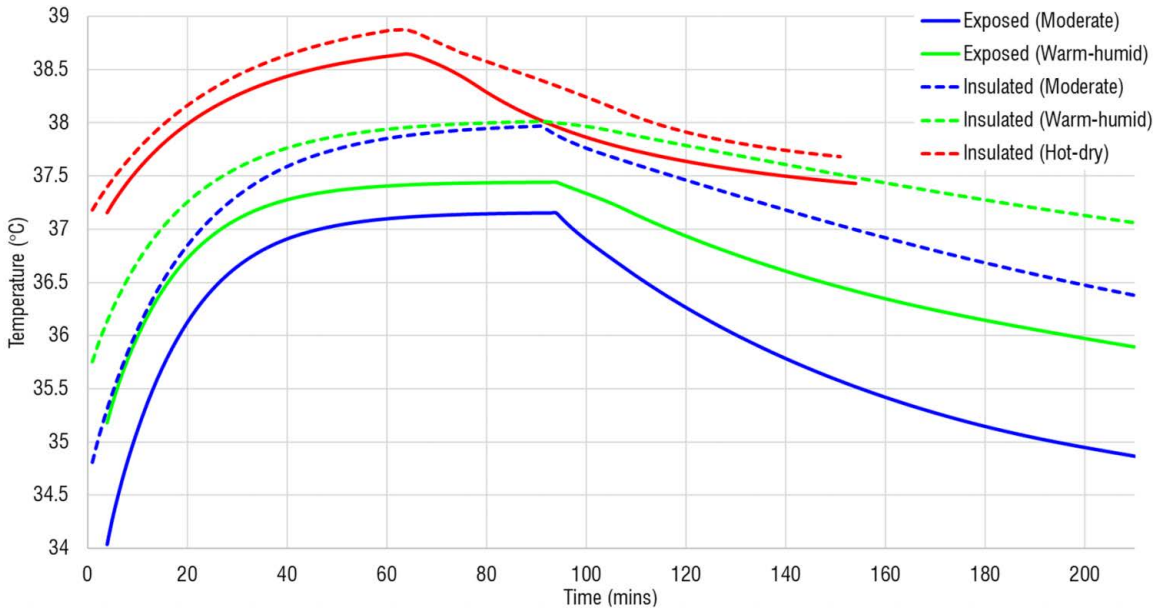


Figure 4.18. Insulation increases the temperature during exercise and time for recovery

In the hot-dry condition, this temperature rises to close to 39°C, which is the temperature the WHO recommend keeping tissue below to avoid thermal damage.[211,212]

Again, this model requires validation against empirical data to confirm the magnitude of the responses. It would be useful to have a validated bioheat model that can predict this temperature increase, to help prosthetists and end-users know how to best design the prosthetic socket and to care for the residuum.

4.6. A geometrically accurate model

From the previous section, it is obvious that geometry is important. It is also useful for designing a prosthetic socket that better matches the thermal load of the body, to know the changes across the skin's surface. This could, in future, be linked to CAD/CAM with multi-material printing, smart materials or adaptable microstructure printing to target cooling at certain areas of the socket to reduce the thermal load (see Section 5.1 for a discussion on these possibilities).

A benefit of using FEA techniques is that if the same mesh element sizes are used as the cylindrical model, increasing the accuracy of the shape does not increase the model run-time, because each mesh element is analysed individually, rather than the shape as a whole. This section explores realistic geometries, importing .stl files that were developed based on MRI data into COMSOL Multiphysics.

BodyParts3D provides a freely available anatomical database, where MRI images from a male volunteer have been constructed and segmented by body part and tissue type.[213] Each body part, divided by tissue type, has been stored as an individual object file with locational information so that it can be easily fitted correctly to other body parts. BodyParts3D was chosen over the other commonly used free dataset; the Visible Human Project,[214] because highly detailed vasculature is not required, and the BodyParts3D model has lower resolution and smaller data sizes. It is also based on a living volunteer, rather than a cadaver, and therefore avoids inaccuracies caused by tissue deterioration, such as collapsed blood vessels. This anatomical dataset supports the development of finite element analysis (FEA) models to simulate body functions using internal anatomical accuracies.

COMSOL requires manifold objects, has difficulty with meshing narrow regions, and its FEA calculations are computationally heavy, so it would take a super-computer to

simulate a highly complex mesh, which reduces the usefulness of the simulation for clinicians. COMSOL also has limited capabilities in CAD modelling and manipulation or meshing of imported data. It was therefore not feasible to import the BodyParts3D object files directly into COMSOL. The recommended method for importing complex models into COMSOL is to use ScanIP software. It takes input from an .stl file and generates the mesh as an .mph file, for importation into COMSOL. This is much more successful than COMSOL's inbuilt mesh generator. However, I did not have access to this specialised imaging software, so have generated simpler meshes, more distanced from the original MRI data, in order to enable COMSOL to load and mesh the files.

To achieve this, all muscles of the right thigh were opened simultaneously in Autodesk Meshmixer. These were made manifold using the *close cracks* and *inspector* tools. The muscles were then combined into a single object with the correct outward shapes, but with surfaces added between each muscle and internal walls removed to create a single manifold shape. This model was smoothed using uniform triangles to remove any narrow regions, so that it would be easier to mesh in COMSOL. The file was saved as a solid .stl model (Figure 4.19). The femur and fat files required little manipulation. They were also made manifold and smoothed using uniform triangles to remove narrow and highly detailed mesh regions. Skin was added as a 2 mm thickness around the fat layer in COMSOL directly, rather than importing an additional surface.

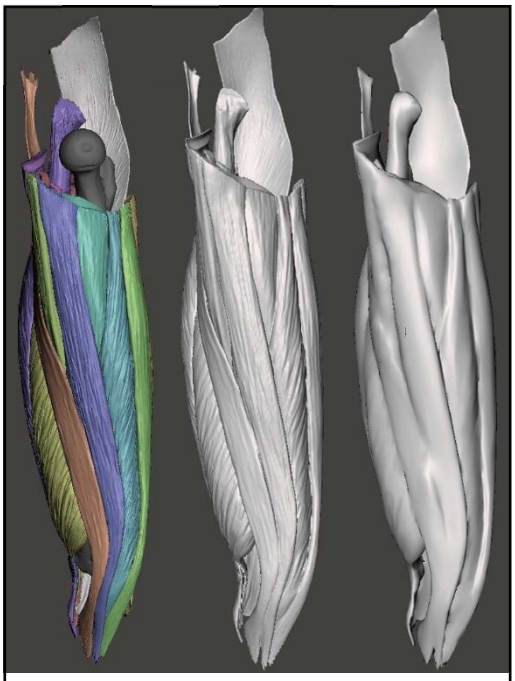


Figure 4.19. Joining and smoothing thigh muscles in Meshmixer
A. Individual manifold muscles, B. All muscles combined into a solid object, C. Smoothed muscles

The femoral vein and artery were modelled because they have a large enough radius that Pennes bioheat equation is invalid due to convection dominating the heat transfer (see theory in Section 3.4.2).[182,183] Using Autodesk Meshmixer, the vein and artery were correctly positioned, running alongside one another, but they were smoothed and encased in a 5mm sheath of muscle that was merged with the surrounding muscle layer but cut into the bone

where the veins touched the bone, to simplify meshing and calculations in COMSOL Multiphysics.

To create the amputee version of the model, for demonstration of the concept, this healthy leg model was amputated using the *plane cut* and *sculpt* tools in Meshmixer. The model was then imported into the cylindrical model file in COMSOL, to make sure all variables remained the same, and the material properties were added to the correct tissue domains. A sensitivity analysis showed that the mesh element sizes of the cylindrical model were suitable for the anatomical model.

Figure 4.20 shows screen shots of the model at rest, after the exercise and at the end of the 2-hour recovery for the moderate temperature condition. This shows visually that the muscles heat during exercise and have almost recovered after 2 hours. After meshing the model, it only takes 2.5 minutes to run when using *intermediate* time-stepping with a maximum of 1-minute time-steps. This can be sped up further by increasing the maximum time increment as the temperature stabilises. Using this method, with simplified meshes designed from MRI data, significantly improves the anatomical accuracy over any previous models, while remaining fast enough to compute in a clinical setting, to give prosthetists additional information to feed into prosthetic socket design.

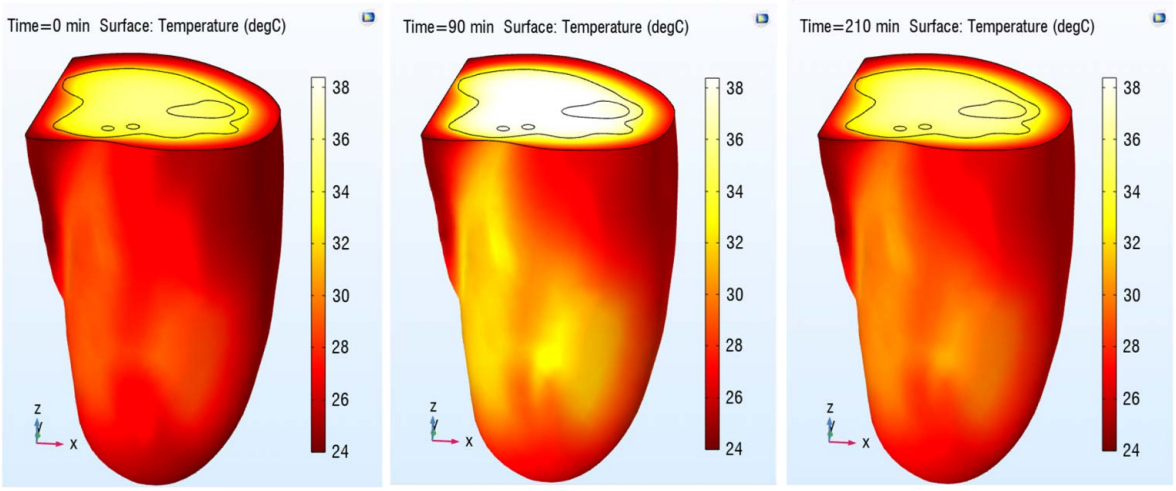


Figure 4.20. Anatomical model skin temperatures at rest, end of exercise and after recovery

A clearer view of the internal temperatures can be seen in Figure 4.21, which has been presented as slices through the limb. Note that the hottest point is in the centre of the muscle

mass at this time-point and the blood vessels have a noticeable effect on the surrounding tissue.

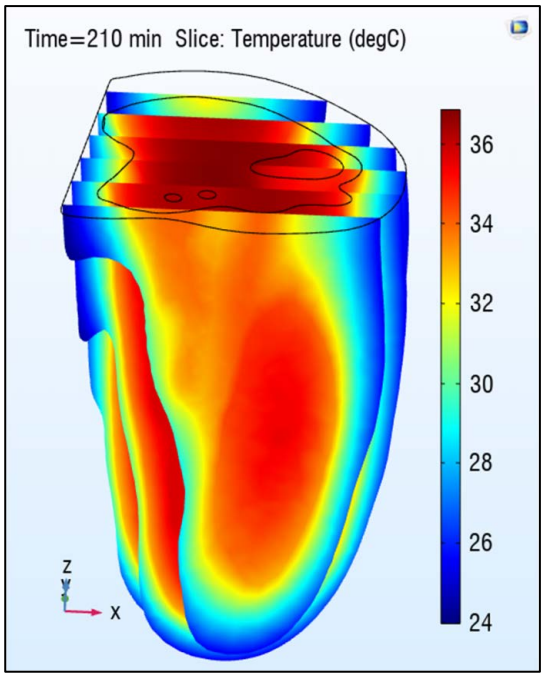


Figure 4.21 Slices through the residual limb show internal temperature variations

This model has not been validated because of the lack of empirical data. However, it shows the feasibility of using FEA for bioheat modelling of an amputee's residual limb during exercise and post-exercise recovery, using an isolated segment model with a predicted arterial temperature entering the leg segment. The results are in a sensible temperature range and align with the scientific literature regarding temperatures of the muscles and skin during exercise and post-exercise recovery. The model outputs show variations in temperature across the residual limb, with greater heating in the centre of the muscle mass, and different temperature heating and cooling rates near the major blood vessels, where the blood circulates from the rest of the body, bringing heat into the limb when resting, and transporting heat from the muscles during and after exercise.

The bioheat model is complex, with large numbers of variables, many of which are modelled based on empirical data. During the testing of the model, each variable was adjusted and the model re-run to provide an indication of the impact of each variable on the overall output. The next stage of the model development would be to run a full sensitivity analysis to assess how each of these variables impacts the model outputs. This could increase the understanding of the relationships between input and output variables, provide

information on the robustness of the model, and determine how to reduce the uncertainty to improve its robustness. It could also enable the model to be simplified by fixing or removing inputs that have little or no effect on the output.

Validating the amputee bioheat model using amputees is challenging because of the difficulties in non-invasively collecting muscle temperatures. Using in-socket sensors and methods of insulating the skin so it rises to close to the muscle temperatures[119,120] may be useful for improving the amputee model and validating it. Amputees could use different prosthetic sockets with known thermal properties. The different sockets could then be compared to see how they affect skin temperatures, and whether the results match the predicted temperatures from the simulation results (more detail is provided in the Future Directions in section 6.1.2).

Physical models can also be used for validation of the bioheat model. A thigh-shaped structure could be built using materials that have the correct thermal properties to represent the different tissues and tubes for fluid flow to represent the blood vessels. The heating of the muscle-like material, blood-like fluids and environment could be controlled, and these heating inputs could also be programmed into the computational model to enable comparison of the outputs of the physical and computational models.

Bioheat models could enable different prosthetic materials and designs to be tested and optimised via simulation for pre-clinical analysis, reducing trial-and-error, time, and manufacturing costs. They can easily be adapted to an individual user's physiology, environment, exercise conditions and prosthesis, and can overcome participant limitations in physical trials such as challenges with donning and doffing the prosthesis, fitness levels affecting data collection timespans, and challenges recruiting a large enough sample size for statistical power. This research is a step towards the long-term goal of developing a data-orientated approach to socket optimisation, to improve design for individual thermal comfort under a range of environmental and exercise conditions.

The more anatomically accurate amputee model uses the same computational methods and calculations as the non-amputee cylindrical model. This assumes that an amputation would not significantly affect blood flow and heat transfer properties within the residuum. However, there is research that shows that blood flow is reduced with amputation, and

particularly with vascular disease.[122] Amputees also have worse muscle conditioning in the residual limb, and the thigh muscles of transfemoral amputees are mostly not functional after the knee has been removed, so the work done in the muscles might be done by higher up muscles such as the gluteal muscles. The residual limb also has soft-tissue that is not designed for load-bearing. It therefore, changes its structural properties in response to the load. These differences may explain why the amputated limb skin temperature is typically colder than the contralateral limb. There may be less heat generated in the thigh muscles during exercise, but it cannot dissipate as quickly, so the muscles are likely to store more than this current model predicts and take longer to recover. Now that this research has developed a way to model thermoregulation in an amputee's residual limb, future research is required to learn how the healthy thermoregulatory system and heat transfer is disrupted in an amputated limb.

4.7. Key findings and contributions

The work presented in Chapter 4 demonstrates the feasibility of realistically modelling a body segment under exercise and post-exercise recovery conditions. The model is the first to use finite element analysis to determine temperature distributions through the thigh during exercise and post-exercise recovery. It is based on previous bioheat models. However, this research developed a way to predict temperatures in the arterial blood flowing into the thigh and to model the large blood vessels to increase the accuracy of predictions of muscle temperatures during exercise and post-exercise recovery. The chapter explores the effect of the environment on muscle temperatures, and is the first research found that compares computational model outputs to empirical data of muscle temperatures during exercise and post-exercise recovery. Even using a simple cylindrical geometry, the model was able to show good correlation with the empirical data. It demonstrates that muscles can heat by more than 3°C during exercise and take over two hours to recover, even without the effect of insulation and amputation. The active thermoregulatory system successfully keeps the temperatures from rising too high in a healthy, uninsulated leg, but the model predicts that with insulation, the temperature, when exercising in a hot climate, rises to near the 39°C limit that the WHO recommends tissue should remain below to avoid thermal damage.[211,212]

The model outputs suggest that thermal responses of individuals are varied and complex. It is, therefore, important to develop bioheat models that can be adjusted for an individual in

order to predict temperature responses to exercise, rather than using an average across a population. As discussed in Section 4.6, the model is likely to require adjustment to be used with transfemoral amputees. There has been little research into amputee muscle use and temperatures, so further empirical work is required to develop a better understanding of the adjustments that might need to be made to the bioheat model.

A bioheat model could be used by prosthetists in the clinic to predict the heating patterns of an individual's leg during the prosthetic socket casting process. The model ran in under 10 minutes, so is feasible to use during clinical visits. COMSOL provides the option to develop easy-to-use web-based applications that can be run on computers without COMSOL installed (see Section 6.3.3). The bioheat model could therefore be set up so the clinician can input the amputee's measurements and test the model with different environmental or exercise conditions. It could also have options for selecting the socket material and thickness from a list of commonly used materials. The app could then provide simple visual outputs and graphs to show the clinician where the limb is likely to heat up, and how high the muscle temperatures might get if a socket is made using the material and thickness selected. This visual guide could help prosthetists to choose appropriate socket designs and materials for the individual, and to see which areas of the limb would benefit from reduced thermal loading. Prosthetists and technicians could create holes in certain areas of the socket to change the breathability, thin the material or change the type of material to modify the thermal conductivity or porosity, or add active cooling processes such as fans or water channels through the material to change the microenvironment around the limb and to support the body's active thermoregulatory processes.

Computer-aided design processes could be used to support prosthetists in making these design decisions, based on the outputs of the bioheat model. As understanding of the human body's response to exercise, environmental conditions and prosthetic socket designs increases, this knowledge can be programmed into future computational models. The outputs of a bioheat model, as presented in this chapter, could be linked directly into a machine-learning algorithm, along with simulations from other models, such as one that assesses pressure distributions in the socket, and information from sensors and prosthetists. This setup could enable objective selection of the best socket design or computer-aided adjustments to

the socket design for an individual. Once the knowledge and technology has reached a level to be able to support computer-aided design, computer-aided manufacturing becomes an obvious choice for converting this virtual design into a physical prosthetic socket. Additive manufacturing is proposed as a solution for enabling this kind of system. Chapter 5 focuses on assessing whether additive manufacturing processes are currently capable of, or show promise for one day, supporting the manufacture of computer-aided prosthetic socket designs, informed by sensors and mechanical modelling.

5. Feasibility of using 3D printing

5.1. Opportunity provided by 3D printing technologies

5.1.1. 3D printing capabilities

Transferring the information provided by a simulation to the design of a physical product requires a data-supported manufacturing process. Additive manufacturing is proposed as a solution for directly implementing simulation results into product design and manufacture, replacing the conventional artisanal manufacturing methods. Additive manufacturing, more commonly referred to as 3D printing, is an industrial production technique that enables a 3D digital model to be converted into a physical model by printing it layer by layer. Because of its ability to manufacture directly from a 3D model, 3D printing provides an opportunity to design customised prosthetic sockets using a data-driven approach. This enables information from simulations, sensors, previous designs and machine-learning to be incorporated into designs, potentially reducing trial-and-error in fitting, and increasing comfort. 3D printing using multi-materials or adaptable microstructures may also support the development of sockets with varying properties across the socket to meet different design priorities.[58] The cost effectiveness of 3D printing technology for manufacturing one-off prints, and reduction in labour also increase the appeal of using 3D printing for prosthetic socket manufacture. Because 3D printing could play an important role in the development of data-driven customisation of prosthetic sockets, this chapter assesses the feasibility of using 3D printing to support data-driven customisation of functional and durable prosthetic sockets.

Conventional prosthetic sockets are fitted by creating a mould of the residual limb using plaster casting.[10,11] More recently, 3D scanning and digital rectification of the socket has become popular because it is faster, creates less mess, and can be digitally stored for future use or comparison.[12,13] Both processes require significant knowledge and skill from the prosthetist to rectify the shape so that it stays on, distributes the pressure in a way that the user can tolerate, and improves function. Residual limbs are often unusually shaped;

sometimes they are conical, but often they have bulbous areas due to the initial trauma, the surgery, or the way the tissue and scarring has healed and adapted under loadbearing conditions. Prosthetists manually modify the socket shape to fit the individual based on many factors. For example, scarring may affect which areas of tissue are sensitive, posture may need to be accounted for, and the socket might require adjustment to reduce gait asymmetry.

The geometrical complexity of the fitting processes used by skilled prosthetists is challenging to replicate using objective, digital methods. The use of 3D scans, indentation tools that can assess tissue hardness and soft-tissue movement, sensors and computer simulation tools can help with quantifying these necessary changes to the socket design, but until the technology is significantly advanced, manual prosthetist input into the digital designs is vital for creating comfortable sockets. The conventional manufacturing processes develop a socket with a solid outer layer, typically made of a single material, which is not ideal for supporting soft-tissue deformation and shape changes during dynamic loading. A 3D scanning and printing approach could enable prosthetists to have more freedom to adjust the socket design by enabling the use of different materials in different areas of the socket. For example, areas most important for load-bearing and pressure distribution might be designed to be solid and strong, while flexibility might be prioritised in areas that change shape due to soft-tissue deformation, and areas that heat or sweat significantly might be focused on breathability.

The chapter gives an overview of the capabilities, limitations and future possibilities of 3D printing technology, and assesses the efficacy and effectiveness of current 3D printed medical devices.

For decades, 3D printing has been used for rapid prototyping, but the recent advances in the available materials, speed, resolution, accuracy, reliability, cost and repeatability of 3D printing technologies have broadened the possibilities for clinical uses.[215,216]

The latest advancements in 3D printing include conductive printing, where conductive nanomaterials are incorporated into high-resolution 3D printing processes to enable the design of macro-scale electronics including flexible electronics, sensors and microbatteries.[217] These could be embedded into prosthetic sockets to monitor the device-user interface. Micro- and nano-scale printing also enables the manufacture of complex wire and fibre structures. Bioprinting provides amazing possibilities for organ-on-a-chip,

regenerative tissue engineering and targeted drug delivery devices. Using biocompatible materials to develop scaffolds and structures that mimic the body's processes can increase the strength of the attachment of new tissue and surgical healing times. Multimaterial bioprinting has created composite materials with properties that closely match the stiffness and elasticity of cartilage, which has not been previously achieved.[217] Smart materials have also been developed to change their shape or functional properties under certain stimuli. The stimuli used are typically temperature, electric current, or the presence of light or water. These materials can be programmed to change shape, concentration or have a piezoelectric response, changing energy from mechanical stresses to electric current or vice versa. These have potential for developing muscle-like tissues that could control prosthetic joints,[218] controlling microsensors, and changing the stiffness and flexibility of a prosthetic socket to more closely mimic the movements of a natural leg.

These new 3D printing technologies hold promise for changing clinical practice in the future, but the possibilities have not yet been realised in commercial products. The advanced medical devices and biocompatible materials are in the process of undergoing laboratory trials and remain far off for use in clinical practice. Until these technologies have been through clinical trials and are available commercially, they remain a distant hope for improving prosthetic socket design.

Of particular interest when considering the design of data-driven customised prosthetic sockets are the areas of adaptive microstructure printing to change the material properties in different areas of the prosthetic socket to meet various design priorities, and the options for remote fitting and manufacturing of prosthetic sockets to increase global access to high-quality prosthetics and associated services.

5.1.2. Adaptive material microstructures

There are numerous factors to take into consideration in the design of a functional and durable prosthetic socket that fits more naturally and comfortably onto the patient's residual limb and adapts to the individual's changing socket requirements. These factors include the variability in temperatures across the limb and the temperature fluctuations that occur over time, as well as changes in stresses, pressure and friction under dynamic loading conditions.

The geometry and body composition differences across the limb also affect the areas of the socket that undergo the highest loading forces, or need to account for the greatest volume fluctuation (due to movement, muscle contractions and other forces), and areas that must accommodate greater heat fluctuations or sweating.

A uniform material, as is conventionally used in prosthetic sockets, does not support this level of design optimisation for comfort. Ideally, it would be useful to have changing material properties across the socket surface to provide flexibility to enable the socket to remould to the changing shape of the limb, while keeping the necessary rigidity and strength in the direction of loading, and provide breathability, moisture-wicking properties, and thermal conductivities that limit the thermal load on the body, while maintaining a vacuum-seal to reduce friction and improve pressure distributions, to make the prosthetic socket as 'invisible' as possible to the wearer so they forget it is there. A socket that can meet all these requirements is a distant reality. However, recent advances in simulations and monitoring provide additional information on the requirements of an ideal prosthetic socket and 3D printing technology enables this data-driven design process to link directly into the manufacturing process, providing possibilities for patient-specific device development. The development of a variable-impedance prosthetic socket demonstrated proof-of-concept for changing the material properties according to individual anantomy,[58] but it used a multi-material 3D printer, which creates weak boundaries between materials and the materials typically degrade under heat and UV lighting.[219] An emerging area of research is the development of varied 3D-printable microstructures that create different macro-material properties from a single printing material, overcoming the issues of multimaterial printing.[220] Current 3D printers typically print using a homogenous layer-by-layer method, but revolving axis printers, tilted beds and options for programming the directions of the printing over time can create new material structures and properties. An area for future research is the development of 3D-printable microstructures to provide variation across the socket in mechanical strength to meet dynamic loading requirements, breathability and thermal coefficients to improve thermal comfort, and elasticity to enable the socket to respond to changes residual limb size and shape, along with developing smooth, durable transitions between these printed structures to ensure the structural integrity of the sockets. Smart material printing, where the material properties change with a stimulus, may provide solutions such as enabling the prosthetic socket to have holes for breathability under loading

and to provide a vacuum seal when lifting the leg in swing phase. These 3D printing material properties can then be used as constraints within multiphysics simulations to develop the optimised prosthetic socket designs for individuals.

5.1.3. CAD/CAM for developing countries

Another issue with current artisanal manufacturing methods of developing prosthetic sockets is that they are time, cost and skill-intensive. Due to ageing populations, the increase in vascular-related diseases, and the migration to cities increasing population density and with it, the occurrences of traffic accidents, the number of amputees is growing faster than the expansion of prosthetics services.[3] The World Health Organization estimates a global shortage of about 40,000 prosthetists.[7] A new digital manufacturing solution could improve worldwide access to high quality prosthetics.

The research presented in this thesis contributes to knowledge on the physiological responses of lower-limb amputees during physical activity. It also develops a computational model to simulate an amputee's physiological responses under varied exercise and environmental conditions; results that are challenging to obtain empirically. This improved understanding of device-user interactions can be used in the development of software to digitally and objectively optimise a prosthetic socket for an individual, to improve fit, comfort, tissue health and repeatability of the design and manufacturing process. Linking this computer-aided design method with 3D printing technology can reduce labour costs and increase access to prosthetics services because it is based on simple scans fed into simulation software, so healthcare workers with little prosthetics training can work on the ground, supported by prosthetists further afield via video calls.[65] This reduces the requirements for amputees to come into the city for months be fitted and rehabilitated with a prosthesis, and alleviates some of the workload on already overstretched prosthetists. This is particularly beneficial for people living in rural and remote communities, where it is often too expensive for amputees and their families to take time off work to travel to the city for prosthetic fitting, rehabilitation and maintenance.

Companies such as ProsFit[221] are already setting up support for this type of digitised prosthetic socket fitting system, working with countries such as India, to create 3D printed

prosthetic sockets. Due to the high quality of print required, they have centralised manufacturing facilities, but the customised fitting software allows orders for sockets to be sent from rural and remote locations and the sockets are posted to the clients. This overcomes issues of poor durability and manufacturing quality that are encountered when prostheses are created on consumer printers. Because digitising the design, manufacture and fitting processes can increase socket fit, possibly enable remote fitting, and can reduce the time and costs of fittings, computer aided manufacturing of prosthetics in developing countries has shown great increases in number of amputees fitted with prosthetics.[15]

5.1.4. Necessity of critically appraising 3D printed prosthetics

Because of the importance 3D printing could play in the development of data-driven customisation of prosthetic sockets, a systematic review of 3D printed limb prostheses that included a human trial was undertaken to understand the efficacy and effectiveness of current devices. For a new therapy to be accepted by healthcare regulatory bodies or recommended for reimbursement by insurance companies, its efficacy and effectiveness must be shown. *Efficacy* is defined as the performance of the device under ideal and controlled conditions, and *effectiveness* is defined as its performance under everyday conditions.[222] In reviewing the relevant literature, the level of evidence[223] and the quality of the study[224] can be assessed using published tools. In particular, this determines whether the reported trial is designed to ask an appropriate question that relates to how the device is to be used – i.e. *external validity* – and whether the study answers the research question in an unbiased way – i.e. *internal validity*.[225]

Most 3D printed prosthetic devices are for transradial or partial-hand amputations because these devices have less complexity than above-elbow devices, and arms, unlike legs, do not need to take high loading forces. Open-source databases such as E-Nable[226] and Open Bionics[227] have developed readily available 3D printed designs of prosthetic hands for printing on consumer printers. These allow amputees to modify, print and trial their own devices without requiring any specialist equipment.

When a prosthetic limb does not work as intended, it can cause a number of issues for the amputee. If it is unreliable, the user is likely to fear performing tasks with it, and therefore will not make use of it. If this unreliability results in device failure, this could cause harm.

For example, a load-bearing prosthetic leg socket splitting could cause a fall. Also, the weight, shape and function of the device can affect the compensatory movements of the user, which could create other health issues, such as back pain. It is therefore, important to assess and control the quality of prosthetic devices.

Despite the growing popularity of 3D printed prosthetics, no review of their efficacy and effectiveness has been carried out. This review aims to assess the evidence for the clinical efficacy and effectiveness of 3D printed prosthetic limbs by performing a systematic literature search, categorising studies by their level of evidence, and critically appraising their scientific quality.

5.1.5. Systematic review methodology

The systematic review of literature was performed using PubMed, Web of Science and OVID to find all relevant publications up to March 2019 that reported human trials of 3D printed prosthetics. The review follows the Preferred Reporting Items for Systematic Reviews and Meta-Analyses (PRISMA) guidelines.[228]

The 89 terms included in the search covered areas under three Medical Subject Headings (MeSH):

1. **Health care evaluation mechanisms**

"Randomized controlled" OR "randomised controlled" OR RCT OR "randomized control" OR "randomised control" OR "clinical trial" OR "clinical study" OR "clinical evaluation" OR "case-control" or "case control" OR "case study" OR "case report" OR "pilot study" OR efficacy OR effectiveness OR evaluation OR validation OR feasibility OR cohort OR observational OR longitudinal OR retrospective OR comparative OR exploratory OR subjects OR participant OR participants

2. **Printing, three-dimensional**

AND ("Printing, Three-Dimensional" OR ("three dimensional" OR "Three-dimensional" OR "3 Dimensional" OR 3D OR "3-D" AND (printing OR print OR printed))

OR “3D-printing” OR “3D-print” OR “3D-printed” OR “computer-aided manufacturing” OR stereolithography OR “laser melting” OR “electron beam melting” OR “fused deposition modeling” OR “fused deposition modelling” OR “selective laser sintering” OR “rapid manufacturing” OR “rapid prototyping” OR “layered manufacturing” OR “digital manufacturing” OR “3D prototyping” OR “3D fabrication” OR “rapid fabrication” OR “freeform fabrication”)

3. Prostheses and implants

AND (“prostheses and implants” OR prosthetic OR prosthetics OR prosthesis OR prostheses OR artificial OR bionic OR robotic

AND (finger OR hand OR wrist OR arm OR forearm OR “above-elbow” OR “below-elbow” OR toe OR foot OR Syme’s OR ankle OR leg OR “above-knee” OR “below-knee” OR calf OR thigh OR limb OR extremity OR transradial OR “trans-radial” OR transhumeral OR “trans-humeral” OR transtibial OR “trans-tibial” OR transfemoral OR “trans-femoral”))

The title and abstract of each publication were reviewed to assess whether the paper met the relevance inclusion criterion of reporting on a trial with human participants that tested a 3D printed external limb prosthesis.

A full-text review of the included studies was undertaken and any cited references that met the inclusion criteria were added. The studies were then rated according to their level of evidence, based on the Oxford Centre for Evidence-based Medicine (CEBM) Levels of Evidence (Table 5.1).[223]

Table 5.1. CEBM Levels of Evidence

Level	Types of study
1	Randomised controlled trials (RCTs)
2	Cohort studies
3	Case-control studies Poor quality estimates of data that include sensitivity analyses incorporating clinically sensible variations
4	Case-series studies
5	Case reports Studies that do not provide quantitative evidence to support a hypothesis

A summary of the included studies, including the type of device, details of participants and primary outcomes was tabulated, and the Downs and Black Quality Index was used to

critically analyse the studies under review.[224] It has 27 questions divided into 'reporting', 'external validity', 'internal validity' both in regards to bias and confounding, and 'power'. Instead of assigning weights to the items in the scale, the responses have been left in their raw form (yes/no/unable to determine/not applicable) and presented in a table to enable the reader to visualise the trends, as recommended by the Cochrane Handbook for Systematic Reviews of Interventions.[225]

5.1.6. Critical appraisal of 3D printed prosthetic device studies

After removing duplicates, 651 papers were identified. Of these, 31 met the relevance inclusion criterion. Another 3 papers were identified through the reference lists and forward citation reports from each database (Figure 5.1). The studies were then rated according to their level of evidence. All were small, non-randomised trials and though 7 studies compared the 3D printed device to a conventional prosthesis, only one had more than one participant and met the level 3 criteria for a controlled study. Twenty-eight studies were level 5, testing the prosthesis on a single amputee, only trialling the device with able-bodied participants, or providing no quantitative results (Figure 5.1).

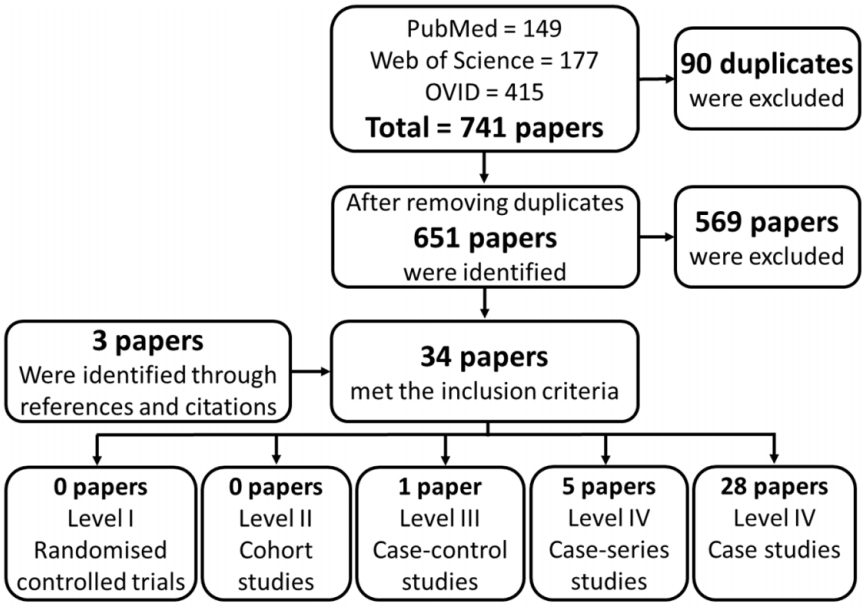


Figure 5.1 Flow chart of selection and sorting of 3D printed prosthetics studies

The 34 studies evaluated are summarised in Table 5.2. Most studies were of upper-limb devices: 13 were of prosthetic hands, 5 were of partial hands, 3 were of hand attachments

and 1 was of an above-elbow prosthesis. The lower-limb devices were mostly sockets, with 7 studies specifically on transtibial sockets, 1 included a transradial socket and a transtibial socket, and 1 mentioned both transfemoral and transtibial sockets but did not assess either. There was also a study on a titanium implant for an osseointegrated transtibial prosthesis, a study on a prosthetic knee component, and one on a prosthetic foot component.

Table 5.2. Summary of human trials with a 3D printed prosthesis

Author, date	Device	Participants	Aim	Outcomes
[229] Alvial, 2018	Partial hand prosthesis with silicone-embedded components	1 amputee Age: 51 Sex: M	To compare use of the 3D printed prosthesis to using no prosthesis using the Jebsen Hand Function Test.	The patient performed faster on daily tasks and completed more tasks when using the prosthesis than when not using any aid.
[230] Atallah, 2017	3D printed titanium transtibial osseointegrated implant	5 amputees Age: 56-84 Sex: 2 M, 3 F	To assess pain, time wearing the prosthesis, mobility, walking ability, quality of life and adverse events over 12 months.	At 12 months postoperatively, 4 patients were pain-free and all 5 were using the osseointegrated prosthesis. Two patients had a single episode of superficial soft-tissue infection.
[231] Belter, 2016	Body-powered below-elbow prosthesis	12 able-bodied participants Age: 18-36 Sex: 6 M, 6 F, 2 amputees Age and sex not provided	To compare the 3D printed Yale Multigrasp Hand to a split-hook hand and a voluntary closing hand with two active fingers using the Box and Blocks test and the SHAP test.	The three devices performed similarly ($p = 0.81$-0.86). The Yale Multigrasp hand was as effective as the commercial devices for able-bodied participants but scored lower for the amputees.
[232] Cañizares, 2017	Myoelectric below-elbow prosthesis	3 able-bodied participants. Age and sex not provided	To demonstrate the feasibility of using 3D printing to build a prototype of a myoelectric hand.	The 3D printed myoelectric hand was able to open, close, grip and hold.
[233] Faustini, 2005	Transtibial prosthetic socket with compliant features	1 amputee Age: 53 Sex: M	To compare pressure measurements recorded from three prototype SLS sockets with the same topology but differing levels of compliance.	The socket with the greatest compliance reduced the average and peak pressure by 22% and 45% at the distal tibia, respectively, and 19% and 23% at the fibula head, respectively.
[234] Gretsch, 2016	Robotic below-elbow prosthesis	1 amputee Age: 13 Sex: F	To design and test an inexpensive, externally powered 3DP prosthesis that does not require a functional wrist.	The patient said that the biggest advantages were the individual thumb movement, the ability to grasp objects with all fingers and the low weight compared to other externally powered prostheses.
[235] Herbert, 2005	Resin-coated transradial and transtibial prosthetic sockets	2 amputees Age and sex not provided	To demonstrate that it is possible to produce 3D printed sockets that patients find comfortable.	The patients felt that the 3D printed sockets were as comfortable as those made by traditional methods.
[236] Hofmann, 2015	Prosthetic hand customised attachments	2 amputees Age: 9 and 27 Sex: 1 M, 1 F	To test the process of prototyping customised prosthetic hand attachments.	The process produced customised and affordable attachments for different prosthetics.
[237] Hofmann, 2016	Prosthetic hand customised attachments	3 amputees Age: 9, 27, 47 Sex: 2 M, 1 F	To understand the requirements for end user involvement in rapidly prototyping task-specific prosthetic attachments.	Co-designing customised attachments for different prosthetics resulted in unique devices that met participants' needs.
[238] Hsu, 2010a	Polyester resin-coated prosthetic transtibial socket	1 amputee Age: 59 Sex: M	To measure the pressure distribution in the socket.	Interface pressures exerted on the socket were similar to other sockets presented in literature during the stance phase.

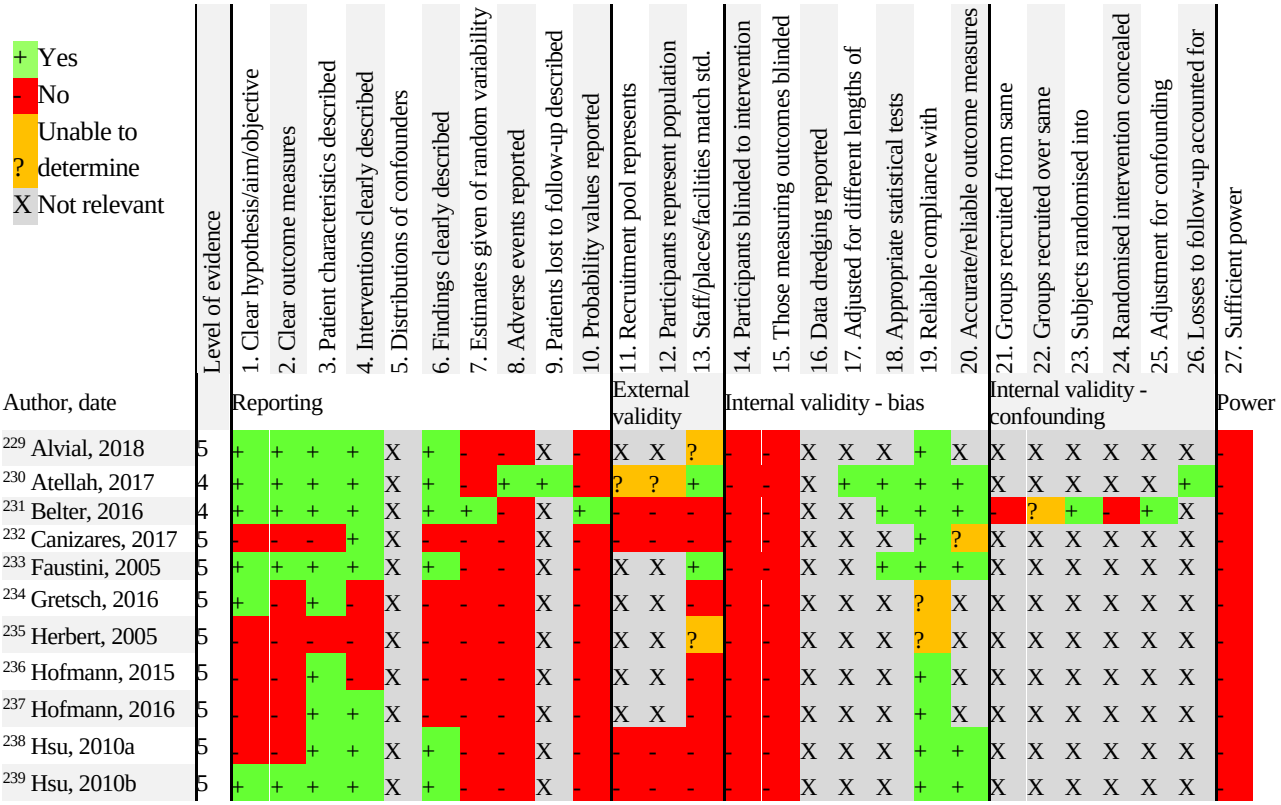
[239] Hsu, 2010b	Polyester resin-coated prosthetic transtibial socket	1 amputee Age: 61 Sex: M	To compare a conventional plaster-cast socket with two resin-enhanced 3D printed sockets on pressure distributions while walking.	The 3D printed sockets produced higher pressures on the residuum's pressure-tolerant areas and lower pressures elsewhere, compared to the conventional socket.
[240] Hsu, 2018	Polyester resin-coated prosthetic transtibial socket	1 amputee Age: 26 Sex: M	To compare a conventional socket with a resin-enhanced 3D printed socket on gait, pressure distributions and user satisfaction.	The conventional socket outperformed the 3D printed socket on gait, pressure distributions and user satisfaction.
[241] Jacobsen, 2016	Realistic prosthetic hand from 3D scan	Researcher tested but no participants or information	To assess the feasibility of creating a low-cost reverse-engineered prosthesis from a scan of a human hand.	The hand opened and closed but was unable to pick up small or smooth objects.
[242] Jeong, 2017	Myoelectric below-elbow prosthesis	5 amputees Age: 40-67 Sex: 4 M, 1 F	To compare functional outcome measurements after one month using the low cost myoelectric prosthetic hand to pre-treatment functionality.	The functional outcome measurements after a month obtained using the Orthotics Prosthetics User Survey [OPUS])2 demonstrated improved function compared to pre-treatment scores.
[243] Kontoudis, 2015	Robotic hand	1 able-bodied participant. Age and sex not provided	To test the efficacy of the hand design through experimental paradigms involving gestures and grasping of objects.	The fingers could move independently using a single motor, and the user was able to grasp objects of varied sizes and shapes.
[244] Lee, 2017	Pressure-sensored prosthetic hand (conventional PP socket)	1 amputee Age: 52 Sex: M	To compare a pressure-sensored hand with a conventional myoelectric hand on a standard suite of upper-limb function tests.	The 3D printed hand showed lower grip strength and decreased dexterity compared to the conventional myoelectric prosthesis.
[245] Lee, 2018	Silicone thumb prosthesis	1 amputee Age: 67 Sex: M	To compare hand function with and without the prosthesis using a standard suite of hand function tests.	All but one of the functions tested improved after applying the prosthesis.
[246] Low, 2015	Soft pneumatic finger actuator	5 able-bodied participants Age: 25±2.5 Sex: 3 M, 2 F	To evaluate the capability of the soft actuators to grasp and hold different sizes and weights of objects.	The prototype was able to grasp the four items firmly, move them in all three axis directions and rotate the objects 90°.
[247] Nabeel, 2016	Vibrotactile feedback for a 3D printed prosthetic hand	1 amputee Age: not provided Sex: M	To see whether the participant preferred the hand with or without vibrotactile sensation.	The participant preferred having vibrotactile sensation.
[248] Rajestari, 2017	One-DoF SLA prosthetic finger	1 amputee Age: not provided Sex: M	To grasp and lift circular objects of varying diameters.	The object contact with metacarpals was lost when grasping small objects, and the low coefficient of friction of the material made the grasping unstable.
[249] Ramakrishnan, 2017	Prosthetic knee	1 amputee Age: 37 Sex: F	To compare a 3D printed knee to the Ossur Total Knee 2000 using motion capture and force plate data collection.	The participant had longer step times on both legs, higher peak flexion, and the average peak knee angle asymmetry of the 3D printed knee was larger when using the 3D printed knee than when using the Ossur Total Knee.
[59] Rogers, 2007	SLS transtibial sockets (TSB and PTB)	4 amputees Age and sex not provided	To compare the biomechanics of an SLS socket to a conventional socket after two weeks of wearing.	There were no significant differences between conventional and SLS sockets in biomechanics or comfort. One SLS socket failed.

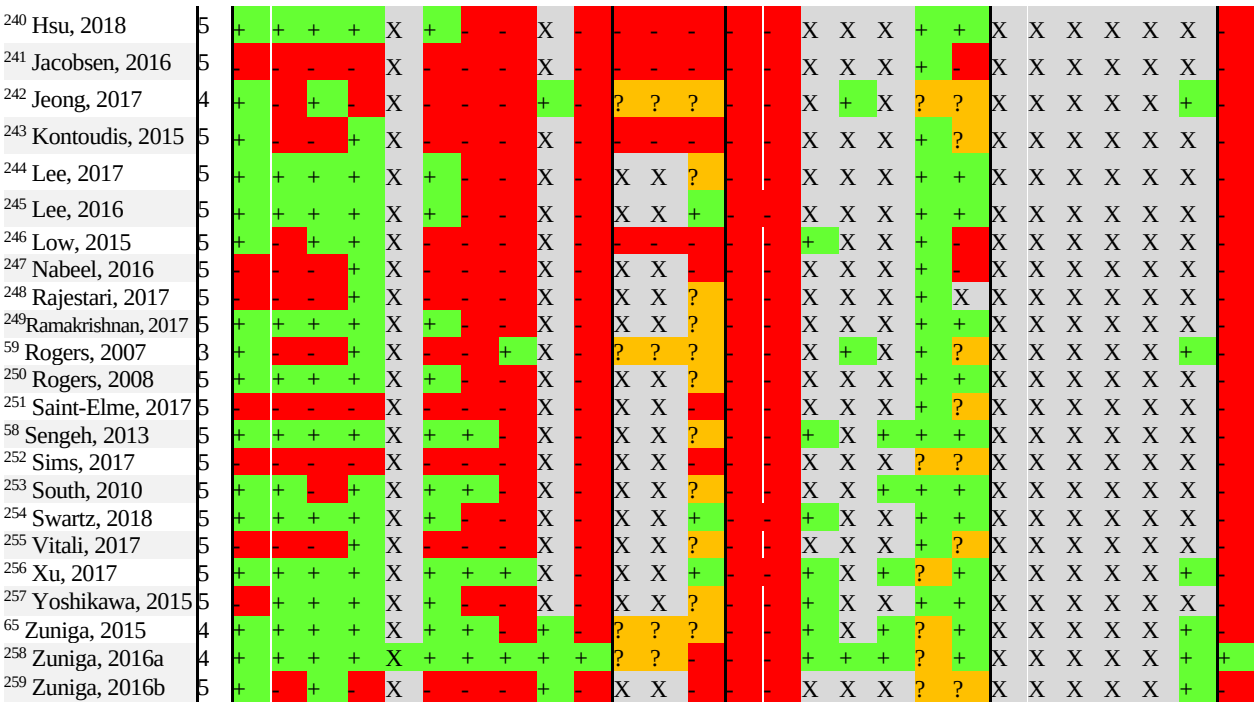
[250] Rogers, 2008	Transtibial prosthetic socket with compliant features	1 amputee Age: 47 Gender: M	To compare pressure measurements recorded from three prototype SLS sockets with the same topology but differing levels of compliance.	The more compliant the socket, the faster the cadence and walking speed, and the lower the pressure over the distal tibia and fibula head.
[251] Saint-Elme, 2017	EEG/EMG controlled hand based on bone, ligament and tendon structures	3 participants Age and sex not provided	To assess the success rate of activating hand motions using EEG and EMG.	EMG actuated the hand with an 80% success rate, while EEG actuated the hand with a 68% success rate.
[58] Sengeh, 2013	Transtibial prosthetic socket with compliant features	1 amputee Age: not provided Sex: M	To compare the 3D printed socket with a conventional state-of-the-art carbon prosthetic socket on interface pressures and gait.	Peak contact pressures at the device-user interface were lower for the 3D printed socket compared with the conventional socket (17% and 15% reduction on the fibula head region for the first and second peaks, and 8% and 7% reduction along the tibia). Preferred walking speed was faster using the 3D printed socket (0.84 m/s instead of 0.72 m/s).
[252] Sims, 2017	Pediatric specific-task terminal devices prototyped using 3D printing	8 amputees Age: 8-15 Sex: 4 M, 4 F	To get end-user input into design and qualitative evaluation of terminal device designs.	Several prototypes were developed of task-specific prosthetic devices that are suitable for further development and refinement.
[253] South, 2010	SLS elastic energy storage and return foot	1 amputee, Age: 45 Sex: not provided	To compare kinetic and kinematic data between carbon fibre and SLS feet.	The SLS framework produced prosthetic feet with mechanical properties that were similar to the carbon fibre foot properties.
[254] Swartz, 2018	Voluntary-closing body-powered thumb	1 amputee Age: 50 Gender: M	To evaluate the effectiveness of the device using the Box and Blocks Test and the Patient-Specific Functional Scale	Prior to device use, the participant was unable to grasp items and rated tasks as 0/10 (unable to perform), but with the prosthesis he moved 23 blocks in 1-minute and rated tasks as 5/10 (moderate difficulty).
[255] Vitali, 2017	Transtibial and transfemoral prosthetic sockets	A few case studies, no information provided	To assess the feasibility of digitising socket design and manufacture using 3D printing.	The initial results suggest this design method may improve digitisation of the socket design and manufacturing process.
[256] Xu, 2017	Child's wrist activated voluntary-closing hand	1 amputee Age: 8 Sex: M	To test function at 1 and 3 months follow-up using the CAPP score and UNB test.	At 3 month follow-up, CAPP-PSI score was 35, CAPP-FSI score was 28, and UNB spontaneity and UNB skill scores increased ($p<.001$).
[257] Yoshikawa, 2015	Electric below-elbow prosthesis	1 amputee Age: 40s Sex: M	To assess whether the Rehand enabled an amputee to do everyday activities, using the Southampton Hand Assessment Procedure.	All light-object tasks were completed in 100 seconds. For heavy-object tasks, the sphere task and the lateral task were unable to be completed. Most Activities of Daily Living tasks were completed, but those that required fine manipulation were not.
[65] Zuniga, 2015	Child's wrist activated voluntary-closing hand	11 amputees Age: 3 to 16 Sex: 7 M, 2 F, 2 information not provided	To test a prosthesis fitting methodology that can be performed at a distance.	No differences were found between the anthropometric and range-of-motion measurements taken directly from the upper limbs of subjects versus those extracted from photographs.
[258] Zuniga, 2016a	Child's wrist activated voluntary-closing hand	5 amputees Age: 3 to 10 Sex: 3 M, 2 F	To identify anthropometric, range of motion (ROM) and strength changes after using the prosthesis for 6 months.	Forearm circumference increased ($p=0.02$), as did ROM for flexion ($p=0.02$) and extension ($p=0.04$). No change was found for wrist flexion, extension strength or ROM for ulnar or radial deviation ($p>0.05$).
[259] Zuniga, 2016b	Mechanical shoulder prosthesis	1 amputee Age: 7 Sex: M	To test whether an inexpensive mechanical shoulder prosthesis could assist an amputee in performing bi-manual activities.	A partial correction of the patient's spinal deviation was noted due to the counterweight of the device. The family reported improved balance and performance of some bimanual activities after 2 weeks.

Of the 7 studies that compared the 3D printed prosthetic device to a conventional device, 5 had only a single participant, and the study by Belter et al.[231] tested 12 able-bodied participants, using a bypass socket, to compare the 3D printed hand to a commercial hand. Because participants were able-bodied, the study did not fit the CEBM Levels of Evidence criteria for a control study. The largest comparative study with amputees was by Rogers et al.,[59] where 4 participants wore a conventional transtibial socket for 2 weeks and a 3D printed socket, designed to be identical in fit to the control socket, for two weeks. Within the two-week period, one of the 3D printed sockets fractured.

The studies that evaluated 3D printed sockets assessed pressure distributions, biomechanics, and walking speed with mixed outcomes. Eight of the upper-limb device studies evaluated the function of the terminal device using standard hand assessment procedures which showed that the participants performed tasks faster and more accurately with a prostheses than without one, and improved in the months after fitting it, but the two devices that were compared to conventional devices scored lower on grip strength, dexterity, time and ability to complete grasp-and-release tasks than their conventional counterparts.[231,244]

Table 5.3. Critical appraisal of 3D printed prosthetic device studies





A critical appraisal of the studies shows that no studies blinded the participants or those measuring the outcomes to the intervention, or demonstrated external validity (Table 5.3, with abridged Quality Index questions). Seven studies included short-term follow-up but only one had sufficient power to detect a clinically important effect.

5.1.7. Outcomes and limitations of studies

Outcomes reported were mainly on 3D printed device kinematics, especially of prosthetic hands. Qualitative functional assessment was highly positive across studies. Despite this, the two upper-limb terminal devices that were compared to conventional devices performed worse.[231,244] This may be due to them being prototype devices, rather than well-established commercial products, and is possibly also because the participants were already familiar with using some of the commercial products.

The 3D printed lower-limb sockets that were compared to conventional sockets reduced pressures at the load-sensitive areas and sometimes improved gait symmetry and walking speed.[58,239] They also found that increasing compliance of the socket improved the pressure distribution and gait.[233,250] However, the 3D printed knee and foot components showed similar or worse biomechanical gait properties than their conventional equivalents.[249,253] Rogers et al.[59] had one of 4 sockets fail due to poor manufacturing strength, and Sengeh et al.[58] increased the thickness of the socket substantially, adding significant weight, to provide

the required strength. Lee et al.[244] found that the 3D printed hand had low grip strength, and only one report of an above-elbow prosthesis was found,[259] potentially reflecting the difficulty of meeting the basic strength requirements. Only one study followed up 6 months after fitting the prosthesis, and this study reported that 3 of the 5 devices broke or malfunctioned in this time-period,[258] so there is limited information on durability and wear of the devices and signs of brittleness and poor durability. 3D printed material is highly anisotropic, with different mechanical properties depending on loading direction, and prosthetics are subjected to complex, cyclic loading. The strength of 3D printing is typically lower than an injection moulded equivalent.[260] 3D printing materials and designs need to be carefully chosen in order to ensure that they have the necessary strength and durability to support everyday use.

A key benefit to using 3D printing for medical applications is its ability to print devices customised to the patient. Most of the studies customised the overall size of device for the participant. However, research into using 3D printing to support a data-driven approach to customisation, such as feeding information from simulations, scans or sensors into the digital model to improve comfort or to match the limb shape to the contralateral one, have only been minimally explored.[58,59] Before the potential of 3D printing to improve personalisation can be realised, the sensors and predictive models that provide quantitative input into the design of the socket must be developed. One study showed no significant mean difference between anthropometric measures taken on the subject's arm and those taken from photographs, suggesting that there may be potential for remote fitting of 3D printed prostheses. However, they made no assessment of the outcomes of fittings provided in this way.[65] The main reported advantages of 3D printing from the studies were low manufacturing costs for one-off prints, ease-of-access for the researchers, customisability, and options for making the designs open-source.

Non-trained professionals frequently provide 3D printed prosthetics services, often resulting in poor fit, inadequate rehabilitation support and secondary complications.[2] There is a danger that users who self-print their device may not receive the support they require to maximise their function.[261] Also, given the brittleness of many of the devices presented in this review, the material choices and printing processes require more consideration and

durable designs are unlikely to be able to be printed on low-cost consumer 3D printers. Therefore, the implementation of any 3D printing prosthetics service will require careful design and monitoring.

Although 3D printed devices have already demonstrated some benefits over conventional prosthetics, particularly in the area of customisable prosthetic socket design, the studies remain under-powered and lack internal and external validity. Therefore, the results and conclusions of the studies must be used with caution. A large number of 3D printed prosthetics exist that have not been clinically trialled, and many of the papers presented in this review come from the same research groups, reporting on the same devices as one another. Therefore, the body of evidence is smaller and less representative of the field than it initially appears.

Providing a critical appraisal of the efficacy and effectiveness of 3D printed devices gives healthcare professionals a resource to assess the validity of the devices, and provides researchers with an overview of areas that require further research and validation. Comparing a device to current devices and procedures, and understanding the long-term implications of the device's use is important for validating the device and ensuring best patient outcomes. The studies in this review mainly focused on describing the designs and providing a limited assessment of their functionality rather than assessing the devices' clinical efficacy and effectiveness. No papers presented randomised controlled trials, and there was not enough data to perform a meta-analysis to assess the efficacy of 3D printing for limb prosthetics. It is therefore imperative that before 3D printed prostheses are widely promoted and distributed, randomised controlled trials of the efficacy and effectiveness of using 3D printed devices are performed with long-term follow-up. The field is young and fast-growing, with more than 75% of the reviewed manuscripts having been published between 2015 and 2018. The 3D printing industry is likewise growing substantially, with broader options becoming available for materials and printing processes, which holds promise for overcoming the issues of current 3D printed prosthetic designs. Therefore, it is recommended that this review be updated in a few years to better understand the possibilities provided by 3D printing technologies.

5.2. Clinical efficacy and effectiveness of 3D printing

5.2.1. Overview of 3D printed medical devices

The systematic review that was focused on 3D printed prosthetics assessed all studies that include a human trial, regardless of whether they assessed device efficacy. This is because so few papers provided an assessment of the efficacy and effectiveness of 3D printed prosthetic limbs. Because using 3D printing for prosthetics is a new field with limited clinical evidence to support it, it is worthwhile understanding how 3D printing technologies are influencing personalised healthcare in other medical fields. A broader systematic review was undertaken to assess the efficacy and effectiveness of 3D printed patient-specific medical devices across all medical fields so the findings could be translated to the field of prosthetics to provide insight into what makes a patient-specific 3D printed device successful and to assess whether 3D printing is suitable for supporting a data-driven approach to the design of prosthetic sockets.

Due to the rapidly advancing improvements to 3D printing technologies in print quality and material options, 3D printing is likely to play a pivotal role in transforming healthcare and clinical practice because it provides the opportunity to create customised devices designed for the complexity and individual variances of the patient populations.[262] Many medical fields use 3D printing to manufacture custom surgical tools, guides, dose delivery devices, implants, external prosthetics or orthotics, and devices for preoperative planning or education.[215,263,264] Tailoring devices and procedures to the patient is expected to reduce the time required for surgery, treatment or recovery, while increasing the accuracy and success of the outcome.[262] The worldwide 3D printing industry's revenue from products and services is over $4 billion and fast-growing, with 13.1% of the industry attributed to the medical sector.[265]

In most medical fields, 3D printing applications are still in the research and development stage or have only just entered clinical practice within the last decade, and hence there has been a lack of research into the clinical efficacy, effectiveness and long-term follow-up in

comparison to traditional technologies.[266] The Food and Drug Administration (FDA) states that 3D printed medical devices are required to meet the same regulations as their non-3D printed counterparts. Because 3D printed devices can have different safety and efficacy issues than the equivalent devices, additional testing may be required to demonstrate safety, efficacy and effectiveness.[267] Hospitals and clinics will need to adopt new medical product procedures when they want to introduce 3D printing for healthcare, and more evidence of device efficacy and effectiveness will help make an informed discussion before prescribing 3D printed devices for patients. Providing a critical appraisal of the efficacy and effectiveness of 3D printed medical devices gives healthcare professionals a resource to assess the validity of the devices, and provides researchers with an overview of areas that require further research and validation.

Previous systematic reviews summarise 3D printed medical devices being used in specific medical fields, such as plastic and reconstructive surgery,[268] preoperative planning for liver resections,[269] and increasingly available 3D printing processes used in dentistry and mandibular reconstructions.[270–272] Systematic reviews on the advantages of 3D printed devices over conventional methods in surgery have found improved clinical outcomes, and reductions in operating times and manufacturing costs.[264,273] However, the reviews do not critically appraise the studies, and are therefore subject to bias. The only systematic review that did assess bias for a very specific field found no difference in patient outcomes when 3D printed instrumentation for total knee replacements was compared to conventional instrumentation.[274] This highlights the need for a systematic review that incorporates a critical appraisal of the studies that are included.

This review aims to assess the clinical efficacy and effectiveness of 3D printed devices through performing a systematic literature search, categorising reports of 3D printed device usage by medical field and purpose, and assessing the reports' scientific quality. The key findings of studies that compare 3D printed medical devices to their non-3D printed counterparts are presented, and the gaps in research highlighted.

5.2.2. Systematic review methodology

5.2.2.1. Search strategy

The applied protocol used systematic methods to search for relevant studies, screen them for eligibility, and assess their quality. The review follows the Preferred Reporting Items for Systematic Reviews and Meta-Analyses (PRISMA) guidelines.[275]

A literature search was performed using PubMed, Web of Science, OVID, IEEE Xplore and Google Scholar. A combination of 45 relevant keywords were used to collect all studies that included a 3D printed device and a clinical trial (Table 5.4). Due to the word and character limit search restrictions in IEEE Xplore and Google Scholar, a narrower search of 15 terms was performed for these databases. The search includes all publications up to January 2017.

Table 5.4. Systematic literature search method for 3D printed medical devices

1. database search		***IEEE Xplore and Google Scholar required a simplified search.***				
	Database	PubMed (All article types)	ISI Web of Science (Article, review, case report, clinical trial, book or report)	OVID (Journal OR book)	IEEE Xplore (All article types)	Google Scholar (Exclude patents and citations)
	Search Term	"**health care evaluation mechanisms**" OR "randomized controlled trial" OR "randomised controlled trial" OR "clinical trial" OR (efficacy OR effectiveness OR validation OR validity OR feasibility OR cohort OR observational OR longitudinal OR retrospective OR comparative OR "exploratory study" OR "case-control study" OR "case study" AND (clinical OR medical OR hospital OR biomedical OR assistive OR "health care" OR patients OR patient)) AND ("**Printing, Three-Dimensional**" OR "Three Dimensional Printing" OR "Three-Dimensional Printing" OR "3 Dimensional Printing" OR "3D Printing" OR "3-D Printing" OR stereolithography OR "laser melting" OR "electron beam melting" OR "fused deposition modeling" OR "fused deposition modelling" OR "rapid manufacturing" OR "rapid prototyping" OR "layered manufacturing" OR "digital manufacturing" OR bioprinting OR "3D prototyping" OR "3D fabrication" OR "rapid fabrication" OR "freeform			randomized controlled trial OR "clinical trial" OR (efficacy OR validation OR feasibility OR "case study" AND (clinical OR medical OR hospital OR assistive OR "health care")) AND ("Three Dimensional Printing" OR "3D Printing" OR "rapid prototyping" OR "additive manufacturing")	"randomized controlled" OR "clinical trial" efficacy OR validation OR feasibility OR "case study" clinical OR medical OR hospital OR assistive OR "health care" "Three Dimensional Printing" OR "3D Printing" OR "rapid prototyping" OR "additive manufacturing"
	Number of studies	913	700	1158	754	980
					Number of studies: 4505	
2. Duplicate removal		***The first four databases were combined, then relevant additional results from Google Scholar were added.***				
					Number of studies: 3084	

5.2.2.2. Study selection

After removing all duplicates from the databases, the title and abstract of each publication was reviewed to determine eligibility for inclusion.

The inclusion criteria were:

- Relevance - papers were required to report first-hand on the results of a clinical study that assessed the efficacy and effectiveness of a 3D printed device.
- Language - only papers written or translated into English were included in the review.
- Peer-review - records that had no peer-review or where the level of peer-review could not be traced were excluded from the review.

Included articles underwent a full-text review and references cited in these studies were also examined for relevance using the same inclusion criteria.

5.2.2.3. Quality assessment

The studies were then rated according to their level of evidence, based on the Oxford Centre for Evidence-based Medicine (CEBM) Levels of Evidence.[223] Systematic reviews and opinion papers were excluded because they cannot provide the original data in a suitable format to be assessed using the quality assessment method used in this review. Where studies used 3D printed devices but the hypothesis, aim or objective was focused on an outcome other than the effect of the 3D printed device, the paper has been graded as the level of evidence shown for the device. All levels of evidence were included in the review but only those that used a control group (Levels 1 to 3) were critically analysed.

Studies were then placed in medical fields based on the International Classification of Diseases (ICD) chapter divisions[276] and categorised by the purpose of the device. The three categories were; devices used for preoperative planning, devices to aid surgery, and therapeutic devices.

To analyse the quality of the studies under review, critical appraisal tools were assessed to find one that met the following criteria:

- Suitable for assessing the quality of both randomised and non-randomised studies,
- Well-regarded and commonly used for quality assessments in systematic reviews.
- Demonstrates internal consistency, test-retest reliability and criterion validity.
- Assesses the risk of bias, the participant selection methods, the study protocol, and the validity, reliability and responsiveness of the study’s results.

- Simple and intuitive to interpret.
- Does not assign weights to the items in the scale where there is a lack of empirical evidence to support the assignment.[225]

The Downs and Black Quality Index[224] meets all but the final criterion on this list. To overcome this limitation, responses have been left in their raw form (yes/no/unable to determine/not applicable, in accordance with the definitions provided by Downs and Black[224]) and presented in a table to enable the reader to visualise the category trends, as recommended by the Cochrane Handbook for Systematic Reviews of Interventions.[225]

The study details and data relating to the quality of study design and reporting were manually extracted from each paper by one reviewer (LD). The study details included medical field, study design, device category, device purpose, number of participants, age and gender of participants, and aims and outcomes of the study. The data relating to study design and reporting were extracted according to the criteria used by the Downs and Black Quality Index, divided into reporting, external validity, bias, confounding and power. Where there were uncertainties as to how the study fitted with the Downs and Black Quality Index criteria, the other two authors were consulted and in all cases, an agreement was reached.

5.2.3. Critical appraisal of randomised controlled trials

The search yielded 4505 records and, after removing duplicates, 3084 abstracts were screened. A total of 350 studies met the inclusion criteria and were included in the review (Figure 5.2).

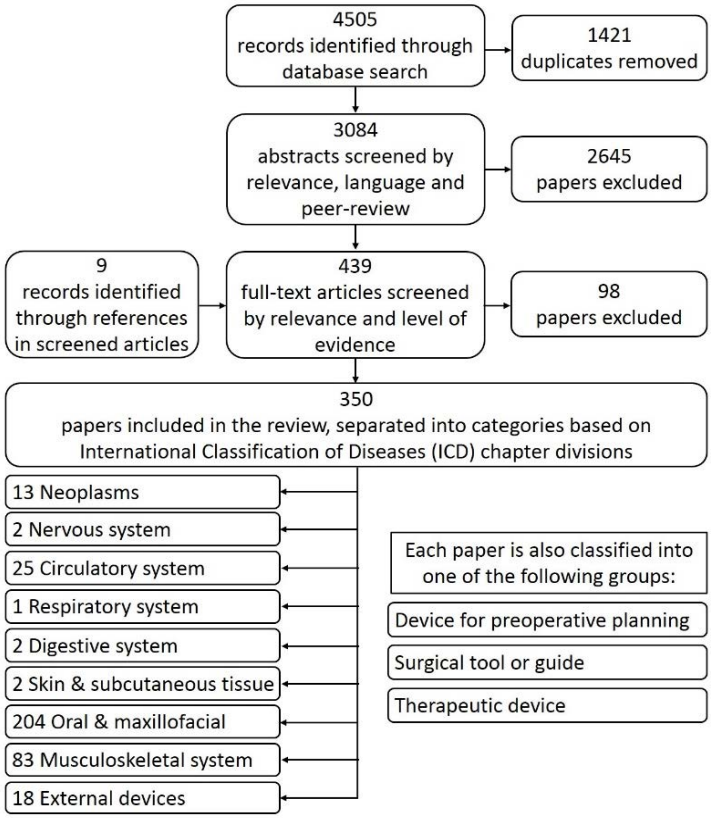


Figure 5.2. Flow chart of selection and sorting of 3D printed medical device studies

Due to the large number of included studies, this chapter gives an overview of the level of evidence found for 3D printed medical devices in each medical field and then focuses on the outcomes of the Level 1 studies, with a brief overview of the content and quality of Level 2 and 3 studies.

A wide range of 3D printed devices have been developed and clinically trialled. The most common device types were anatomical models for preplanning surgeries (40.9%), followed by guides to aid in surgery (37.1%). The studies covered 9 medical fields, with the majority (58.3%) of studies falling into the Oral and Maxillofacial Surgery field, which included dentistry and orthopaedic surgery of the jaw, face and skull, and those covering the Musculoskeletal System (23.7%) making up the second group. Some studies spanned multiple medical fields, such as neoplasms that occur in the circulatory system. In these cases, the most prominent field of the paper was selected. Only 14.0% of included studies used a control group (Levels 1 to 3 in Figure 5.3), whereas 41.4% were level 5 studies. The average number of participants per controlled trial was 41 (36 for RCTs), compared to 17 for all studies.

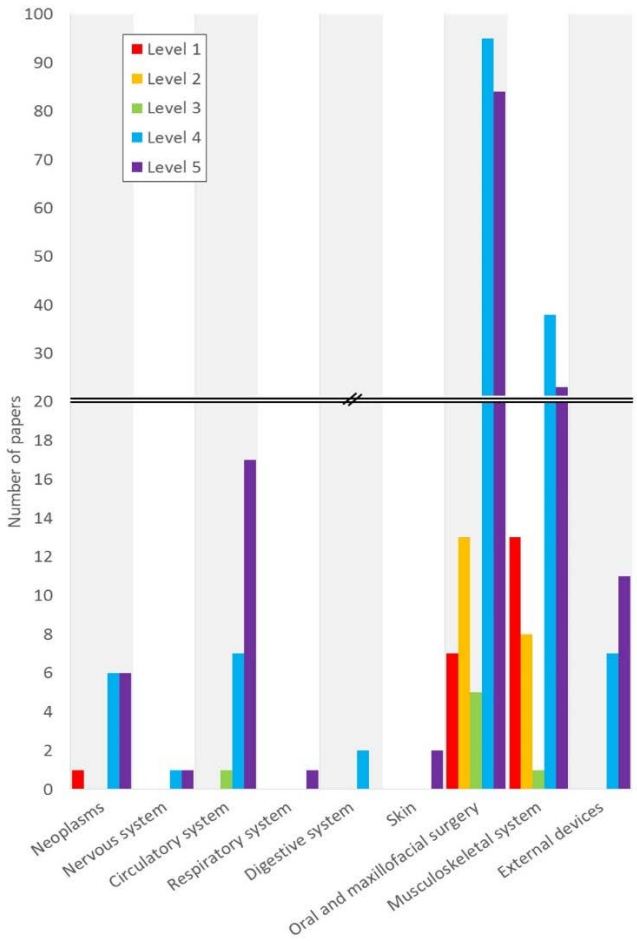


Figure 5.3. Number of studies per level of evidence given by medical field.

Levels of evidence are colour coded and fields are visually separated by alternating between white and grey columns.

All 21 Level 1 studies fell within the Oral and Maxillofacial Surgery or Musculoskeletal System categories, with one cross-field study fitting in both Oral and Maxillofacial Surgery and Neoplasms (Table 5.5 summarises all RCTs). All Level 1 studies, with the exception of Stephens et al.,[277] used objective measures as their indicators of device efficacy and effectiveness. Of these, the 7 models used for preoperative planning were all modelling bone or fracture fixation plates, though the locations spanned skull, face, mandible, arm, spine, hip and ankle. All aimed to assess the effectiveness of using the models for surgical planning in treating specific conditions. Six out of 7 studies used operating time, 4 used accuracy of the surgery and 3 used blood loss as key indicators of device effectiveness. Aesthetics, recovery time and post-surgery function were also used as indicators of device effectiveness. All Level 1 studies of 3D printed models for preoperative planning that used time, accuracy

or blood loss as indicators of device effectiveness reported that the test group had better outcomes than the control group, with statistical significance at $p<0.05$ found for 4 studies that assessed operating time, 3 studies that assessed accuracy, and 2 studies that assessed blood loss. The two studies that assessed recovery time found no difference between groups, one of the two studies that assessed user function found statistically significant differences in the test group, and the other found no difference between groups.

Of the 11 RCTs that assessed 3D printed guides or templates that supported navigation and surgery (of the mandible, teeth, shoulder, spine, hip or knee), 9 studies used accuracy of positioning as an indicator of device effectiveness, all of which found an improvement when using the guide or template, and 8 of which showed statistically significant results at $p<0.05$. All 4 studies that used time as an indicator of device effectiveness showed decreased operating times when using the guide or template (all with $p<0.05$), and 5 of the 6 studies that used changes at the operation site (blood loss, inflammatory response, tactile sensation or aesthetics) found statistically significant improvements at $p<0.05$.

Only 3 therapeutic devices were tested using RCTs. These were zirconia crowns, which were found to have a better marginal gap and internal fit than the conventional crowns tested ($p<0.05$), cranial implants, which showed less vertical ridge resorption over time ($p<0.05$), and osteosynthesis plates for intercondylar humeral fractures, which showed a reduction in operating time ($p<0.05$) but no difference in elbow function during recovery.

While most Level 1 studies found statistically significant improvements at $p<0.05$ when using the 3D printed device, none performed an analysis on the clinical relevance of these improvements.

Table 5.5. Summary of RCTs

(Type: P = preoperative planning, S = surgical tool or guide, T = therapeutic device)

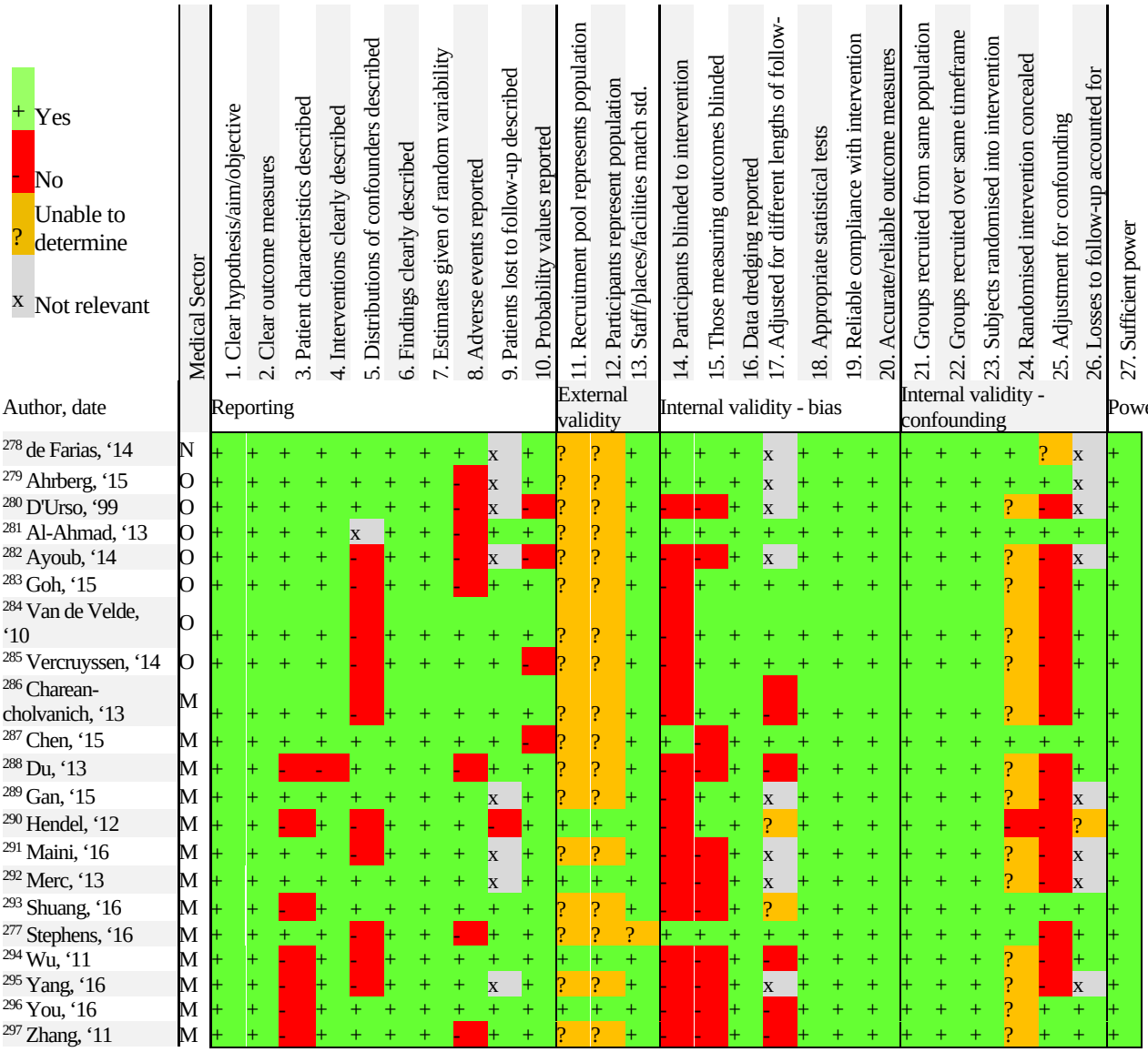
Sector	First author, date	Device	Type	Size (n)	Participant details	Aim	Outcomes
Neoplasms	[278] de Farias, 2014	Mandible model	P	37 (Test = 17, Control = 20)	Age: 9 to 74 years (Test mean = 39.57 years, Control mean = 53.11 years). Test = 14M/3F, Control = 15M/5F	Aim: to evaluate the efficacy of using 3D printed models to plan head and neck surgeries.	Reconstruction time decreased; Test = 43.7 mins, Control = 127.7 mins, p = 0.001. Though statistical significance was not demonstrated, the size of the bone flap taken for reconstruction was typically smaller, and the aesthetic results better in the test group.
Oral and Maxillofacial	[279] Ahrberg, 2015	All-ceramic zirconia crowns	T	25 (Same participants used for test and control)	Age: >18 years 10M/15F	Aim: to evaluate the marginal and internal fit of 3D printedzirconia crowns and three-unit fixed dental prostheses resulting from direct versus indirect digitalization.	The marginal gap was smaller; Test = 61.08 ± 24.77 μm, Control = 70.40 ± 28.87 μm, $p<0.05$, and the fit was better at the centro-occlusal site; Test = 155.57 ± 49.85, Control = 171.51 ± 60.98, $p<0.05$. The fit improved at the mid-axial wall and axio-occlusal transition but the results lacked statistical significance.
	[280] D'Urso, 1999	Cranio-maxillofacial model	P	30 (Test = 15, Control = 15)	No information provided	Aim: to assess whether biomodels in addition to standard imaging have greater utility in patient education, diagnosis and operative planning than the standard imaging alone.	3D printed models improved operative planning accuracy; Test = 82.21%, Control = 44.09%, $p<0.01$ and diagnosis accuracy; Test = 95.23%, Control = 65.63%, $p<0.01$. Measurement accuracy improved; Test error = 7.91%, Control error = 44.14%, $p<0.05$). Surgeons estimated that operating time over 45 operations was also reduced by 17.63%.
	[281] Al-Ahmad, 2013	Surgical guide for sagittal splitting ramus osteotomy	S	8 (One side used as test, the other as control)	Age: 18-30 years (mean = 23 years)	Aim: to evaluate the effectiveness of sagittal splitting ramus osteotomy in reducing the incidence and severity of neurosensory alterations, using a 3D printed surgical guide.	The Semmes–Weinstein monofilament tactile threshold was considered abnormal at >2.83 on the χ^2 test. At 1 week after surgery; Test = 67% abnormal, Control = 83% abnormal. This difference showed statistical significance ($p<0.05$) at 3 months post-surgery for chin and 6 months post-surgery for lower lip. For the two-point discrimination, the lower lip showed statistical significance at 1 week (Test = 9 mm, Control = 22 mm), and the chin at 6 months (Test = 11 mm, Control = 30 mm).
	[282] Ayoub, 2014	Guide for mandibular reconstruction	S	20 (Test = 10, Control = 10)	Age: Test = 52.3 ± 19.2 years, Control = 54.7 ± 14.2 years). Test = 4M/6F, Control = 6M/4F	Aim: to evaluate the benefits of computer-assisted mandibular reconstruction with iliac crest bone grafts regarding the intraoperative time for transplant shaping, ischemia, duration of surgery, amount of bone removed and the change in postoperative condyle position compared to conventional surgery.	Computer-assisted surgery shortened the time of transplant ischemia; Test = 96.1 ± 15.8 mins, Control = 122.9 ± 20.4 mins, $p<0.005$, and defect reconstruction; Test = 6.2 ± 4.9 mins, Control = 20.3 ± 7.4 mins, $p<0.001$. There was less bone harvested; Test = no difference regarding defect size, Control = 16.8 ± 5.6 mm larger transplant size than defect size, $p<0.001$. The intercondylar distance before compared to after surgery was less affected; Test = 1.3 ± 0.2 mm, Control = 5.5 ± 2.5 mm, $p<0.001$.
	[283] Goh, 2015	Polycapro-lactone scaffold for ridge preservation	T	13 (Test = 6, Control = 7)	Age: 29–60 years (mean = 46.8 years). 7M/7F (1 lost to follow-up, so excluded from results)	Aim: to evaluate the feasibility and effectiveness of using a polycaprolactone scaffold in fresh extraction sockets for ridge preservation.	The test group showed less vertical ridge resorption in all aspects (mesio-buccal, mid-buccal and disto-buccal) with statistically significant results in the mesio-buccal aspect; Test = 0.13 ± 0.96 mm, Control = -2.18 ± 1.02mm, p = 0.008), with better maintenance of ridge height after 6 months.

	[284] Van de Velde, 2010	Maxilla surgical guide	S	13 (Test = 36 tooth implants, Control= 34 tooth implants)	Age: 39-75 years (mean = 55.7 years), 4M/9F	Aim: to compare the outcome of dental implants placed using a flapless protocol with a 3D printed guide and immediate loading with a conventional protocol and loading.	The height of the attached mucosa at 1 week post-surgery was less; Test = 3.26 ± 1.57 mm, Control = 6.01 ± 1.10 mm, p<0.05. Marginal bone levels were not statistically significantly different between test and control implants; Test = 1.95 mm ± 0.70 and 1.93mm ± 0.42 after 18 months. Opinion about speech, function, aesthetics and self-confidence was statistically significantly better for the test side after 1 week when using a VAS rating scale, p<0.05.
	[285] Vercruyssen, 2014	Surgical guides for edentulous jaws	S	59 (72 jaws, 12 in each group)	Age:31-78 years 31 male jaws, 41 female jaws	Aim: To assess the accuracy of guided surgery compared to mental navigation or the use of a surgical template, in fully edentulous jaws.	There was lower deviation at the entry point (1.4mm), at the apex (1.6 mm) and angular deviation (3.0°) when using the 3D printed guiding systems (all p<0.05). There were negligible differences between bone and mucosa support or type of guidance.
Musculoskeletal	[286] Charean-cholvanich, 2013	Cutting guides for total knee replacement	S	80 (Test = 40, Control= 40)	Age: 55-84 years (mean = 69.5 years) 6M/34F	Aim: to compare patient-specific cutting guides with conventional instrumentation in total knee replacement.	The tibial component in the test group was marginally closer to neutral alignment; Test = 89.8 ± 1.2°, Control = 90.5 ± 1.6°, p=0.03. The 3D printed guides also shortened the bone-cutting time by 3.6 mins (p<0.001) and the operating time by 5.1 mins (p=0.019), without differences in post-operative blood loss (p=0.528) or need for blood transfusion (p=0.789). These minimal advantages of the 3D printed guides are unlikely to be clinically relevant.
	[287] Chen, 2015	Guide plate for pedicle screw fixation	S	43 (Test=20, Control= 23)	Age: Test = 35-70 years (mean = 52.3 years), Control = 37-72 years (mean = 55.4 years). Test = 9M/11F, Control = 12M/11F	Aim: to evaluate the clinical efficacy of use of a 3D printing guide plate in posterior lumbar pedicle screw fixation.	Placement time for each screw was shorter (Test = 4.9 ± 2.1 mins, Control = 6.5 ± 2.2 mins), the amount of hemorrhage was less (Test = 8.0 ± 11.1 mL, Control = 59.9 ± 13.0 mL), and the fluoroscopy times of each screw placement was lower (Test = 0.5 ± 0.4 mins, Control = 1.2 ± 0.7 mins), p<0.05 for all tests. The excellent and good screw placement rate was 100% in the test group and 98.4% in the control group, with no statistical difference. No complications were reported.
	[288] Du, 2013	Templates to aid in pin placement in hip resurfacing arthroplasty	S	34 (Test-16, Control = 18)	Ages: 37-55 years	Aim: To assess whether 3D printed patient-specific templates aid in accurate intraoperative pin placement.	The prosthesis stem shaft angle was greater; Test = 138.68 ± 8.85°, Control = 118.9 ± 12.8, p=0.001. The locating template can provide precise and dependable location for hip resurfacing femoral components during arthroplasty and ensure the valgus stem placement necessary for optimal outcomes.
	[289] Gan, 2015	Navigational template for total knee arthroplasty	S	70 (Test = 35, Control = 35)	Age: Test = 63-75 years (mean = 68 years), Control = 64-72 years (mean = 67.8 years). Test = 10M/25F, Control=9M/26 F	Aim: to validates a novel patient-specific navigational template for total knee arthroplasty.	The 3D printed navigational template reduced operation time (Test = 45 ± 8 mins, Control = 60 ± 10 mins, p<0.001) and blood loss (Test = 200 ± 45 mL, Control = 290±60 mL, p<0.001). The mean deviation from the neutral axis also decreased for the frontal femoral component (Test = 1.0±0.8°, Control = 2.6±1.8°, p<0.001) and the frontal tibial component (Test = 1.2±1.0°, Control = 2.8±1.5°, p<0.001).
	[290] Hendel, 2012	Guide for determining glenoid component position	S	31 (Test = 15, Control = 16)	No information provided	Aim: to compare patient-specific instruments with standard surgical instruments in determining glenoid component position.	The 3D printing technology decreased the average deviation of implant position for inclination; Test = 2.9 ± 3.4°, Control = 11.6 ± 7.0°, p<0.0001, and medial-lateral offset; Test = 1.0±0.9mm, Control = 1.9±1.0mm, p<0.05. The greatest benefit was observed in patients with retroversion >16˚; Test = 1.2±2.0˚, Control = 10±4.4˚, p<0.001.

	[291] Maini, 2016	Plate for acetabulum fracture fixation	P	21 (Test = 10, Control = 11)	Age: 18-60 years (mean = 38.7 years) Test = 9M/1F, Control = 9M/2F	Aim: to evaluate the accuracy of patient-specific pre-contoured plates.	Greater reduction was achieved, as evaluated by CT scan; Test = 8.36 ± 5.82 mm, Control = 2.99 ± 1.34mm, p<0.05. Reduced blood loss; Test = 620 ± 247 mL, Control = 720 ± 286 mL, and surgical time; Test = 120 ± 38 mins, Control = 132 ± 41 mins, were observed but the results were not statistically significant (p>0.05). All plates fitted well to the pelvis intra-operatively.
	[292] Merc, 2013	drill guide for screw placement	S	19 (Test = 9 (54 screws), Control = 10(54 screws))	Age: Test = 59 ± 5 years, Control = 62 ±12 years. Test = 4M/5F, Control = 5M/5F	Aim: to evaluate the accuracy of a multi-level drill guide template for lumbar and first sacral pedicle screw placement and to compare it with the freehand technique under fluoroscopy supervision.	The incidence of cortex perforation was reduced; Test = 0, Control = 8, p<0.05. So was the deviation of pedicle screw position in the sagittal plane; Test = 2 ± 10˚, Control = -12 ± 8˚, p<0.05, but there was no discernable difference in the transverse plane deviation or displacement in sagittal or transverse planes.
	[293] Shuang, 2016	Osteosynthesis Plates	T	13 (Test = 6, Control = 7)	Age: Test = 31-62 years (mean = 46.2 years), Control = 27-59 years (mean = 40.3 years). Test = 4M/2F, Control = 6M/1F	Aim: to evaluate the efficacy custom 3D printed osteosynthesis plates in the treatment of intercondylar humeral fractures.	Operative time was shorter; Test = 70.6 ± 12.1 mins, Control = 92.3 ± 17.4 mins, p<0.05. The mean time to bone union was 3.4 months. No difference was found in the rate of patients with good elbow function, or in the ranges of elbow flexion/extension and pronation/supination (all p>0.05).
	[277] Stephens, 2016	Bone models	P	58 (Test = 29, Control = 29)	Age: >60 years (mean = 73 years) 5M/53F	Aim: to investigate the efficacy of 3D printed bone models as a tool to facilitate initiation of bisphosphonate treatment among individuals who are newly diagnosed with osteoporosis.	Using the 9-item Brief Illness Perception Questionnaire with a 0-10 rating scale, the test group were more emotionally affected by osteoporosis immediately after the interview (Test = 4.08±0.41, Control = 2.89 ± 0.40, p>0.05) and reported a greater understanding of osteoporosis at the 2 month follow-up (Test = 7.19 ± 0.51, Control = 5.72 ± 0.49, p<0.04).
	[294] Wu, 2011	Spine model	P	62 (Test = 34, Control = 28) 677 screws inserted	Age: 4-22 years (mean = 11 years)	Aim: to compare the accuracy and safety of pedicle screw placement in congenital scoliosis using the 3D printing technique versus conventional fluoroscopy.	Results for thoracolumbar and lumbar, respectively: Shorter operation time; Test = 6.5 and 5.1 hours, Control = 8.5 and 6.3 hours, p<0.05. Higher scoliosis correction ratio; Test = 83.8 and 81.8, Control = 76.6 and 64.7, p<0.05. Accuracy of screw placement; Test = 94.4% and 91.6%, Control = 86.1% and 82.0%, p<0.05.
	[295] Yang, 2016	Model of trimalleolar fracture	P	30 (Test = 15, Control = 15)	Age: 31-42 years (mean = 36.5 years) 16M/14F	Aim: to evaluate the effectiveness of using 3D printed models for surgical planning in treating trimalleolar fractures and in physician-patient communication.	Shorter operation time; Test = 184.32 ± 4.65 mins, Control = 212.32 ± 8.17 mins, p<0.001. Less blood loss; Test = 846.68 ± 26.11 mL, Control = 1029.65 ± 72.18 mL, p<0.001. No statistically significant differences were observed in complication rate, length of hospital stay, and postoperative radiological outcomes (all, p>0.05).
	[296] You, 2016	Proximal humeral fracture model	P	66 (Test = 34, Control = 32)	61-76 years (Test = 66.09±4.09 years, Control = 66.28± 4.10 years) 27M/39F	Aim: to investigate the feasibility and clinical potential of using 3D printed models versus the conventional thin-layer CT scan for the treatment of proximal humeral fractures in old people.	Surgery time decreased; Test = 77.65 ± 8.09 mins, Control = 92.03 ± 10.31 mins, p<0.05, there was less blood loss; Test = 235.29 ± 63.40 mL, Control = 281.25 ± 57.85 mL, p<0.05, and a lower number of fluoroscopy; Test = 7.12 ± 1.57, Control = 10.59 ± 1.36, p<0.05. The results showed no statistically significant difference in time to union (p>0.05).
	[297] Zhang, 2011	Acetabular navigational template	S	22 (Test = 11, Control = 11)	Age: Test=48.6 ± 6.8 years, Control=49.3 ± 4.9 years Test=7M/4F, Control=5M/6F	Aim: to compare a customised 3D printed acetabular navigational template for total hip arthroplasty (THA) to conventional THA in adult single development dysplasia of the hip.	The templates facilitated accurate placement of acetabular components in dysplasia of acetabulum. At 1 year follow-up there were smaller differences from the predetermined angles of 45° abduction and 18° anteversion; Test = 1.6 ± 0.4°, 1.9 ± 1.1°, Control = 5.8 ± 2.9°, 3.9 ± 2.5°, p<0.05.

Critical appraisal of the RCTs from each medical field are shown in Table 5.7. The table includes the abridged quality index questions. These RCTs typically rated highly across all areas assessed using the quality index. However, many of the RCTs did not demonstrate external validity, and did not blind participants or those measuring the outcomes, or assess confounding factors between groups. Only 57% of the RCTs included follow-up.

Table 5.6. Critical appraisal of studies with the highest level of evidence from each medical field
Medical sector: N = Neoplasms, O = Oral and Maxillofacial, M = Musculoskeletal



An overview of the papers that met the level 2 and 3 evidence criteria from each medical field are shown in Table 5.7, with a critical appraisal of the papers presented in Table 5.8. Studies with higher levels of evidence typically rated better across all areas assessed using the quality index.

Table 5.7. Overview of studies with levels 2 and 3 of evidence from each medical field

Sector	First author, date	Device	Level	Type	Size (n)	Participant details	Aim	Outcomes
Oral and Maxillofacial	[298] Arisan, '13	Guides for dental implants	2	S	54 (Mucosa-support = 12, Bone-support = 15, Control = 27)	Age: 28-74 years (mean = 52.5 years). 23 male, 31 female	Aim: to compare the dental implant positioning errors related to the use of freehand and computer-aided treatment methods.	+ Interproximal emergence, insuf!cient interimplant distance, and improper parallelism errors were higher in implants placed using the freehand method ($p < .0001$, $p < .0001$, and $p < .001$ respectively).
	[299] Azuma, '14	Mandible model	2	S	28 (Test = 12, Control = 16)	Age: Test = 34-91, Control = 55-82. 18 male, 10 female	Aim: To evaluate the clinical efficacy and esthetic outcome of using preoperatively manufactured reconstruction plates, produced using AM models, in mandibular reconstruction.	+ The mandibular symmetry in patients receiving the AM-model-based prebent plates was better than that in patients receiving conventional reconstructive surgery ($p<0.05$).
	[300] Brown, '15	Orthodontic bracket system	2	T	96 (G1: Test = 31, G2: Direct bonded conventional = 33, G3: Indirect bonded conventional = 32)	Age: G1 = 13.42 years, G2 = 3.58 years, G3 = 13.42 years. G1 (AM) = 17 male, 15 female; G2 = 16 male, 15 female; G3 = 17 male, 16 female	Aim to retrospectively compare: patients who were indirectly bonded with CAD/CAM self-ligating appliances with those direct bonded with conventional self-ligating appliances, and those indirectly bonded with conventional self-ligating appliances.	+ No statistically significant difference was found on ABO Cast-Radiograph Evaluation scores among the 3 treatment groups ($p=0.13$). The mean treatment times were different ($p<0.05$, G1: 13.8 ± 3.4 months, G2: 21.9 ± 5.0 months; G3: 16.9 ± 4.1 months.
	[301] Calvo-Guirado, '11	Composite powder molding for bone grafts	2	P	20 (Test = 10, Control = 10)	No information	Aim: to validate the use of AM bioreplicas for calculating bone volumes prior to planning bone regeneration surgery.	NS No differences were recorded for measurements of bone defect between patient bone and the biological models ($p>0.05$) but there were also no differences between the test group and control group arising from post-surgical complications observed at the post-operatory fifteen and thirty day examinations.
	[302] Hanasono '12	Guide for mandibular reconstruction	2	S	76 (Test = 38, Control = 38 defect-matched)	Age: Test = 51.0 ± 14.4 years, Control = 56.4 ± 15.1 years. Test = 26 male, 12 female; Control = 28 male, 10 female	Aim: to evaluate the use of AM modeling to improve the speed and accuracy of mandibular reconstruction.	+ The operative time for the test group was faster than the operative time defect-matched control group ($p=0.0006$). The change in position of selected bony landmarks was less in the test group than in the control group ($p=0.001$).
	[303] Inokoshi '12	AM complete dentures	2	T	10 (Same participants used for test and control)	Age: 78.1 ± 5.6 years	Aim: to compare an AM method for complete dentures with the conventional method.	NS Prosthotontists rated esthetics and stability lower for the AM method ($p<0.05$), but chair time as faster ($p<0.01$). No significant differences were found between the two methods in regards to patient scores.
	[304] Kozakiewicz '11	Model for developing patient-specific orbital wall implants	2	P	24 (Test = 12, Control = 12)	Age: Test = 36 ± 10 years, Control = 40 ± 20 years Test = 9 male, 3 female, Control = 9 male, 3 female	Aim: to compare the functional results, 1 year after treatment, of using an AM reconstruction method for orbital wall repair with a conventional reconstruction method.	+ At 1 year follow up, the test group had better outcomes than the control group (diplopia: $p=0.021$, upgaze vertical visual disparity reduction: $p=0.007$)

	[305] Lee '09	AM prefabricated prostheses for cranioplasty	2	T	131 (Autograft (G1) = 91, conventional prosthesis (G2) = 23, AM prefabricated prosthesis (G3) = 17)	Age: G1 = 43.84 ± 17.91 years, G2 = 40.96 ± 15.48 years, G3 = 40.24 ± 11.97 years. G1 = 62 male, 29 female; G2 = 14 male, 9 female; G3 = 12 male, 5 female	Aim: to assess whether prefabricated AM prostheses outperform intra-operatively moulded prostheses and perform comparably to the gold-standard of autograft bone flaps in reducing operating time, blood loss and surgical complications in elective delayed cranioplasty operations, after decompressive craniectomy, to repair large (> 100 cm2) cranial defects.	+ G3 patients required less operating time than G2 patients ($p<0.001$), and operating time did not differ significantly between G1 and G3 ($p>0.05$). Intra-operative blood loss was lower for G3 than G2 ($p=0.015$) and did not differ significantly between G1 and G3 ($p>0.05$). The infection rate for G3 was lower than for G2 and was comparable to G1.
	[306] Modabber '12a	Guide for jaw reconstruction	2	S	10 (Test = 5, Control = 5)	Age: 37-74 years (mean = 52.4 years). 8 male, 2 female	Aim: to assess whether the AM method has an influence on the duration of the surgery and the amount of bone removed in fibular reconstruction of maxillary or mandibular defects.	+ Shaping procedure and ischaemic time was shorter for the test group than the control ($p=0.014$). There was no change between the defect size of the fibula and the necessary transplant size for the test group, but a mean change of 1.92cm occured for the control ($p=0.001$).
	[307] Resnick '16	Surgical splint for orthognathic surgery	2	T	43 (symmetry, single-segment = 19, asymmetry, single-segment = 17, multi-segment = 7).	All groups compared AM to manual splint fabrication. No information on age or gender.	Aim: to retrospectively compare time and cost differences between virtual surgical planning and 3D printed orthognathic splints with conventional planning and manufacture techniques.	+ The average times and costs were 194 ± 14.1 minutes and $2,765.94, respectively, for VSP and 540.9 ± 99.5 minutes and $3,519.18, respectively, for standard planning. All time and cost differences were statistically significant ($p<0.001$).
	[308] Rogers-Vizena, '16	Craniofacial model	2	P	29 (Test = 9, Control = 20)	Age: Test = 11.4 ± 3.0 years, Control = 11.1 ± 4.7 years. Test = 4 male, 5 female Control = 11 male, 9 female	Aim: to retrospectively assess the benefit of AM models used in planning surgeries in regards to safety, operative time and cost.	NS 7 complications occurred in 6 of the control group, whereas none occurred in the test group. The test group had a 31.3 minute (7.8%) reduction in operative time (not significant), and time-based cost savings were $1036.
	[309] Sumida, '15	membranes for bone augmentation in implant treatment	2	T	26 (Test = 13, Control = 13)	Age: Test = 48.6 ± 9.4 years, Control = 47.8 ± 8.8 years. Test = 4 male, 9 female; Control = 3 male, 10 female	Aim: to compare titanium AM devices with conventional methods for reconstructing alveolar bone for implantation.	+ There was no significant difference between groups in occurance of mucosal rupture ($p=0.27$). However, the operation time was shorter for the test group ($p<0.01$), and fewer screws were used to retain the membrane than the control group ($p<0.01$).
	[310] Zhang, '11b	Titanium plate to guide temporomandibular joint reconstruction	2	S	35 (Test = 11, Control = 24)	Age: Test = 14-65 years (mean = 42.3 years), Control = 24-56 years (mean = 34.9). Test = 5 male, 6 female; Control = 14 male, 10 female	Aim: to compare the operative time between temporomandibular joint reconstruction surgery using AM guides and conventional surgery.	+ Operative time was shorter for the test group than the control ($p<0.05$). The outcome of the surgeries was good, with the condyle-incisor, condyle–mental foramen, and condyle-angle from the postoperative CT scan showing no significant difference between the 2 sides ($p>0.05$).
Musculoskeletal	[311] Hirao, '14	Guide for total ankle arthroplasty	2	S	38 (Test = 24, Control = 14)	No information	Aim: to retrospectively compare the accuracy and stability of bone cutting for total ankle arthroplasty when using AM surgical guides to using conventional guides.	+ The error angle of the tibial bone cut was smaller ($p = 0.02$), and the tilting angle between components was smaller in the test group than the control group ($P = 0.01$).
	[312] Iannotti, '15	Template for glenoid implant positioning	2	P	46 (Test = 25, Control = 21)	No information	Aim: to assess whether 3D imaging and the use of patient-specific instrumentation results in more accurate placement of the glenoid component than 3D imaging and standard instrumentation.	NS There was no significant difference between the test group and the control group in achieving the desired implant position, but both performed better than a retrospective sample that used 2D imaging with standard instrumentation.

	[313] Karlin, '17*	Spine model	2	P	17 (Test = 7, Control = 10)	Age: children	Aim: to retrospectively review children for whom AM spine models were used for surgical planning (Test) and compare them through subjective and objective criteria to a similar group that had no models (Control).	NS The models improved planning and performance of patient-specific spinal instrumentation that was secure and low profile. The efficiency of the surgery as measured by intraoperative fluoroscopy time and blood loss and the extent of the deformity correction was comparable or superior in the test group.
	[314] Li, '15a	Lumbar vertebral model	2	P	37 (Test = 15, Control = 22)	Age: Test = 52.36 ± 4.57 years, Control = 50.83 ± 3.60 years. Test = 9 male, 6 female; Control = 15 male, 7 female	Aim: to evaluate the effectiveness of 3-D rapid prototyping technology in revision lumbar discectomy.	+ The test group had a shorter operation time ($p<0.001$) and less blood loss ($p<0.001$) than the control group. There was no difference between groups for complication rate or clinical metrics.
	[315] Li, '16a	Model of pelvis and pelvic fracture	2	P	157 (Test = 81, Control = 76)	Age: Test = 34.0 ± 8.2 years, Control = 32.2 ± 9.4 years. Test = 55 male, 26 female; Control = 51 male, 25 female	Aim to compare the two groups on length of surgical procedure, intra-operative complications, intra- and postoperative blood loss, postoperative pain, postoperative nausea and vomiting (PONV), length of stay, and type of discharge.	+ The test group experienced shorter surgery time ($p=0.035$), less blood loss (31.0±8.2 g/L vs. 36.2± 7.4 g/L), less pain (2.5±2.3 NRS score vs. 2.8±2.0 NRS score), and shorter recoveries (7.8±2.0 days vs. 10.2±3.1 days before discharge).
	[316] Schweizer, '16	Guide for Reconstructions of Scaphoid Fractures	2	S	22 (Test = 9, Control = 13)	Age: Test = 15-47 years (mean = 27). Control = 14-41 years (mean = 24) All male	Aim: to assess the accuracy of the reduction of surgically reconstructed scaphoid nonunions or fractures using 3-dimensional computer-based planning with and without patient-specific guides.	+ In the test group, average residual displacement was 7˚ after surgery, and 8 of 9 scaphoids healed after 2 to 6 months, with partial nonunion after 9 months observed in one patient. In the control group, residual displacement after surgery was 26˚, and 11 of 13 scaphoids healed between 2 and 34 months. 2 scaphoids in the control did not consolidate. The difference in the accuracy of reconstruction was significant ($p=0.001$). Average operation time was shorter ($p=0.01$) for the test group.
	[317] Yang, '14	Upper cervical spine model and navigation template	2	S	49 (Test = 21, Control = 28)	Age: 5-81 years (mean = 37.6 years). 21 male, 28 female	Aim: to evaluate the clinical efficacy of AM models in surgical treatments for atlantoaxial instability.	+ The test group had lower intraoperative fluoroscopy frequency ($p<0.001$), operation time (posterior $p=0.001$, anterior $p=0.004$) and blood loss for the posterior approach ($p=0.006$) than the control group. The screw malposition rate showed no difference between the two groups.
	[318] Yang, '15	Spine model	2	P	126 (Test-50, Control=76)	Age: Test = 12.52 ± 5.45 years, Control = 12.11 ± 6.42 years. Test = 12 male, 38 female, Control = 33 male, 43 female	Aim: to retrospectively evaluate the effectiveness of AM technology in corrective surgery for Lenke 1 adolescent idiopathic scoliosis (AIS) patients based on operation time, perioperative blood loss, transfusion volume, postoperative hemoglobin (Hb), postoperative complications, and length of hospital stay.	+ The test group had shorter operation time, less blood loss and transfusion volume, and higher postoperative Hb (all, $P<0.001$). However, no significant differences were observed in complication rate, length of hospital stay, and postoperative radiological outcomes between 2 groups (all, $P>0.05$).

Circulatory	[319] Schievano, '07	Model of the right ventricular outflow tract and pulmonary trunk	3	P	12 (4 did not undergo percutaneous pulmonary valve implantation (PPVI), 4 had successful PPVI, and 4 had unsuccessful PPVI)	Age: 9-39 years (mean 20 years) 7 male, 5 female	Age: 9-39 years (mean 20 years) 7 male, 5 female	NS Both cardiologists correctly determined from the models that the 4 subjects who did not undergo PPVI were unsuitable for PPVI. Of the 8 subjects who underwent PPVI, only 4 were successful. Both cardiologists correctly identified the suitability of 5 of these subjects from the models. Therefore the cardiologists had a 75% accuracy when selecting patient suitability for PPVI using 3D models.
Oral and Maxillofacial	[320] Adolphs, '14	Splint for orthognathic surgery	3	T	10 (Same participants used for test and control)	No information provided	No information provided	NS 8 of 10 AM splints, and 6 out of conventional splints could be used clinically to achieve and maintain final occlusion after orthognathic surgery. In the five patients where both types of splints were available, their occlusal fitting was assessed as being equivalent, and in one case the AM splint showed better occlusal fitting than the traditional splint.
	[321] Arisan, '10	Dental screw placement guides	3	S	54 (28 guides in system I, 32 guides in system II)	Age: 28-73 years (mean = 48.4 years) 16 male, 38 female	Age: 28-73 years (mean=48.4 years) 16 male, 38 female	+ Implants that were placed by bone-supported guides had higher deviations than implants that were placed by mucosa-supported guides ($p<0.05$) but there was no difference in deviation between implant brands ($p<0.08$).
	[322] Morris, '13	Mandible or midface model	3	P	20 (Test = 10, Control = 10)	Age: Test = 40.5 ± 5.6 years, Control = 66.1 ± 3.0 years Test = 6 male, 4 female, Control = 8 male, 2 female	Age: Test=40.5 ± 5.6 years, Control=66.1 ± 3.0 years Test=6 male, 4 female, Control=8 male, 2 female	- No significant differences were observed for total operative time between groups, but the total reconstructive time was lower in the control group ($p=0.05$).
	[323] Shahbazian, '13	Surgical guide for autotransplantation of teeth	3	S	40 (Test = 20, Control = 20)	Age: Test = 9-18 years (mean = 11 years), Control = 9-18 years (mean = 12 years) Test = 12 male, 8 female, Control = 13 male, 7 female	Age: Test=9-18 years (mean=11 years), Control=9-18 years (mean=12 years) Test=12 male, 8 female, Control=13 male, 7 female	NS 6 from the control group showed 1 or more complications, compared to 2 from the test group.
	[324] Weitz, '11	Templates for navigated dental implantation	3	S	10 (Same participants used for test and control)	Age: 19-46 years (mean = 29.9 years) 6 male, 4 female	Age: 19-46 years (mean = 29.9 years) 6 male, 4 female	NS The conventional templates enabled excellent fitting accuracy but the accuracy of implants fitted with the AM templates was not sufficient and could result in significant iatrogenic complications.
Musculoskeletal	[325] Otsuki, '13	Cutting guide for curved peri-acetabular osteotomy	3	S	18 (Test = 7, Control = 11)	Age: No information provided Test = all 7 female, Control = No information provided	Age: No information provided Test =All 7 female, Control = No information provided	NS The rate of osteotomy-related complications did not differ significantly between the two groups ($p>0.1$). The actual cutting line corresponded almost exactly to the planned cutting line in all patients.

Table 5.8. Critical appraisal of studies with levels 2 or 3 of evidence from each medical field

			Reporting											External validity			Internal validity - bias							Internal validity - confounding							Power
Author, date	Sector (**O**ral & maxillofacial, **M**usculoskeletal, **C**irculatory)	Level of evidence	1. Clear hypothesis/aim/objective	2. Clear outcome measures	3. Patient characteristics described	4. Interventions clearly described	5. Distributions of confounders described	6. Findings clearly described	7. Estimates given of random variability	8. Adverse events reported	9. Patients lost to follow-up described	10. Probability values reported	11. Recruitment pool represents population	12. Participants represent population	13. Staff/places/facilities match std. treatment	14. Participants blinded to intervention	15. Those measuring outcomes blinded	16. Data dredging reported	17. Adjusted for different lengths of follow-up	18. Appropriate statistical tests	19. Reliable compliance with intervention	20. Accurate/reliable outcome measures	21. Groups recruited from same population	22. Groups recruited over same timeframe	23. Subjects randomised into intervention	24. Randomised intervention concealed	25. Adjustment for confounding	26. Losses to follow-up accounted for	27. Sufficient power
[298] Arisan, '13	O	2	+	+	+	+	+	+	+	-	+	+	?	?	+	-	+	+	+	+	+	+	+	+	-	X	+	+	+
[299] Azuma, '14	O	2	+	+	+	+	-	+	+	-	-	-	?	?	+	-	-	+	-	+	+	+	?	?	-	X	-	-	+
[300] Brown, '15	O	2	+	+	+	+	+	+	+	-	X	+	+	+	+	-	+	+	X	+	+	+	?	?	-	X	+	X	+
[301] Calvo-Guirado, '11	O	2	+	+	-	+	-	+	+	-	+	-	?	?	+	-	-	+	+	+	+	+	+	?	?	?	?	+	-
[302] Hanasono '12	O	2	+	+	-	+	+	+	+	-	+	+	?	?	+	-	-	+	-	+	+	+	-	+	-	X	-	+	+
[303] Inokoshi '12	O	2	+	+	+	+	-	+	+	-	X	-	?	?	?	-	-	+	X	+	+	-	X	X	-	X	-	X	+
[304] Kozakiewicz '11	O	2	+	+	+	+	-	+	-	-	+	+	+	+	+	-	-	+	+	+	+	+	+	-	-	X	-	+	+
[305] Lee '09	O	2	+	+	+	+	-	+	+	-	-	+	+	+	+	+	+	+	-	+	+	+	+	+	?	-	?	?	+
[306] Modabber '12a	O	2	+	+	-	+	-	+	+	+	X	+	?	?	+	-	-	+	X	+	+	+	+	+	+	?	-	X	+
[307] Resnick '16	O	2	+	+	+	+	-	+	+	-	X	+	?	?	+	-	-	X	X	+	+	+	-	-	?	X	-	X	+
[308] Rogers-Vizena, '16	O	2	+	+	-	+	-	+	+	+	X	+	?	?	+	-	-	X	X	+	+	+	?	?	-	X	-	X	-
[309] Sumida, '15	O	2	+	+	-	-	+	+	+	-	X	+	?	?	?	-	-	?	X	+	+	+	?	?	?	X	-	X	+
[310] Zhang, '11b	O	2	-	+	-	+	-	-	-	-	+	-	+	+	+	-	-	+	?	+	+	+	-	-	-	X	-	+	+
[311] Hirao, '14	M	2	-	+	-	+	-	+	+	+	+	+	?	?	+	-	-	?	+	+	+	+	?	?	-	X	-	+	+
[312] Iannotti, '15	M	2	+	+	-	+	-	+	+	-	X	+	?	?	+	-	+	+	X	+	+	+	-	-	-	?	-	X	+
[313] Karlin, '17*	M	2	+	+	+	+	?	+	?	?	?	?	?	?	+	-	-	X	?	?	?	?	-	?	-	X	?	?	?
[314] Li, '15a	M	2	+	+	+	+	+	+	+	+	+	+	?	?	+	-	-	+	-	+	+	+	?	+	-	X	+	+	+
[315] Li, '16a	M	2	+	+	+	+	+	+	+	+	X	+	+	+	+	-	-	X	X	+	+	+	+	+	-	X	+	X	+
[316] Schweizer, '16	M	2	+	+	-	+	-	+	+	+	+	+	?	?	+	-	-	+	-	+	+	+	?	?	-	X	-	+	+
[317] Yang, '14	M	2	+	+	+	+	+	+	+	+	+	+	+	+	+	-	-	+	+	+	+	+	?	?	-	X	-	+	+
[318] Yang, '15	M	2	+	+	+	+	+	+	+	+	+	+	?	?	+	-	-	+	?	+	+	+	?	+	-	X	-	+	+
[319] Schievano, '07	C	3	+	+	-	+	-	+	+	-	X	-	-	-	+	-	+	X	X	+	+	+	?	?	-	-	-	X	-
[320] Adolphs, '14	O	3	+	+	-	+	X	-	-	-	X	-	?	?	+	-	-	?	X	+	+	?	X	X	X	X	X	X	-
[321] Arisan, '10	O	3	+		+	+	+	+	+	-	-	+	?	?	+	-	-	+	-	+	+	+	+	?	-	X	-	+	+
[322] Morris, '13	O	3	+	+	-	+	+	+	+	-	X	+	?	?	+	-	-	X	X	+	+	+	?	?	-	X	-	X	+
[323] Shahbazian, '13	O	3	+	+	-	+	+	+	-	+	-	-	?	?	+	-	+	+	-	+	+	+	-	-	-	X	-	?	-
[324] Weitz, '11	O	3	+	-	-	-	-	+	+	+	X	-	?	?	?	-	-	?	X	+	+	+	X	X	X	X	X	X	-
[325] Otsuki, '13	M	3	+	+	-	+	-	-	+	+	+	-	?	?	+	-	-	+	-	+	+	+	-	?	-	X	-	+	-

+ Yes
- No
? Unable to determine
x Not relevant

* Karlin et al. provided access to the first page only, so ? has been used for unknown answers.

5.2.4. Outcomes and limitations

The results show that a wide range of 3D printed devices have been clinically trialled but few papers have rigorously assessed the efficacy or effectiveness of clinical 3D printed devices. The 3D printed devices tested were mainly designed for planning surgeries, particularly using anatomical models or surgical guides to aid cutting or navigating, with

little attention dedicated to 3D printed interventions. This is likely due to the lower complexity of the anatomical models and surgical guides and the smaller risk to the patient than therapeutic devices, resulting in less rigorous regulation and safety testing requirements. Approximately twice as many studies were in Oral and Maxillofacial Surgery than in the Musculoskeletal System, the two largest fields, but the Musculoskeletal System, despite its more recent uptake of 3D printing, had almost double the number of Level 1 studies. This is perhaps because clinical trials in musculoskeletal surgery typically aim to demonstrate quantitative clinical outcomes, driving more rapid growth in the level of evidence of studies than oral and maxillofacial surgery where aesthetics is a priority and individual outcomes are harder to quantify.

The RCT listed under Neoplasms was an anatomical model used for planning mandibular surgery, but with a focus on tumour removal, fitting into both categories. Therefore no RCTs were found outside the Oral and Maxillofacial Surgery or Musculoskeletal System fields. The primary indicators of success used to determine the efficacy and effectiveness of 3D printed devices across all medical fields were operating time, accuracy of surgery or positioning, fit, changes at the operation site (particularly blood loss, inflammation and aesthetics), recovery time and functional outcomes. From the studies that compared against a control, the 3D printed devices used for preoperative planning and aiding surgery consistently found decreases in operating time and increases in surgical accuracy, the two most commonly reported indicators of effectiveness. Operating time is an obvious choice as an indicator for device success because it is easy to measure and quantify and corresponds to decreased blood loss and faster recovery. The main aims of anatomical models and surgical guides are to provide better information to the surgeon on the surgical site and to guide the surgeon's hand. Therefore measuring the accuracy of the surgeries indicates whether these aims have been met. To make more decisive conclusions regarding the performance of 3D printed medical devices in Oral and Maxillofacial Surgery and Musculoskeletal Surgery it is important to assess the long-term effects. Few papers assessed the long-term differences of using the 3D printed devices and those that did had mixed results as to whether there were any differences in recovery times and outcomes. The other aspect that should be addressed in future studies is the appropriate choice of outcome measures. In the studies analysed in this review there appears to be no evaluation of how the selected outcome measures match the purpose of the device.

Therapeutic devices such as implants, prosthetic limbs and orthotics offer the promise of revolutionising the medical industry because of their ability to be custom-made for the patient, but most therapeutic devices are still early-stage, with little research into their efficacy and effectiveness in a clinical setting. There were not enough therapeutic devices tested against a control group to find and evaluate repeated measures of success.

Most studies reviewed were poor quality, meaning that their study designs demonstrated levels of evidence for the 3D printed device of 4 or 5, with no use of a control group. The 41.4% of papers that reported on individual case studies or provided only qualitative results did not clinically validate the devices that they reported on, and therefore add little value to their fields. Few included follow-up, or addressed the external validity, bias or confounding factors. The vast majority of papers reported positive outcomes for the patients, but few studies demonstrated clinically significant findings. Even the Level 1 studies demonstrated limited external validity and rarely blinded participants or those measuring the outcomes to the intervention.

The RCTs all demonstrated statistically significant results in favour of using the 3D printed device over the current clinical practice to which it was compared. However, one RCT[286] concluded that the improvement with 3D printing was too small to provide a clinical advantage and none performed an analysis on the clinical relevance of these differences. The studies consistently used p-values of <0.05 as their measure of device success, but taking into consideration the false discovery rate, it is likely that this will only show a real effect about 70% of the time under ideal testing conditions.[326] While the critical analysis in Table 5.6. shows all Level 1 studies as adequately powered, this is because the Quality Index bases its definition of "adequately powered" on whether a difference due to chance is less than 5%. Therefore, given that all Level 1 studies had 40 or fewer participants in each group, many of these studies are likely to be underpowered.[326] Considering the possibility of underpowered studies, the publication bias towards positive trials, and the fact that all RCTs in this review were single site trials, the likelihood that the results shown in these papers reflect a real effect is lower than suggested by the reviewed studies.[327] Until independent groups start validating 3D printed devices, it is also difficult to avoid researcher bias.

Most 3D printed device studies that were excluded from this review had uses in medical training, or as moulds for manufacturing and therefore did not meet the inclusion requirements. A few other studies were excluded because they had not been translated into English.

Previous reviews have documented the uses of 3D printing for developing patient-specific medical devices. However, there has been limited research into assessing the efficacy and effectiveness of these devices. This rigorous systematic review design is the first to compare 3D printed devices across all medical fields and assess their efficacy and effectiveness, describing key benefits that have been found from using 3D printed devices clinically. The progress made in different medical fields is compared using validated quality assessment and clinical level of evidence tools. It demonstrates that the fields of Oral and Maxillofacial Surgery and the Musculoskeletal System are leading the way in validating 3D printed devices for clinical use. Multiple high-quality studies have been performed on surgical guides for maxillofacial, hip and knee surgeries. This growing body of comparable high-quality research sets an example for other fields to emulate in order to demonstrate the efficacy and effectiveness required to integrate these 3D printed devices into clinical practice.

A critical appraisal of the efficacy and effectiveness of 3D printed devices across medical fields provides clinicians with an evidence-based approach to determine the applicability of 3D printing within their field. It also gives researchers an overview of areas that require further research and validation. It encourages investigators to discover what methods have been successfully validated in other medical fields and promotes potential collaborations between fields.

3D printing provides a way of customising devices to improve patient outcomes. Available techniques and materials will increase, as 3D printing technology continues to be developed. There is therefore a growing need for validation of new devices, materials and techniques to ensure best patient outcomes. Much research has already gone into developing 3D printed devices for medical purposes. However, this drive for new technology development has not yet been matched with a drive for critical appraisal of the devices to demonstrate their efficacy and effectiveness. Even the fields that are leading the way in critically evaluating new 3D printed devices will be required to increase their output as 3D printing continues to grow in popularity and functionality.

The early research covered by this review shows that 3D printing can be valuable for use in medicine. The next important step to take is growing the body of research that focuses on validating 3D printed devices. All fields require more rigorous and long-term assessments into the efficacy, effectiveness and safety of 3D printed devices before they are introduced into standard clinical practice. The study is limited to a critical appraisal of individual studies, rather than a meta-analysis, because of the breadth of uses for anatomical models, surgical guides and therapeutic devices and the lack of comparable hypotheses. Funders can take an active role in promoting not only early technological development, but also the subsequent clinical trials. Demonstration of clinical efficacy, effectiveness and device safety will become increasingly important as higher risk 3D printed devices are developed and unconventional manufacturers, such as hospitals and clinics, incorporate 3D printing of patient-specific medical devices into standard clinical practice.

Fields such as Oral and Maxillofacial surgery, who were early in the uptake of 3D printing, are beginning to stabilise, with a steady number of studies being published each year, but other fields, such as Musculoskeletal and Circulatory Systems, are more recently gaining traction, with increasing numbers of studies performed each year. 3D printed drug delivery devices and biological 3D printing technologies for printing tissue show huge promise, but have not been clinically trialled and so are not included here.[328] This is likely to change within the near future. It is therefore recommended that in this fast-growing and dynamic environment, this review is updated every few years.

5.2.5. Application of findings to prosthetic socket design

The findings of this wider review demonstrate that strength and precision can both be attained using 3D printing techniques; attributes that had not been demonstrated in the prosthetic-specific review. The printing methodologies used to develop strong, durable devices for dentistry, skull reconstruction, orthotics and back braces may be transferable to the field of prosthetics, to overcome some of the weaknesses of current devices. Dentistry and musculoskeletal fields have also developed digital systems that can take data from scans and develop accurate custom 3D printed devices. These successful design, fitting and manufacturing processes should be observed in more detail to assist in bridging the step in

the prosthetics field between collecting data through scans, and using the data to manufacture custom devices. No fields have yet provided clinically trialled processes to include data from simulations into their 3D printed devices.

This research demonstrates the importance of running large clinical trials to validate 3D printed devices, rather than relying on the outcome of individual studies. For example, many knee reconstruction studies, performed with 3D printed devices, came out with positive results. However, a larger review showed no overall clinical benefit to the 3D printed devices for this purpose.[274] No 3D printed prosthetic devices have yet been through a randomised controlled trial and none have included long-term follow-up.

In summary, 3D printing shows promise for supporting prosthetic socket design that is informed by sensors and mechanical modelling. However, due to the infancy of the field, there are many technical issues and challenges with product validation methods to overcome. No studies have yet been published that assess whether 3D printing can be used to improve thermal comfort.

6. Future directions

6.1. Validation of the amputee model

Future work includes validation of the bioheat model for use with amputees. This is required before the information from this model can be used to inform future prosthetic socket designs for improved thermal comfort.

6.1.1. Prosthetic socket materials

The first stage of future research is to undertake a study with the amputee model, adding various insulating materials and thicknesses to match those of commonly used prosthetic sockets and liners, and compare the simulated outputs to the thermal properties measured by Klute et al.[25] and Williams et al.[329] to compare materials and validate the model. Plastics used for prosthetic sockets typically have low thermal conductivities. This means they are good insulators, which is not necessarily beneficial in hot conditions and during exercise. A socket that has a low thermal conductivity will store excess heat from the body, but one with high thermal conductivity will be overly affected by external environmental conditions, so will easily get hot and cold. Materials such as high density polyethylene (HDPE), polypropylene copolymer (PPC), acrylonitrile butadiene styrene (ABS) and carbon-fibre lay-up, have thermal conductivities of 0.49, 0.22, 0.1 and 0.148 W/(m·K), respectively, and are often cast about 4.2-4.6 mm thick for a prosthetic socket.[25] Likewise, common prosthetic liners are between 0.085 and 0.266 W/(m·K), with thicknesses between 3 and 6 mm.[25] These thermal properties are not dissimilar to the thermal conductivity of skin (0.37 W/(m·K)), but are much lower than metals (for example, aluminium has a thermal conductivity of 205 W/(m·K)) and even glass and water at moderate ambient temperatures have properties of 0.8 and 0.6 W/(m·K), respectively. PPC is often used as a rigid, outer layer for a prosthetic socket. It has low moisture absorption, is extremely tough and rigid, and yet is flexible, providing excellent crack resistance and durability. However, it is not as impact-resistant as the polyethylenes. HDPE is easy to fabricate, durable, strong, lightweight and low cost. ABS is less common in conventional prosthetic sockets, but has been used in 3D printed sockets because it is easy to manufacture (print and thermoform), and it is tough, rigid and impact

resistant. A carbon-fibre lay-up uses carbon and fibreglass braids over an inner plastic. More research is required to determine which of these materials provide better thermal comfort, what designs can use these materials in ways that increase thermal comfort, and whether there are other materials that can out-perform these commonly used ones.

Given the importance of sweat and evaporation in the body's thermoregulatory process, breathability and sweat absorption are also measures that need to be considered to adequately predict thermal comfort and the best materials and designs for prosthetic thermal comfort.

6.1.2. Collecting muscle temperature data from amputees

Accurate collection of muscle temperature data during exercise requires an invasive and expensive procedure. However, Flouris et al. have developed and validated sensors that insulate the skin and cause the skin to heat to close to muscle temperature, enabling prediction of muscle temperatures without the invasive proceedure.[119,120] Plans have been developed, subject to research funding, to collect skin and muscle temperatures from transfemoral amputees during everyday physical activity in hot and humid climates, along with measures of discomfort and visible signs of tissue damage. These empirical results would be compared to the simulated results, to validate the simulator's ability to predict temperatures and the risk of tissue damage. As part of this research, different socket types would be included in the data-collection and simulation, and compared on their thermal properties and on thermal discomfort experienced by the wearer.

A physical model could also be developed for validation of the bioheat model, using materials that have suitable thermal properties to represent the different tissues. Controlled heating of the materials and environment would provide temperature outputs that could be compared to the computational model outputs.

6.2. Future model developments

6.2.1. Increasing accuracy

This model has demonstrated that individual body size has a significant impact on the temperatures of the muscles. However, it remains unknown how much other human factors, such as sex, age, ethnicity, fitness, hydration and amount of hair affect muscle temperatures.

These variables have not yet been assessed because there is, at present, not enough empirical data to validate the model's findings.

The other model input variables, such as those used to determine sweat rate and metabolic rate also have not been validated. As mentioned in the discussion in Section 4.6, a sensitivity analysis of the bioheat model should be undertaken to assess how each input variable in the model affects the output variables. This could provide information on the robustness and uncertainty in the model and enable the model to be simplified by fixing or removing inputs that have little or no effect on the output.

This research briefly demonstrated that the model can be used with accurate geometries, developed from MRI data (Section 4.6). However, this area has also not been studied in detail, due to the lack of empirical data to validate the findings against. Funding is being sought to collaborate with researchers at Flinders University, Australia, who have expertise in FEA to assess soft-tissue damage.[330–333] The project includes collection of MRI scans of the residual limbs of transfemoral amputees, without the prosthesis and with the prosthesis (both with the leg unloaded and loaded). These would be collected before and after a 12-month clinical trial to assess changes in soft-tissue over time. A grant application has been submitted to further develop and validate the thermal model presented in this dissertation and add temperature monitoring into the data collected in their study, to give a more rounded approach to assessing how an amputee's residual limb changes over time and with prosthesis wear. The MRI data collected can be used to improve the accuracy of the thermal model and to better assess how temperature response varies with individual geometry (see Section 6.2.2 for more about this research).

It may also be useful to separate out the individual muscles in the model, rather than treating them as a single lump volume, as the strain, homogeneity and intermuscular sliding may affect heating, particularly that generated by friction.[334] This also has implications when studying the biomechanical properties of the limb. However, including this level of detail would significantly increase the complexity and run-time of the model, so it is more useful for research purposes than for a real-time application in a clinical setting. Adding this increased level of detail to the model is not planned for the immediate future.

6.2.2. Assessing tissue damage

Pressure ulcers can develop in soft-tissue well before there are any external signs of injury, and extensive tissue damage may have already occurred by the time there are visual signs. Peripheral neuropathy may also limit the warning an amputee has of tissue damage. This is particularly important to consider in the reconstructed soft tissue pad in the residual limb because the tissue is not accustomed to load-bearing and it is put under sustained cyclic loading when wearing a prosthesis.[335] Not only is the effect of loading on the deep tissue under-researched, the adaption and breakdown of skin when under abnormal load bearing also requires further research.[37,336] Monitoring tissue heat may be able to be used as a pre-warning of tissue inflammation, and being able to simulate and compare different prosthetics and loading conditions could assist in reducing or preventing tissue damage.

The study planned with transfemoral amputees in Australia includes a questionnaire of patient discomfort, a clinical assessment of the health condition of the residual limb,[39] a clinical gait study, EMG recordings of muscle groups in the thigh, and measures of socket pressures, heart rate and skin temperature during and post-exercise. Joint movement, tissue deformation, temperature, pressure and shear forces can be calculated based on these measurements and the MRI images. There is little knowledge of how an amputation changes the body's thermal and pressure distributions, and how the prosthesis interacts with the body. This study will aim to create the first detailed dataset for understanding commonality and differences between tissue responses in amputees, which can inform individualised patient care.

6.2.3. Incorporating pressure and friction analysis under dynamic loading

To create a systemic approach to developing user-specific prosthetic sockets that overcome the discomfort and tissue damage issues of current sockets, it is important to understand the anatomy of the residual limb and the effect current sockets have on an amputee’s physiological responses during physical activity. Informed socket design is likely to require patient-specific geometry, material properties and pressure tolerance measurements. It is important to integrate thermal modelling with biomechanical modelling, as high internal tissue temperatures negatively affect the skin’s mechanical stiffness and strength.[335] This can lead to tissue damage. Also, moisture in the socket, due to sweat not

being able to dissipate, causes the skin to soften and changes the friction coefficient. This can cause skin irritation and result in high shear forces at the skin-socket interface.[335] Some FEA models exist that simulate prosthesis interface pressures and internal soft tissue stresses and strains.[337] However, few studies have yet considered full dynamic loading conditions, and none have included the effect of heating as well as loading. Some work is being done to analyse prosthetic componentry using FEA.[335] Experts in the field have recommended that soft-tissue modelling needs to move towards subject-specific analysis, due to the large inter-subject variations in many factors.[335]

It is hoped that the information collected in the Australian clinical study can be used to add information to the COMSOL multiphysics FEA model or that links can be created between FEA models to improve model predictions of soft-tissue deformation, contact pressure between the residual limb and the prosthetic socket and tissue temperature. Using the data collected from the clinical study will allow model validation using a leave-one-out cross validation method. This uses all data but that of one participant to predict the one participant's results, then cycles through each participant, comparing the model prediction to the corresponding measurements in each participant.

The following stage of research is to use this multiphysics model to inform prosthetic socket design to reduce the risk of tissue damage and discomfort. This may include the development of an optimisation algorithm to design a prosthetic socket that interfaces as seamlessly as possible with the individual's residual limb. It is expected that different sections of the limb will favour different material properties, based on variables such as proximity of the bone or blood vessels to the skin, direction of loading, and tissue movement during dynamic loading. The effect of different prosthetic material properties and socket structures on the internal tissues can be examined through simulation of temperature, pressure and tissue deformation, to determine the relative importance of each variable at each location around the socket. It is not feasible, financially, to require the extensive input used in the clinical trial and model development for each prosthetic socket design. Therefore, the model must be able to predict the optimal design for an amputee whose data was not used in the design of the optimisation algorithm. Therefore, it is recommended that a leave-one-out cross validation method is again used to create the optimised socket for each

participant, based on the data from the other participants, along with a scan of the individual's external limb shape and measures of tissue compliance around the limb.

With a multiphysics model of the effect of the prosthetic socket on the body, the model can be used to modify the socket design, iteratively comparing each change to optimise the socket to minimise the thermal disruption on the body without adversely affecting other aspects of comfort and durability.

6.3. Further uses of the model

6.3.1. Athlete training protocols and post-exercise recovery interventions

The non-amputee model can provide useful information for athletes. Understanding an individual's muscle temperatures during exercise and post-exercise recovery can provide insight into monitoring tissue health and developing training protocols and post-exercise recovery interventions. It has been shown that increased muscle temperature leads to increased muscle power for short-duration exercise, but reduces the time to fatigue.[338] However, there is a ceiling above which increasing the ambient temperature does not improve the power output, and the benefit of higher muscle temperatures is lost under repeated-sprints or if core temperature also increases.[338] Overexertion or exercising in hot weather can cause rhabdomyolysis, muscular pain, swelling, and fatigue.[109,110] A bioheat model can be used to predict how changes in heat load might affect an individual, looking at the effect of the environmental conditions and the length and vigour of exercise, along with recovery times between exercise bouts. This can support the optimisation of exercise routines, and reduce the risk of injury and fatigue.

6.3.2. Design guides for prosthetists

Using this bioheat model to assess the feasibility of adding real-time user-specific simulation into the socket design and fitting process and into new socket designs will help direct the future of the prosthetic socket industry. A more data-driven approach to design and fitting could provide better patient outcomes. However, even without the software on-hand to provide real-time simulation of a patient's limb, design guides, developed using the bioheat model, could provide prosthetists and end-users with a greater understanding of the

thermal benefits of using one type of socket over another. They could also inform prosthetists on what changes could be made to a socket if the current one is causing thermal discomfort. These design guides could be as simple as showing a comparison of different commonly used socket materials and designs with the pros and cons of each.

6.3.3. Web application for prosthetists

In its current form, the bioheat model is designed for research purposes. However, COMSOL Multiphysics provides the option to develop easy-to-use web-based applications based on the simulations. Once the simulations have been developed into an app, they can be run on computers without COMSOL installed. The developer can control which parameters the end-user can manipulate and ensure the app provides simple visual outputs and graphs, so a non-specialised consumer can benefit from software developed in COMSOL. This could be beneficial for training clinicians to use the simulations in the prosthesis fitting process.

6.4. Monitoring temperature in the prosthesis

6.4.1. Reason for monitoring skin temperature

A thermal model can feed directly into computer-aided design and 3D printing of sockets, or provide prosthetists with additional information to assist with socket design and material selections (see Section 4.7). To validate the socket designs, sensors can be used to assess whether the socket performs as the bioheat model predicted. This feedback on the real-life activities of the prosthesis-users and the corresponding temperatures in the socket can be used to improve the thermal modelling, which can then feed into better socket designs. Sensors can also be used to monitor changes in the residual limb and socket fit over time, to provide warning of residual limb health issues and the need for socket replacement.

This research has demonstrated the importance of understanding muscle temperatures when investigating amputee discomfort and tissue health. Skin temperature and moisture are also important indicators of tissue health, and give some indication of the soft tissue overheating. Pressure and friction also create heat, so skin temperature can be used to indicate how well the socket fits. Therefore, there is value in monitoring the skin temperature

in the prosthesis, even though it cannot adequately determine changes in internal tissue heating. Temperature varies substantially across the residual limb, and may provide an indication of areas of the residual limb with poor blood-flow, which can help with diagnosing further issues associated with vascular disease. Finding a way to map the heat across the residual limb continuously could not only be useful for monitoring long-term tissue health and socket fit, it could also feed into the validation and improvement of the bioheat model to improve future prosthetic socket designs. Monitoring the device-user interface can indicate whether the socket performs as intended, which is particularly necessary if novel design processes are developed, such as varying the material properties across the prosthetic socket to more closely match the limb's requirements.

The more data that can be collected from amputees, the easier it will be to develop and validate data-driven prosthetic socket designs. The International Society for Prosthetics and Orthotics (ISPO) UK is developing and trialling an online anonymised registry for Amputee Reported Outcome Measures (AMPROM),[339] and the Assisting Living and Learning Institute and the Global Cooperation on Assistive Technology (GATE) are focused on creating a systemic approach to fitting and disseminating prosthetics globally.[5] These organisations could perhaps be a starting-point for collecting and disseminating empirical data from sensors in prosthetic sockets.

A few research groups have monitored pressures in the prosthetic socket over time,[60] and others have developed sensors that have been tested within a laboratory setting that measure pressure,[340] interface shear stresses,[61] and temperature.[66–70] However, none of the previous sensor systems are suitable for within the clinic or for long-term monitoring of temperature at the socket-user interface. This section gives a brief overview of the options available for monitoring skin temperature in the prosthesis, and the pros and cons of each.

6.4.2. Comparing temperature sensing methods

There are many ways to measure temperature.[341] Temperature sensing methods can be divided into those suitable for clinicians to use in assessing the design and fit of a socket in the clinic, and those that may be able to be used for long-term monitoring outside the clinic. The previous studies that have measured skin temperatures under laboratory settings used IC chips in a grid across the residual limb, or a thermal camera before and after wearing the prosthesis.[66–70] None have yet been designed for long-term monitoring. Thermal cameras

and thermochromic liquid crystals (TLCs) can be used with transparent check-sockets to assist with design and fitting of a definitive socket. A grid made of IC chips, fibre-optics or resistive threads have more potential to be developed for long-term monitoring, though fibre-optics remains prohibitively expensive, so will not be considered in detail here.

6.4.2.1. Thermal camera

A thermal camera is a contactless method of collecting a 2D temperature map. Objects react to incident radiation according to their material properties, either absorbing, reflecting or transmitting the incident ray. A thermal camera lens focuses the infrared light emitted or reflected by objects on an infrared detector. Many thermal cameras monitor voltage with constant current using thermistors. The absorption of infrared energy heats the detection element. These measurable changes can be detected by external instrumentation. High-end thermal cameras can detect changes of 0.1◦C, with a response rate that is fast enough for 30 frames per second and a resolution of 640 x 480 pixels.[342] Conventional definitive prosthetic sockets are not transparent in the infrared range, so it is not possible to monitor skin temperature through them. However, prosthetists often use a check-socket to allow the amputee to try the socket for a while to assess its comfort and fit before making the definitive socket. The main material used for check-sockets is polyethylene terephthalate glycol-modified thermoplastic (PETG) which is a visibly transparent plastic. The human body radiates heat at wavelengths of around 9.3 μm. The amount of infrared light transmitted through PETG near the 9.3 μm range varies according to the specifications of the specific PETG, so it is necessary to test the accuracy of temperature recordings through it before using it in trials. PETG also has similar thermal conductivity (0.15 to 0.24 W/(m·K)) and moisture permeability properties to other plastics used for definitive prosthetic sockets.[25] If enough of the infrared light passes through the PETG, thermal cameras may be useful in the clinical evaluation of socket comfort and fit. A benefit of using thermal cameras for monitoring temperature is that the temperatures can be easily collected from the contralateral limb at the same time to observe the effect of vascular disease, amputation, and a prosthetic socket on the residual limb, compared to a healthy limb.

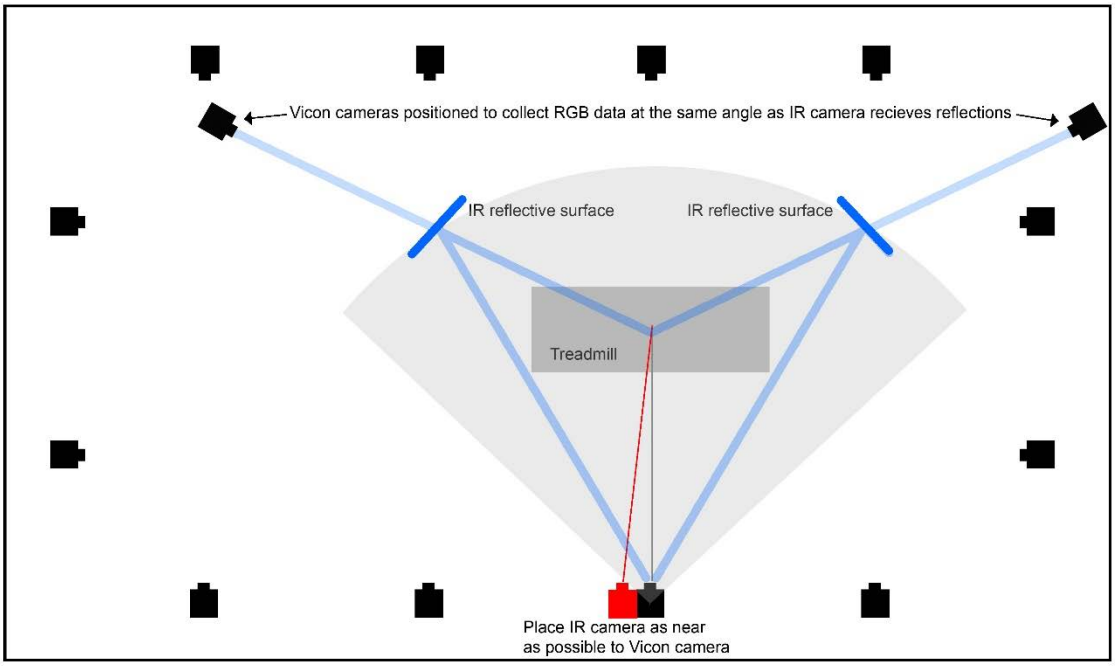


Figure 6.1. Aerial view of suggested gait lab setup for dynamic 3D thermal imaging

A disadvantage of using a thermal camera is that it only collects a 2D map from a single view-point, so only shows part of the limb at a time. Thermal imaging cameras are thousands of pounds each, so purchasing numerous cameras in order to calibrate them and collect 3D thermal information is not feasible. However, a novel idea is to use infrared reflective plates to mirror the body during exercise in a controlled environment such as a gait lab, so that the thermal camera can collect data from multiple angles simultaneously. Plexiglas (PMMA) reflects infrared light wavelengths between 2.8 µm and 25 µm but passes wavelengths up to 2.8 µm. Given that the human body radiates heat at wavelengths of around 9.3 µm, a Plexiglas sheet can be used as an infrared mirror without blocking visible light cameras. Figure 8 gives a suggestion of how the gait lab might be able to be set up to make the most of the Vicon motion capture system. The Vicon motion capture system triangulates the 3D position of a marker between cameras calibrated to provide overlapping projections. Its cameras use optical-passive motion capture, using retroreflective markers placed on the participant, that are tracked using short-wave infrared wavelengths.[343] Unfortunately, these cameras do not capture the range of wavelengths required for thermal imaging. Retroreflective markers reflect the incident ray back in the same direction it came from regardless of the angle of incidence. This effect is achieved by using a sphere made of a material with a refractive index that is exactly 2 times the refractive index of the medium from which the radiation is incident. This causes the sphere surface to behave as a concave

spherical mirror with the required curvature for retroreflection.[344] The cameras filter out other wavelengths so that the markers shine brightly on the cameras' images.

The design in Figure 8 places a high-quality infrared thermal imaging camera as near as possible to one of the calibrated motion capture cameras, to view the participant from the same angle. By positioning Plexiglas sheets that reflect infrared light on the far side of participant, it may be possible to capture other angles of the participant in the reflections that return to the thermal camera, while the sheets remain transparent to the motion capture cameras.

The Oxford Gait Lab has 12 fixed cameras and two portable cameras that can be calibrated. If the two portable cameras are placed behind the Plexiglas sheets so that they capture the same angle and distance as the reflected images, they can be used to calibrate the angles of the reflections. The Engineering Science Department has a FLIR thermal imaging camera. FLIR Systems offers training on how to combine the FLIR infrared data with other cameras in MATLAB. Vicon's DataStream SDK streams data from the Vicon system to third-party programs and plug-ins, including MATLAB.[345] Combining the Vicon data streaming with the FLIR thermal imaging in MATLAB should enable the thermal maps from the warm body to be overlaid onto the 3D positional data. The accuracy of the point matching when overlaying the thermal images would require testing and validation. The thermal images would not provide a perfect 360◦ thermal reconstruction, as the limited number of reflected angles means that when one part of the body crosses in front of another between the camera or Plexiglas, a section of skin will momentarily pass through a 'blind' region in the thermal camera's display. Another possible issue with this system is that the infrared wavelength that the Vicon cameras use may be within the region that is blocked by the Plexiglas, stopping the cameras from detecting the markers on the participant. This method of collecting skin temperature requires expensive equipment, so might be useful for clinicians in the UK, but is not transferable to lower-income countries.

6.4.2.2. Thermochromic liquid crystals (TLCs)

TLCs are molecules sprayed onto a surface that reflect light in an optically active range of temperatures. These coatings are temperature sensitive, selectively reflecting light. The liquid crystal structure is made up of layers of molecules that are aligned when they are in their solid crystal phase, but as they heat, the layers twist away from each other, and reflect incident white light (Figure 6.2.). They twist further as they heat, so that the wavelength of light that can travel through and reflect back slowly changes through the visible spectrum. Eventually they heat to the point where the bonds break and they function as a liquid. The wavelengths reflected respond directly to the temperature, responding the same whether heating or cooling.

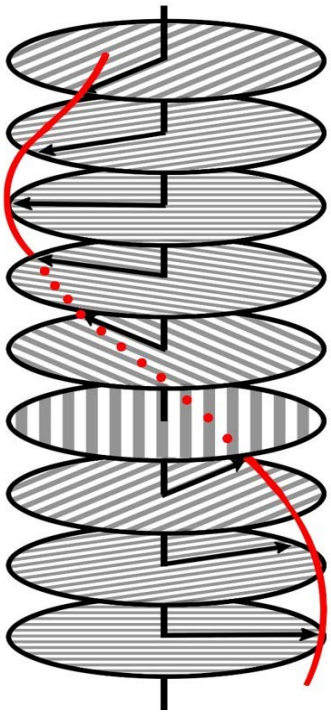


Figure 6.2. Thermochromic liquid crystal structure

TLC products are designed with different colour bandwidths, anywhere between -30°C and 115°C. Skin temperature measurements would require a bandwidth of around 28°C to 38°C. The narrower the bandwidth, the higher the resolution that can be detected.[346] The benefits of using thermochromic liquid crystals for mapping the temperature include that they do not require expensive equipment, they do not require connection to a data-collection system or electrical power (thus allowing the wearer to ambulate freely), and their output is visually easy to interpret. They would need to be against the skin to accurately measure skin temperatures, and require visualisation, meaning that they are only useful inside transparent sockets, either sprayed as a layer within the socket or on a thin sock that can be worn within the socket. Though this need for visibility makes them inappropriate for definitive sockets, the method may be viable for incorporating into the current check-socket designs to give prosthetists increased information about what type and shape of socket might suit the user before the definitive socket is made. No studies have used TLCs to assist prosthetists in assessing check-sockets.

The TLC spray paint is expensive, costing approximately £10 per socket, as well as being time-consuming to apply and calibrate. Therefore, coating inside each participant's

check-socket is not as efficient as painting a transparent gel liner that can be worn in the check-socket. These liners come in standard sizes, rather than requiring individual fitting, so could be used for multiple amputees as part of the fitting process. The TLCs are durable and should last for many tests before beginning to wear off the socket, even with the bending and rubbing of a liner as it is placed on the residual limb and into the prosthetic socket.

To calibrate the thermochromic liquid crystals, they would need to be tested against more accurate sensors, such as thermocouples, on a flat surface with a known heat dissipation curve, then the effect of adding PETG plastic over the top would need to be assessed. This would show the correlation curve between the input temperature and the wavelength reflected, to test whether the resolution is fine enough to capture small changes in temperature at the residual limb. An issue with using thermochromic liquid crystals is that they typically come with a spectral range of 1°C or 20°C. Neither of these are ideal for detecting changes in temperature of the skin, given that there is approximately 4°C difference between the proximal and distal ends of the residual limb, but only small changes in temperature found during changing physical activity. One group overcame this by using a pattern of different ranges across a fabric, but it makes the outcome much harder to visually interpret.[347]

For research purposes it is useful to quantify the changes in colour. This could be done with careful calibration of a camera so that the colours at each location are accurately recorded under the specific ambient lighting conditions. A challenge of developing this method is that viewing angle changes the wavelength seen, so must be calibrated for, particularly with wide bandwidths. A study of how curves affect the reflected wavelength would be required to estimate the calibration requirements for the different areas of a prosthesis, based on the general shape of a prosthesis.

Another area to be wary of is that pressure and shear forces can also induce changes in colour in TLCs, so the colour change may not be purely based on temperature. However, the low forces of human locomotion, are unlikely to significantly affect temperature outputs. The paint’s effect on the thermal properties of the socket also would require testing. TLCs

are also susceptible to contamination by UV and organic solvents, so may need protective coatings.

6.4.2.3. Temperature sensor grid

Previous studies have used temperature sensors (either thermistors[66–69] or integrated circuit (IC) temperature sensors[70]) placed on the skin. ICs are a sensible choice if considering adding individual sensors to measure discrete points within the prosthetic socket, rather than thermocouples, resistance temperature detectors (RTDs) or thermistors. This is because IC temperature sensors have a linear response (so do not require linearisation or other circuitry), they have the highest output and are small and inexpensive. An IC sensor is a silicon temperature transducer with a two-terminal integrated circuit that produces a current or voltage directly proportional to the temperature.

To collect temperatures across the limb, many sensors would be required in a grid formation.[348] This is impractical due to expense, challenges with calibration, and the likelihood of the sensors to interfere with socket comfort and integrity. Embedding wires and sensors in a liner is also likely to destroy the liner's structural integrity, and placing the sensors directly onto the skin provides positioning challenges and is likely to cause chaffing and skin irritation.[349] Other issues are that ICs do not directly measure the skin temperature, they create self-heating errors that can affect the temperature output, and the accuracy is relatively low compared to the small temperature changes expected on the skin during short, intermittent exercise.[135] Creating a grid of ICs allows monitoring of the skin temperatures outside the laboratory, and within a definitive prosthesis, but the method is not ideal for long-term monitoring of tissue health and socket fit.

6.4.2.4. Fibre optics

Fibre optics have been used to map temperature in areas that are difficult to measure with thermal cameras, because they can wrap around complex surfaces for 3D mapping.[350] The optical fibres are thin strands of glass about the diameter of a human hair. Light is scattered and attenuated as it travels along the fibre optic cable. A physical disturbance, such as a change in temperature, changes the reflected wavelength of the light. Optical fibre sensors then detect the variations in the scattering spectrum. A frequently used sensor is based on a Fibre Bragg Grating, where gratings are created within the fibre. The spacing between gratings changes with temperature, which causes the refractive index to change, and

therefore a shift in the reflected wavelength. This technology is extremely expensive and typically used for monitoring temperature over large spatial fields and temperature ranges, such as temperature air flows in jet engines.[350]

6.4.2.5. Wire grid

Wires change resistance when heated or bent. The relationship between temperature and resistance of a wire can be written as:

$$R = R_0(1 + \alpha(T - T_0))$$

where R is the resistance of the wire at the present temperature, R_0 is the resistance of the wire at the initial (or reference) temperature, α is the temperature coefficient of resistance and T and T_0 are the present and initial temperatures, respectively. This resistance at a fixed temperature can be determined by the length and thickness of the wire:

$$R = r\frac{l}{A}$$

where r is the resistivity of the metal, l is the length of the wire and A is the cross-sectional area. Resistance temperature detectors (RTDs) use this relationship to provide the temperature from the changes in the resistance of a single length of wire over time. However, this method is unable to detect where the temperature change occurred along the wire, or differentiate between temperature changes and mechanical loading. Weaving thin conductive fibres into a fabric can create a mesh of sensors that monitor temperature changes across a surface. This has been considered a poor method of mapping temperature in the past, because it is difficult to pinpoint where along the wire the temperature change occurred that caused the change in resistance along the wire. If only using two weave directions, as in most fabrics, a change in resistance in some of the fibres could mean a change at the point where those fibres meet, or multiple changes elsewhere Figure 6.3.

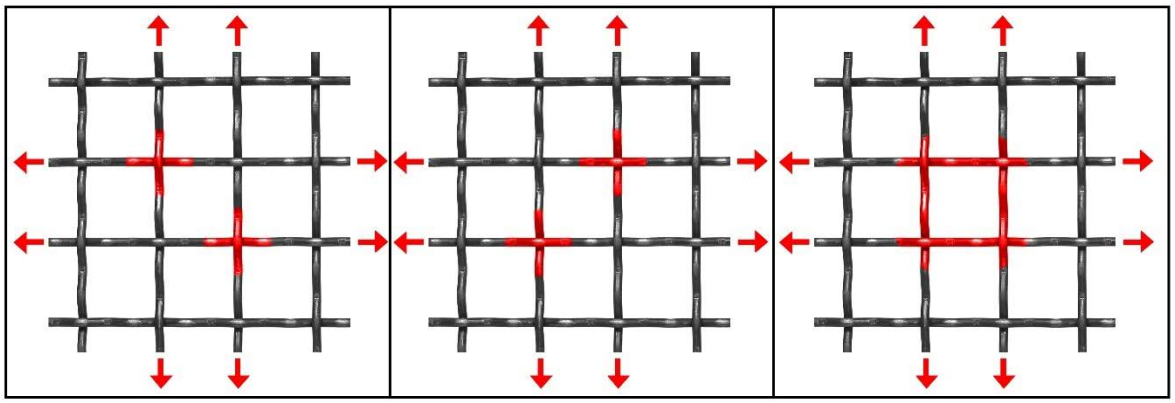


Figure 6.3. Example of temperature patterns that cannot be differentiated with a 2-direction weave

A novel idea in sensor design is to weave more angles through each point and use an inverse Radon transform to back-project the measured changes in resistance at the ends of the threads to the location of the change along the threads. This significantly increases the accuracy of location predictions of temperature changes. The inverse Radon transform is an integral transform used in reconstructing images from CT scans.[351] CT scanners collect varying levels of signal from many more angles than can be woven through a fabric, but the fabric does not need to provide as detailed an image, so the same theory may be able to be transferred to reconstructing a temperature map from a wire grid.

The hex-axial weave pattern shown in Figure 6.4 has six weave directions instead of the normal two. The weave shown is most commonly seen in decorative basket weaving, and has not been published in sensor design.

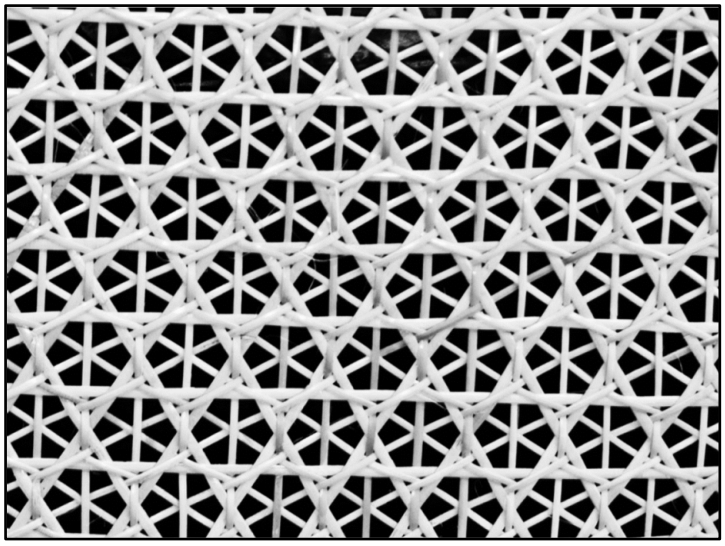


Figure 6.4. A hex-axial weave pattern typically used in basket weaving

Using thin resistive fibres, I created a weave pattern with 12 directions. This design could also double each conductive thread, weaving two wires parallel to each other at each point, to take advantage of the fact that metals have unique temperature coefficients. As with thermocouple design, various pairs of metals can be used to differentiate between changes in temperature and changes in mechanical loading. This can be used to decrease the signal noise when measuring temperature, or maybe with reference fibres, also be used to detect changes in mechanical loading. A stainless steel or silver coated yarn paired with a constantan fibre have shown high potential difference and a good linear relationship.[352,353] Polymer wires might also be feasible if they have an even spread of nanoparticles to enable the back projection.

The largest challenge with developing this type of sensor is likely to be having detectors with high enough accuracy to read the changes in resistance, as the temperature variation across the skin is only a few degrees and a leg is not large enough to easily weave long wires through. It is important to remove the noise created by mechanical strains, as this creates a larger signal than the temperature changes. A Wheatstone bridge might make this possible.

Sweat may also affect the resistivity and needs to be taken into consideration. Another challenge is developing a non-flat weave. The tested basket weave would require significant distortion of the grid to reach the top of the socket, providing the poorest spatial resolution at the base of the residuum.

Future research could focus on designing a thin sock that can be worn inside the prosthetic socket that maps the changes in temperature and mechanical loading at the skin interface using this wire-grid method. A phone app could be developed to wirelessly receive this data. This low-cost, unobtrusive sensing system may enable a comparison of empirical results with the simulated results for validation purposes and provide long-term monitoring to give early warning of changes in socket performance and fit.

Table 6.1. Comparison of temperature sensing methods

	IC chips	**Thermal camera**	**TLCs**	**Resistive grid**
Cost (including analysis)	Very high	Very high	Low	Moderate
360° view	Yes (discrete points)	Maybe (with mirrors)	Yes	Yes (discrete points)
Quantitative output	Yes	Challenging	Challenging	Yes
Freedom to test in varied environments	Yes (power required)	Some	Yes (requires calibration to quantify output)	Yes (power required)
Able to be combined with other sensors	Yes (increases bulk and power requirements)	Possibly	No	Yes
Useable by clinicians or end-users	Possibly	No	Yes	Probably
Possible consumer end product	Possibly	No	Possibly	Yes
Novel engineering research	Not much	Perhaps the mirror method for a 360° view	Yes	Yes
Comparable to contralateral side	Not without affecting heating	Yes	No	Not without affecting heating
Able to be transferred to any socket	Limited (affects socket integrity)	No	No	Yes
Spatial mapping	Discrete points	Yes	Yes	Many discrete points
Continuous time mapping	Yes	Yes	Yes	Yes

The comparison of temperature sensing methods in Table 6.1 does not consider the weighting of each of the considered factors. However, the resistive grid appears to be the most obvious solution because it can be used in all prosthetic sockets and rated ok on all factors considered. However, this method is far from being a commercial solution and requires extensive research to assess its validity before it can be used in the field of prosthetics.

7. Conclusions

Conventional manufacture of prosthetic sockets often leads to discomfort and tissue damage. This research shows that heat-related issues were the main type of discomfort experienced by amputees in Bangalore, India, and that socket comfort was the biggest area of dissatisfaction with current prosthetics. The research increases knowledge of the body's heat transfer mechanisms and the effect of amputation and wearing a prosthesis on heat transfer and thermal discomfort through reviewing literature, running a clinical study with amputees and developing a computational bioheat model.

This study is the first to compare amputee skin temperature to heat discomfort and to compare the temperatures between the amputated and healthy limbs. It also addresses a different demographic to previous studies, that were on highly active, and generally younger amputees with traumatic aeteology.[66–70] Given that the majority of leg amputations are attributed to vascular diseases, and older amputees are at risk of low levels of total physical activity, the present study provides important insight into a large demographic that has not been previously studied. The study focused on intermittent short exercise durations, which has not been assessed before. It found that skin temperatures did not explain the thermal discomfort experienced on the amputated limb during exercise. This might signal that the heat generated by the muscles in the residual limb during exercise is stored in the muscles.

The bioheat model is designed to explore muscle temperatures during exercise and post-exercise recovery in hot and humid climates. It is the first FEA model to focus on the muscle temperatures during exercise and to provide validation against empirical data. The model uses a novel method of predicting temperatures in the arterial blood flowing into the thigh, and models the large blood vessels separately, to improve the prediction of temperature distributions in the thigh. It shows that muscles can heat by more than 3°C during exercise and take over two hours to recover, even without the effect of insulation and amputation. The active thermoregulatory system successfully keeps the temperatures from rising too high in a healthy, uninsulated leg, but the model predicts that with insulation, the temperature, when exercising in a hot climate, rises to near the 39°C limit that the WHO recommends tissue should remain below to avoid thermal damage.

Based on the thermal modelling of a healthy leg and the literature and clinical study findings on amputee thermoregulation, it is reasonable to conclude that the decrease in blood flow in the residual limb, and the insulating properties of conventional prosthetic sockets are likely to cause the muscles in the residual limb to store excess heat during exercise, explaining the thermal discomfort often experienced by amputees. However, the amputee model requires future validation against empirical data.

The model also shows the importance of individual geometry and body composition in determining muscle temperatures. It is set up as a FEA model, which enables accurate geometries to be imported and used with the same physics, without significantly increasing the complexity and run-time. This model can be used to assess which parts of the prosthetic socket to target for cooling, showing that the heat is greater near the large muscles, and that the large blood vessels carry the heat from the core to the legs during rest and carry the heat from the legs away to the core during exercise.

This research demonstrates that thermal issues within a prosthetic socket are frequent, but the thermal responses of individuals are varied and complex. The bioheat model increases knowledge of the heat transfer factors to consider in developing user-specific prosthetic sockets that reduce the thermal load on the body. This model can benefit prosthetists, providing a greater understanding of the thermal benefits of using one type of socket over another, which can feed into their decision-making process when fitting an amputee with a new socket, and it can feed directly into the data-based clinical measurement methods being developed for the provision and assessment of prosthetic devices. Using this bioheat model to assess the feasibility of adding real-time user-specific simulation into the socket design and fitting process and into new socket designs will help direct the future of the prosthetic socket industry to determine if a more data-driven approach to design and fitting could provide better patient outcomes.

The systematic reviews on the effectiveness of 3D printing personalised prosthetics and other medical devices showed promise for integrating simulations, such as this bioheat model, with computer-aided design and 3D printing technology to improve data-driven customisation of prosthetic sockets. However, the technology still lacks research and clinical validation.

References

1. Gallagher, P & Desmond, D. Measuring quality of life in prosthetic practice: Benefits and challenges. *Prosthet. Orthot. Int.* **2007**; 31 (2) 167–176.

2. Khasnabis, C. Standards for prosthetics and orthotics service provision. *World Health Organization*. **2015**.

3. WHO. Global Disability Action Plan 2014-2021: Better health for all people with disability. *World Health Organization*. **2015**.

4. Tebbutt, E *et al*. Assistive products and the Sustainable Development Goals (SDGs). *Global. Health*. **2016**; 12 (79) 1–6.

5. MacLachlan, M. Systems thinking for assistive technology: Redesigning the future. in *ISPO UK Annual Scientific Meeting*. **2018**.

6. Borg, J, Lindstrom, A & Larsson, S. Assistive technology in developing countries: a review from the perspective of the Convention on the Rights of Persons with Disabilities. *Prosthet. Orthot. Int.* **2011**; 35 (1) 20–29.

7. Guidelines for training personnel in developing countries for prosthetics and orthotics services. *World Health Organization*. **2005**.

8. Prosthetics service review. **2018**. Available at: www.england.nhs.uk/commissioning/spec-services/npc-crg/group-d/d01.

9. Lake, C. The evolution of upper limb prosthetic socket design. *J. Prosthetics Orthot.* **2008**; 20 (3) 85.

10. Lee, PVS, Lythgo, N, Laing, S, Lavranos, J & Thanh, NH. Pressure casting technique for transtibial prosthetic socket fit in developing countries. *J. Rehabil. Res. Dev.* **2014**; 51 (1) 101–110.

11. Zettl, JH & Traub, JE. Premodified casting for the patellar-tendon-bearing prosthesis. *Artif. Limbs*. **1971**; 15 (l) 1–14.

12. Chitresh, N, Singh, A & Himanshu, C. Customised prosthetic socket fabrication using 3D scanning and printing. in *4th International Conference on Additive Manufacturing Technologies*. **2014**.

13. Thannhauser, SV. Biomechanical assessment of CAD/CAM and hand-cast prostheses for transtibial amputees. (*Thesis: University of Calgary*). **2009**.

14. Gholizadeh, H, Abu Osman, NA, Eshraghi, A, Ali, S & Razak, NA. Transtibial prosthesis suspension systems: Systematic review of literature. *Clin. Biomech.* **2014**; 29 (1) 87–97.

15. Andrysek, J. Lower-limb prosthetic technologies in the developing world: A review of literature from 1994–2010. *Prosthet. Orthot. Int.* **2010**; 34 (4) 378–98.

16. LeTourneau Prosthetics. Suspension choice a key element of prosthetic success. **2016**. Available at: www.llop.com/choice-key-element-prosthetic-success.

17. Sanders, JE & Fatone, S. Residual limb volume change: Systematic review of measurement and management. *J. Rehabil. Res. Dev.* **2011**; 48 (8) 949–986.

18. Board, WJ, Street, GM & Caspers, C. A comparison of trans-tibial amputee suction and vacuum socket conditions. *Prosthet. Orthot. Int.* **2001**; 25 (3) 202–209.

19. Nair, A, Hanspal, RS, Zahedi, MS, Saif, M & Fisher, K. Analyses of prosthetic episodes in lower limb amputees. *Prosthet. Orthot. Int.* **2008**; 32 (1) 42–49.

20. Oxford University Hospitals. Transfemoral prosthesis information for patients. *NHS Trust*. **2015**.

21. Nottingham University Hospitals. Advice following discharge with a prosthesis. *NHS Trust*. **2017**.

22. P&O Care. Prosthetic timeline. **2018**. Available at: www.pandocare.com/prosthetic-timeline.

23. The Leads Teaching Hospitals. The Prosthetic Limb Service. *NHS Trust*. **2012**.

24. Gholizadeh, H *et al.* Evaluation of new suspension system for limb prosthetics. *Biomed. Eng. Online*. **2014**; 13 (1) 1–13.

25. Klute, GK, Rowe, GI, Mamishev, a V & Ledoux, WR. The thermal conductivity of prosthetic sockets and liners. *Prosthet. Orthot. Int.* **2007**; 31 (3) 292–299.

26. Tsikandylakis, G, Berlin, Ö & Brånemark, R. Implant survival, adverse events, and bone remodeling of osseointegrated percutaneous implants for transhumeral amputees. *Clin. Orthop. Relat. Res.* **2014**; 472 (10) 2947–2956.

27. Hebert, JS, Rehani, M & Stiegelmar, R. Osseointegration for lower-limb amputation: A systematic review of clinical outcomes. *JBJS Rev.* **2017**; 5 (10) 1–12.

28. Dillingham, TR, Pezzin, LE, MacKenzie, EJ & Burgess, AR. Use and satisfaction with prosthetic devices among persons with trauma-related amputations: A long-term outcome study. *Am. J. Phys. Med. Rehabil.* **2001**; 80 (8) 563–571.

29. Biddiss, E, Beaton, D & Chau, T. Consumer design priorities for upper limb prosthetics. *Disabil. Rehabil. Assist. Technol.* **2007**; 2 (6) 346–357.

30. Hagberg, K & Brånemark, R. Consequences of non-vascular trans-femoral amputation: A survey of quality of life, prosthetic use and problems. *Prosthet. Orthot. Int.* **2001**; 25 (3) 186–194.

31. Ghoseiri, K & Safari, MR. Prevalence of heat and perspiration discomfort inside prostheses: literature review. *J. Rehabil. Res. Dev.* **2014**; 51 (6) 855–68.

32. Biddiss, EA & Chau, TT. Upper limb prosthesis use and abandonment: A survey of the last 25 years. *Prosthet. Orthot. Int.* **2007**; 31 (3) 236–257.

33. Cordella, F *et al.* Literature review on needs of upper limb prosthesis users. *Front. Neurosci.* **2016**; 10 (209) 1–14.

34. Østlie, K *et al.* Prosthesis rejection in acquired major upper-limb amputees: a population-based survey. *Disabil. Rehabil. Assist. Technol.* **2012**; 7 (4) 294–303.

35. Nagaraja, VH, Bergmann, JH, Sen, D & Thompson, MS. Examining the needs of affordable upper limb prosthetic users in India: A questionnaire-based survey. *Technol. Disabil.* **2016**; 28 (3) 101–110.

36. Hagberg, K. Transfemoral amputation, quality of life and prosthetic function. *Department of Orthopaedics, Göteborg University*. **2006**.

37. Sanders, JE, Goldstein, BS & Leotta, DF. Skin response to mechanical stress: adaptation rather than breakdown--a review of the literature. *J. Rehabil. Res. Dev.* **1995**; 32 (3) 214–226.

38. Dudek, NL, Marks, MB, Marshall, SC & Chardon, JP. Dermatologic conditions associated with use of a lower-extremity prosthesis. *Arch. Phys. Med. Rehabil.* **2005**; 86 (4) 659–663.

39. Highsmith, JT & Jason, T. Identifying and managing skin issues with lower-limb prosthetic use. *inMotion - A Publ. Amputee Coalit.* **2011**; 21 (1) 41–43.

40. Highsmith, MJ *et al.* Interventions to manage residual limb ulceration due to prosthetic use in individuals with lower extremity amputation: A systematic review of the literature. *Technol. Innov.* **2016**; 18 (2–3) 115–123.

41. Biddiss, E & Chau, T. Upper-limb prosthetics: critical factors in device abandonment. *Am. J. Phys. Med. Rehabil.* **2007**; 86 (12) 977–987.

42. Chamlian, TR. Use of prostheses in lower limb amputee patients due to peripheral arterial disease. *Einstein (São Paulo)*. **2014**; 12 (4) 440–446.

43. Pupulin, E. A manual for the rehabilitation of people with limb amputation. *World Health Organization*. **2004**.

44. Meulenbelt, HEJ, Geertzen, JHB, Jonkman, MF & Dijkstra, PU. Skin problems of the stump in lower limb amputees: 1. A clinical study. *Acta Derm. Venereol.* **2011**; 91 (2) 133–137.

45. Black, JM *et al.* Medical device related pressure ulcers in hospitalized patients. *Int. Wound J.* **2010**; 7 (5) 358–365.

46. Safari, MR & Meier, MR. Systematic review of effects of current transtibial prosthetic socket designs—Part 1: Qualitative outcomes. *J. Rehabil. Res. Dev.* **2015**; 52 (5) 491–508.

47. Safari, MR & Meier, MR. Systematic review of effects of current transtibial prosthetic socket designs—Part 2: Quantitative outcomes. *J. Rehabil. Res. Dev.* **2015**; 52 (5) 509–526.

48. Ahmad, N, Thomas, GN, Gill, P, Chan, C & Torella, F. Lower limb amputation in England: prevalence, regional variation and relationship with revascularisation,

deprivation and risk factors. A retrospective review of hospital data. *J. R. Soc. Med.* **2014**; 107 (12) 483–489.

49. Ziegler-Graham, K, MacKenzie, EJ, Ephraim, PL, Travison, TG & Brookmeyer, R. Estimating the prevalence of limb loss in the United States: 2005 to 2050. *Arch. Phys. Med. Rehabil.* **2008**; 89 (3) 422–429.

50. Stewart, CPU & Jain, AS. Cause of death of lower limb amputees. *Prosthet. Orthot. Int.* **1992**; 16 (2) 129–132.

51. Langford, J, Dillon, MP, Granger, CL & Barr, C. Physical activity participation amongst individuals with lower limb amputation. *Disabil. Rehabil.* **2019**; 41 (9) 1063–1070.

52. Deans, S, Burns, D, McGarry, A, Murray, K & Mutrie, N. Motivations and barriers to prosthesis users participation in physical activity, exercise and sport: A review of the literature. *Prosthet. Orthot. Int.* **2012**; 36 (3) 260–269.

53. Sorensen, L, Molyneaux, L & Yue, DK. The relationship among pain, sensory loss, and small nerve fibers in diabetes. *Diabetes Care*. **2006**; 29 (4) 883–887.

54. Sengeh, DM. Advanced prototyping of variable impedance prosthetic sockets for trans-tibial amputees: Polyjet matrix 3D printing of comfortable prosthetic sockets using digital anatomical data. (*Thesis: Massachusetts Institute of Technology*). **2012**.

55. Sanders, JE, Severance, MR & Allyn, KJ. Computer-socket manufacturing error: How much before it is clinically apparent? *J. Rehabil. Res. Dev.* **2012**; 49 (4) 567.

56. Sanders, JE *et al.* CAD/CAM transtibial prosthetic sockets from central fabrication facilities: How accurate are they? *J. Rehabil. Res. Dev.* **2007**; 44 (3) 395.

57. Smith, DG & Burgess, EM. The use of CAD/CAM technology in prosthetics and orthotics - current clinical models and a view to the future. *J. Rehabil. Res. Dev.* **2001**; 38 (3) 327–334.

58. Sengeh, DM & Herr, H. A variable-impedance prosthetic socket for a transtibial amputee designed from magnetic resonance imaging data. *J Prosthet Orthot*. **2013**; 25 (3) 129–137.

59. Rogers, B *et al.* Advanced trans-tibial socket fabrication using selective laser sintering. *Prosthet. Orthot. Int.* **2007**; 31 (1) 88–100.

60. Pirouzi, G *et al.* Review of the socket design and interface pressure measurement for transtibial prosthesis. *Sci. World J.* **2014**; 1–9.

61. Laszczak, P *et al.* Development and validation of a 3D-printed interfacial stress sensor for prosthetic applications. *Med. Eng. Phys.* **2015**; 37 (1) 132–7.

62. Mak, AF, Zhang, M & Boone, DA. State-of-the-art research in lower-limb prosthetic biomechanics-socket interface: a review. *J. Rehabil. Res. Dev.* **2001**; 38 (2) 161–174.

63. Al-Fakih, EA, Abu Osman, NA & Mahmad Adikan, FR. Techniques for interface stress measurements within prosthetic sockets of transtibial amputees: A review of the past 50 years of research. *Sensors (Basel)*. **2016**; 16 (7) 1–30.

64. Stech, N. MovAid - Movement Assistive Devices: Manufacturing of personalised Kineto-Dynamics parts and products for workers, elderly and children. in *ISPO UK Annual Scientific Meeting*. **2018**.

65. Zuniga, J *et al.* Cyborg beast: a low-cost 3d-printed prosthetic hand for children with upper-limb differences. *BMC Res. Notes*. **2015**; 8 (1) 10.

66. Peery, JT, Ledoux, WR & Klute, GK. Residual-limb skin temperature in transtibial sockets. *J. Rehabil. Res. Dev.* **2005**; 42 (2) 147–154.

67. Huff, E a., Ledoux, WR, Berge, JS & Klute, GK. Measuring residual limb skin temperatures at the skin-prosthesis interface. *JPO J. Prosthetics Orthot.* **2008**; 20 (4) 170–173.

68. Klute, GK, Huff, E & Ledoux, WR. Does activity affect residual limb skin temperatures? *Clin. Orthop. Relat. Res.* **2014**; 472 (10) 3062–3067.

69. Segal, AD & Klute, GK. Residual limb skin temperature and thermal comfort in people with amputation during activity in a cold environment. *J. Rehabil. Res. Dev.* **2016**; 53 (5) 619–628.

70. Cutti, AG, Perego, P, Fusca, MC, Sacchetti, R & Andreoni, G. Assessment of lower limb prosthesis through wearable sensors and thermography. *Sensors (Switzerland)*. **2014**; 14 (3) 5041–5055.

71. Census of India 2011: C-29 Disabled population by type of disability, educational level and sex. *Government of India*. **2011**. Available at: www.censusindia.gov.in/2011census/population_enumeration.html.

72. World Health Organistaion. World Report on Disability. *Geneva, Switzerland*. **2011**.

73. Cochrane, H, Rosario, D, Singh, A & Ghosh, R. Prosthetics & orthotics impact assessment: India and Bangladesh. *International Society for Prosthetics and Orthotics*. **2015**.

74. Adelmanesh, F *et al.* Reliability, validity, and sensitivity measures of expanded and revised version of the Short-Form McGill Pain Questionnaire (SF-MPQ-2) in Iranian patients with neuropathic and non-neuropathic pain. *Pain Med.* **2012**; 13 (12) 1631–1636.

75. Dworkin, RH *et al.* Development and initial validation of an expanded and revised version of the Short-form McGill Pain Questionnaire (SF-MPQ-2). *Pain*. **2009**; 144 (1–2) 35–42.

76. Menezes Costa, L da C, Maher, CG, McAuley, JH & Costa, LOP. Systematic review of cross-cultural adaptations of McGill Pain Questionnaire reveals a paucity of clinimetric testing. *J. Clin. Epidemiol.* **2009**; 62 (9) 934–943.

77. Flouris, AD & Schlader, ZJ. Human behavioral thermoregulation during exercise in the heat. *Scand. J. Med. Sci. Sport.* **2015**; 25 (1) 52–64.

78. Gagge, AP, Stolwijk, JAJ & Hardy, JD. Comfort and thermal sensations and associated physiological responses at various ambient temperatures. *Environ. Res.* **1967**; 1 (1) 1–20.

79. Kimberger, O & Quast, S. The significance of core temperature - Pathophysiology and measurement methods. *Dräger Medical*. **2014**.

80. McMurray, RG, Soares, J, Caspersen, CJ & McCurdy, T. Examining variations of resting metabolic rate of adults: A public health perspective. *Med. Sci. Sports Exerc.* **2014**; 46 (7) 1352–1358.

81. Despopoulos, A & Silbernagl, S. Color atlas of physiology. *Thieme*. **2003**.

82. Lim, CL, Byrne, C & Lee, JKW. Human thermoregulation and measurement of body temperature in exercise and clinical settings. *Ann. Acad. Med. Singapore*. **2008**; 37 (4) 347–353.

83. Van Beek, JHGM *et al.* Simulating the physiology of athletes during endurance sports events: Modelling human energy conversion and metabolism. *Philos. Trans. R. Soc. A Math. Phys. Eng. Sci.* **2011**; 369 (1954) 4295–4315.

84. Venes, D. Taber's Cyclopedic Medical Dictionary. *F.A. Davis*. **2017**.

85. Romanovsky, AA. Skin temperature: Its role in thermoregulation. *Acta Physiologica*. **2014**; 210 (3) 498–507.

86. Deng, ZS & Liu, J. Mathematical modeling of temperature mapping over skin surface and its implementation in thermal disease diagnostics. *Comput. Biol. Med.* **2004**; 34 (6) 495–521.

87. Marieb, EN & Hoehn, K. Human Anatomy & Physiology. *Pearson*. **2007**.

88. Parsons, K. Human Thermal Environments. *The Effects of Hot, Moderate, and Cold Environments on Human Health, Comfort, and Performance*. *CRC Press*. **2014**.

89. Blatteis, CM. Physiology and pathophysiology of temperature regulation. *World Scientific*. **1998**.

90. Tilkens, MJ, Wall-Scheffler, C, Weaver, TD & Steudel-Numbers, K. The effects of body proportions on thermoregulation: an experimental assessment of Allen's rule. *J. Hum. Evol.* **2007**; 53 (3) 286–291.

91. Dervis, SM *et al.* A comparison of thermoregulatory responses to exercise between mass-matched groups with large differences in body fat. *J. Appl. Physiol.* **2016**; 120 (6) 615–623.

92. Kenny, GP & Jay, O. Thermometry, calorimetry, and mean body temperature during heat stress. *Compr. Physiol.* **2013**; 3 (4) 1689–1719.

93. Kenny, GP & McGinn, R. Restoration of thermoregulation after exercise. *J. Appl. Physiol.* **2017**; 122 (4) 933–944.

94. Sawka, MN, Montain, SJ & Latzka, WA. Hydration effects on thermoregulation and performance in the heat. *Comp. Biochem. Physiol. - A Mol. Integr. Physiol.* **2001**; 128

(4) 679–690.

95. Charkoudian, N. Mechanisms and modifiers of reflex induced cutaneous vasodilation and vasoconstriction in humans. *J. Appl. Physiol.* **2010**; 109 (4) 1221–1228.

96. Kenny, GP, Stapleton, JM, Yardley, JE, Boulay, P & Sigal, RJ. Older adults with type 2 diabetes store more heat during exercise. *Med. Sci. Sports Exerc.* **2013**; 45 (10) 1906–1914.

97. Poirier, MP, Gagnon, D, Friesen, BJ, Hardcastle, SG & Kenny, GP. Whole-body heat exchange during heat acclimation and its decay. *Med. Sci. Sports Exerc.* **2015**; 47 (2) 390–400.

98. Kenny, GP *et al.* Postexercise hypotension causes a prolonged perturbation in esophageal and active muscle temperature recovery. *Am. J. Physiol. Regul. Integr. Comp. Physiol.* **2006**; 291 (3) R580-8.

99. Neves, EB *et al.* Different responses of the skin temperature to physical exercise: Systematic review. *Conf. Proc. Annu. Int. Conf. IEEE Eng. Med. Biol. Soc.* **2015**; 1307–1310.

100. Bandeira, F, Moura, MAM De, Souza, MA De, Nohama, P & Neves, EB. Pode a termografia auxiliar no diagnóstico de lesões musculares em atletas de futebol? *Rev. Bras. Med. do Esporte*. **2012**; 18 (4) 246–251.

101. Ferreira, JJA *et al.* Exercise-associated thermographic changes in young and elderly subjects. *Ann. Biomed. Eng.* **2008**; 36 (8) 1420–1427.

102. Ghoseiri, K, Zheng, YP, Hing, LLT, Safari, MR & Leung, AK. The prototype of a thermoregulatory system for measurement and control of temperature inside prosthetic socket. *Prosthet. Orthot. Int.* **2015**; 40 (6) 751–755.

103. Ferres, HM. The effect of pressure on sweating. *J. Physiol.* **1960**; 151 591–597.

104. Miller, AA, Knight, KL, Feland, JB & Draper, DO. Neoprene thigh sleeves and muscle cooling after exercise. *J. Athl. Train.* **2005**; 40 (4) 264–270.

105. Ingraham, P. Heat Therapy: The Complete Guide to Treating Pain with Heat. **2016**. Available at: www.painscience.com/articles/heating.

106. Nadler, SF *et al.* Continuous low-level heatwrap therapy for treating acute nonspecific low back pain. *Arch. Phys. Med. Rehabil.* **2003**; 84 (3) 329–334.

107. Mayer, JM *et al.* Continuous Low-Level Heat Wrap Therapy for the Prevention and Early Phase Treatment of Delayed-Onset Muscle Soreness of the Low Back: A Randomized Controlled Trial. *Arch. Phys. Med. Rehabil.* **2006**; 87 (10) 1310–1317.

108. Draper, DO *et al.* Hot-pack and 1-MHz ultrasound treatments have an additive effect on muscle temperature increase. *J. Athl. Train.* **1998**; 33 (1) 21–24.

109. Whitman, TJ, Deiss, RG & Ferguson, TM. Update: Exertional rhabdomyolysis, active

component, U.S. Army, Navy, Air Force, and Marine Corps, 2011-2015. *Med. Surveill. Mon. Rep.* **2016**; 23 (3) 21–24.

110. Scalco, RS *et al.* Exertional rhabdomyolysis: physiological response or manifestation of an underlying myopathy? *BMJ Open Sport Exerc. Med.* **2016**; 2 (1)

111. Lin, H, Chie, W & Lien, H. Epidemiological analysis of factors influencing an episode of exertional rhabdomyolysis in high school students. *Am. J. Sports Med.* **2006**; 34 (3) 481–486.

112. Seese, TM, Harasaki, H, Saidel, GM & Davies, CR. Characterization of tissue morphology, angiogenesis, and temperature in the adaptive response of muscle tissue to chronic heating. *Lab. Investig.* **1998**; 78 (12) 1553–1562.

113. Périard, JD, Thompson, MW, Caillaud, C & Quaresima, V. Influence of heat stress and exercise intensity on vastus lateralis muscle and prefrontal cortex oxygenation. *Eur. J. Appl. Physiol.* **2013**; 113 (1) 211–222.

114. Walter, EJ & Carraretto, M. The neurological and cognitive consequences of hyperthermia. *Crit. Care*. **2016**; 20 (199) 1–8.

115. Junglee, NA *et al.* Exercising in a hot environment with muscle damage: effects on acute kidney injury biomarkers and kidney function. *Am J Physiol Ren. Physiol*. **2013**; 305 (6) 813–820.

116. Faulds, M & Meekings, T. Temperature management in critically ill patients. *Contin. Educ. Anaesthesia, Crit. Care Pain*. **2013**; 13 (3) 75–79.

117. Yarmolenko, PS *et al.* Thresholds for thermal damage to normal tissues: an update. *Int. J. Hyperth.* **2011**; 27 (4) 320–343.

118. González-Alonso, J, Quistorff, B, Krustrup, P, Bangsbo, J & Saltin, B. Heat production in human skeletal muscle at the onset of intense dynamic exercise. *J. Physiol.* **2000**; 524 (2) 603–15.

119. Flouris, AD *et al.* Non-invasive measurement of tibialis anterior muscle temperature during rest, cycling exercise and post-exercise recovery. *Physiol. Meas.* **2015**; 36 (7) 103–113.

120. Flouris, AD, Webb, P & Kenny, GP. Noninvasive assessment of muscle temperature during rest, exercise, and postexercise recovery in different environments. *J. Appl. Physiol.* **2015**; 118 (10) 1310–1320.

121. Williams, RJ, Takashima, A, Ogata, T & Holloway, C. A pilot study towards long-term thermal comfort research for lower-limb prosthesis wearers. *Prosthet. Orthot. Int.* **2019**; 43 (1) 47–54.

122. Harden, RN, Gagnon, CM, Gallizzi, M, Khan, AS & Newman, D. Residual limbs of amputees are significantly cooler than contralateral intact limbs. *Pain Pract.* **2008**; 8 (5) 342–347.

123. Seminati, E. Reliability of 3 different methods of assessing amputee residuum volume. in *ISPO UK Annual Scientific Meeting*. **2018**.

124. Gappmaier, E. The Submaximal Clinical Exercise Tolerance Test (SXTT) to establish safe exercise prescription parameters for patients with chronic disease and disability. *Cardiopulm. Phys. Ther. J.* **2012**; 23 (2) 19–29.

125. Jones, DR, Speier, J, Canine, K, Owen, R & Stull, GA. Cardiorespiratory responses to aerobic training by patients with postpoliomyelitis sequelae. *JAMA J. Am. Med. Assoc.* **1989**; 261 (22) 3255–3258.

126. McAuley, P, Myers, J, Abella, J & Froelicher, V. Evaluation of a specific activity questionnaire to predict mortality in men referred for exercise testing. *Am. Heart J.* **2006**; 151 (4) 1–7.

127. Khalfallah, K *et al.* Noninvasive galvanic skin sensor for early diagnosis of sudomotor dysfunction: Application to diabetes. *IEEE Sens. J.* **2012**; 12 (3) 456–463.

128. Villarejo, MV, Zapirain, BG & Zorrilla, AM. A stress sensor based on galvanic skin response (GSR) controlled by ZigBee. *Sensors (Switzerland)*. **2012**; 12 (5) 6075–6101.

129. Braune, S & Schady, W. Changes in sensation after nerve injury or amputation: the role of central factors. *J. Neurol. Neurosurg. Psychiatry*. **1993**; 56 (4) 393–399.

130. Aftanas, M & Zubek, JP. Cutaneous sensitivity of unilateral arm amputees. *Can. J. Psychol.* **1964**; 18 (2) 101–105.

131. Stevens, JC & Choo, KK. Temperature sensitivity of the body surface over the life span. *Somatosens. Mot. Res.* **1998**; 15 (1) 13–28.

132. Nothnagel, H *et al.* How stable are quantitative sensory testing measurements over time? Report on 10-week reliability and agreement of results in healthy volunteers. *J. Pain Res.* **2017**; 10 2067–2078.

133. Waris, T *et al.* Regeneration of cold, warmth and heat-pain sensibility in human skin grafts. *Br. J. Plast. Surg.* **1989**; 42 (5) 576–580.

134. Fiala, D, Lomas, KJ & Stohrer, M. Computer prediction of human themoregulatory and temperature responses to a wide range of environmental conditions. *Int J Biometeorol*. **2001**; 45 (3) 143–159.

135. MacRae, BA, Annaheim, S, Spengler, CM & Rossi, RM. Skin temperature measurement using contact thermometry: A systematic review of setup variables and their effects on measured values. *Front. Physiol.* **2018**; 9 (29)

136. Kenny, GP *et al.* Muscle temperature transients before, during, and after exercise measured using an intramuscular multisensor probe. *J. Appl. Physiol.* **2003**; 94 (6) 2350–2357.

137. Peery, JT, Klute, GK, Blevins, JJ & Ledoux, WR. A three-dimensional finite element model of the transibial residual limb and prosthetic socket to predict skin temperatures. *IEEE Trans. Neural Syst. Rehabil. Eng.* **2006**; 14 (3) 336–343.

138. Gao, T *et al.* Three-Dimensional Printed Thermal Regulation Textiles. *ACS Nano*.

2017; 11 (11) 11513–11520.

139. Portnoy, S, Siev-Ner, I, Shabshin, N & Gefen, A. Effects of sitting postures on risks for deep tissue injury in the residuum of a transtibial prosthetic-user: a biomechanical case study. *Comput. Methods Biomech. Biomed. Engin.* **2011**; 14 (11) 1009–1019.

140. Taylor, NAS, Tipton, MJ & Kenny, GP. Considerations for the measurement of core, skin and mean body temperatures. *J. Therm. Biol.* **2014**; 46 72–101.

141. Duc, S. Efficiency and Thermography in Cycling during a Graded Exercise Test. *J. Exerc. Sport. Orthop.* **2015**; 2 (3) 1–8.

142. Ring, E. The historical development of thermometry and thermal imaging in medicine. *J. Med. Eng. Technol.* **2006**; 30 (4) 192–198.

143. De Andrade Fernandes, A *et al.* Measuring skin temperature before, during and after exercise: A comparison of thermocouples and infrared thermography. *Physiol. Meas.* **2014**; 35 (2) 189–203.

144. Fernandes, A de A, Amorim, PR dos S, Brito, CJ, Sillero-Quintana, M & Marins, JCB. Regional skin temperature response to moderate aerobic exercise measured by infrared thermography. *Asian J. Sports Med.* **2016**; 7 (1) 1–8.

145. Niedermann, R *et al.* Prediction of human core body temperature using non-invasive measurement methods. *Int. J. Biometeorol.* **2014**; 58 (1) 7–15.

146. Casa, DJ *et al.* Validity of devices that assess body temperature during outdoor exercise in the heat. *J. Athl. Train.* **2007**; 42 (3) 333–342.

147. Morris, C, Atkinson, G, Drust, B, Marrin, K & Gregson, W. Human core temperature responses during exercise and subsequent recovery: An important interaction between diurnal variation and measurement site. *Chronobiol. Int.* **2009**; 26 (3) 560–575.

148. Yoshioka, Y *et al.* Noninvasive measurement of temperature and fractional dissociation of imidazole in human lower leg muscles using 1 H-nuclear magnetic resonance spectroscopy. *J. Appl. Physiol.* **2005**; 98 (1) 282–287.

149. Rieke, V & Pauly, KB. MR thermometry. *J. Magn. Reson. Imaging*. **2008**; 27 (2) 376–390.

150. Katić, K, Li, R & Zeiler, W. Thermophysiological models and their applications: A review. *Build. Environ.* **2016**; 106 286–300.

151. Stańczyk, M, Leeuwen, GMJ Van & Steenhoven, AA Van. Discrete vessel heat transfer in perfused tissue—model comparison. *Phys. Med. Biol.* **2007**; 52 (9) 2379–2391.

152. Chen, MM & Holmes, KR. Microvascular Contributions in Tissue Heat Transfer. *Ann. N. Y. Acad. Sci.* **1980**; 335 (1) 137–150.

153. Wissler, EH. Steady-state temperature distribution in man. *J. Appl. Physiol.* **1961**; 16 (4) 734–740.

154. Stolwijk, JAJ. A mathematical model of physiological temperature regulation in man.

NASA CR-1855. Yale University School of Medicine. **1971**.

155. Fiala, D, Lomas, KJ & Stohrer, M. A computer model of human thermoregulation for a wide range of environmental conditions: the passive system. *J. Appl. Physiol.* **1999**; 87 (5) 1957–1972.

156. Huizenga, C, Hui, Z & Arens, E. A model of human physiology and comfort for assessing complex thermal environments. *Build. Environ.* **2001**; 36 (6) 691–699.

157. Lai, D & Chen, Q. A two-dimensional model for calculating heat transfer in the human body in a transient and non-uniform thermal environment. *Energy Build.* **2016**; 118 114–122.

158. Miller, TR, Nelson, DA, Kuznetz, L & Bue, G. Dynamic simulation of human thermoregulation and heat transfer for spaceflight applications. in *41st International Conference on Environmental Systems*. **2011**.

159. Tanabe, S, Kobayashi, K, Nakano, J, Ozeki, Y & Konishi, M. Evaluation of thermal comfort using combined multi-node thermoregulation(65MN) and radiation models and computational fluid dynamics (CFD). *Energy Build.* **2002**; 34 637–646.

160. van Treeck, C *et al.* Integrated thermal comfort analysis using a parametric manikin model for interactive real-time simulation. *J. Build. Perform. Simul.* **2009**; 2 (4) 233–250.

161. Fiala, D *et al.* Physiological modeling for technical, clinical and research applications. *Front. Biosci. S2*. **2010**; 2 (3) 939–968.

162. Kobayashi, Y & Tanabe, SI. Development of JOS-2 human thermoregulation model with detailed vascular system. *Build. Environ.* **2013**; 66 1–10.

163. Wölki, D *et al.* Individualisation of virtual thermal manikin models for predicting thermophysical responses. *12th Int. Conf. Indoor Air Qual. Clim. 2011*. **2011**; 1 432–437.

164. Zhang, H, Huizenga, C, Arens, E & Yu, T. Considering individual physiological differences in a human thermal model. *J. Therm. Biol.* **2001**; 26 (4–5) 401–408.

165. Sun, X, Eckels, S & Zheng, ZC. An improved thermal model of the human body. *HVAC&R Res.* **2012**; 18 (3) 323–338.

166. Ferreira, MS & Yanagihara, JI. A transient three-dimensional heat transfer model of the human body. *Int. Commun. Heat Mass Transf.* **2009**; 36 (7) 718–724.

167. Werner, J & Buse, M. Temperature profiles with respect toinhomogeneity and geometry of the human body. *Appl. Physiol.* **1988**; 65 1110–8.

168. Li, F, Wang, Y & Li, Y. A transient 3-D thermal model for clothed human body considering more real geometry. *J. Comput.* **2013**; 8 (3) 676–684.

169. Kalra, M, Bahrami, M & Sparrey, CJ. The effects of physiological thermoregulation

on the efficacy of surface cooling for therapeutic hypothermia. *Med. Biol. Eng. Comput.* **2015**; 53 (3) 205–213.

170. Trobec, R & Depolli, M. Simulated temperature distribution of the proximal forearm. *Comput. Biol. Med.* **2011**; 41 (10) 971–979.

171. Mitchell, J, Galvez, T, Hengle, J, Myers, G & Siebecker, K. Thermal response of human legs during cooling. *J. Appl. Physiol.* **1970**; 29 (6) 859–865.

172. González-Alonso, J. Human thermoregulation and the cardiovascular system. *Exp. Physiol.* **2012**; 97 (3) 340–346.

173. Kenny, GP *et al.* Heat balance and cumulative heat storage during intermittent bouts of exercise. *Med. Sci. Sports Exerc.* **2009**; 41 (3) 588–596.

174. Kenny, GP & Jay, O. Sex differences in postexercise esophageal and muscle tissue temperature response. *Am. J. Physiol. Integr. Comp. Physiol.* **2007**; 292 (4) 1632–1640.

175. Kenny, GP, Webb, P, Ducharme, MB, Reardon, FD & Jay, O. Calorimetric measurement of postexercise net heat loss and residual body heat storage. *Med. Sci. Sports Exerc.* **2008**; 40 (9) 1629–1636.

176. Long, BC, Cordova, ML, Brucker, JB, Demchak, TJ & Stone, MB. Exercise and quadriceps muscle cooling time. *J. Athl. Train.* **2005**; 40 (4) 260–263.

177. Bristow, GK, Sessler, DI & Giesbrecht, GG. Leg temperature and heat content in humans during immersion hypothermia and rewarming. *Aviat. Sp. Environ. Med.* **1994**; 65 (3) 220–226.

178. Pennes, H. Analysis of tissue and arterial blood temperatures in the resting human forearm. *J. Appl. Physiol.* **1948**; 1 (2) 93–122.

179. Shih, T-C, Kou, H-S, Liauh, C-T & Lin, W-L. Thermal Models of Bioheat Transfer Equations in Living Tissue and Thermal Dose Equivalence Due To Hyperthermia. *Biomed. Eng. Appl. Basis Commun.* **2002**; 14 (02) 86–96.

180. Chiesa, ST, Trangmar, SJ & González-Alonso, J. Temperature and blood flow distribution in the human leg during passive heat stress. *J. Appl. Physiol.* **2016**; 120 (9) 1047–1058.

181. Fiala, D, Havenith, G, Bröde, P, Kampmann, B & Jendritzky, G. UTCI-Fiala multi-node model of human heat transfer and temperature regulation. *Int. J. Biometeorol.* **2012**; 56 (3) 429–441.

182. Salloum, M, Ghaddar, N & Ghali, K. A new transient bio-heat model of the human body. in *ASME Summer Heat Transfer Conference*. **2005**.

183. Stergiopulos, N, Young, DF & Rogge, TR. Computer simulation of arterial flow with applications to arterial and aortic stenoses. *J. Biomech.* **1992**; 25 (12) 1477–1488.

184. COMSOL Multiphysics. Fluid Flow: Conservation of Momentum, Mass, and Energy. *Multiphysics Cyclopedia*. **2018**. Available at: uk.comsol.com/multiphysics/fluid-flow-conservation-of-momentum-mass-and-energy.

185. Caro, CG, Pedley, T., Schoroter, R. & Seed, W. The Mechanics of the Circulation. *Oxford Medical Publications*. **1978**.

186. Cengel, YA & Ghajar, AJ. Heat and Mass Transfer: Fundamentals & Applications. *McGraw-Hill Education*. **2011**.

187. Wissler, EH. A mathematical model of the human thermal system. *Bull. Math. Biophys.* **1964**; 26 147–166.

188. Stolwijk, JA & Hardy, JD. Partitional calorimetric studies of responses of man to thermal transients. *J. Appl. Physiol.* **1966**; 21 (3) 967–977.

189. Ainsworth, BE *et al.* 2011 compendium of physical activities: A second update of codes and MET values. *Med. Sci. Sports Exerc.* **2011**; 43 (8) 1575–1581.

190. Wyndham, CH *et al.* Inter- and intra-individual differences in energy expenditure and mechanical efficiency. *Ergonomics*. **1966**; 9 (1) 17–29.

191. Plagenhoef, S, Gaynor Evans, F & Abdelnour, T. Anatomical Data for Analyzing Human Motion. *Res. Q. Exerc. Sport*. **1983**;

192. Byrne, NM. Metabolic equivalent: one size does not fit all. *J. Appl. Physiol.* **2005**; 99 (3) 1112–1119.

193. Givoni, B & Goldman, RF. Predicting rectal temperature response to work, environment, and clothing. *J. Appl. Physiol.* **1972**; 32 (6) 812–822.

194. Gonzalez, RR, McLellan, TM, Withey, WR, Chang, SK & Pandolf, KB. Heat strain models applicable for protective clothing systems: comparison of core temperature response. *J. Appl. Physiol.* **1997**; 83 (3) 1017–1032.

195. Arens, E & Hui, Z. The skin's role in human thermoregulation and comfort. in *Thermal and Moisture Transport in Fibrous Materials*. **2006**.

196. Wang, L, Yin, H, Di, Y, Liu, Y & Liu, J. Human local and total heat losses in different temperature. *Physiol. Behav.* **2016**; 157 270–276.

197. Bolineni, S, Stratbücker, S & van Treeck, C. Development of reduced order flow responsive models of convective heat transfer for human body segments. *Build. Simul.* **2015**; 8 (4) 393–404.

198. Thirumaleshwar, M. Fundamentals of Heat and Mass Transfer. *Dorling Kindersley*. **2009**.

199. Alduchov, OA & Eskridge, RE. Improved Magnus Form Approximation of Saturation Vapor Pressure. *Journal of Applied Meteorology*. **1996**; 35 (4) 601–609.

200. Kalra, M. Development of a Novel Portable Cooling Device for Inducing Mild Hypothermia. (*Thesis: Simon Fraser University*). **2014**.

201. Potter, AW, Blanchard, LA, Friedl, KE, Cadarette, BS & Hoyt, RW. Mathematical

prediction of core body temperature from environment, activity, and clothing: The heat strain decision aid (HSDA). *J. Therm. Biol.* **2017**;

202. Wakat, DK, Johnson, RE, Krzywicki, HJ & Gerber, LI. Correlation between body volume and body mass in men. *Am. J. Clin. Nutr.* **1971**;

203. Havenith, G, Heus, R & Lotens, WA. Clothing ventilation, vapour resistance and permeability index: Changes due to posture, movement and wind. *Ergonomics*. **1990**;

204. Joyner, MJ & Casey, DP. Regulation of increased blood flow (Hyperemia) to muscles during exercise: A hierarchy of competing physiological needs. *Physiol. Rev.* **2015**; 95 (2) 549–601.

205. COMSOL Multiphysics. The Finite Element Method (FEM): Mesh Convergence. *Multiphysics Cyclopedia*. **2017**. Available at: uk.comsol.com/multiphysics/finite-element-method.

206. Schlegel, F. Understanding Stabilization Methods. *COMSOL Multiphysics*. **2014**. Available at: comsol.com/blogs/understanding-stabilization-methods.

207. Vaughan, N, Dubey, VN, Wee, MYK & Isaacs, R. Parametric model of human body shape and ligaments for patient-specific epidural simulation. *Artif. Intell. Med.* **2014**; 62 (2) 129–140.

208. Lorbeer, R *et al.* Reference values of vessel diameters, stenosis prevalence, and arterial variations of the lower limb arteries in a male population sample using contrast-enhanced MR angiography. *PLoS One*. **2018**; 13 (6) e0197559.

209. Chavhan, GB, Parra, DA, Mann, A & Navarro, OM. Normal doppler spectral waveforms of major pediatric vessels: Specific patterns. *Radiographics*. **2008**; 28 (3)

210. Calbet, JAL *et al.* Chronic hypoxia increases arterial blood pressure and reduces adenosine and ATP induced vasodilatation in skeletal muscle in healthy humans. *Acta Physiol.* **2014**; 211 (4) 574–584.

211. Sienkiewicz, Z, Van Rongen, E, Croft, R, Ziegelberger, G & Veyret, B. A closer look at the thresholds of thermal damage: workshop report by an ICNIRP task group. *Health Phys.* **2016**; 111 (3) 300–306.

212. Van Rhoon, GC *et al.* CEM43°C thermal dose thresholds: A potential guide for magnetic resonance radiofrequency exposure levels? *Eur. Radiol.* **2013**; 23 (8) 2215–2227.

213. Mitsuhashi, N *et al.* BodyParts3D: 3D structure database for anatomical concepts. *Nucleic Acids Res.* **2009**; 37 782–785.

214. Spitzer, V, Ackerman, MJ, Scherzinger, a L & Whitlock, D. The visible human male: a technical report. *J. Am. Med. Informatics Assoc.* **1996**; 3 (2) 118–130.

215. Banks, J. Adding value in additive manufacturing: Researchers in the United Kingdom and Europe look to 3D printing for customization. *IEEE Pulse*. **2013**; 4 (6) 22–26.

216. Royal Academy of Engineering. Additive Manufacturing : Opportunities and

Constraints. *Royal Academy of Engineering*. **2013**.

217. Chang, J *et al.* Advanced material strategies for next-generation additive manufacturing. *Materials*. **2018**;

218. Miriyev, A, Stack, K & Lipson, H. Soft material for soft actuators. *Nat. Commun.* **2017**; 8 (1) 596.

219. Moore, JP & Williams, CB. Fatigue properties of parts printed by PolyJet material jetting. *Rapid Prototyp. J.* **2015**; 21 (6) 675–685.

220. Schumacher, C *et al.* Microstructures to control elasticity in 3D printing. *ACM Trans. Graph.* **2015**; 34 (4) 1–13.

221. Prosfit. The Pandofit solution. Available at: https://prosfit.com/.

222. Revicki, DA & Frank, L. Pharmacoeconomic evaluation in the real world: Effectiveness versus efficacy studies. *PharmacoEconomics*. **1999**; 15 (5) 423–434.

223. Oxford Centre for Evidence-based Medicine. Levels of Evidence. *University of Oxford*. **2009**. Available at: www.cebm.net.

224. Downs, SH & Black, N. The feasibility of creating a checklist for the assessment of the methodological quality both of randomised and non-randomised studies of health care interventions. *J. Epidemiol. Community Health*. **1998**; 52 (6) 377–384.

225. Higgins, JPT & Green, S. Cochrane Handbook for Systematic Reviews of Interventions Version 5.1.0. *The Cochrane Collaboration*. **2011**.

226. E-NABLE. Enabling the future. **2015**. Available at: enablingthefuture.org.

227. Open Bionics. The next generation of bionics. **2016**. Available at: www.openbionics.com.

228. Moher, D, Liberati, A, Tetzlaff, J & Altman, DG. Preferred Reporting Items for Systematic Reviews and Meta-Analyses: The PRISMA Statement. *Ann. Intern. Med.* **2009**; 151 (4) 264–269.

229. Alvial, P *et al.* Quantitative functional evaluation of a 3D–printed silicone-embedded prosthesis for partial hand amputation: A case report. *J. Hand Ther.* **2018**; 31 (1) 129–136.

230. Atallah, R *et al.* Osseointegrated Transtibial Implants in Patients with Peripheral Vascular Disease: A Multicenter Case Series of 5 Patients with 1-Year Follow-up. *J. Bone Joint Surg. Am.* **2017**; 99 (18) 1516–1523.

231. Belter, JT, Leddy, MT, Gemmell, KD & Dollar, AM. Comparative clinical evaluation of the Yale Multigrasp Hand. in *International Conference on Biomedical Robotics and Biomechatronics*. **2016**. 528–535.

232. Cañizares, A, Pazos, J & Benítez, D. On the Use of 3D Printing Technology Towards

the Development of a Low-Cost Robotic Prosthetic Arm. in *IEEE International Autumn Meeting on Power, Electronics and Computing*. **2017**.

233. Faustini, MC, Crawford, RH, Neptune, RR, Rogers, WE & Bosker, G. Design and analysis of orthogonally compliant features for local contact pressure relief in transtibial prostheses. *J. Biomech. Eng.* **2005**; 127 (6) 946–951.

234. Gretsch, KF *et al.* Development of novel 3D-printed robotic prosthetic for transradial amputees. *Prosthet. Orthot. Int.* **2016**; 40 (3) 400–403.

235. Herbert, N, Simpson, D, Spence, WD & Ion, W. A preliminary investigation into the development of 3-D printing of prosthetic sockets. *J. Rehabil. Res. Dev.* **2005**; 42 (2) 141.

236. Hofmann, MK. Making Connections: Modular 3D Printing for Designing Assistive Attachments to Prosthetic Devices. in *International ACM SIGACCESS Conference on Computers & Accessibility*. **2015**. 353–354.

237. Hofmann, M, Harris, J, Hudson, SE & Mankoff, J. Helping Hands: Requirements for a Prototyping Methodology for Upper-limb Prosthetics Users. in *SIGCHI Conference on Human Factors in Computing Systems*. **2016**. 1769–1780.

238. Hsu, LH, Huang, GF, Lu, CT, Hong, DY & Liu, SH. The development of a rapid prototyping prosthetic socket coated with a resin layer for transtibial amputees. *Prosthet. Orthot. Int.* **2010**; 34 (1) 37–45.

239. Hsu, LH *et al.* Introduction to a type of resin-reinforced rapid prototyping transtibial socket. in *Conference on Engineering Systems Design and Analysis*. **2010**.

240. Hsu, CH, Ou, CH, Hong, WL & Gao, YH. Comfort level discussion for prosthetic sockets with different fabricating processing conditions. *Biomed. Eng. Online*. **2018**;

241. Jacobsen, C, Ashe, E & Noorani, R. The recreation and evaluation of a human hand using low-cost reverse engineering and 3D printing systems. in *ASME International Mechanical Engineering Congress and Exposition, Proceedings*. **2016**.

242. Jeong, E & Lee, G. The Use of a Low-Cost Three- Dimensional Printed Single Channel Myoelectric Interfaced Prosthesis for Transradial Amputees : Preliminary Report. *Plast Reconstr Surg Glob Open*. **2017**; 5 (9) 147–148.

243. Kontoudis, GP, Liarokapis, M V., Zisimatos, AG, Mavrogiannis, CI & Kyriakopoulos, KJ. Open-source, anthropomorphic, underactuated robot hands with a selectively lockable differential mechanism: Towards affordable prostheses. in *IEEE International Conference on Intelligent Robots and Systems*. **2015**. 5857–5862.

244. Lee, KH *et al.* Hand functions of myoelectric and 3D-printed pressure-sensored prosthetics: A comparative study. *Ann. Rehabil. Med.* **2017**; 41 (5) 875–880.

245. Lee, KH *et al.* Three-dimensional printed prosthesis demonstrates functional improvement in a patient with an amputated thumb: A technical note. *Prosthet. Orthot. Int.* **2018**; 42 (1) 107–111.

246. Low, JH, Ang, MH & Yeow, CH. Customizable soft pneumatic finger actuators for hand orthotic and prosthetic applications. in *IEEE International Conference on*

Rehabilitation Robotics. **2015**. 380–385.

247. Nabeel, M, Aqeel, K, Ashraf, MN, Awan, MI & Khurram, M. Vibrotactile stimulation for 3D printed prosthetic hand. in *2016 2nd International Conference on Robotics and Artificial Intelligence*. **2016**. 202–207.

248. Rajestari, Z, Feizi, N, Taghvaei, S & Jalisi, M. Optimal kinematic synthesis and fabrication of a one-DoF prosthetic finger. *J. Brazilian Soc. Mech. Sci. Eng.* **2017**; 39 (8) 2925–2934.

249. Ramakrishnan, T, Schlafly, M & Reed, KB. Evaluation of 3D printed anatomically scalable transfemoral prosthetic knee. in *IEEE International Conference on Rehabilitation Robotics*. **2017**. 1160–1164.

250. Rogers, B *et al.* Case report: variably compliant transtibial prosthetic socket fabrication using solid freeform fabrication. *JPO J. Prosthetics Orthot.* **2008**; 20 (1) 1–7.

251. Saint-Elme, E *et al.* Design of a Biologically Accurate Prosthetic Hand. in *International Symposium on Wearable Robotics and Rehabilitation*. **2017**.

252. Sims, T, Cranny, A, Metcalf, C, Chappell, P & Donovan-Hall, M. Participatory design of pediatric upper limb prostheses: Qualitative methods and prototyping. *Int. J. Technol. Assess. Health Care*. **2017**; 33 (6) 629–637.

253. South, BJ, Fey, NP, Bosker, G & Neptune, RR. Manufacture of Energy Storage and Return Prosthetic Feet Using Selective Laser Sintering. *J. Biomech. Eng.* **2010**; 132 (1) 015001.

254. Swartz, AQ, Turner, K, Miller, L & Kuiken, T. Custom, rapid prototype thumb prosthesis for partial-hand amputation: A case report. *Prosthet. Orthot. Int.* **2018**; 42 (2) 187–190.

255. Vitali, A, Rizzi, C & Regazzoni, D. Design and Additive Manufacturing of Lower Limb Prosthetic Socket. in *International Mechanical Engineering Congress and Exposition*. **2017**.

256. Xu, G *et al.* Three-dimensional-printed upper limb prosthesis for a child with traumatic amputation of right wrist. *Med. (United States)*. **2017**; 96 (52) 1–5.

257. Yoshikawa, M, Sato, R, Higashihara, T, Ogasawara, T & Kawashima, N. Rehand: Realistic electric prosthetic hand created with a 3D printer. in *Proceedings of the Annual International Conference of the IEEE Engineering in Medicine and Biology Society*. **2015**. 2470–2473.

258. Zuniga, JM, Peck, J, Srivastava, R, Katsavelis, D & Carson, A. An Open Source 3D-Printed Transitional Hand Prosthesis for Children. *J Prosthet Orthot*. **2016**; 28 (3)

259. Zuniga, JM *et al.* The development of a low-cost three-dimensional printed shoulder , arm , and hand prostheses for children. *Prosthet. Orthot. Int.* **2017**; 41 (2) 205–209.

260. Ahn, S, Montero, M, Odell, D, Roundy, S & Wright, PK. Anisotropic material properties of fused deposition modeling ABS. *Rapid Prototyp. J.* **2002**; 8 (4) 248–257.

261. Biddiss, E & Chau, T. The roles of predisposing characteristics, established need, and enabling resources on upper extremity prosthesis use and abandonment. *Disabil. Rehabil. Assist. Technol.* **2007**; 2 (2) 71–84.

262. Zadpoor, AA & Malda, J. Additive Manufacturing of Biomaterials, Tissues, and Organs. *Ann. Biomed. Eng.* **2017**; 45 (1) 1–11.

263. Lee Ventola, C. Medical applications for 3D printing: Current and projected uses. *P T.* **2014**; 39 (10) 704–711.

264. Tack, P, Victor, J, Gemmel, P & Annemans, L. 3D-printing techniques in a medical setting: a systematic literature review. *Biomed. Eng. Online.* **2016**; 15 (1) 115.

265. Caffrey, T & Wohlers, T. Additive manufacturing state of the industry. *Manuf. Eng.* **2015**; 154 (5) 67–78.

266. Mulford, JS, Babazadeh, S & Mackay, N. Three-dimensional printing in orthopaedic surgery: Review of current and future applications. *ANZ J. Surg.* **2016**; 86 (9) 648–653.

267. Technical Considerations for Additive Manufactured Devices - Draft Guidance for Industry and Food and Drug Administration Staff. *Food and Drug Administration (FDA)*. **2016**.

268. Bauermeister, AJ, Zuriarrain, A & Newman, MI. Three-Dimensional Printing in Plastic and Reconstructive Surgery: A Systematic Review. *Ann. Plast. Surg.* **2016**; 77 (5) 569–576.

269. Soon, DSC *et al.* 3D haptic modelling for preoperative planning of hepatic resection: A systematic review. *Ann. Med. Surg.* **2016**; 10 1–7.

270. Patzelt, SBM, Spies, BC & Kohal, RJ. CAD/CAM-fabricated implant-supported restorations: A systematic review. *Clin. Oral Implants Res.* **2015**; 26 (11) 77–85.

271. Bidra, AS, Taylor, TD & Agar, JR. Computer-aided technology for fabricating complete dentures: Systematic review of historical background, current status, and future perspectives. *Journal of Prosthetic Dentistry*. **2013**; 109 (6) 361–366.

272. Tarsitano, A, Del Corso, G, Ciocca, L, Scotti, R & Marchetti, C. Mandibular reconstructions using computer-aided design/computer-aided manufacturing: A systematic review of a defect-based reconstructive algorithm. *J. Cranio-Maxillofacial Surg.* **2015**; 43 (9) 1785–1791.

273. Martelli, N *et al.* Advantages and disadvantages of 3-dimensional printing in surgery: A systematic review. *Surgery (United States)*. **2016**; 159 (6) 1485–1500.

274. Zhang, QM *et al.* No Evidence of Superiority in Reducing Outliers of Component Alignment for Patient-specific Instrumentation for Total Knee Arthroplasty: A Systematic Review. *Orthopaedic Surgery*. **2015**; 7 (1) 19–25.

275. Liberati, A *et al.* The PRISMA statement for reporting systematic reviews and meta-analyses of studies that evaluate health care interventions: explanation and elaboration. *J. Clin. Epidemiol.* **2009**; 62 (10) 1–34.

276. International Statistical Classification of Diseases and Related Health Problems (ICD) 10th Revision. *World Health Organization*. **2010**.

277. Stephens, MH *et al.* 3-D bone models to improve treatment initiation among patients with osteoporosis: A randomised controlled pilot trial. *Psychol. Health.* **2016**; 31 (4) 487–497.

278. de Farias, TP *et al.* Use of prototyping in preoperative planning for patients with head and neck tumors. *Head Neck.* **2014**; 36 (12) 1773–1782.

279. Ahrberg, D, Lauer, HC, Ahrberg, M & Weigl, P. Evaluation of fit and efficiency of CAD/CAM fabricated all-ceramic restorations based on direct and indirect digitalization: a double-blinded, randomized clinical trial. *Clin. Oral Investig.* **2016**; 20 (2) 291–300.

280. D'Urso, PS *et al.* Stereolithographic biomodelling in cranio-maxillofacial surgery: a prospective trial. *J. cranio-maxillo-facial Surg.* **1999**; 27 (1) 30–37.

281. Al-Ahmad, HT, M Saleh, MW & Hussein, AM. Evaluation of an innovative computer-assisted sagittal split ramus osteotomy to reduce neurosensory alterations following orthognathic surgery: a pilot study. *Int. J. Med. Robot. Comput. Assist. Surg.* **2013**; 9 (2) 134–41.

282. Ayoub, N *et al.* Evaluation of computer-assisted mandibular reconstruction with vascularized iliac crest bone graft compared to conventional surgery: a randomized prospective clinical trial. *Trials*. **2014**; 15 114.

283. Goh, BT, Teh, LY, Tan, DBP, Zhang, Z & Teoh, SH. Novel 3D polycaprolactone scaffold for ridge preservation - a pilot randomised controlled clinical trial. *Clin. Oral Implants Res.* **2015**; 26 (3) 271–277.

284. Van de Velde, T, Sennerby, L & De Bruyn, H. The clinical and radiographic outcome of implants placed in the posterior maxilla with a guided flapless approach and immediately restored with a provisional rehabilitation: A randomized clinical trial. *Clin. Oral Implants Res.* **2010**; 21 (11) 1223–1233.

285. Vercruyssen, M *et al.* A randomized clinical trial comparing guided implant surgery (bone- or mucosa-supported) with mental navigation or the use of a pilot-drill template. *J. Clin. Periodontol.* **2014**; 41 (7) 717–723.

286. Chareancholvanich, K, Narkbunnam, R & Pornrattanamaneewong, C. A prospective randomised controlled study of patient-specific cutting guides compared with conventional instrumentation in total knee replacement. *Bone Joint J.* **2013**; 95-B 354–359.

287. Chen, HL, Wu, DY, Yang, HL & Guo, KJ. Clinical Use of 3D Printing Guide Plate in Posterior Lumbar Pedicle Screw Fixation. *Med. Sci. Monit.* **2015**; 21 3948–3954.

288. Du, H *et al.* Use of patient-specific templates in hip resurfacing arthroplasty: Experience from sixteen cases. *Int. Orthop.* **2013**; 37 (5) 777–782.

289. Gan, Y, Ding, J, Xu, Y & Hou, C. Accuracy and efficacy of osteotomy in total knee arthroplasty with patient-specific navigational template. *Int. J. Clin. Exp. Med.* **2015**; 8 (8) 12192–12201.

290. Hendel, MD *et al.* Comparison of patient-specific instruments with standard surgical instruments in determining glenoid component position: a randomized prospective clinical trial. *J. Bone Joint Surg. Am.* **2012**; 94 (23) 2167–75.

291. Maini, L, Sharma, A, Jha, S, Sharma, A & Tiwari, A. Three-dimensional printing and patient-specific pre-contoured plate: future of acetabulum fracture fixation? *Eur. J. Trauma Emerg. Surg.* **2018**; 44 (2) 215–224.

292. Merc, M, Drstvensek, I, Vogrin, M, Brajlih, T & Recnik, G. A multi-level rapid prototyping drill guide template reduces the perforation risk of pedicle screw placement in the lumbar and sacral spine. *Arch. Orthop. Trauma Surg.* **2013**; 133 (7) 893–899.

293. Shuang, F, Hu, W, Shao, Y, Li, H & Zou, H. Treatment of Intercondylar Humeral Fractures With 3D-Printed Osteosynthesis Plates. *Medicine (Baltimore).* **2016**; 95 (3) 2461.

294. Wu, Z-X *et al.* Accuracy and safety assessment of pedicle screw placement using the rapid prototyping technique in severe congenital scoliosis. *J. spinal Disord. {&} Tech.* **2011**; 24 (7) 444–450.

295. Yang, L *et al.* Application of 3D Printing in the Surgical Planning of Trimalleolar Fracture and Doctor-Patient Communication. *Biomed Res. Int.* **2016**; 1–5.

296. You, W *et al.* Application of 3D printing technology on the treatment of complex proximal humeral fractures (Neer3-part and 4-part) in old people. *Orthop. Traumatol. Surg. Res.* **2016**; 102 (7) 897–903.

297. Zhang, YZ *et al.* Preliminary application of computer-assisted patient-specific acetabular navigational template for total hip arthroplasty in adult single development dysplasia of the hip. *Int. J. Med. Robot. Comput. Assist. Surg.* **2011**; 7 (4) 469–474.

298. Arisan, V, Karabuda, CZ, Mumcu, E & Ozdemir, T. Implant positioning errors in freehand and computer-aided placement methods: a single-blind clinical comparative study. *Int. J. Oral Maxillofac. Implants*. **2013**; 28 (1) 190–204.

299. Azuma, M *et al.* Mandibular reconstruction using plates prebent to fit rapid prototyping 3-dimensional printing models ameliorates contour deformity. *Head Face Med.* **2014**; 10 45.

300. Brown, M *et al.* Effectiveness and efficiency of a CAD/CAM orthodontic bracket system. *Am J Orthod Dentofac. Orthop*. **2015**; 148 (6) 1067–1074.

301. Calvo-Guirado, J-L, Maté-Sánchez, J-E, Delgado-Ruiz, R & Ramírez-Fernández, M-P. Calculation of bone graft volume using 3D reconstruction system. *Med. Oral Patol. Oral Cir. Bucal*. **2011**; 16 (2) e260-4.

302. Hanasono, MM & Skoracki, RJ. Computer-assisted design and rapid prototype modeling in microvascular mandible reconstruction. *Laryngoscope*. **2013**; 123 (3) 597–604.

303. INOKOSHI, M, KANAZAWA, M & MINAKUCHI, S. Evaluation of a complete denture trial method applying rapid prototyping. *Dent. Mater. J.* **2012**; 3 (31) 40–46.

304. Kozakiewicz, M, Elgalal, M, Piotr, L, Broniarczyk-Loba, A & Stefanczyk, L. Treatment with individual orbital wall implants in humans - 1-year ophthalmologic evaluation. *J. Cranio-Maxillofacial Surg.* **2011**; 39 (1) 30–36.

305. Lee, STSC, Wu, CT, Lee, STSC & Chen, PJ. Cranioplasty using polymethyl methacrylate prostheses. *J. Clin. Neurosci.* **2009**; 16 (1) 56–63.

306. Modabber, A *et al.* Evaluation of computer-assisted jaw reconstruction with free vascularized fibular flap compared to conventional surgery: A clinical pilot study. *Int. J. Med. Robot. Comput. Assist. Surg.* **2012**; 8 (2) 215–220.

307. Resnick, CM *et al.* Is There a Difference in Cost Between Standard and Virtual Surgical Planning for Orthognathic Surgery? *J. Oral Maxillofac. Surg.* **2016**; 74 (9) 1827–1833.

308. Rogers-Vizena, C, Sporn, S, Daniels, K, Padwa, B & Weinstock, P. Cost-Benefit Analysis of Three-Dimensional Craniofacial Models for Midfacial Distraction: A Pilot Study. *Cleft Palate Craniofac J.* **2017**; 54 (5) 612–617.

309. Sumida, T *et al.* Custom-made titanium devices as membranes for bone augmentation in implant treatment: Clinical application and the comparison with conventional titanium mesh. *J. Cranio-Maxillofacial Surg.* **2015**; 43 (10) 2183–2188.

310. Zhang, S *et al.* Application of rapid prototyping for temporomandibular joint reconstruction. *J. Oral Maxillofac. Surg.* **2011**; 69 (2) 432–438.

311. Hirao, M *et al.* Use of a custom-made surgical guide in total ankle arthroplasty in rheumatoid arthritis cases. *Tech. Orthop.* **2014**; 29 (2)

312. Iannotti, JP *et al.* Three-dimensional imaging and templating improve glenoid implant positioning. *J. Bone Joint Surg. Am.* **2015**; 97 (8) 651–658.

313. Karlin, L, Weinstock, P, Hedequist, D & Prabhu, SP. The surgical treatment of spinal deformity in children with myelomeningocele: The role of personalized three-dimensional printed models. *J. Pediatr. Orthop. Part B.* **2017**; 26 (4) 375–382.

314. Li, C *et al.* Application of the polystyrene model made by 3-D printing rapid prototyping technology for operation planning in revision lumbar discectomy. *J. Orthop. Sci.* **2015**; 20 (3) 475–480.

315. Li, B *et al.* Comparative use of the computer-aided angiography and rapid prototyping technology versus conventional imaging in the management of the Tile C pelvic fractures. *Int. Orthop.* **2016**; 40 (1) 161–166.

316. Schweizer, A, Mauler, F, Vlachopoulos, L, Nagy, L & Fürnstahl, P. Computer-assisted 3-dimensional reconstructions of scaphoid fractures and nonunions with and without the use of patient-specific guides: Early clinical outcomes and postoperative assessments of reconstruction accuracy. *J. Hand Surg. Am.* **2016**; 41 (1) 59–69.

317. Lin, X *et al.* Application of three-dimensional model in the management of irreducible atlanto-axial dislocation. *Acta Orthop. Traumatol. Turc.* **2014**; 48 (3) 298–302.

318. Yang, M *et al.* Application of 3D rapid prototyping technology in posterior corrective surgery for Lenke 1 adolescent idiopathic scoliosis patients. *Med.* **2015**; 94 (8) e582.

319. Schievano, S *et al.* Percutaneous pulmonary valve implantation based on rapid prototyping of right ventricular outflow tract and pulmonary trunk from MR data. *Radiology*. **2007**; 242 (2) 490–497.

320. Adolphs, N, Liu, W, Keeve, E & Hoffmeister, B. RapidSplint: virtual splint generation for orthognathic surgery – results of a pilot series. *Comput Aided Surg*. **2014**; 19 1092–9088.

321. Arısan, V, Karabuda, ZC & Özdemir, T. Accuracy of Two Stereolithographic Guide Systems for Computer-Aided Implant Placement: A Computed Tomography-Based Clinical Comparative Study. *J. Periodontol.* **2010**; 81 (1) 43–51.

322. Morris, L, Sokoya, M, Cunningham, L & Gal, TJ. Utility of stereolithographic models in osteocutaneous free flap reconstruction of the head and neck. *Craniomaxillofac. Trauma Reconstr.* **2013**; 6 (212) 87–92.

323. Shahbazian, M *et al.* Validation of the cone beam computed tomography-based stereolithographic surgical guide aiding autotransplantation of teeth: Clinical case-control study. *Oral Surg. Oral Med. Oral Pathol. Oral Radiol.* **2013**; 115 (5) 667–675.

324. Weitz, J *et al.* Accuracy of templates for navigated implantation made by rapid prototyping with DICOM datasets of cone beam computer tomography (CBCT). *Clin. Oral Investig.* **2011**; 15 (6) 1001–1006.

325. Otsuki, B *et al.* Developing a novel custom cutting guide for curved peri-acetabular osteotomy. *Int. Orthop.* **2013**; 37 (6) 1033–1038.

326. Colquhoun, D. An investigation of the false discovery rate and the misinterpretation of p-values. *R. Soc. Open Sci.* **2014**; 1 (3) 1–16.

327. Ioannidis, JPA. Why most published research findings are false. *PLoS Medicine*. **2005**; 2 (8) 0696–0701.

328. Shafiee, A & Atala, A. Printing Technologies for Medical Applications. *Trends Mol. Med.* **2016**; 22 (3) 254–265.

329. Williams, RJ, Washington, ED, Miodownik, M & Holloway, C. The effect of liner design and materials selection on prosthesis interface heat dissipation. *Prosthet. Orthot. Int.* **2018**; 42 (3) 275–279.

330. Al-Dirini, RMA, Reed, MP & Thewlis, D. Deformation of the gluteal soft tissues during sitting. *Clin. Biomech.* **2015**; 30 (7) 662–668.

331. Al-Dirini, RMA, Nisyrios, J, Reed, MP & Thewlis, D. Quantifying the in vivo quasi-static response to loading of sub-dermal tissues in the human buttock using magnetic resonance imaging. *Clin. Biomech.* **2017**; 50 70–77.

332. Taylor, M, Perilli, E & Martelli, S. Development of a surrogate model based on patient weight, bone mass and geometry to predict femoral neck strains and fracture loads. *J. Biomech.* **2017**; 55 121–127.

333. Martelli, S, Calvetti, D, Somersalo, E & Viceconti, M. Stochastic modelling of muscle recruitment during activity. *Interface Focus*. **2015**; 5 (2) 20140094-.

334. Lee, V, Gross, P, Spense, W, Solomonidis, S & Paul, J. Two dimensional finite element model of a transverse section of the trans-femoral amputee's stump. in *Computer methods in biomechanics & biomedical engineering 2*. (eds. Middleton, J., Jones, M. & Pande, G.) *Overseas Publishers Association*. **1998**. 577–583.

335. Dickinson, AS, Steer, JW & Worsley, PR. Finite element analysis of the amputated lower limb: A systematic review and recommendations. *Med. Eng. Phys.* **2017**; 43 1–18.

336. Sanders, JE. Thermal response of skin to cyclic pressure and pressure with shear: A technical note. *J. Rehabil. Res. Dev.* **2000**;

337. Portnoy, S *et al.* Internal mechanical conditions in the soft tissues of a residual limb of a trans-tibial amputee. *J. Biomech.* **2008**;

338. Racinais, S & Oksa, J. Temperature and neuromuscular function. *Scandinavian Journal of Medicine and Science in Sports*. **2010**;

339. Sullivan, J & Young, C. National Amputee Prosthetics Outcomes Registry (AMPROM). in *ISPO UK Annual Scientific Meeting*. **2018**.

340. Sahandi, R, Sewell, P, Noroozi, S & Hewitt, M. Remote monitoring of lower-limb prosthetic socket fit using wireless technologies. *J. Med. Eng. Technol.* **2012**;

341. Childs, PRN, Greenwood, JR & Long, CA. Review of temperature measurement. *Review of Scientific Instruments*. **2000**;

342. FLIR A655sc Infrared Camera. **2016**. Available at: www.flir.com/science/display/?id=46802.

343. Vicon Motion Systems. Motion Capture. **2016**. Available at: www.vicon.com/what-is-motion-capture.

344. Nation Master Encyclopaedia. Retroreflective. **2003**. Available at: www.statemaster.com/encyclopedia/Retroreflective.

345. Vicon Motion Systems. Vicon DataStream SDK Developer's Manual. **2013**.

346. LCR Hallcrest. Handbook of Thermochromic Liquid Crystal Technology.

347. LeSar, JD *et al.* A novel thermochromic liquid crystal fabric design for the early detection of high-risk foot complications: A proof-of-concept study. *J. Am. Podiatr. Med. Assoc.* **2017**;

348. Schäfer, T. Temperature Grid Sensor for the Measurement of Spatial Temperature Distributions at Object Surfaces. *Sensors*. **2013**; 13 1593–1602.

349. Mathur, N, Glesk, I & Buis, A. Skin Temperature Prediction in Lower Limb Prostheses. *Ieee J. Biomed. Heal. Informatics*. **2016**; 20 (1) 158–165.

350. Lomperski, S, Gerardi, C & Pointer, WD. Fiber optic distributed temperature sensor mapping of a jet-mixing flow field. *Exp. Fluids*. **2015**;

351. Aundal, TP. The Radon Transform-Theory and Implementation. (*University of Denmark*). **1996**.

352. Van Langenhove, L. Advances in Smart Medical Textiles: Treatments and Health Monitoring. *Advances in Smart Medical Textiles: Treatments and Health Monitoring*. **2015**.

353. Mandal, S & Song, G. Thermal sensors for performance evaluation of protective clothing against heat and fire: a review. *Text. Res. J.* **2015**; 85 (1) 101–112.